

**DESIGN OF HYBRID MARINE CONTROL SYSTEMS
FOR DYNAMIC POSITIONING**

NGUYEN TRONG DONG

(B.Eng. (Hons.), HCMUT)

A THESIS SUBMITTED IN PARTIAL FULFILLMENT OF THE
REQUIREMENT FOR THE DEGREE OF DOCTOR OF PHILOSOPHY
DEPARTMENT OF CIVIL ENGINEERING
NATIONAL UNIVERSITY OF SINGAPORE

2005

Acknowledgements

First of all, I would like to thank my supervisor, Professor Quek Ser Tong, at the Department of Civil Engineering, NUS, for his encouraging and introducing me this wonderful research. His trust and scientific excitement inspired me through my research and I am so lucky to work with him.

I am grateful to my co-supervisor, Professor Asgeir J. Sørensen at the Marine Technology Department, Norwegian University of Science and Technology (NTNU), for inviting me to research stay at NTNU. He always shares his knowledge regarding the marine control systems and this helps me a lot in my research.

I would like to thank my colleagues at NUS and NTNU for their invaluable helps and supporting me in my research work. I would like to say that it was a pleasure to work with Øyvind and especially Torgeir Wahl who valuably helped me to conduct experiments with Cybership III at the Marine Cybernetics Laboratory, NTNU. I want to thank you all for all your kindly help, support, interest and valuable hints.

I also want to thank my parents and brother, who taught me the value of hard working by their own examples. They are always my strong support during the whole difficult time of my research. The acknowledgement would not be complete without the mention of my girlfriend who is always with me whenever I fell lonely far from home.

The work has been carried out and supported by the National University of Singapore Research Scholarship. In addition, Keppel Corporation is great is greatly acknowledged for sponsoring me the Keppel Professorship Fund for my research stay at NTNU. Finally, the presentations of three conference papers in the Sixteenth, Seventeenth and Eighteenth KKCNN Symposums on Civil Engineering were made possible with financial support from Lee Foundation.

Summary

Dynamic positioning is critical in floating structures to keep it operational especially for offshore exploration. Marine vessels should optimally be able to operate in different environmental conditions and different speed regimes but it is not efficient to have a wide operational window using a single control system. Hence, the objectives of this thesis are to present the concept of an *integrated hybrid control dynamic positioning system* (or so-called “*super system*”) for marine control, integrating DP, maneuvering and transit operations under calm, moderate, rough and extreme environmental conditions. The choice of controller to use is influenced by three main parameters, namely function, environment and speed regime. Changes in these parameters will result in changes in control objectives, constraints, dynamic responses and disturbance characteristics. Once the choice is decided, switching can be performed manually or automatically.

Manually switched hybrid marine control system integrating functions for DP, low speed maneuvering and transit operations was developed. For smooth performance during switching, weighting functions for the controllers were used. Guidance and navigation is necessary to smoothly change the desired speed or set-point. The smooth transformation was verified experimentally using the model ship, Cybership III, for operating from DP to PM and vice versa.

Automatic switch hybrid control was performed via a switching logic adopting the concept of supervisory switching, and was developed in this thesis for DP system under calm to extreme seas. Although station keeping of floating structures under moderate sea conditions has been well studied, the solutions are not adequate for extreme sea conditions. Nonlinear passive observer without wave frequency (WF)

filtering was studied by stability analysis, numerical simulations and experiments with the model ship, Cybership III, to validate this observer proposed by Sørensen et al. (2002) for extreme seas. The study showed that in extreme seas nonlinear passive observer without WF filtering stabilized the DP vessel and performed better than nonlinear passive observer with WF filtering. In addition, the acceleration feedback with PID, in short AFB controller, was studied for its effectiveness in extreme seas. The experiments with the Cybership III under three sea states, i.e. moderate, moderately rough and rough seas, showed that AFB controller improved the performance of DP vessel compared with that using PID controller only and the level of improvement seems to increase with increasing sea states. The observer without WF filtering and AFB controller were recommended for the DP system in extreme seas.

The hybrid control for DP system handling changes of environmental conditions from calm to extreme sea integrates the conventional controllers for normal seas and output AFB or output PID without WF filtering from the observer. The hybrid control DP system adopting the concept of supervisory switching has the ability to automatically switch among a set of controllers. Stability analysis, numerical simulations and experiments for the proposed hybrid control using supervisory control were provided. The performances of the hybrid control DP vessel in simulations and experiments in varying environmental conditions did not show instability when switching and performed better than the single controller DP vessel. Those suggest that the switching may not have a negative effect on the stability of the whole system and can be expand the weather window for DP system to extreme conditions by implementing hybrid control concept.

Table of Content

Acknowledgements	i
Summary	ii
Table of Content	iv
List of Tables	x
List of Figures	xii
Chapter 1 Introduction	1
1.1 Background	1
1.2 Literature Review	2
1.2.1 Hybrid Control and Supervisory Control	2
1.2.2 Station Keeping of Marine Vessels	4
1.2.3 Low Speed Maneuvering and Transit.....	11
1.3 Objectives and Scopes	12
1.4 Organization of Thesis.....	16
Chapter 2 Modelling of Marine Vessels	18
2.1 Introduction.....	18
2.2 Notation and Kinematics	19
2.2.1 Reference Frames and Notations	19
2.2.2 Kinematics.....	20
2.3 Floater Dynamics.....	21
2.3.1 Low Frequency Model	22
2.3.2 Environmental Loads.....	26

2.3.3 Mooring Loads	28
2.3.4 Wave Frequency Model	32
 Chapter 3 Concept of Hybrid Marine Control Systems (HyMarCS).....	35
3.1 Introduction.....	35
3.2 Multi Operational Regime Controller Objectives.....	35
3.2.1 Changes in Operation Mode.....	35
3.2.2 Changes in Speed	37
3.2.3 Changes in Environment	37
3.2.4 Fault-Tolerant Control.....	39
3.3 Control Structure.....	39
3.3.1 Actuator Controller (Low Level).....	39
3.3.2 Plant Controller (High Level).....	39
3.3.3 Local Optimization.....	40
3.4 Concept of Hybrid Controller.....	40
3.4.1 Concept of Supervisory Control.....	41
3.4.2 Properties of Supervisory Control	43
3.4.3 Scale-Independent Hysteresis Switching Logic	45
3.5 Conclusions.....	46
 Chapter 4 Multi-Operational Hybrid Controller Structure for Station Keeping and Transit Operations of Marine Vessels.....	51
4.1 Introduction.....	51
4.2 Autopilot in Transit Regime	52
4.2.1 Observer Design	52
4.2.2 Controller Design	54
4.3 Station Keeping – Dynamic Positioning.....	54

4.3.1	Observer Design	54
4.3.2	Controller Design	57
4.4	Controller for Transition from Autopilot to DP.....	57
4.5	Station Keeping – Positioning Mooring System.....	58
4.5.1	Observer Design	58
4.5.2	Controller Design	59
4.6	Station Keeping – Transition from DP to PM and vice versa	59
4.7	Experimental Results	60
4.7.1	Switching from DP Mode to SPM Mode	61
4.7.2	Switching from STL Mode to DP Mode	62
4.7.3	Discussions	63
4.8	Conclusions.....	63
 Chapter 5 Design of Observer and Controller for Dynamic Positioning in Moderate and Extreme Seas		 80
5.1	Introduction.....	80
5.2	Observer with Parametrically Adaptive WF Filtering.....	82
5.2.1	Formulation	83
5.2.2	Simulation and Experimental Results	85
5.3	Observer without WF Filtering.....	86
5.3.1	Formulation	86
5.3.2	Simulation Results.....	86
5.3.3	Experimental Results.....	87
5.4	Experiments with AFB in different sea states	88
5.4.1	Overview of Experiments.....	88
5.4.2	Results and Discussions	88

5.5 Conclusions.....	90
Chapter 6 Design of Hybrid Controller for Dynamic Positioning from Calm to Extreme Seas..... 100	
6.1 Introduction.....	100
6.2 Hybrid Controller DP System Using Multi-output PID Controllers with Position Measurement.....	101
6.2.1 Output PID Controller for Calm and Moderate Seas (Models 1 and 2).....	102
6.2.2 Output PID Controller for Extreme Seas (Model 4)	105
6.2.3 Output PID for Transition Regime between Moderate and Extreme Seas (Model 3).....	107
6.3 Hybrid Controller DP System Using Multi-output PID and AFB Controllers with Position and Acceleration Measurements.....	107
6.3.1 Output AFB Controller for Extreme Seas (Model 4)	108
6.3.2 Output PID and AFB for Transition Regime between Moderate and Extreme Seas (Model 3)	110
6.4 Hybrid Controller DP System Using Multi-output PID and AFB Controllers with Position, Velocity and Acceleration Measurements	110
6.4.1 Output PID Controller for Calm and Moderate Seas (Model 1 and 2).....	111
6.4.2 Output AFB Controller for Extreme Seas (Model 4)	113
6.4.3 Output PID and AFB for Transition Regime between Moderate and Extreme Seas (Model 3)	115
6.5 Stability Analysis.....	115
6.5.1 Multi-output PID and AFB Controllers, with Position and Acceleration Measurements	115
6.5.2 Tuning for Supervisory Control	117

6.6 Numerical Simulation Results	118
6.6.1 Overview of Simulation	118
6.6.2 Results	119
6.6.3 Discussions	119
6.7 Experimental Results	120
6.7.1 Overview of Experiments.....	120
6.7.2 Results and Discussions	121
6.8 Conclusions.....	124
 Chapter 7 Conclusions and Recommendations for Further Work	140
7.1 Conclusions.....	140
7.2 Recommendations for Further Work	143
 References	145
 Appendix A Stability Analysis of Hybrid Control for DP System.....	155
A.1 Fundamental Stability Analysis	155
A.2 Stability Analysis of Observer without WF Filtering for Output PID.....	156
A.3 Stability Analysis of Observer without WF Filtering for Output AFB	158
A.4 Proof of Proposition 1	159
Part 1	160
Part 2	161
Part 3	162
 Appendix B Marine Cybernetics Laboratory.....	166
 Appendix C Cybership III	168
C.1 General Configurations of Cybership III	168

C.2 Bollard Pull Tests of Cybership III.....	170
C.2.1 Cybership III Thruster Configuration.....	170
C.2.2 Experimental Setup	171
C.2.3 Thruster Characteristics.....	172
Appendix D Marine Systems Simulator	174
D.1 Introduction.....	174
D.2 Simulation of Second-Order Wave Load for DP Vessel	174
D.2.1 Formulation	175
D.2.2 Simulation results	176
Appendix E Publications and Submitted Paper during this Period	180
E.1 Journal papers	180
E.2 Conference papers.....	180

List of Tables

Table 2.1. Notation for position and velocity (after SNAME, 1950).	33
Table 3.1. Typical Operational Profiles of a PSV, a Shuttle Tanker, an FPSO, and Drilling & well-intervention vessel.....	48
Table 3.2. Sub-Functions for Marine Operational Objectives	48
Table 4.1. Summary of Experiments: Switching from DP to SPM Mode.....	64
Table 4.2. Environmental Conditions.....	64
Table 4.3. Summary of operation modes from SPM to DP.....	64
Table 4.4. Summary of Experiments: Switching from STL to DP.....	64
Table 4.5. Summary of Operation Modes from STL to DP.....	64
Table 5.1. Performance and consumed energy indicators (standard deviation values) normalized with respect to value obtained by single output PID control.	92
Table 5.2. Experiments to investigate effects of AFB.	92
Table 5.3. Empirical performance indicators (standard deviation and RMS values) normalized with respect to values obtained by conventional PID-control.	92
Table 6.1. Definition of Sea State codes (Price and Bishop, 1974).	125
Table 6.2. Sea state definition based on PFW.	125
Table 6.3. Observers and controllers for proposed hybrid DP system using multi-PID and multi-PID + AFB.....	125
Table 6.4. Environmental conditions	125
Table 6.5. Simulation and experimental setup.....	126
Table 6.6. Performance and consumed energy indicators (standard deviation values) normalized with respect to value obtained by Case 2.	126
Table 6.7. Experiments with hybrid control for DP vessel under changes of environmental conditions from short to long waves (constant H_s).	126
Table 6.8. Experiments with hybrid control for DP vessel under changes of environmental conditions from calm to rough seas (varying H_s).....	126
Table 6.9. Performance and consumed energy indicators (standard deviation values) normalized with respect to value obtained by single output PID control (constant H_s). Experiments with varying environmental conditions from short to long waves.....	127

Table 6.10. Performance and consumed energy indicators (standard deviation values) normalized with respect to value obtained by single output PID control (varying H_s). Experiments with varying environmental conditions from calm to rough sea.	127
Table C.1. Supply vessel main particulars.....	169
Table C.2. Thruster specifications	170
Table C.3. Thrust characteristics	173
Table D.1. Simulation results of Case (a): the fixed vessel.....	177
Table D.2. Simulation results of Case (b): the DP vessel.....	177

List of Figures

Figure 2.1. Earth-fixed, reference-parallel and body-fixed frame.	34
Figure 2.2. 6-DOF mode of motion.	34
Figure 3.1. Control objectives for different marine operations.	49
Figure 3.2. Control structure (Sørensen, 2005b).....	49
Figure 3.3. Switched DP system.	49
Figure 3.4. Injected DP system in cascade with process based on Hespanha (2001)...	50
Figure 3.5. Scale-independent hysteresis switching logic, Hespanha (2001).	50
Figure 4.1. Various marine operations of a shuttle tanker.	65
Figure 4.2. Concept of hybrid controller for marine operations from transit to station keeping.	65
Figure 4.3. Weighting function α_1 and α_2 , with $q = 8$, $p = 2.5$, $r = 12$	66
Figure 4.4. The Cybership III with SPM.	66
Figure 4.5a. Test 1a: performance of switching from DP to SPM mode and vice versa of the shuttle tanker: measured position and heading (solid) and their LF estimation (grey).	67
Figure 4.5b. Test 1a: control force and moment: force and moment produced by thrusters (solid), force and moment produced by the mooring system (dash).....	67
Figure 4.6a. Test 2a: performance of switching from DP to SPM mode and vice versa of the shuttle tanker: measured position and heading (solid) and their LF estimation (grey).	68
Figure 4.6b. Test 2a: control force and moment: force and moment produced by thrusters (solid), force and moment produced by the mooring system (dash).....	68
Figure 4.7a. Test 3a: performance of switching from DP to SPM mode and vice versa of the shuttle tanker: measured position and heading (solid) and their LF estimation (grey).	69
Figure 4.7b. Test 3a: control force and moment: force and moment produced by thrusters (solid), force and moment produced by the mooring system (dash).....	69

Figure 4.8a. Test 4a: performance of switching from DP to SPM mode and vice versa of the shuttle tanker: measured position and heading (solid) and their LF estimation (grey)	70
Figure 4.8b. Test 4a: control force and moment: force and moment produced by thrusters (solid), force and moment produced by the mooring system (grey)	70
Figure 4.9a. Test 5a: performance of switching from DP to SPM mode and vice versa of the shuttle tanker: measured position and heading (solid) and their LF estimation (grey)	71
Figure 4.9b. Test 5a: control force and moment: force and moment produced by thrusters (solid), force and moment produced by the mooring system (dash).....	71
Figure 4.10a. Test 6a: performance of switching from DP to SPM mode and vice versa of the shuttle tanker: measured position and heading (solid) and their LF estimation (grey)	72
Figure 4.10b. Test 6a: control force and moment: force and moment produced by thrusters (solid), force and moment produced by the mooring system (dash).....	72
Figure 4.11. STL model: four mooring lines connected to the floating turret which can be connected and disconnected to the bow of the Cybership III. The turret can be freely rotated relatively to the mooring system.	73
Figure 4.12. Three mooring system configurations.	73
Figure 4.13a. Test 1b: performance of switching from STL to DP mode of the shuttle tanker: measured position and heading (solid) and their LF estimation (grey)	74
Figure 4.13b. Test 1b: control force and moment: force and moment produced by thrusters (solid), force and moment produced by the mooring system (dash).....	74
Figure 4.14a. Test 2b: performance of switching from STL to DP mode of the shuttle tanker: measured position and heading (solid) and their LF estimation (grey)	75
Figure 4.14b. Test 2b: control force and moment: force and moment produced by thrusters (solid), force and moment produced by the mooring system (dash).....	75
Figure 4.15a. Test 3b: performance of switching from STL to DP mode of the shuttle tanker: measured position and heading (solid) and their LF estimation (grey)	76

Figure 4.15b. Test 3b: control force and moment: force and moment produced by thrusters (solid), force and moment produced by the mooring system (dash).....	76
Figure 4.16a. Test 4b: performance of switching from STL to DP mode of the shuttle tanker: measured position and heading (solid) and their LF estimation (grey)	77
Figure 4.16b. Test 4b: control force and moment: force and moment produced by thrusters (solid), force and moment produced by the mooring system (dash).....	77
Figure 4.17a. Test 5b: performance of switching from STL to DP mode of the shuttle tanker: measured position and heading (solid) and their LF estimation (grey)	78
Figure 4.17b. Test 5b: control force and moment: force and moment produced by thrusters (solid), force and moment produced by the mooring system (dash).....	78
Figure 4.18a. Test 6b: performance of switching from STL to DP mode of the shuttle tanker: measured position and heading (solid) and their LF estimation (grey)	79
Figure 4.18b. Test 6b: control force and moment: force and moment produced by thrusters (solid), force and moment produced by the mooring system (grey)	79
Figure 5.1. Concept of adaptive observer	93
Figure 5.2. Estimated peak frequency of wave from observer with parametrically adaptive WF filtering – simulation result.....	94
Figure 5.3. Measured position and heading (grey) and corresponding LF (black) estimates from observer with parametrically adaptive WF filtering – simulation result	94
Figure 5.4. Estimated peak frequency of wave from observer with parametrically adaptive WF filtering – experimental result.....	95
Figure 5.5. Measured position and heading (grey) and corresponding LF (black) estimates from observer with parametrically adaptive WF filtering – experimental result	95
Figure 5.6. Standard deviation of (a) position; and (b) commanded control force and moment, in increasing sea states of the DP vessel using observer with WF filtering	96
Figure 5.7. Performance of DP vessel using observer with WF filtering and output PID in extreme sea (Test 1a)	96

Figure 5.8. Performance of DP vessel using observer without WF filtering and output PID in extreme sea (Test 1b).....	96
Figure 5.9. Performance of DP vessel using observer without WF filtering and output AFB in extreme sea (Test 1c).....	96
Figure 5.10. Performance of PID in moderate sea, Test 2a	97
Figure 5.11. Performance of AFB in moderate sea, Test 2a.....	97
Figure 5.12. Performance of PID in moderately rough sea, Test 2b.	98
Figure 5.13. Performance of AFB in moderately rough sea, Test 2b.	98
Figure 5.14. Performance of PID in rough sea, Test 2c.....	99
Figure 5.15. Performance of AFB in rough sea, Test 2c.	99
Figure 6.1. Concept of hybrid controller DP system using discrete switching signal.	128
Figure 6.2. Weighting function in (a) test 1b and 1c, (b) test 2b and 2c.	128
Figure 6.3. Position and heading of DP vessel in Case 1 using single output PID.....	129
Figure 6.4. Estimated PFW in Case 1.....	129
Figure 6.5. Position and heading of DP vessel in Case 2 with hybrid controller using multi-output PID.	130
Figure 6.6. Estimated PFW and switching signal, σ , in Case 2.....	130
Figure 6.7. Performance of DP vessel in Case 3 with hybrid controller using multi-output PID and AFB.....	131
Figure 6.8. Estimated PFW and switching signal, σ , in Case 3.....	131
Figure 6.9. Performance of DP vessel in Test 1a using single output PID controller from short to long waves.....	132
Figure 6.10. Estimated PFW in Test 1a	132
Figure 6.11. Performance of DP vessel in Test 1b using hybrid controller using multi-PID controller.....	133
Figure 6.12. Estimated PFW and switching signal, σ , in Test 1b.....	133
Figure 6.13. Performance of DP vessel in Test 1c using hybrid controller using multi output PID and AFB.....	134
Figure 6.14. Estimated PFW and switching signal, σ , in Test 1c.....	134
Figure 6.15. Performance of DP vessel in Test 2a using single output PID controller from calm to rough sea.....	135

Figure 6.16. Estimated PFW in Test 2a	135
Figure 6.17. Estimated WF motion in 7 sea states (Test 2a)	136
Figure 6.18. Performance of DP vessel in Test 2b using hybrid controller using multi-PID controller.....	136
Figure 6.19. Estimated PFW and switching signal, σ , in Test 2b.....	137
Figure 6.20. Estimated WF motion in 7 sea states (Test 2b)	137
Figure 6.21. Performance of DP vessel in Test 2c using hybrid controller using multi output PID and AFB.....	138
Figure 6.22. Estimated PFW and switching signal, σ , in Test 2c.....	138
Figure 6.23. Estimated WF motion in 7 sea states (Test 2c)	139
Figure B.1. The basin of the MCLab	167
Figure B.2. The single flap wave generator of the MCLab.	167
Figure B.3. Four cameras mounted on the towing carriage for capturing position of model vessel.....	167
Figure C.1. Cybership III.....	169
Figure C.2. PC in control room.....	170
Figure C.3. Thruster distance.....	170
Figure C.4. Experimental setup for test (a) Port Main thruster at 0° , (b) Starboard Main thruster at 0° , (c) Port Main thruster at 30° , (d) Starboard Main thruster at 30° , and (e) Front Azimuth thruster at 0°	171
Figure C.5. Experimental setup for test (f) Front Azimuth thruster at 90° , and (g) Tunnel thruster.....	171
Figure C.6. Thrust characteristics for (a) Port Main at thruster 0° , (b) Starboard Main thruster at 0° , (c) Port Main thruster at 30° , (d) Starboard Main thruster at 30° , (e) Front Azimuth thruster at 0° , (f) Front Azimuth thruster at 90° , and (g) Tunnel thruster.....	172
Figure D.1. An example of to simulating DP vessel using MSS.....	175
Figure D.2. Second-order wave-drift load acting on fixed vessel.	177
Figure D.3. Performance of DP vessel with mean wave-drift load simulation.	178
Figure D.4. Mean wave-drift load acting on the DP vessel.	178

Figure D.5. Performance of DP vessel with *filtered* Newman second-order wave-drift load simulation 179

Figure D.6. Filtered Newman second-order wave-drift load acting on the DP vessel.179

Chapter 1 Introduction

1.1 Background

Marine business covers three main clusters: shipping/transportation, offshore exploration and exploitation of hydrocarbons, and aquaculture/fisheries. In all three clusters, marine vessel is one major common element. Nowadays, marine vessels are required to operate in different environmental conditions and different speed regimes. Safety and cost effectiveness are primary considerations in such operations. It is important to increase the operational availability making it possible to conduct all-year marine operation, such as sub-sea installation and intervention, offloading, diving, drilling, and laying of pipes in harsh environments. In particular, when conducting marine operations in deep water, the operations are more time consuming, and hence more sensitive to changes in sea states. Therefore, marine control systems must be designed so that vessel can operate in many different operational and environmental conditions.

This motivates the design of nonlinear control since the dynamics of the process, the constraints, and the objectives of the controllers change significantly in the different operational conditions. There are two obvious solutions for this nonlinear problem: design one unique nonlinear controller or combine different controllers. The design of a unique nonlinear controller may be complicated or even impossible since the dynamics of the process changes significantly with various operational regimes. In addition, it is difficult to satisfy many control objectives within only one controller. It is therefore not surprising that few industrial applications adopt this control strategy.

The combination of many controllers, denoted as hybrid control, on the other hand, may appear to be a simpler solution. In this control strategy, the dynamics of the process is simplified in each operational regime. The design of controller corresponding to a particular operational regime is straightforward since the simplified dynamics of the process are well-formulated linear/nonlinear systems. With a multi-operational hybrid controller structure, it is easier to satisfy different control objectives. Although the drawback could be a bundle of controllers with chattering problem, this control strategy has been implemented widely in many industrial applications using ad-hoc solutions.

The state of research in hybrid control to integrate different controllers into a system will be reviewed in the following section. Conventional hybrid control using ad-hoc solutions in flight control and control of land-based vehicles will be presented. The literature review will focus on the theory of supervisory control developed systematically for hybrid control. Review on the control for station keeping and transit of the marine vessel in different environmental conditions will also be presented. Based on these reviews, the feasibilities of adopting hybrid control in marine control system will be explored.

1.2 Literature Review

1.2.1 Hybrid Control and Supervisory Control

Gain scheduling has been commonly used in the flight control due to its simplicity (McLean, D., 1990; Wang and Balakrishnan, 2002; and Oosterom and Babuška, 2005). The nonlinear dynamics of conventional aircraft is linearized for different operational conditions associated with different speed regimes. A set of linear controllers are designed corresponding to those linear systems. Although the controllers may be similar, the controller gains are different. For a vector-thrust

Vertical and/or Short Take-Off and Landing (VSTOL) aircraft, the aircraft's dynamics is simplified into three modes: Conventional Take-Off and Landing (CTOL), Vertical Take-Off and Landing (VTOL) and TRANSITION. The simplified state space equations are nonlinear with non-minimal phase. Stability in the sense of Lyapunov has been used to prove the stability of this system across switching boundary (Oishi and Tomlin, 1999 and 2000). There has been an attempt to combine human factors and other controllers since the pilot can also be considered as a controller (Oishi et al., 2002).

In land-based vehicle control, the strategy for combination of controllers, known as local network control (LNC), is similar to gain scheduling presented above. A set of empirically parametric first-order linear models, valid locally in some operational regimes, have been used to mathematically model the nonlinear dynamics of the process (Hunt et al., 1996a). It is noted that these linear models do not necessarily contain any physical equilibriums. The local controller designs are based upon those linear models and combined by weighting functions (Hunt et al., 1997). An illustration of this control strategy is the LNC designed for autonomous vehicle steering (Hunt et al., 1996b).

In marine control system, Smogeli et al. (2004) proposed the hybrid thruster controller to combine torque control for low and moderate loading conditions of thruster, and power control for high loading condition. In low loading, the control objective is to produce accurate propeller torque. In high loading, the objective is to avoid unintended oscillations and peaks in power consumption preventing blackout. By combining these two controllers, the operational regime of a thruster can be extended to provide safer high loading conditions.

The strategies presented above have been developed for specific problems. Furthermore, those strategies are applicable for a small number of candidate controllers. In some applications, the switching among the controllers may lead to instability (Liberzon and Morse, 1999). Therefore, more general approaches need to be developed to prevent instability and chattering. Extensive work has focused on systematic approach to combine a set of controllers (Hespanha, 2001; Hespanha and Morse (2002); Hespanha, et al., 2003; and the references therein). This control strategy, so-called *supervisory control*, aims to switch among the linear or nonlinear controllers according to their operational regimes through a specially designed discrete logic to guarantee the stability of the whole system. It is therefore a *switched* and *hybrid system*. Supervisory control is more advantageous than adaptive control (Åström and Wittenmark, 1995) in terms of rapid adaptation, flexibility and modularity, and decoupling between supervision and control. One of the applications of supervisory switching control was illustrated by Böling et al. (2005) on multi-model PID controller for a nonlinear pH neutralization process.

In the following subsections, an overview of station keeping and transit for marine control systems will be addressed. In addition, previous studies on station keeping in moderate and extreme seas will also be presented. These serve as background for the hybrid marine control systems developed in this thesis.

1.2.2 Station Keeping of Marine Vessels

The floating vessels are kept in position by *position mooring* without or with thruster assistance (PM) systems, or exclusively by only thrusters known as *dynamic positioning* (DP). The term *positioning control* is here used to denote either PM or DP (Sørensen, 2005b).

1.2.2.1 Dynamic positioning in moderate seas.

DP is implemented in marine vessel to maintain a fixed position and heading as well as to precisely maneuver a predetermined track exclusively by means of the vessel's propulsion system. In the 1960s, the first DP systems were introduced to control horizontal modes of motion (surge, sway and yaw). In 1980, there were about 65 DP-equipped vessels, and by 1985, this number increased to 150. In 2002 and 2003, approximately 200 vessels equipped with DP systems were built worldwide each year. Currently, there are over 1000 vessels with DP system specialized for many functions (Sørensen, 2004). Marine vessels with DP system are mostly used in oil and gas industrial activities such as coring, exploration drilling, production drilling, platform supply, shuttle tanker off-take and floating production, cable laying, pipe laying, and anchor handling vessels. DP systems are increasingly being used on other ship types than those in the offshore industry such as cruise vessels, navy ships, and fishing vessels. It is interesting to note that cruise vessels operating in Caribbean are not allowed to anchor due to possible damage to the coral reefs, thus requiring DP system in this case. Navy ships require accurate position so that military equipment can aim at the right targets. Therefore, the market of DP systems has high prospects.

The early DP systems used conventional low-pass and/or notch filters and single-input-single-output PID for controller. The drawbacks of low-pass and/or notch filter observer are the introduction of phase lag and poor wave filtering properties. In addition, non-measurable states such as velocity are not available. Also in case of loss of measurements the controller does not have any model prediction or dead reckoning possibilities. From a hydrodynamic point of view, the surge, sway and yaw motions are coupled, but the single-input-single-output PID controller considers each motion as uncoupled and hence it may deteriorate the performances of marine vessels with such

systems. More advanced techniques involving the model-based observer using Kalman filter theory to avoid the time delay in estimation and the multi-variable output feedback PID controller for better performances have been proposed by Balchen et al. (1976, 1980) and Sælid et al. (1983). The relationship between notch filter and Kalman filter observers has been shown by Grimble (1978). The Kalman filter and the multi-output PID controller led to further developments such as the extended Kalman filtering techniques and stochastic optimal control theory, described in Grimble et al. (1979, 1980a, b), Fung and Grimble (1983), Grimble and Johnson (1989) and Fossen (1994).

The Kalman filter observer state space equations are based on the linearized marine vessel's dynamics at different vessel's heading angles in terms of a rotational matrix, to approximate the actual nonlinear dynamics behaviour, similar to that in robotic applications. The linearization results in large sets of observer gain matrices for tuning and design. This has motivated the development of the nonlinear passive observer (Fossen and Strand, 1999; and Strand and Fossen, 1999). The advantage of this observer is the significant reduction of observer gain matrices since the state space equations of nonlinear observer are based on the nonlinear ship's dynamics. Fossen and Strand (1999) introduced the passive nonlinear observer with formal stability proof and proposed the design of observer gains based on the passivity. In order to have more effective filtering for the wave frequency (WF) motions, Strand and Fossen (1999) extended the earlier passive nonlinear observer with the addition of recursive adaptive wave filtering. The disadvantage of the nonlinear passive observer with recursively adaptive WF filtering (Strand and Fossen, 1999) is the difficulty in tuning.

The multi-variable output PID controller, used in the previous studies so far, consists of proportional, derivative and integral terms. While the feedback proportional

and derivative control actions are used to compensate dynamical environmental loads, the integral controller is used to counteract the mean environmental loads induced by wind, wave and current. The vessel performances depend significantly on the tuning of the PID controller gain matrices. For example, the vessel can drift away, so-called *drift-off*, if the integral controller is not properly tuned. For this reason, Sørensen et al. (1996) proposed a design for controller gain matrices based on the LQG algorithm. Strand (1999) proposed the nonlinear back-stepping controller.

In the above-mentioned studies on DP systems, the major concerns are the observer and controller. As recognized by Fossen (1994, 2002) and Sørensen et al. (1996), other aspects have also been studied such as thruster control, optimal thrust allocation and reference model. Sørensen (2005b) generalized these aspects into the structure of a general DP system at three levels: actuator control level (low level), plant control level (high level) and local optimization level. At the low level, actuators including thrusters, propellers, rudders, etc. have their own controllers to ensure the appropriate control force and moment commanded from the plant control level. At high level, the control systems focus on observer, controller (mentioned above) and optimal thrust allocation. At the local optimization level, the guidance and navigation control (GNC) system provides appropriate desired paths or set-points.

Researchers have also considered that changes in control objectives will result in changes of components at the three levels. For example, the conventional output-PID controller at plant control level has been modified to include the roll and pitch damping in the design of controller for small-waterplane-area marine vessels (Sørensen and Strand, 2000). Drilling vessels operating in deep-water are required to keep the riser angles within a limited offset. The DP vessel must then follow the optimal set-point (Sørensen et al., 2001) rather than the fixed set-point as in

conventional DP operations to ensure small riser angles. The marine vessels operating under changes of environmental directions are required to keep the heading angle such that the main environmental direction attacks through the center line of the ship to minimize resulting moment acting on the ship (Fossen and Strand, 2001).

1.2.2.2 Positioning mooring in moderate seas

The control of a PM vessel is quite similar to that of a DP vessel since the main objective of PM is to keep the vessel in a fixed position. The vessel's oscillations caused by ocean disturbances are attenuated mainly by the mooring systems. Hence, the effect of the mooring system must be taken into account. In rough weather conditions, the use of thruster is necessary in PM system in order to avoid large tension in the mooring lines; hence, the secondary objective of PM is to keep the line tension within a limited range to prevent line break. In an earlier study, Strand et al. (1998) focused on the modelling and proposed a control strategy for thruster assisted positioning mooring system to satisfy the main objective of keeping the vessel in a fixed position. Later, Aamo and Fossen (1999) worked on controlling the line tension in PM to satisfy both the main and secondary objectives.

Another type of PM vessel is the single point moored interconnected structure which is specially developed for aquaculture/fisheries industry. Berntsen et al. (2003 and 2004) studied the modelling of single point moored interconnected structures. The first vessel in the chain of interconnected structure is kept in a fixed position by the mooring system. The other vessels are connected together and to the moored vessel via rigid or flexible connectors which contribute the restoring and damping forces to the motion of the individual structure. The latter paper then proposed the control law to satisfy the three objectives: 1) to keep the line tension within an acceptable limit; 2) to keep the chain of vessels aligned transversally to the incoming current; and 3) to

ensure positive strain in the connectors between vessels. Leira et al. (2004) further specified the limit for the tension of the mooring lines which is the structural reliability of the mooring lines.

A special type of mooring configuration is the single point mooring (SPM) system which consists of a buoy and a hawser. The buoy is moored to the seafloor and the vessel is connected to the buoy by the hawser. At the loading site, the SPM system is used for station keeping to offload the oil from the field to the vessel. In this mooring configuration, the oscillation of vessel may produce large mooring line forces and therefore break the mooring line. Sørheim (1981) developed the control strategy for the dynamic positioning of the vessel to reduce the tension in the SPM system. The study showed that the slowly-varying motion of the vessel and the hawser tension were effectively minimized by using the proposed solution. However, the approaching and connecting, staying in moor, and disconnecting operations of the vessel to the SPM system become significantly difficult when the sea state increases and therefore still remain for further studies.

1.2.2.3 Station keeping of marine vessels in harsh seas

The studies mentioned in 1.2.2.1 and 1.2.2.2 have been developed for the station keeping of marine vessels up to certain weather condition. Recently, some work to improve the performance of the DP vessels under harsh environments has been attempted.

Under normal conditions, the DP system counteracts the low frequency (LF) motions caused by wind, current and slowly-varying drift wave loads rather than counteracting the wave frequency (WF) motions commonly caused by first-order wave loads. The conventional observers with wave filtering are able to estimate the WF motions, and hence isolate the LF motions from the total motions for feedback control.

In moderate sea states, this philosophy works well. However, in extreme sea states when the WF motions are of low frequency and within the LF domain, separating WF and LF motions becomes ambiguous. The swell waves, often large with long periods, may be present in addition to wind-generated waves (Torsethaugen, 1996); hence both WF and LF motions must be compensated by the DP control system. Addressing this problem, Sørensen et al. (2002) proposed an observer without WF filtering for the output PID controller. The estimated states are the total motions rather than only LF motions as in normal environmental conditions.

Due to the accuracy and availability of inertia measurement units (IMU), Lindegaard (2003) proposed using acceleration feedback (AFB) to increase the performance of DP systems. AFB will provide a virtual mass in addition to the physical mass of the vessel. Therefore, the vessel becomes less sensitive to environmental excitations. It is noted that the AFB denoted here is the extension of the output-PID controller to include an output acceleration feedback.

While the work of Sørensen et al. (2002) and Lindegaard (2003) focused on the observer design and the controller design at plant control level, the thruster control (low level) for extreme seas has been developed by Smogeli et al. (2005). The latter study showed the losses of torque and shaft speed when the thruster is not fully submerged which causes a sharp thrust reduction at high shaft speed. Consequently, a thruster control scheme was proposed in the sense that the normal thruster control is automatically switched to anti-spin thruster control in which the shaft speed is forced to reduce if high thrust losses are detected. The anti-spin thruster control reduces transients in the power system, optimizes the thrust production and hence efficiency in transient operation regimes, and reduces the wear and tear of the propulsion unit.

As shown above, station keeping of floating structures under moderate sea conditions has been well studied. However, the solutions are not adequate for extreme sea conditions. The observer without WF filtering was theoretically developed, but still not verified experimentally. AFB was shown to have better performances but the effects of AFB in harsh environmental have not been carefully studied.

In addition, there has been no published research on station keeping for marine vessels operating under changes from calm to extreme seas.

1.2.3 Low Speed Maneuvering and Transit

In low speed maneuvering control, the marine vessel is forced to follow a path and keep its speed assignment along that path. In conventional low speed maneuvering, those two objectives have been usually solved separately (Pettersen, 2001). The control system automatically cruise the ship along the predetermined path while the speed assignment is done by the operator. Skjetne et al. (2005) and Skjetne (2005) proposed the adaptive maneuvering control which merges the two control objectives into one single task. This work was the extension of the robust output maneuvering for the class of nonlinear systems proposed by Skjetne et al. (2004).

The autopilot system forces the ship to transit in a fixed heading or changed heading. Nomoto (1957) proposed the model for the vessel's heading angle and the PID controller for the heading. Norrin (1970) added the nonlinear damping into the control plant model. Fossen (2005) developed the nonlinear state space equation for low speed maneuvering and station keeping. This work was motivated by Bailey et al. (1998) who proposed a unified mathematical model describing the maneuvering of a ship travelling in a seaway.

From the literature review, we can see marine control system must nowadays satisfy different objectives in different operations and environmental conditions.

However, there has not been any systematic attempt to integrate the different controllers into one control system.

1.3 Objectives and Scopes

The objectives of this thesis are to

- (1) present an *integrated system* (a so-called “*super system*”) as a novel concept for marine control system integrating DP, maneuvering and transit operations subjected to changes in the environmental conditions;
- (2) develop a hybrid marine control system integrating station keeping and transit in normal environmental conditions;
- (3) present a nonlinear observer with parametric adaptive WF filtering as an alternative for the nonlinear observer with recursively adaptive WF filtering;
- (4) develop a control strategy using the observer without WF filtering and acceleration feedback for DP vessel operating in extreme environmental conditions; and
- (5) develop a hybrid DP system for marine vessels operating under changing environmental conditions from calm to extreme seas by adopting the supervisory control theory and combining the four controllers for calm, moderate, high and extreme seas.

The scopes of this thesis are as follows:

- (1) The integrated system is conceptually introduced by showing the possibilities of combining different controllers into a hybrid marine control system. The conceptual hybrid control system combines different controllers for marine vessels operating in different speed regimes, environmental conditions, operation functions and fault tolerance with different control objectives, vessel’s dynamics and characteristics of environmental loads at various

control levels, i.e. local optimization for optimal set-point chasing or for guidance and navigation, plant control level, and actuator control level (Sørensen, 2005b).

(2) In the hybrid marine control system integrating station keeping control and transit, the controllers considered here are

- autopilot control for transit mode;
- DP for station keeping; and
- PM for station keeping.

The switching from DP to PM mode (Single Point mooring – SPM and Submerged Turret Loading – SLT) and vice versa was experimentally examined by the model vessel (Cybership III). Experiments were carried out in the Marine Cybernetic Laboratory (MCLab) at the Norwegian University of Technology and Science (NTNU). Due to the limitation of the tower tank at the MCLab, the experiment for switching from/to autopilot to/from DP is not done.

(3) The environmental excitations are wind, wave and current. While some areas such as Gulf of Mexico, Northern England, Southern Norway, and South Africa experience extreme conditions in terms of currents, in the North seas, extreme conditions usually refer to the very long and high waves. The observer without WF filtering is developed here for DP system in extreme conditions only in terms of the wave effects. The WF motions need to be controlled by the DP system; thus, the estimation is done by observer without WF filtering for extreme seas rather than by observer with WF filtering for moderate seas. Experiments with DP Cybership III using observer without

WF filtering were carried out in the MCLab to verify the ship's stability and the improved performances in very long waves.

- (4) The acceleration feedback adopted here is applicable for extreme environmental conditions in terms of wave, wind and current effects. The effect of acceleration feedback is to “add” more mass to the vessel; thus the vessel is less influenced by any external loads. However, the external excitation load in the experiments with Cybership III to verify the validity of acceleration feedback is only the wave load. The experiments were carried out in different sea conditions from moderate to harsh seas to see the effectiveness of acceleration feedback under different wave height conditions. The acceleration feedback in extreme sea was not done due to the limitation of the wave generator in the MCLab.
- (5) In the supervisory control for hybrid DP vessels subjected to change of environmental conditions from calm to extreme seas, the controllers considered here are
- observer with adaptive WF filtering and output PID controller for calm sea;
 - observer with adaptive WF filtering and output PID controller for moderate sea;
 - observer without WF filtering and output PID (or AFB) controller for extreme sea; and
 - smooth transformation of observers and controllers from moderate to extreme seas.

This hybrid control was examined by the experiments with Cybership III in the MCLab from calm to high seas considering only the wave effects.

The concept of hybrid marine control system is broad and novel. It should provide a framework to combine different controllers in marine control system. Some examples of combining different controllers that can be built using the conceptual hybrid marine control are

- 1) At actuator level (low level): hybrid control for changes of environmental from calm to extreme seas,
- 2) At plant control level (high level): hybrid control for changes of environmental conditions, for changes of operational functions, as well as for changes of vessel's speed,
- 3) At local optimization level: hybrid control for changes of environmental conditions, for changes of set-point chasing in station keeping mode, for changes of trajectory path in low pass maneuvering, or for route planning in transit operation mode.

The experimental results of acceleration feedback in different sea conditions may provide useful information on the effectiveness of acceleration feedback to improve the vessel's performance under harsh environments. The proposed observer with parametric adaptive WF filtering should provide an alternative to observer with recursive adaptive WF filtering for DP system in calm and moderate sea conditions. The observer with parametric adaptive WF filtering is much simpler than the observer with recursively adaptive WF filtering in terms of observer gain tuning; hence it is easier to implement in industrial applications. Implementing the hybrid DP system for marine vessels operating from calm to extreme seas should increase the operational availability (expand the operational weather window) making it possible to conduct all-year marine operation, e.g. sub-sea installation and intervention, drilling, pipe laying, etc., in harsh environments.

1.4 Organization of Thesis

The thesis is organized into seven chapters.

In Chapter 2, the mathematical model of marine vessel is presented. The marine vessel is modelled as a rigid body with six degrees of freedom under the excitations of wind, wave and current. For moored vessel, there is an additional load from the mooring system. Modelling is essential since most of the control strategies and controller design for marine vessel are based on the model of the vessel, and often known as model-based control.

Chapter 3 presents the concept for hybrid marine control system. By reviewing the different control objectives, the changing dynamics, as well as the different mode of control of marine vessel under various environmental conditions, the motivation for the development of hybrid control for marine control system will be addressed. General concept of hybrid control and supervisory control is discussed. The structure of marine control system is presented to show the feasibilities of hybrid control at different levels.

In Chapter 4, an example of hybrid control for marine vessels operating from transit to station keeping will be developed. Experiments will be presented to validate this hybrid control strategy.

Chapter 5 studies the acceleration feedback controller and observer without wave filtering for dynamic positioning in extreme seas. The nonlinear passive observer without wave filtering will be theoretically and experimentally studied. Experiments with a model vessel under different sea states will be carried out to evaluate the effectiveness of acceleration feedback to improve performance of dynamic positioning. In addition, the performance of the observer with parametrically adaptive wave filtering will be verified by numerical simulations and experiments. The observer

without wave filtering and acceleration feedback will be used as the input for the hybrid control for dynamic positioning from calm to extreme seas.

Chapter 6 focuses on the development of the hybrid control for DP vessels operating in environmental conditions changing from calm to extreme seas. The hybrid control using multi-PID and multi-PID+AFB will be developed. Stability analysis, numerical simulation and experiments will be provided to verify and validate the proposed hybrid control systems.

Chapter 7 summarizes the key research findings and recommends possible future work.

Chapter 2 Modelling of Marine Vessels

2.1 Introduction

From previous studies, it has been found that model-based control is preferable for marine control system where the dynamics of floaters are basically described by the state space equations. For example, a model-based PID controller has been used for positioning of floating structures since 1960s. Subsequently, conventional optimal control and Kalman filter theory proposed by Balchen et al. (1976 and 1980) have been employed using the equations of motion of marine vessel. Since then, this model has been used and improved by researchers such as Fossen (1994), Sørensen et al. (1996), Strand (1999), Fossen (2002) and Lindegaard (2003) for other positioning control problems.

The modelling for a general control problem may be formulated at two complexity levels (Sørensen, 2005a and b), namely a process plant model and a control plant model. The *process plant model*, which simulates as close as possible the real physics of vessel's dynamics including process disturbance, sensor outputs and control inputs, is for numerical analysis of the stability and performance of the closed-loop system. The *control plant model*, which is simplified from the process plant model, is used for controller design and analytical study of stability (such as in the sense of Lyapunov). Different control plant models for different control objectives and operational regimes of the vessel will be presented in Chapters 4, 5, and 6.

In this chapter, the process plant model including the kinematics and dynamics will be discussed. The reference frame and notation will be presented in Section 2.2, where the geometrical aspects are treated in the kinematics part. In Section 2.3, the

dynamics of the floating structure will be analyzed in both the wave frequency (WF) and low frequency (LF) regime.

2.2 Notation and Kinematics

Dynamic motions have to be described with respect to some reference point or coordinate system. Three reference frames in which the state variables of the control system are defined will be presented and the transformation between different frames will be obtained based on kinematics.

2.2.1 Reference Frames and Notations

According to Sørensen (2005a), the definitions of common frames for station keeping and transit of floating structures are shown in Figure 2.1 and summarized as follows.

Definition 2.1 (Earth-fixed reference frame) *The Earth-fixed reference frame is denoted as the $X_EY_EZ_E$ -frame, in which the vessel's position and orientation coordinates are measured relative to a defined origin (centre of the Earth). Each position reference system (such as GPS and hydro-acoustics) has its own local coordinate system, which has to be transformed into the common Earth-fixed reference frame.*

Definition 2.2 (Body frame) *The body frame XYZ is fixed to the vessel and thus moving along with it. For convenience, the body frame is often positioned at the vessel's center of gravity.*

For modelling purpose, the hydrodynamics coefficients of the vessels, such as added mass, damping and restoring forces (Faltinsen, 1990) are described in the so-called hydrodynamics frame which is defined below.

Definition 2.3 (Hydrodynamic frame) *The $X_hY_hZ_h$ -frame is generally moving along the path of the vessel with the x -axis being positive in the forward direction, y -axis*

positive to the starboard, and z -axis positive downward. The X_hY_h -plane is assumed fixed at and parallel to the mean water surface. The vessel is assumed to oscillate with small amplitudes about this frame such that linear theory may apply when modeling the perturbations. In forward speed sea keeping analysis, the hydrodynamic frame is moving forward with constant vessel speed U . In station keeping operations about the desired position x_d , y_d , and heading angle ψ_d , the hydrodynamic frame is Earth-fixed and denoted as the reference-parallel frame $X_RY_RZ_R$. It is rotated to the desired heading angle ψ_d and the origin is translated to the desired x_d and y_d position coordinates for the particular station keeping operation studied. As such, a frame for this reference position and orientation is defined as reference-parallel frame.

Earth-fixed, reference-parallel and body-fixed frames are shown in Figure 2.1.

For a 6-DOF model of a vessel shown in Figure 2.2, the notation of the general motion of the marine vessel is described by the Society of Naval Architects & Marine Engineers (SNAME, 1950) as in Table 2.1. To characterize the operation of a vessel in a local area, the position and orientation of the vessel are described relative to the inertial frame which is approximated by the $X_EY_EZ_E$ -frame whereas the linear and angular velocities of the vessel are expressed in the XYZ -frame (body).

2.2.2 Kinematics

The Euler angle transformation matrix, $\mathbf{J}_1(\boldsymbol{\eta}_2) \in \mathbf{SO}(3)$, is employed to transform linear velocity in the body-fixed frame, $\mathbf{v}_1 \in \mathbb{R}^3$, to the Earth-fixed frame, $\dot{\mathbf{q}}_1 \in \mathbb{R}^3$, (Fossen, 2002), according to

$$\dot{\mathbf{q}}_1 = \mathbf{J}_1(\boldsymbol{\eta}_2) \mathbf{v}_1, \quad (2.1)$$

$$\text{where } \mathbf{J}_1(\boldsymbol{\eta}_2) = \begin{bmatrix} c\psi c\theta & -s\psi c\theta + c\psi s\theta s\phi & s\psi s\phi + c\psi c\phi s\theta \\ s\psi c\theta & c\psi c\phi + s\phi s\theta s\psi & -c\psi s\phi + s\theta s\psi c\phi \\ -s\theta & c\theta s\phi & c\theta c\phi \end{bmatrix}. \quad (2.2)$$

and $\mathbf{SO}(3)$ denotes special orthogonal group of order 3.

The angular velocity vector, $\mathbf{v}_2 \in \mathbb{R}^3$, and the Euler rate vector, $\dot{\mathbf{n}}_2 \in \mathbb{R}^3$, are related through a transformation matrix $\mathbf{J}_2(\mathbf{n}_2) \in \mathbb{R}^{3 \times 3}$ according to:

$$\mathbf{v}_2 = \mathbf{J}_2(\mathbf{n}_2) \dot{\mathbf{n}}_2, \quad (2.3)$$

$$\text{where } \mathbf{J}_2(\mathbf{n}_2) = \begin{bmatrix} 1 & s\phi t\theta & c\phi t\theta \\ 0 & c\phi & -s\theta \\ 0 & s\phi/c\theta & c\phi/c\theta \end{bmatrix}, \quad c\theta \neq 0. \quad (2.4)$$

The relationship between the Earth-fixed position and orientation and body-fixed velocity is then given as

$$\dot{\mathbf{n}} = \begin{bmatrix} \mathbf{J}_1(\mathbf{n}_2) & \mathbf{0}_{3 \times 3} \\ \mathbf{0}_{3 \times 3} & \mathbf{J}_2(\mathbf{n}_2) \end{bmatrix} \mathbf{v}. \quad (2.5)$$

The rotation matrices $\mathbf{J}_1(\mathbf{n}_2) \in \mathbf{SO}(3)$ and $\mathbf{J}_2(\mathbf{n}_2) \in \mathbb{R}^{3 \times 3}$ are defined in (2.2) and (2.4). If only surge, sway and yaw (3-DOF) are considered, the transformation (2.5) is simplified as follows:

$$\dot{\mathbf{n}} = \mathbf{R}(\psi) \mathbf{v}, \quad (2.6)$$

$$\text{or } \begin{bmatrix} \dot{x} \\ \dot{y} \\ \dot{\psi} \end{bmatrix} = \begin{bmatrix} c\psi & -s\psi & 0 \\ s\psi & c\psi & 0 \\ 0 & 0 & 1 \end{bmatrix} \begin{bmatrix} u \\ v \\ r \end{bmatrix}, \quad (2.7)$$

where $c(\cdot) = \cos(\cdot)$, $s(\cdot) = \sin(\cdot)$, and $t(\cdot) = \tan(\cdot)$.

2.3 Floater Dynamics

In modelling the dynamics of floating structure, a simplification can be made by considering two possible models (Balchen et al., 1980; Fossen, 1994 and 2002; and Sørensen, 2005a), namely, low frequency (LF) model and wave frequency (WF) model. WF model is primarily for motions due to first-order wave loads whereas LF

model accounts predominantly for motions due to second-order mean and slowly varying wave loads, currents and wind loads.

It is noticed that Bailey et al. (1989) described the maneuvering of a ship through a unified mathematical model where both WF and LF motion can be modelled in one equation using a frequency-dependent vessel model. The drawback is the appearance of both the frequency and the time in this equation. However, the frequency-dependent coefficients can be transformed to equivalent time-domain representation using Cummins' equation (Cummins, 1962).

In this thesis, the WF and LF motions of marine vessel are modelled by two separate equations as follows.

2.3.1 Low Frequency Model

This 6-DOF LF model formulation is based on Fossen (2002) and Sørensen (2005a). The equations of motion for nonlinear low-frequency model of a floating vessel is given by

$$\mathbf{M}\ddot{\mathbf{v}} + \mathbf{C}_{RB}(\mathbf{v})\mathbf{v} + \mathbf{C}_A(\mathbf{v}_r)\mathbf{v}_r + \mathbf{D}(\mathbf{v}_r) + \mathbf{G}(\boldsymbol{\eta}) = \boldsymbol{\tau}_{env2} + \boldsymbol{\tau}_{moor} + \boldsymbol{\tau}_{thr}. \quad (2.8)$$

The various terms are described below.

a) Generalized inertia forces, $\mathbf{M}\ddot{\mathbf{v}}$:

The system inertia matrix $\mathbf{M} \in \mathbb{R}^{6 \times 6}$ including the added mass is defined as

$$\mathbf{M} = \begin{bmatrix} m - X_{\dot{u}} & 0 & -X_{\dot{w}} & 0 & mz_G - X_{\dot{q}} & 0 \\ 0 & m - Y_{\dot{v}} & 0 & -mz_G - Y_{\dot{p}} & 0 & mx_G - Y_{\dot{r}} \\ -Z_{\dot{u}} & 0 & m - Z_{\dot{w}} & 0 & -mx_G - Z_{\dot{q}} & 0 \\ 0 & -mz_G - K_v & 0 & I_x - K_{\dot{p}} & 0 & -I_{xz} - K_{\dot{r}} \\ mz_G - M_{\dot{u}} & 0 & -mx_G - M_{\dot{w}} & 0 & I_y - M_{\dot{q}} & 0 \\ 0 & mx_G - N_{\dot{v}} & 0 & -I_{zx} - N_{\dot{p}} & 0 & I_z - N_{\dot{r}} \end{bmatrix} \quad (2.9)$$

where m is the vessel mass, I_x , I_y and I_z are the moments of inertial about the x -, y - and z -axes and $I_{xz} = I_{zx}$ are the products of inertia. The zero-frequency added mass

coefficients $X_{\dot{u}}$, $X_{\dot{w}}$, $X_{\dot{q}}$, $Y_{\dot{v}}$, $Y_{\dot{p}}$, $Y_{\dot{r}}$, $Z_{\dot{u}}$, $Z_{\dot{w}}$, $Z_{\dot{q}}$, $K_{\dot{v}}$, $K_{\dot{p}}$, $K_{\dot{r}}$, $M_{\dot{u}}$, $M_{\dot{w}}$, $M_{\dot{q}}$, $N_{\dot{v}}$, $N_{\dot{p}}$, and $N_{\dot{r}}$ at low speed in surge, sway, heave, roll, pitch and yaw due to accelerations along the corresponding and the coupled axes are defined as in Faltinsen (1990). Hence, it can be shown that the system inertia matrix is symmetrical and positive definite, i.e. $\mathbf{M}=\mathbf{M}^T > 0$. In addition, $\dot{\mathbf{M}}=0$.

b) Generalized Coriolis and centripetal forces, $\mathbf{C}_{RB}(\mathbf{v})\mathbf{v} + \mathbf{C}_A(\mathbf{v}_r)\mathbf{v}_r$:

The matrix $\mathbf{C}_{RB}(\mathbf{v}) \in \mathbb{R}^{6 \times 6}$ is the skew-symmetric Coriolis and centripetal matrix, written as (Fossen, 1994)

$$\mathbf{C}_{RB}(\mathbf{v}) = \begin{bmatrix} 0 & 0 & 0 & c_{41} & -c_{51} & -c_{61} \\ 0 & 0 & 0 & -c_{42} & -c_{52} & -c_{62} \\ 0 & 0 & 0 & -c_{43} & -c_{53} & -c_{63} \\ -c_{41} & c_{42} & c_{43} & 0 & -c_{54} & -c_{64} \\ c_{51} & -c_{52} & c_{53} & c_{54} & 0 & -c_{65} \\ c_{61} & c_{62} & -c_{63} & c_{64} & c_{65} & 0 \end{bmatrix}, \quad (2.10)$$

where

$$\begin{aligned} c_{41} &= mz_G r & c_{42} &= mw & c_{43} &= m(z_G p - v) \\ c_{51} &= m(x_G q - w) & c_{52} &= m(z_G r + x_G p) & c_{53} &= m(z_G q + u) & c_{54} &= I_{xz} p - I_z r \\ c_{61} &= m(v + x_G r) & c_{62} &= -mu & c_{63} &= mx_G p & c_{64} &= I_y q \\ c_{65} &= I_x p + I_{xz} r \end{aligned} \quad (2.11)$$

The effect of current is divided into 2 parts: potential and viscous parts. The potential part of current includes the so called Munk moment and is formulated according to Sørensen et al. (1996) as

$$\mathbf{C}_A(\mathbf{v}_r) = \begin{bmatrix} 0 & 0 & 0 & 0 & -c_{a51} & -c_{a61} \\ 0 & 0 & 0 & -c_{a42} & 0 & -c_{a62} \\ 0 & 0 & 0 & -c_{a43} & -c_{a53} & 0 \\ 0 & c_{a42} & c_{a43} & 0 & -c_{a54} & -c_{a64} \\ c_{a51} & 0 & c_{a53} & c_{a54} & 0 & -c_{a65} \\ c_{a61} & c_{a62} & 0 & c_{a64} & c_{a65} & 0 \end{bmatrix}, \quad (2.12)$$

where

$$\begin{aligned} c_{a42} &= -Z_{\dot{w}}w - Z_{\dot{w}}u_r - Z_{\dot{q}}q & c_{a43} &= Y_{\dot{p}}p + Y_{\dot{v}}v_r + Y_{\dot{r}}r \\ c_{a51} &= Z_{\dot{q}}q + Z_{\dot{w}}w + X_{\dot{w}}u_r & c_{a53} &= -X_{\dot{q}}q - X_{\dot{u}}u_r - X_{\dot{w}}w & c_{a54} &= Y_{\dot{r}}v_r + K_{\dot{r}}p + N_{\dot{r}}r \\ c_{a61} &= -Y_{\dot{v}}v_r - Y_{\dot{p}}p - Y_{\dot{r}}r & c_{a62} &= X_{\dot{u}}u_r + X_{\dot{w}}w + X_{\dot{q}}q & c_{a64} &= X_{\dot{q}}u_r + Z_{\dot{q}}w + M_{\dot{q}}q \\ c_{a65} &= Y_{\dot{v}}v_r + K_{\dot{v}}p + K_{\dot{r}}r \end{aligned} \quad (2.13)$$

$\mathbf{v}_r \in \mathbb{R}^6$ is the relative velocity between the vessel and current according to

$$\mathbf{v}_r = [u - u_c \quad v - v_c \quad w \quad p \quad q \quad r]^T. \quad (2.14)$$

The horizontal current components in surge and sway are defined as:

$$u_c = V_c \cos(\beta_c - \psi), \quad v_c = V_c \sin(\beta_c - \psi), \quad (2.15)$$

where V_c and β_c are the current velocity and direction respectively, represented in Figure 2.1. The total relative current vector is then defined as

$$U_{cr} = \sqrt{u_r^2 + v_r^2}, \quad (2.16)$$

where $u_r = u - u_c$, and $v_r = v - v_c$.

The relative drag angle is found from the following relation:

$$\gamma_r = \text{atan} 2(-v_r, u_r), \quad (2.17)$$

where atan2 is the four quadrant arctangent function of the real parts of the elements of X and Y, such that $-\pi \leq \text{atan} 2(Y, X) \leq \pi$. The nonlinear damping is assumed to be caused by turbulent skin friction and viscous eddy-making, also described as vortex shedding, Faltinsen (1990).

c) Generalized damping and current forces, $\mathbf{D}(\mathbf{v}_r)$:

The damping vector may be divided into a nonlinear and a linear component

$$\mathbf{D}(\mathbf{v}_r) = \mathbf{D}_L \mathbf{v} + \mathbf{d}_{NL}(\mathbf{v}_r, \gamma_r). \quad (2.18)$$

Furthermore, the effect of current normally included in the nonlinear damping term as a function of the relative velocity vector $\mathbf{v}_r \in \mathbb{R}^6$ in (2.14).

Nonlinear damping and current forces: Assuming small vertical motion, the 6-dimensional nonlinear damping vector is often formulated as:

$$\mathbf{d}_{NL} = 0.5 \rho_w L_{pp} \begin{bmatrix} DC_{cx}(\gamma_r) |U_{cr}| U_{cr} \\ DC_{cy}(\gamma_r) |U_{cr}| U_{cr} \\ BC_{cz}(\gamma_r) |w| w \\ B^2 C_{c\phi}(\gamma_r) |p| p + z_{py} DC_{cy}(\gamma_r) |U_{cr}| U_{cr} \\ L_{pp} BC_{c\theta}(\gamma_r) |q| q + z_{px} DC_{cx}(\gamma_r) |U_{cr}| U_{cr} \\ L_{pp} DC_{cy}(\gamma_r) |U_{cr}| U_{cr} \end{bmatrix}, \quad (2.19)$$

where $C_{cx}(\gamma_r)$, $C_{cy}(\gamma_r)$, $C_{cz}(\gamma_r)$, $C_{c\phi}(\gamma_r)$, $C_{c\theta}(\gamma_r)$ and $C_{cy}(\gamma_r)$ are the non-dimensional drag coefficients estimated from model tests for the specific vessel under consideration (defined at specified location of the origin); and B is the breadth. The second contributions to roll and pitch are the moments caused by the nonlinear damping and current forces in surge and sway, respectively, attacking in the corresponding centers of pressure located at z_{py} and z_{px} .

Linear damping: It is important to notice that for velocities of vessel close to zero, linear damping becomes more significant than nonlinear damping. The strictly positive linear damping matrix \mathbf{D}_L caused by linear wave drift damping and the laminar skin friction is written as

$$\mathbf{D}_L = - \begin{bmatrix} X_u & 0 & X_w & 0 & X_q & 0 \\ 0 & Y_v & 0 & Y_p & 0 & Y_r \\ Z_u & 0 & Z_w & 0 & Z_q & 0 \\ 0 & K_v & 0 & K_p & 0 & K_r \\ M_u & 0 & M_w & 0 & M_q & 0 \\ 0 & N_v & 0 & N_p & 0 & N_r \end{bmatrix}. \quad (2.20)$$

The coefficients can be calculated by special software or found by model tests.

d) Generalized restoring forces, $\mathbf{G}(\eta)$:

Here it is assumed the roll and pitch angles are small, such that the restoring vector can be linearized to $\mathbf{G}\eta$, where $\mathbf{G} \in \mathbb{R}^{6 \times 6}$ is a matrix of linear generalized

gravitation and buoyancy force coefficients and is for xz -plane symmetry (Figure 2.2) written as

$$\mathbf{G} = - \begin{bmatrix} 0 & 0 & 0 & 0 & 0 & 0 \\ 0 & 0 & 0 & 0 & 0 & 0 \\ 0 & 0 & Z_z & 0 & Z_\theta & 0 \\ 0 & 0 & 0 & K_\phi & 0 & 0 \\ 0 & 0 & M_z & 0 & M_\theta & 0 \\ 0 & 0 & 0 & 0 & 0 & 0 \end{bmatrix}, \quad (2.21)$$

where the coefficients are defined as

$$Z_z \triangleq -\rho_w g A_{WP}, \quad (2.22)$$

$$Z_\theta = M_z \triangleq \rho_w g \iint_{A_{WP}} x dA, \quad (2.23)$$

$$K_\phi \triangleq -\rho_w g \nabla(z_G - z_B) - \rho_w g \iint_{A_{WP}} y^2 dA = -\rho_w g V \overline{GM}_T, \quad (2.24)$$

$$M_\theta \triangleq -\rho_w g \nabla(z_G - z_B) - \rho_w g \iint_{A_{WP}} x^2 dA = -\rho_w g V \overline{GM}_L. \quad (2.25)$$

Here, ρ_w is the density of water, g is the acceleration due to gravity, A_{WP} is the waterplane area, $dA = dx dy$, ∇ is the displaced volume of water, and \overline{GM}_T and \overline{GM}_L are the transverse and longitudinal meta-centric heights, respectively.

The right-hand side of (2.8) represents the generalized external forces acting on the vessel. These comprise the environmental loads and mooring loads to be presented in the following Sections.

2.3.2 Environmental Loads

In the LF model, the slowly-varying environmental loads, $\boldsymbol{\tau}_{env2}$, consists of wind load and wave load, given by Fossen (1994),

$$\boldsymbol{\tau}_{env2} = \boldsymbol{\tau}_{wind} + \boldsymbol{\tau}_{wave2}. \quad (2.26)$$

The current load is already included in the damping term (2.18).

a) Wind load model:

The effects of wind may be divided into mean, slowly-varying and rapidly-varying wind loads. If the relative wind velocity is defined as

$$\mathbf{v}_{rw} = [u - u_w, v - v_w, w, p, q, r]^T, \quad (2.27)$$

where u_w and v_w are components of wind velocities, defined as

$$u_w = V_w \cos(\beta_w - \psi), \quad v_w = V_w \sin(\beta_w - \psi), \quad (2.28)$$

where V_w is the wind velocity and β_w is the wind direction (Figure 2.1), then the total relative wind velocity is then given according to

$$U_{wr} = \sqrt{u_{rw}^2 + v_{rw}^2}. \quad (2.29)$$

The wind load is given by (Fossen, 1994),

$$\boldsymbol{\tau}_{wind} = 0.5 \rho_a \begin{bmatrix} A_x C_{wx}(\gamma_w) | U_{rw} | U_{rw} \\ A_y C_{wy}(\gamma_w) | U_{rw} | U_{rw} \\ 0 \\ A_y L_{yz} C_{wx}(\gamma_w) | U_{rw} | U_{rw} \\ -A_x L_{xz} C_{wx}(\gamma_w) | U_{rw} | U_{rw} \\ A_y L_{oa} C_{wy}(\gamma_w) | U_{rw} | U_{rw} \end{bmatrix}, \quad (2.30)$$

where ρ_a is the density of air; L_{oa} is the overall length of vessel; L_{xz} and L_{yz} are the vertical distances between transverse and longitudinal origin and the wind load point of attack; A_x and A_y are the lateral and longitudinal areas of the non-submerged part of the ship projected on the xz -plane and yz -plane; $\gamma_w = \beta_w - \psi$ is the relative wind angle; and $C_{wx}(\gamma_w)$, $C_{wy}(\gamma_w)$, and $C_{wy}(\gamma_w)$ are the non-dimensional wind coefficients in surge, sway and yaw respectively. These coefficients are often found by model testing or by semi-empirical formulas as presented in Isherwood (1972).

b) Wave load model:

The linear wave forces are purely oscillatory loads which oscillate at the wave frequency, while higher order wave forces have magnitudes which are proportional to

the square (or higher order) of the wave amplitudes. The second-order wave effects include mean loads, slowly-varying loads due to frequency difference and rapidly-varying wave loads due to frequency summation. The effects of rapidly-varying wave loads can be neglected for dynamic positioning control application.

According to Faltinsen (1979), the second-order wave force τ_{wave2} can be approximated as a summation of second-order ‘transfer’ functions of difference frequency wave components as:

$$\tau_{wave2}^i = \sum_{j=1}^N \sum_{i=1}^N A_j A_k [T_{jk}^{ic} \cos((\omega_k - \omega_j)t + (\varepsilon_k - \varepsilon_j)) + T_{jk}^{is} \sin((\omega_k - \omega_j)t + (\varepsilon_k - \varepsilon_j))], \quad (2.31)$$

where ω_i = wave frequencies; ε_i = random phase angles; N = number of wave components considered; $A_i = \sqrt{2S(\omega_i)\Delta\omega}$ = wave amplitudes determined from the wave spectrum $S(\omega)$; $\Delta\omega = (\omega_{\max} - \omega_{\min})/N$; and T_{jk}^{ic} and T_{jk}^{is} can be interpreted as second-order transfer functions for the difference frequency loads (Faltinsen, 1990). To avoid slow-drift wave force repetition after $2\pi N / (\omega_{\max} - \omega_{\min})$, ω_i were chosen to be random in the interval $[\omega_i - \Delta\omega/2, \omega_i + \Delta\omega/2]$. Simulation of the second-order wave loads in Marine System Simulator (MSS) is presented in Appendix D.2.

2.3.3 Mooring Loads

The mooring system contains a number of mooring lines connected to the vessel directly or through the turret. The dynamics of the mooring lines need to be coupled to the dynamics of the vessel for accurate simulation. First, the elastic catenary equations are presented to study the statics of a mooring line. Solving these equations provide the geometric profile of the mooring line in still water. This profile can then be used as the initial state input for simulating the dynamics.

a) The elastic catenary equations:

The elastic catenary equations of a single mooring line in still water are given by Triantafyllou (1990) as

$$x = \frac{H}{w_0} \left(\sinh^{-1} \left[\frac{V - w_0(L-s)}{H} \right] - \sinh^{-1} \left[\frac{V - w_0L}{H} \right] \right) + \frac{Hs}{EA_0}, \quad (2.32)$$

$$\begin{aligned} z = & \frac{H}{w_0} \left(\sqrt{1 + \left(\frac{V - w_0(L-s)}{H} \right)^2} - \sqrt{1 + \left(\frac{V - w_0L}{H} \right)^2} \right) \\ & + \frac{1}{EA_0} \left(Vs + \frac{w_0}{2} [(L-s)^2 - L^2] \right), \end{aligned} \quad (2.33)$$

$$\tan \varphi = \frac{V}{H} - \frac{\omega_0}{H}(L-s), \quad (2.34)$$

$$V_1 = V - \omega_0 L, \quad (2.35)$$

where L is unstretched mooring line length; s is a parameter running along the cable from 0 to L ; $x(s)$ and $z(s)$ are spatial x - and z -coordinate of points along the cable, respectively; H and V are the horizontal and vertical tension at the upper end; w_0 is the weight of mooring line in water per unit length; E is the Young's modulus of elasticity; A_0 is the cross-sectional area; and V_1 is the vertical tension at the lower end.

b) Partial differential equations for mooring line dynamics:

The PDE equations for mooring line dynamics are derived from the PDE equations for beam dynamics neglecting the bending and torsional stiffness (Triantafyllou, 1990) given by,

$$\rho_0 \frac{\partial \vec{v}(t,s)}{\partial t} = \frac{\partial}{\partial s} (T(t,s) \vec{t}(t,s)) + \vec{f}(t,s)(1+e(t,s)), \quad (2.36)$$

where t is time variable; $\vec{v}(t,s)$ and $\vec{t}(t,s)$ are the velocity and tangential vector of any point along the mooring line; ρ_0 is mass per unit length of the unstretched mooring line; $e(t, s)$ is strain; and $\vec{f}(t,s)$ is the total external forces per unit length acting on

points along the mooring line. Let $\vec{r}(t,s)$ be the position vector. Then, $\vec{t} = \frac{1}{1+e} \frac{\partial \vec{r}}{\partial s}$

and (2.36) becomes

$$\rho_0 \frac{\partial \vec{r}(t,s)}{\partial t^2} = \frac{\partial}{\partial s} \left(EA_0 \frac{e}{1+e} \frac{\partial \vec{r}}{\partial t^2} \right) + \vec{f}(1+e). \quad (2.37)$$

Applying Hooke's law yields

$$\rho_0 \frac{\partial \vec{r}(t,s)}{\partial t^2} = \frac{\partial}{\partial s} \left(EA_0 \frac{e}{1+e} \frac{\partial \vec{r}}{\partial t^2} \right) + \vec{f}(1+e), \quad (2.38)$$

The external excitation forces, \vec{f} , include the gravity, seafloor interaction, hydrostatic and hydrodynamic forces, according to

$$\vec{f} = \vec{f}_{(hg)} + \vec{f}_{(dt)} + \vec{f}_{(dn)} + \vec{f}_{(mn)} + \vec{f}_{(sv)} + \vec{f}_{(st)} + \vec{f}_{(sn)}. \quad (2.39)$$

The gravity and hydrostatic forces is given by

$$\vec{f}_{(hg)} = \rho_0 \frac{\rho_c - \rho_w}{(1+e)\rho_c} \vec{g}, \quad (2.40)$$

where $\vec{g} \in \mathbb{R}^3$ is the gravitational acceleration, ρ_c is density of the mooring line and ρ_w is density of the ambient water.

The hydrodynamic forces, from Morison's equation, contain drag and inertial forces gravity and hydrostatic forces given by

$$\begin{aligned} \vec{f}_{(dt)} &= -\frac{1}{2} C_{DT} d \rho_w |\vec{v} \cdot \vec{t}| (\vec{v} \cdot \vec{t}) \vec{t} = -\frac{1}{2} C_{DT} d \rho_w |\vec{v}_t| \vec{v}_t, \\ \vec{f}_{(dn)} &= -\frac{1}{2} C_{DN} d \rho_w |\vec{v} - (\vec{v} \cdot \vec{t}) \vec{t}| (\vec{v} - (\vec{v} \cdot \vec{t}) \vec{t}) = -\frac{1}{2} C_{DN} d \rho_w |\vec{v}_n| \vec{v}_n, \\ \vec{f}_{(mn)} &= -C_{MN} \frac{\pi d^2}{4} \rho_w (\vec{a} - (\vec{a} \cdot \vec{t}) \vec{t}) = -C_{MN} \frac{\pi d^2}{4} \rho_w \vec{a}_n, \end{aligned} \quad (2.41)$$

where $\vec{f}_{(dt)}$, $\vec{f}_{(dn)}$, and $\vec{f}_{(mn)}$ are tangential drag force, normal drag force and added inertia force per unit length of the unstretched mooring line, respectively; C_{DT} , C_{DN} and C_{MN} are corresponding coefficients; d is the mooring line diameter; $\vec{a}(t,s)$ is the

acceleration; the subscript n and t denote normal and tangential directions, respectively.

The seafloor interaction forces are modelled as three springs when mooring line is in contact with the seafloor. The condition for seafloor interaction to occur is $z > \delta$, where δ is defined as

$$\delta \triangleq D - \frac{w_0}{k_v}. \quad (2.42)$$

Then the seafloor interaction forces are given by

$$\begin{aligned} \vec{\mathbf{f}}_{(sv)} &= h(\delta - z) \frac{k_v}{1+e} (\delta - z), \\ \vec{\mathbf{f}}_{(st)} &= h(\delta - z) \frac{k_{st}}{1+e} \left(\vec{\vartheta} \cdot \vec{\mathbf{t}}_{sf} \right) \vec{\mathbf{t}}_{sf}, \\ \vec{\mathbf{f}}_{(sn)} &= h(\delta - z) \frac{k_{sn}}{1+e} \left(\vec{\vartheta} - \left(\vec{\vartheta} \cdot \vec{\mathbf{t}}_{sf} \right) \vec{\mathbf{t}}_{sf} \right), \end{aligned} \quad (2.43)$$

where z is $\vec{\mathbf{r}}$ projected onto the vertical, that is, $z = \vec{\mathbf{r}} \cdot \vec{\mathbf{k}}$; h is the Heaviside function; D is water depth; k_v is a spring constant; k_{st} and k_{sn} are spring constants in the tangential and normal directions, respectively; $\vec{\mathbf{r}}_{sf}(t, s)$ is the reference configuration, $\vec{\mathbf{t}}_{sf}(t, s)$ is the tangent vector corresponding to the reference configuration; and $\vec{\vartheta}(t, s)$ is the position of the mooring line relative to the reference configuration $\vec{\mathbf{r}}_{sf}(t, s)$, according to

$$\vec{\vartheta}(t, s) = \vec{\mathbf{r}}_{sf}(t, s) - \vec{\mathbf{r}}(t, s). \quad (2.44)$$

By solving the dynamics of the mooring lines, the tension of mooring lines in the horizontal and vertical direction acting on the vessel can be found. On the other hand, the motions of the upper end of the mooring lines follow the dynamics of the vessel.

2.3.4 Wave Frequency Model

The coupled equations of WF motions in surge, sway, heave, roll, pitch and yaw are assumed to be linear, and can be formulated in the body-fixed frame as

$$\mathbf{M}(\omega)\dot{\mathbf{v}}_w + \mathbf{D}_p(\omega)\mathbf{v}_w + \mathbf{G}\dot{\mathbf{\eta}}_{Rw} = \boldsymbol{\tau}_{wave1}, \quad (2.45)$$

where $\dot{\mathbf{\eta}}_w = [\eta_{w1}, \eta_{w2}, \eta_{w3}, \eta_{w4}, \eta_{w5}, \eta_{w6}]^T$ is the WF motion vector in the Earth-fixed frame. $\boldsymbol{\tau}_{wave1} \in \mathbb{R}^6$ is the first order wave excitation vector, which will be modified for varying vessel headings relative to the incident wave direction. $\mathbf{M}(\omega) \in \mathbb{R}^{6 \times 6}$ is the system inertia matrix containing frequency dependent added mass coefficients in addition to the vessel's mass and moment of inertia. $\mathbf{D}_p(\omega) \in \mathbb{R}^{6 \times 6}$ is the wave radiation (potential) damping matrix. The linearized restoring coefficient matrix $\mathbf{G} \in \mathbb{R}^{6 \times 6}$ is the same as in (2.21). The structure of the mass and damping matrices are the same as in (2.9) and (2.20). For anchored vessels, it is assumed that the mooring system will not influence the WF motions.

For small yaw motions in the reference-parallel frame, the WF motion vector becomes

$$\dot{\mathbf{\eta}}_{Rw} = \mathbf{J}(\psi - \psi_d)\mathbf{v}_w, \quad (2.46)$$

$$\text{or } \dot{\mathbf{\eta}}_{Rw} = \mathbf{v}_w. \quad (2.47)$$

Then, (2.45) can be re-formulated in the reference-parallel and Earth-fixed frames as

$$\mathbf{M}(\omega)\ddot{\mathbf{\eta}}_{Rw} + \mathbf{D}_p(\omega)\dot{\mathbf{\eta}}_{Rw} + \mathbf{G}\dot{\mathbf{\eta}}_{Rw} = \boldsymbol{\tau}_{wave1}, \quad (2.48)$$

$$\dot{\mathbf{\eta}}_w = \mathbf{J}(\psi_d)\dot{\mathbf{\eta}}_{Rw}. \quad (2.49)$$

Table 2.1. Notation for position and velocity (after SNAME, 1950).

Position and orientation in Earth-fixed frame Velocity in body-fixed frame	$\boldsymbol{\eta} = [\boldsymbol{\eta}_1 \quad \boldsymbol{\eta}_2]^T = [\underbrace{x \quad y \quad z}_{\text{position}} \quad \underbrace{\phi \quad \theta \quad \psi}_{\text{orientation}}]^T,$ $\boldsymbol{\eta} \in \mathbb{R}^6, \boldsymbol{\eta}_1 \in \mathbb{R}^3, \boldsymbol{\eta}_2 \in \mathbb{R}^3.$
	$\boldsymbol{v} = [\boldsymbol{v}_1 \quad \boldsymbol{v}_2]^T = [\underbrace{u \quad v \quad w}_{\text{linear velocity}} \quad \underbrace{p \quad q \quad r}_{\text{angular velocity}}]^T,$ $\boldsymbol{v} \in \mathbb{R}^6, \boldsymbol{v}_1 \in \mathbb{R}^3, \boldsymbol{v}_2 \in \mathbb{R}^3$

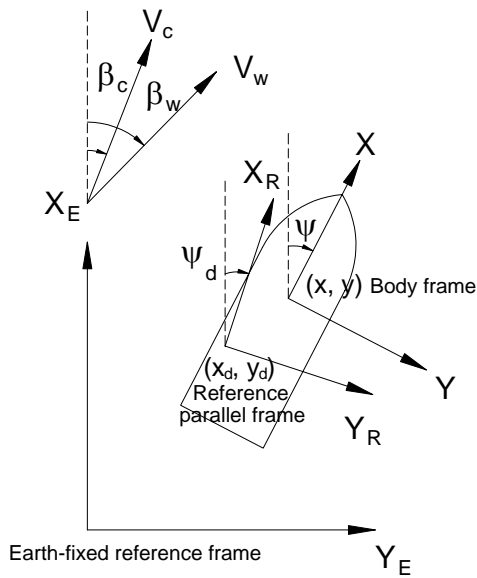


Figure 2.1. Earth-fixed, reference-parallel and body-fixed frame.

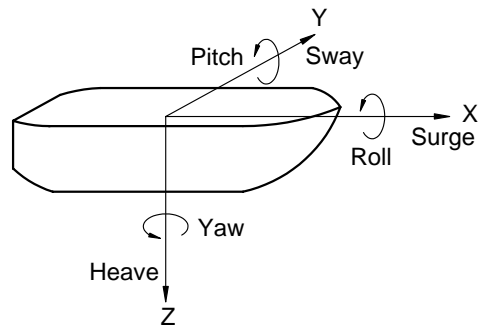


Figure 2.2. 6-DOF mode of motion.

Chapter 3 Concept of Hybrid Marine Control Systems (HyMarCS)

3.1 Introduction

As shown in Chapter 2, the modelling for marine vessels is a complicated and highly nonlinear system. The process plant model can be simplified to different control plant models depending on the control objectives, constraints and dynamic response of the controlled system. The controllers are then designed based on these control plant models rather than the original process plant model. The control objectives can be visually described within a three-dimensional space as depicted in Figure 3.1, with the following three main parameters:

- Functions/mode dependence (x axis),
- Speed dependence (y axis),
- Environmental dependence (z axis).

Changes in these dimensions result in changes in the fundamental components of the motion control problem (namely, objectives, constraints and dynamic response of the controlled system). One can build further upon this setting by considering additional spaces which are fault-tolerant control dependence and interaction between human factor and control system.

3.2 Multi Operational Regime Controller Objectives

3.2.1 Changes in Operation Mode

Marine vessels operate in a variety of modes, such as station keeping including DP and thruster assisted positioning mooring (PM), low speed maneuvering, and moderate to high speed transit. The changes in operation mode are illustrated through

typical operational profiles of a platform supply vessel (PSV), a shuttle tanker, an FPSO and a drilling and well-intervention vessel as summarized in Table 3.1.

Changes in operation mode result in changes in the *control objectives*. For example, a vessel in PM mode may require heading control, damping, line tension control, or single point mooring control for interconnected structures (Aamo and Fossen, 1999; Berntsen et al., 2003; Berntsen et al., 2004; and Strand et al., 1998). Vessel in DP mode requires keeping itself in a fixed position or a pre-determined track exclusively by means of active thrusters (Balchen et al., 1976; and Sørensen et al., 1996). Other objectives associated with the DP system are roll and pitch damping control for small-water-plane-area marine vessel (Sørensen and Strand, 2000), optimal set-point chasing control for deep-water drilling and intervention vessels (Sørensen et al., 2001), and weather optimal positioning control (Fossen and Strand, 2001).

The objectives of low speed maneuvering mode are 1) to force the vessel to follow a path 2) while satisfying time, speed, or acceleration assignment (dynamic task) along the path (Skjetne et al., 2005 and Skjetne, 2005). The objective of low speed tracking is only to force the ship along the pre-determined path. Fossen (2005) proposed a controller that may satisfy the objectives for station keeping and low speed maneuvering by using a unified mathematical model describing the maneuvering of a ship traveling in a seaway (Bailey et al., 1998).

A vessel in transit, on the other hand, may require heading control, heading plus cross-error control, and piece-wise rectilinear path accompanied with active leg switching guidance (Nomoto et al., 1957; Norrbin, 1970; and Fossen, 2002).

A summary of the control objectives for different operational modes is shown in Table 3.2.

3.2.2 Changes in Speed

The changes in speed result in changes in the *dynamic response* of the vessel and will improve or degrade the capacity of the actuators in delivering the desired control action. The latter degradation can be overcome through the control allocation scheme and the low level thruster controller. In the high level controller, the change in speed should be modelled either as changes in the parameters or in the structure of the model and the controller itself. For example, while the effects of nonlinear damping can be neglected in the zero speed regime as in DP application, the effects of nonlinear damping should be included in the control plant model in higher speed regime, e.g. low speed maneuvering and autopilot (Fossen, 2002; Nomoto et al., 1957; Norrin, 1963 and 1970; Skjetne et al., 2005 and Skjetne, 2005).

3.2.3 Changes in Environment

Changes in the environment result in changes of the *disturbance characteristics* (frequency and intensity). However, these changes may also result in the need to change *the control objective*, that is whether to compensate only LF motion in moderate sea or both LF and WF in extreme sea.

The control objective of a vessel performing DP in low to medium sea states is to keep its position by compensating only for the slowly-varying motion induced by mean wave, current and wind loads rather than the higher frequency wave-induced motion (Nguyen et al., 2005b and the references therein). As the sea state increases, the frequency of this wave-induced motion is reduced such that this motion now becomes a significant disturbance to the DP operation. Under extreme seas such as in the North Sea and Barrens Sea, swell waves, often large with long periods, may be present in addition to wind-generated waves (Torsethaugen, 1996). In such case, the

control objectives, the order of the models, as well as the wave filtering functions need to be changed to satisfy the positioning performance and stability requirements.

Recently, there has been some work to achieve the above requirements. At the *plant control level*, Sørensen et al. (2002) proposed that DP system should compensate for both WF and LF motions in extreme seas, especially when swell becomes dominant. Lindegaard (2003) proposed acceleration feedback (AFB) to increase performance of DP systems. Nguyen et al. (2005b) showed that the AFB will have more effect in harsh environments than in moderate seas. At the *actuator control level*, Smogeli (2005) developed an anti-spin control strategy for extreme condition.

Nguyen et al. (2005b) integrated some of these controllers into a hybrid DP system at plant control level in order to extend the weather window of the existing DP system from calm to extreme sea conditions. The concept of hybrid control to operate under changes in environmental condition can also be extended and generalized for other marine control systems as will be shown here.

The control objectives of a PM vessel in low to medium sea states are primarily heading control and damping in surge (e.g. Strand et al., 1998; Aamo and Fossen, 1999) by compensating only for the slowly-varying environment induced motion. The control objective of such vessel in harsh sea is to follow the set-point for the 3-DOF (surge, sway and yaw) motion of the vessel rather than only heading and surge damping in order to guarantee the reliability of the mooring lines by compensating for both the WF and LF motions.

Another example of the change in control objective is the need to incorporate motion damping in roll and pitch of high speed vessels as the sea state increases.

3.2.4 Fault-Tolerant Control

Apart from the natural changes mentioned above, the state of a ship can change as a result of faults in its components, such as sensors, actuators and power generators, at different levels of severity. These faults may effect changes in the dynamic response of the ship, constraints, and the ship's ability to continue with its mission. Contemplation of these eventualities calls for distributed monitoring and diagnostics capabilities and/or effective re-configuration of the control and the objectives, which falls under the field of *fault-tolerant control* (Blanke et al., 2003).

3.3 Control Structure

Sørensen (2005b) addressed the hierarchical levels of marine control systems as shown in Figure 3.2. For the real-time control, the local optimization control provides the plant control system set-points to follow. The plant control then calculates the necessary command forces and moments which are sent to the actuator control block.

3.3.1 Actuator Controller (Low Level)

The actuators of marine systems are normally thrusters, propellers, rudders, interceptors, fins, flaps, T-foils and mooring systems. Other important actuators include pumps, separators, compressors, HVAC, drilling drives, cranes and winches. These actuators are often associated with a local control system which ensures the correct implementation of the control action. Dependent on whether the actuators are mechanically, hydraulically and/or electrically driven, controllers with different properties will be used.

3.3.2 Plant Controller (High Level)

At this level, the control systems focus on ship operational objectives and generate the desired control command (the low level controllers receive the control

command, and adjust the actuators so as to implement the control action). For example in station keeping operations, the DP system is supposed to counteract the disturbances caused by wave (mean and slowly varying), wind and currents loads acting on the vessel. The plant controller calculates the necessary surge and sway forces and yaw moment needed to compensate the disturbances. The computed forces and moments are the inputs to the thrust allocation system which determines the command action of each actuator controller so as to obtain the desired forces. The command generated by the thrust allocation system can be in terms of shaft speed, power or torque. DP systems are usually designed with redundancy in the number of actuators; therefore, in the thrust allocation scheme it is necessary to provide each actuator with the correct command so as to minimize the energy demand and satisfy the constraints. Similar examples may include the ballast and loading controller, power management systems (PMS)/energy management systems (EMS) and motion damping systems.

3.3.3 Local Optimization

At the local optimization level, hybrid control can possibly take the form of switching between operator defined set-point and optimal set-point chasing in DP or PM, and switching amongst route plans (guidance and navigation) in transit operation.

Depending of the actual marine operation that the vessel is involved (such as drilling, weather vaning, pipe laying, tracking operations and transit), optimization of desired set points in conjunction with the appropriate reference models are used. Such level of optimization can also be found in the guidance systems used in transit operations (Fossen, 2002).

3.4 Concept of Hybrid Controller

The *hybrid control system* consists of continuous state multi-controllers and discrete state logics that allow smooth switching among the various controllers for the

particular operations and functions. The concept of hybrid control is also used to automatically switch between appropriate designed controllers handling normal operational conditions to extreme situations such as severe seas and possible failure situations. The selection of which controller to use in the closed loop is decided by an automatic switching logic or by the operator. The level of automation depends on the type of operation. In particular, the operator will be involved in switching among sub-function controllers (Table 3.2). In this hybrid control strategy, the major concern is the switching process and the smooth transition between two controllers. In Chapter 4, a hybrid control system for marine vessel operating from transit to station keeping will be developed by considering the task of the operators.

On the other hand, the hybrid DP system from calm to extreme seas (to be developed in Chapter 6) must be able to automatically switch among controllers designed for various sea states, where the latter may be detected using some simple parameter such as the estimated peak frequency of wave (Nguyen et al., 2005b). In this control strategy, estimator-based *supervisory control* (Hespanha, 2001; Hespanha and Morse, 2002; and Hespanha et al., 2003) is adopted and the main concern is stability when switching among the controllers.

3.4.1 Concept of Supervisory Control

Based on the concept that a hybrid-controller system must have the ability to automatically switch among controllers, one may divide the system into two main blocks, namely, the *supervisor* and the *controller set*. Figure 3.3 shows the general hybrid control system.

In the estimator-based supervision, the supervisor compares the behaviors of some admissible models and the actual process, and decides which model best

describes the ongoing process. This will thus involve multi-estimators which is basically a set of estimators to model the process in different operational regimes,

$$\mathcal{M} := \bigcup_{p \in \mathcal{P}} \mathcal{M}_p . \quad (3.1)$$

There will be at least one controller designed for each model. The set of controllers are denoted as

$$\mathcal{C} := \bigcup_{q \in \mathcal{Q}} \mathcal{C}_q , \quad (3.2)$$

where \mathcal{P} and \mathcal{Q} are the set of estimators and controllers, respectively; p and q are the p th model and q th controller, respectively. The estimator and controller are described by linear or nonlinear systems, represented by

$$\mathcal{M} := \{\dot{\mathbf{x}}_E = \mathbf{A}_E(\mathbf{x}_E, \mathbf{u}, \mathbf{y}), \mathbf{y}_p = \mathbf{C}_E(p, \mathbf{x}_E, \mathbf{u}, \mathbf{y}) : p \in \mathcal{P}\} , \quad (3.3)$$

$$\mathcal{C} := \{\dot{\mathbf{x}}_q = \mathbf{F}_q(\mathbf{z}_q, \mathbf{y}), \mathbf{u} = \mathbf{G}_q(\mathbf{z}_q, \mathbf{y}) : q \in \mathcal{Q}\} . \quad (3.4)$$

As the subscript E denotes “estimator”, \mathbf{x}_E is the state of model set, and \mathbf{y}_p is the estimation vector. \mathbf{x}_q is the state of the controller, and \mathbf{u} is the control force. When switching is made, a *process switching signal* ρ determines which model is selected, and a *switching signal* σ determines which controller is in the loop at each instant of time. Selecting the controller with respect to the estimator is performed by the mapping $\sigma = \chi(\rho) \in \mathcal{Q}$, $\rho \in \mathcal{P}$. For the hybrid-controller DP system considered here, a simple mapping is used, that is, $\sigma = \rho \in \mathcal{P}$, $\mathcal{P} \equiv \mathcal{Q}$.

For formal stability proof of hybrid-controller system, it is convenient to have the following definition.

Definition 1 (Switched System – Hespanha, 2001). The switched system includes the process, controller set, and the estimator set, see Figure 3.3.

$$\dot{\mathbf{x}} = \mathbf{A}_\sigma(\mathbf{x}, \mathbf{w}) , \quad (3.5)$$

$$\mathbf{e}_p = \mathbf{C}_p(\mathbf{x}, \mathbf{w}), \quad p \in \mathcal{P}, \quad (3.6)$$

where \mathbf{x} denotes the states of the process, multi-controller, and multi-estimator, and \mathbf{w} the environmental disturbance. The input to the switched system is the disturbances caused by wind, wave and current loads, and the output is the model error vector, \mathbf{e}_p .

3.4.2 Properties of Supervisory Control

According to Hespanha (2002), the two important properties of the switched systems are *matching* and *detectability*. The switching logic will guarantee *small error* and *non-destabilization* properties.

Matching property: the multi-estimator should be designed such that each particular \mathbf{y}_p provides a “good” approximation of the output \mathbf{y} . This means \mathbf{e}_p is small whenever the process is inside the corresponding \mathcal{M}_p .

Detectability property: The detectability of a system guarantees if the output of that system is small, then the state of that system will eventually be small no matter its initial state. The detectability of the switched system for every fixed estimator, must be detectable with respect to the estimator error \mathbf{e}_p when the switching signal is frozen at $\sigma = \chi(p) \in \mathcal{Q}$.

In order to achieve the detectability property of the switched system in the stability analysis of the switched system, it is convenient to consider the switched system as an interconnection of the process (marine vessel) and the injected system (Figure 3.4). The cascade connection theorem states that if the injected system is input to-state-stable (ISS) and the process is detectable, then the switched system is detectable. Therefore, if the process is assumed to be detectable, then to prove that the switched system is detectable, we only need to prove that the injected system is ISS.

Note that the output of the model (estimator) set is \mathbf{y}_p while the output from the switch is \mathbf{y}_ρ ; which is a sub-vector of \mathbf{y}_p .

The detectability of a system guarantees that if the output of the system is small, then the state must eventually be small, no matter its initial state.

Small error property: the switching logic must guarantee the bound on \mathbf{e}_ρ (the “smallest” sub-vector using any norm of the model error vector, \mathbf{e}_p) for a process switching signal ρ which satisfies $\sigma = \chi(\rho)$, or simply $\sigma = \rho$.

Non-destabilization property preserves the detectability in a temporal sense.

This property is satisfied if:

- switching is slow on the average by using dwell-time switching logic which is used strictly in switching among linear models and controllers only;
- switching stops in finite time by using scale-independent hysteresis switching logic which can be used in switching among linear/nonlinear models and controllers.

The matching property and the detectability property are important for the multi-estimator and multi-controller, respectively. The small error property makes sure that the supervisor switches to the model which has the smallest error between the output of the process and the output of the estimator. When the process is at the “border” of regimes, there may be rapid and frequent switching (*chattering*) affecting the stability of the switched system. In this case, there is a conflict between the desire to switch to the model that has the smallest error and the concern of the chattering problem. Non-destabilization will prevent chattering by providing switching logic, such as dwell-time switching logic and hysteresis switching logic.

The models and the controllers in high-level control of DP systems are nonlinear. Thus, the scale-independent hysteresis switching logic based on Hespanha (2002) will

be adopted rather than the dwell-time switching logic for the hybrid-controller DP system. The term *scale-independent* comes from the fact that the switching signal σ will remain unchanged if all the monitoring signals are simultaneously scaled. The hybrid-controller DP system adopting the scale-independent hysteresis switching logic will be presented in the next Section.

3.4.3 Scale-Independent Hysteresis Switching Logic

The hysteresis switching logic slows down switching based on the observed growth of the estimation errors. Figure 3.5 shows the concept of scale-independent hysteresis switching logic, where μ_p physically is a monitoring signal defined by Hespanha (2001) in terms of the error norm as follows:

Definition 2 (Monitoring signal – Hespanha, 2001)

$$\dot{\mu}_p = -\lambda \mu_p + \gamma(\|\mathbf{e}_p\|), \quad p \in \mathcal{P}, \quad (3.7)$$

where λ denotes a constant non-negative forgetting factor, γ is the class \mathcal{K} function,

$\mu_p(0) > 0$, and $\|\cdot\|$ denotes any norm.

Let h be a positive *hysteresis constant* and $\arg \min \mu_p$ return the index of the minimum values of vector μ_p . The switching procedure could be described in Figure 3.5 and as follows:

- $t = t_0 = 0$,

Let $\mu_p(0) > 0$,

- $\sigma(t_0) = \rho(t_0) = \arg \min \mu_p(t_1)$, $T_1 = t_0$, calculate $\mu_\rho(T_1) = \mu_\rho(t_0)$.
- $t = t_1$ (next time step),
 - calculate $\dot{\mu}_p = -\lambda \mu_p + \gamma(\|\mathbf{e}_p\|)$,
 - if $\mu_\rho(T_1) \leq (1+h)\mu_p(t_1)$,

- then keep the value of $\sigma(t_1) = \sigma(T_1) = \sigma(t_0)$
- else the value of σ is switched to $\sigma(t_1) = \rho(t_1) = \arg \min \mu_p(t_1)$, $T_2 = t_1$, calculate $\mu_p(T_2) = \mu_p(t_1)$.
- $t = t_m$,
- calculate $\dot{\mu}_p = -\lambda \mu_p + \gamma (\|\mathbf{e}_p\|)$,
- if $\mu_p(T_n) \leq (1+h)\mu_p(t_m)$,
 - then keep the value of $\sigma(t_m) = \sigma(T_n) = \sigma(t_{m-1})$
 - else the value of σ is switched to $\sigma(t_m) = \rho(t_m) = \arg \min \mu_p(t_m)$, $T_{n+1} = t_m$, calculate $\mu_p(T_{n+1}) = \mu_p(t_m)$.

Details of hysteresis can be found in Hespanha (2001), Hespanha and Morse (2002), Hespanha et al. (2003), and the references therein.

3.5 Conclusions

This Chapter investigated the possibilities of developing hybrid control for marine control system. The investigation showed that controllers in marine control system can be located in the spaces of three main dimensions: function, environments and speed regimes. Other dimensions are fault-tolerant control and human factor interaction with control system. Changes in those dimensions will results in changes in control objectives, constraints, dynamic responses and disturbance characteristics. Those motivated the development of hybrid control for marine control system. Two main types of hybrid control are the hybrid control involving the operator to manually switch among controllers and the hybrid control adopting the supervisory control to automatically switching among controllers.

In Chapter 4 and Chapter 6, two hybrid control systems for marine operations are presented. The hybrid control system is developed for change of marine operational

functions from transit to station keeping in which the switching involves the operator (Chapter 4). The hybrid DP system subject to change of environmental conditions (Chapter 6) adopts the supervisory control with scale-independent hysteresis switching logic, based on Hespanha (2001).

Table 3.1. Typical operational profiles of a PSV, a shuttle tanker, an FPSO, and drilling & well-intervention vessel

	Station keeping/ Standby	Transit	Port	Others
PSV	30 – 50%	30 – 40%	5 – 10%	5 – 10%
FPSO	90 – 99%	1 – 5%	–	–
Shuttle tanker	20 – 40%	40 – 60%	5 – 15%	–
Drilling and well intervention	70 – 90%	5 – 20%	1 – 5%	–

Table 3.2. Sub-functions for marine operational objectives

Station keeping

- PM/POSMOOR system:
 - Automatic thrust assisted position mooring
 - Station keeping
 - Change of set-point
 - Damping control
 - Line break detection and compensation
 - DP systems:
 - Single point mooring
 - Station keeping
 - Change of set-point (marked position)
 - Optimal heading control
 - Roll and pitch damping
-

Low speed maneuvering

- Follow target (ROV)
 - Low speed way point tracking
-

Transit (autopilot)

- Course keeping
 - Course change
 - High speed way point tracking (guidance and navigation control)
 - Path following
 - Line of sight
-

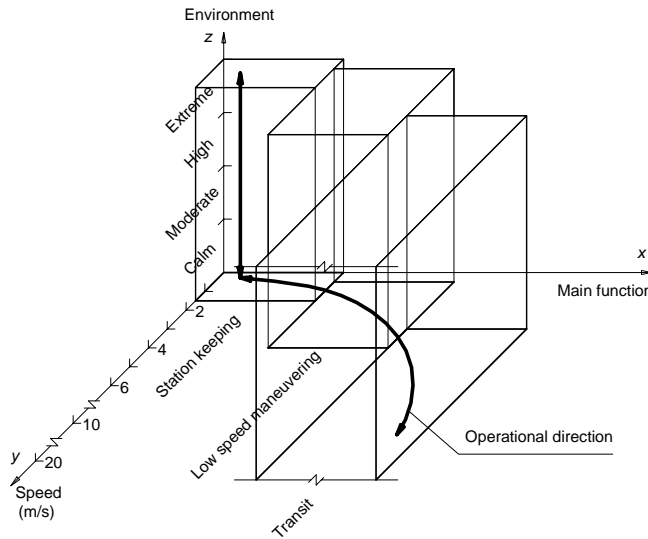


Figure 3.1. Control objectives for different marine operations.

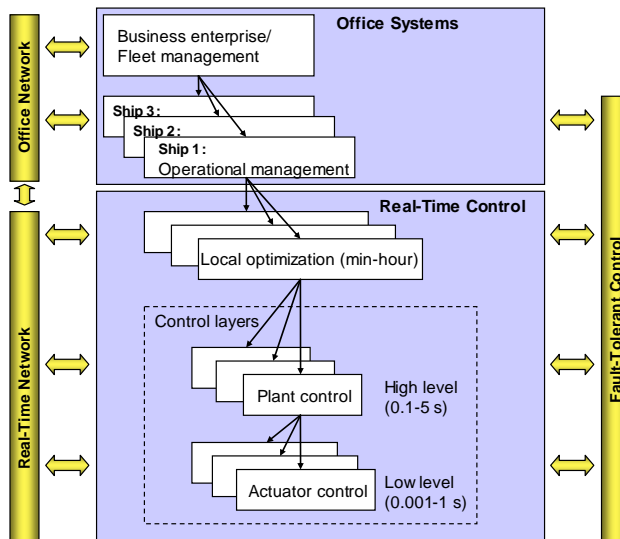


Figure 3.2. Control structure (Sørensen, 2005b).

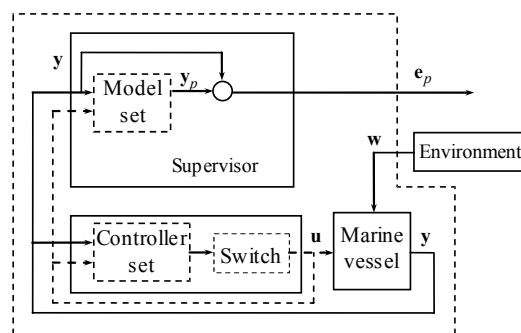


Figure 3.3. Switched DP system.

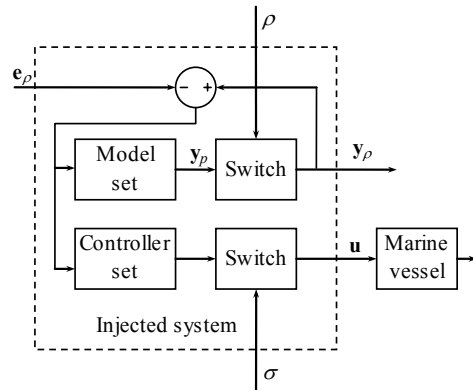


Figure 3.4. Injected DP system in cascade with process based on Hespanha (2001).

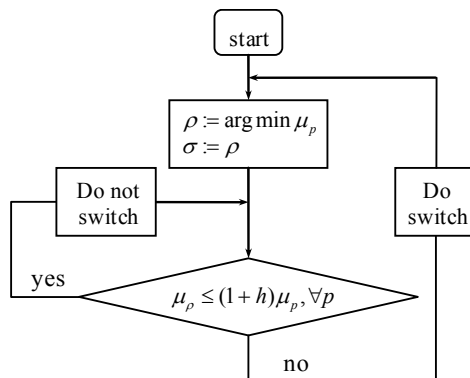


Figure 3.5. Scale-independent hysteresis switching logic, Hespanha (2001).

Chapter 4 Multi-Operational Hybrid Controller Structure for Station Keeping and Transit Operations of Marine Vessels

4.1 Introduction

The typical operations of a shuttle tanker involve transit, low speed maneuvering and station keeping modes, as illustrated in Figure 4.1. In this Chapter, the transit and station-keeping control are combined into a hybrid control system, shown conceptually in Figure 4.2. The shuttle tanker transits between port and the offshore field using an autopilot controller (controller 1). The dynamic positioning (DP) is performed by controller 3. The smooth transformation between autopilot and DP is realized using controller 2. The single point mooring (SPM) or submerged turret loading (STL) mode to connect to the loading buoy or tower is performed with controller 5. Controller 4 is activated by a control strategy for the smooth transformation between DP and SPM/STL.

The purpose of the study presented in this chapter is to illustrate via a shuttle tanker example on the integration of different controllers into a hybrid control system in marine operations. The selection of the controllers inside the hybrid control system may be different from Figure 4.2 as it is application dependent. For example, the low speed maneuvering control proposed by Skjetne et al. (2005) and Skjetne (2005) can be set between DP controller and autopilot if the marine vessel requires the low speed maneuvering. Furthermore, the DP and low speed maneuvering controllers can be replaced by a unified controller for station keeping and low speed maneuvering (Fossen, 2005).

4.2 Autopilot in Transit Regime

The objective of an autopilot is to keep the heading and yaw rate of the vessel in fixed or new set-points commanded by the guidance and navigation control (GNC).

4.2.1 Observer Design

The control plant model is developed by combining the Nomoto ship model (Nomoto et al., 1957) for LF motion and the linear wave model for WF motion, according to

$$\begin{aligned}\dot{\mathbf{z}}_1 &= \mathbf{A}_{p1}\mathbf{z}_1 + \mathbf{B}_{q1}\tau_{q1} + \mathbf{E}_1\mathbf{w}_1, \\ \mathbf{y}_1 &= \mathbf{C}_{p1}\mathbf{z}_1.\end{aligned}\tag{4.1}$$

where τ_{q1} is the control moment in yaw, e.g. from the rudder; $\mathbf{z}_1 \in \mathbb{R}^5$ and $\mathbf{w}_1 \in \mathbb{R}^3$ are the state and disturbance vectors, respectively, given by

$$\mathbf{z}_1 = [\xi_w \quad \psi_w \quad \psi \quad r \quad b]^T,\tag{4.2}$$

$$\mathbf{w}_1 = [w_w \quad w_r \quad w_b]^T,\tag{4.3}$$

in which ψ is LF heading angle; r is yaw rate; b is bias term for rudder offset modelled as a 1st-order Markov process; ψ_w is WF heading angle; and ξ_w and ψ_w are the states of WF model for heading angle following the linear wave model (Fossen, 2002), according to

$$\dot{\xi}_w = \psi_w,\tag{4.4}$$

$$\dot{\psi}_w = -\omega_p^2 \xi_w - 2\lambda \omega_p \psi_w + K_w w_w,\tag{4.5}$$

where ω_p and λ are the peak (dominating) frequency of wave and the damping ratio of WF model (Fossen, 2002), respectively; and K_w is a disturbance scaling parameter.

The system matrices $\mathbf{A}_{p1} \in \mathbb{R}^{5 \times 5}$, $\mathbf{B}_{q1} \in \mathbb{R}^{5 \times 1}$, $\mathbf{E}_1 \in \mathbb{R}^{5 \times 3}$ and $\mathbf{C}_{p1} \in \mathbb{R}^{1 \times 5}$ are given by

$$\mathbf{A}_{p1} = \left[\begin{array}{cc|ccc} 0 & 1 & 0 & 0 & 0 \\ -\omega_p^2 & -2\lambda\omega_p & 0 & 0 & 0 \\ \hline 0 & 0 & 0 & 1 & 0 \\ 0 & 0 & 0 & -1/T & -K/T \\ 0 & 0 & 0 & 0 & -1/T_b \end{array} \right],$$

$$\mathbf{B}_{q1} = \left[\begin{array}{c} 0 \\ 0 \\ \hline 0 \\ K/T \\ 0 \end{array} \right], \quad \mathbf{E}_1 = \left[\begin{array}{c|cc} 0 & 0 & 0 \\ K_w & 0 & 0 \\ \hline 0 & 0 & 0 \\ 0 & 1 & 0 \\ 0 & 0 & 1 \end{array} \right], \text{ and } \mathbf{C}_{p1} = \left[\begin{array}{c} 0 \\ 1 \\ \hline 1 \\ 0 \\ 0 \end{array} \right]^T, \quad (4.6)$$

where T and K are known as the Nomoto time and gain constants, respectively; and T_b is time constant for the bias model.

By copying the control plant model (4.1), the passive observer can be adopted to develop the observer for heading angle (Fossen, 2002) according to

$$\dot{\mathbf{z}}_{p1} = \mathbf{A}_{p1}\mathbf{z}_{p1} + \mathbf{B}_{q1}\tau_{q1} + \mathbf{K}_{p1}(y_1 - y_{p1}), \quad (4.7)$$

$$\mathbf{y}_{p1} = \mathbf{C}_{p1}\mathbf{z}_{p1}. \quad (4.8)$$

The state vector for observer $\mathbf{z}_{p1} \in \mathbb{R}^5$ is written as

$$\mathbf{z}_{p1} = \left[\hat{\xi}_w \quad \hat{\psi}_w \quad \hat{\psi} \quad \hat{r} \quad \hat{b} \right]^T, \quad (4.9)$$

where $\hat{\xi}_w$, $\hat{\psi}_w$, $\hat{\psi}$, \hat{r} , and \hat{b} are the estimated states.

The observer gain $\mathbf{K}_{p1} \in \mathbb{R}^{5 \times 1}$ can be calculated by passivity requirements (Fossen and Strand, 1999; Fossen, 2002), according to

$$\mathbf{K}_{p1} = \left[-2\omega_p(1-\lambda)/\omega_c, 2\omega_p(1-\lambda), \omega_c, K_4, K_5 \right]^T, \quad (4.10)$$

where $\omega_c > \omega_p$ is the filter cut-off frequency, and the remaining gains must satisfy the passivity requirement, such that

$$0 < 1/T_b < K_5/K_4 < \omega_p < \omega_c. \quad (4.11)$$

4.2.2 Controller Design

A PID controller for heading control is used

$$\tau_{q1} = \tau_{FF1} - K_{p1}\tilde{\psi} - K_{d1}\tilde{r} - K_{i1} \int_0^t \tilde{\psi}(\tau) d\tau \quad (4.12)$$

where τ_{FF1} is the feed-forward term; K_{p1} , K_{i1} , and K_{d1} are the non-negative PID controller gains, respectively; and $\tilde{\psi}$ and \tilde{r} are the output feedback error dynamics of heading angle and yaw rate, respectively, given by

$$\tilde{\psi} = \hat{\psi} - \psi_d, \quad \tilde{r} = \hat{r} - r_d, \quad (4.13)$$

in which ψ_d and r_d are the desired heading angle and yaw rate, respectively, provided by the GNC system.

It should be noted that although more sophisticated observer and controller designs may be used instead of presented above, but for the purpose of illustration, conventional well-known designs are selected.

4.3 Station Keeping – Dynamic Positioning

4.3.1 Observer Design

The control plant model in Fossen and Strand (1999) is given as

$$\dot{\mathbf{p}}_w = \mathbf{A}_{pw}\mathbf{p}_w + \mathbf{E}_{pw}\mathbf{w}_{pw}, \quad (4.14)$$

$$\dot{\boldsymbol{\eta}} = \mathbf{R}(\psi)\mathbf{v}, \quad (4.15)$$

$$\dot{\mathbf{b}} = -\mathbf{T}_b\mathbf{b} + \mathbf{E}_b\mathbf{w}_b, \quad (4.16)$$

$$\mathbf{M}\dot{\mathbf{v}} = -\mathbf{D}_L\mathbf{v} + \mathbf{R}^T(\psi)\mathbf{b} + \boldsymbol{\tau}_{q3}, \quad (4.17)$$

$$\mathbf{y} = \boldsymbol{\eta} + \mathbf{C}_{pw}\mathbf{p}_w. \quad (4.18)$$

Assume that the second-order linear model is sufficient to describe the first-order wave-induced motion, then $\mathbf{p}_w \in \mathbb{R}^6$, is the state vector of the WF model (Fossen,

2002). $\mathbf{A}_{pw} \in \mathbb{R}^{6 \times 6}$ is assumed Hurwitz and describes the first-order wave-induced motion as a mass-damper-spring system. $\mathbf{w}_{pw} \in \mathbb{R}^3$ is a zero-mean Gaussian white noise vector. \mathbf{y} is the measurement vector. The WF measurement matrix $\mathbf{C}_{pw} \in \mathbb{R}^{3 \times 6}$ and the disturbance matrix $\mathbf{E}_{pw} \in \mathbb{R}^{6 \times 3}$ are formulated as

$$\mathbf{C}_{pw} = [\mathbf{0}_{3 \times 3} \quad \mathbf{I}_{3 \times 3}], \quad \mathbf{E}_{pw} = \begin{bmatrix} \mathbf{0}_{3 \times 3} \\ \mathbf{K}_w \end{bmatrix}. \quad (4.19)$$

Here, we have assumed a 3-DOF model adopting the notation in (2.6) and (2.7), where $\boldsymbol{\eta} = [x, y, \psi]^T \in \mathbb{R}^3$ and $\mathbf{v} = [u, v, r]^T \in \mathbb{R}^3$ are the LF position vector in the Earth-fixed frame and the LF velocity vector in the body-fixed frame, respectively. The rotation matrix in (2.6) and (2.7) is given by

$$\mathbf{R}(\psi) = \begin{bmatrix} \cos \psi & -\sin \psi & 0 \\ \sin \psi & \cos \psi & 0 \\ 0 & 0 & 1 \end{bmatrix} \quad (4.20)$$

$\mathbf{M} \in \mathbb{R}^{3 \times 3}$ and $\mathbf{D} \in \mathbb{R}^{3 \times 3}$ are the body mass matrix including hydrodynamic added mass and linear damping matrix, respectively. The bias term $\mathbf{b} \in \mathbb{R}^3$ is modelled as Markov processes with positive semi-definite diagonal matrix $\mathbf{T}_b \in \mathbb{R}^{3 \times 3}$ of time constants. $\mathbf{w}_b \in \mathbb{R}^3$ is bounded disturbance vector, and $\mathbf{E}_b \in \mathbb{R}^{3 \times 3}$ and $\mathbf{K}_w \in \mathbb{R}^{3 \times 3}$ are disturbance scaling matrices. $\boldsymbol{\tau}_q$ is the control force. More detail can be found in Fossen (2002), Sørensen (2005a) and the references therein.

By collecting the state $\mathbf{z}_3 \in \mathbb{R}^{15}$, and the disturbance $\mathbf{w}_3 \in \mathbb{R}^6$ according to

$$\mathbf{z}_3 = [\mathbf{p}_w^T \quad \boldsymbol{\eta}^T \quad \mathbf{b}^T \quad \mathbf{v}^T]^T, \quad (4.21)$$

$$\mathbf{w}_3 = [\mathbf{w}_{pw}^T \quad \mathbf{w}_b^T]^T, \quad (4.22)$$

the control plant model can be compactly written as

$$\dot{\mathbf{z}}_3 = \mathbf{T}_{p3}^T(\psi) \mathbf{A}_{p3} \mathbf{T}_{p3}(\psi) \mathbf{z}_3 + \mathbf{B}_{q3} \boldsymbol{\tau}_{q3} + \mathbf{E}_3 \mathbf{w}_3, \quad (4.23)$$

$$\mathbf{y}_3 = \mathbf{C}_{p3} \mathbf{z}_3. \quad (4.24)$$

The subscripts denoting the dimension of zero and identity matrices could be written shortly to save space,

$$\text{i.e. } \mathbf{0}_{i \times j} \triangleq \mathbf{0}_{ij}. \quad (4.25)$$

The transformation matrix $\mathbf{T}_{p3} \in \mathbb{R}^{15 \times 15}$ is given by

$$\mathbf{T}_{p3}(\psi) = \text{diag}(\mathbf{R}^T(\psi), \dots, \mathbf{R}^T(\psi), \mathbf{I}_{33}). \quad (4.26)$$

The system matrices $\mathbf{A}_{p3} \in \mathbb{R}^{15 \times 15}$ and $\mathbf{B}_{q3} \in \mathbb{R}^{15 \times 3}$, and $\mathbf{E}_3 \in \mathbb{R}^{15 \times 6}$ are given by

$$\mathbf{A}_{p3} = \begin{bmatrix} \mathbf{A}_w & \mathbf{0}_{63} & \mathbf{0}_{63} & \mathbf{0}_{63} \\ \mathbf{0}_{36} & \mathbf{0}_{33} & \mathbf{0}_{33} & \mathbf{I}_{33} \\ \mathbf{0}_{36} & \mathbf{0}_{33} & -\mathbf{T}_b^{-1} & \mathbf{0}_{33} \\ \mathbf{0}_{36} & \mathbf{0}_{33} & \mathbf{0}_{33} & -\mathbf{M}^{-1}\mathbf{D}_L \end{bmatrix}, \quad \mathbf{B}_{q3} = \begin{bmatrix} \mathbf{0}_{63} \\ \mathbf{0}_{33} \\ \mathbf{0}_{33} \\ \mathbf{M}^{-1} \end{bmatrix}, \quad \mathbf{E}_3 = \begin{bmatrix} \mathbf{E}_{pw} & \mathbf{0}_{63} \\ \mathbf{0}_{33} & \mathbf{0}_{33} \\ \mathbf{0}_{33} & \mathbf{E}_b \\ \mathbf{0}_{33} & \mathbf{0}_{33} \end{bmatrix}. \quad (4.27)$$

As only positions are measured, the projection $\mathbf{C}_{p3} \in \mathbb{R}^{3 \times 15}$ is

$$\mathbf{C}_{p3} = \begin{bmatrix} \mathbf{C}_{pw} & \mathbf{I}_{33} & \mathbf{0}_{33} & \mathbf{0}_{33} \end{bmatrix}. \quad (4.28)$$

By copying the control plant model in (4.24), the passive nonlinear observer proposed by Fossen and Strand (1999) is

$$\dot{\mathbf{z}}_{p3} = \mathbf{T}_{p3}^T(\psi_y) \mathbf{A}_{p3} \mathbf{T}_{p3}(\psi_y) \mathbf{z}_{p3} + \mathbf{B}_{q3} \boldsymbol{\tau}_{q3} + \mathbf{K}_{p3} (\mathbf{y}_3 - \mathbf{y}_{p3}), \quad (4.29)$$

$$\mathbf{y}_{p3} = \mathbf{C}_{p3} \mathbf{z}_{p3}. \quad (4.30)$$

The state vector for observer $\mathbf{z}_{p3} \in \mathbb{R}^{15}$ is written as

$$\mathbf{z}_{p3} = \begin{bmatrix} \hat{\mathbf{p}}_w^T & \hat{\mathbf{q}}^T & \hat{\mathbf{b}}^T & \hat{\mathbf{v}}^T \end{bmatrix}^T, \quad (4.31)$$

where $\hat{\mathbf{p}}_w$, $\hat{\mathbf{q}}$, $\hat{\mathbf{b}}$, and $\hat{\mathbf{v}}$ are the estimated states.

The observer gain $\mathbf{K}_{p3} \in \mathbb{R}^{15 \times 3}$ is given by

$$\mathbf{K}_{p3} = \begin{bmatrix} \mathbf{K}_{1p3}^T & \mathbf{K}_{2p3}^T & \mathbf{K}_{3p3}^T & \mathbf{K}_{4p3}^T \end{bmatrix}^T. \quad (4.32)$$

The tuning of the observer gain matrices $\mathbf{K}_{1p3} \in \mathbb{R}^{6 \times 3}$, $\mathbf{K}_{2p3} \in \mathbb{R}^{3 \times 3}$, $\mathbf{K}_{3p3} \in \mathbb{R}^{3 \times 3}$, and $\mathbf{K}_{4p3} \in \mathbb{R}^{3 \times 3}$ is based on the passivity requirements (Fossen and Strand, 1999).

4.3.2 Controller Design

The control objective is to keep the vessel in a fixed position and heading $\boldsymbol{\eta}_d \in \mathbb{R}^{3 \times 1}$ such that

$$\boldsymbol{\eta}_d = [x_d, y_d, \psi_d]^T. \quad (4.33)$$

The reference model provides the desired velocity $\mathbf{v}_d \in \mathbb{R}^{3 \times 1}$ and acceleration $\dot{\mathbf{v}}_d \in \mathbb{R}^{3 \times 1}$. The output feedback error dynamics are given by

$$\tilde{\boldsymbol{\eta}} = \hat{\boldsymbol{\eta}} - \boldsymbol{\eta}_d, \quad \tilde{\mathbf{v}} = \hat{\mathbf{v}} - \mathbf{v}_d, \quad (4.34)$$

The nonlinear output-feedback PID control law for model 3 can be written as

$$\dot{\tilde{\boldsymbol{\xi}}}_{q3} = \tilde{\boldsymbol{\eta}}, \quad (4.35)$$

$$\hat{\boldsymbol{\tau}}_{q3} = \boldsymbol{\tau}_{FF3} - \mathbf{K}_{i3} \mathbf{R}^T(\psi_y) \tilde{\boldsymbol{\xi}}_{q3} - \mathbf{K}_{p3} \mathbf{R}^T(\psi_y) \tilde{\boldsymbol{\eta}} - \mathbf{K}_{d3} \tilde{\mathbf{v}}, \quad (4.36)$$

where $\boldsymbol{\tau}_{FF3}$ is the feed-forward term; and $\mathbf{K}_{p3} \in \mathbb{R}^{3 \times 3}$, $\mathbf{K}_{i3} \in \mathbb{R}^{3 \times 3}$, and $\mathbf{K}_{d3} \in \mathbb{R}^{3 \times 3}$ are the non-negative P, I, and D controller gain matrices, respectively.

4.4 Controller for Transition from Autopilot to DP

In the transition regime between autopilot and DP, the controllers of autopilot and DP are combined by weighting-like function

$$\boldsymbol{\tau}_{q2} = \alpha_1(U) \mathbf{H} \boldsymbol{\tau}_{q1} + \alpha_2(U) \boldsymbol{\tau}_{q3}, \quad (4.37)$$

where the weighting functions α_1 and α_2 , which are used to smoothly transform the controller from transit speed to low speed are dependent on the vessel's speed. The latter is given by

$$U = \sqrt{u^2 + v^2}. \quad (4.38)$$

In this regime, the GNC provides the desired vessel's speed from high to zero.

The mapping from control yaw moment in transit operation to 3-DOF is characterized by the matrix $\mathbf{H}^T = [0, 0, 1]^T$.

The weighting functions are assumed to have the following properties:

- $\alpha_i \rightarrow 1$ when the operation is close to the i th regime;
- $\alpha_1(\theta) + \alpha_2(\theta) = 1, \forall \theta$;
- α_i is slowly varying, such that $\frac{d\alpha_i}{dt} = \dot{\alpha}_i \approx 0$.

Examples of appropriate α_1 and α_2 are shown in (4.39), (4.40), and Figure 4.3.

$$\alpha_1(\theta) = 1 - \exp[-k(p\theta)^r], \quad (4.39)$$

$$\alpha_2(\theta) = \exp[-k(p\theta)^r]. \quad (4.40)$$

4.5 Station Keeping – Positioning Mooring System

4.5.1 Observer Design

The control plant model for PM vessel is similar to that for DP vessel, but the restoring loads due to mooring system must be taken into account (Fossen and Strand, 1999). That is, (4.17) becomes

$$\mathbf{M}\ddot{\mathbf{v}} = -\mathbf{D}_L \mathbf{v} - \mathbf{g}_{moor}(\mathbf{x}_{tur}, \boldsymbol{\eta}) + \mathbf{R}^T(\psi)\mathbf{b} + \boldsymbol{\tau}_q, \quad (4.41)$$

where $\mathbf{g}_{moor}(\mathbf{x}_{tur}, \boldsymbol{\eta})$ is the restoring contribution of the mooring system to the vessel's dynamics, in which \mathbf{x}_{tur} is the position of the center of turret in body-fixed frame for STL. The damping contribution of the mooring system to the vessel's dynamics is usually lumped into the linear damping matrix \mathbf{D}_L .

The control plant model can be compactly written as

$$\dot{\mathbf{z}}_5 = \mathbf{T}_{p5}^T(\psi_y) \mathbf{A}_{p5} \mathbf{T}_{p5}(\psi) \mathbf{z}_5 + \mathbf{B}_{q5}(-\mathbf{g}_{moor}(\mathbf{x}_{tur}, \boldsymbol{\eta}) + \boldsymbol{\tau}_{q5}) + \mathbf{E}_5 \mathbf{w}_5, \quad (4.42)$$

$$\mathbf{y}_5 = \mathbf{C}_{p5} \mathbf{z}_5, \quad (4.43)$$

where the state $\mathbf{z}_5 \in \mathbb{R}^{15}$, the disturbance $\mathbf{w}_5 \in \mathbb{R}^6$, the transformation matrix $\mathbf{T}_{p5} \in \mathbb{R}^{15 \times 15}$, the system matrices $\mathbf{A}_{p5} \in \mathbb{R}^{15 \times 15}$, $\mathbf{B}_{q5} \in \mathbb{R}^{15 \times 3}$, $\mathbf{E}_5 \in \mathbb{R}^{15 \times 6}$, and the projection matrix $\mathbf{C}_{p5} \in \mathbb{R}^{3 \times 15}$ are as defined in the DP mode.

By copying the control plant model in (4.24), the passive nonlinear observer is

$$\dot{\mathbf{z}}_{p5} = \mathbf{T}_{p5}^T(\psi_y) \mathbf{A}_{p5} \mathbf{T}_{p5}(\psi_y) \mathbf{z}_{p5} + \mathbf{B}_{q5}(-\mathbf{g}_{moor}(\mathbf{x}_{tur}, \boldsymbol{\eta}) + \boldsymbol{\tau}_{q5}) + \mathbf{K}_{p5}(\mathbf{y}_3 - \mathbf{y}_{p5}), \quad (4.44)$$

$$\mathbf{y}_{p5} = \mathbf{C}_{p5} \mathbf{z}_{p5}. \quad (4.45)$$

The state vector for observer $\mathbf{z}_{p5} \in \mathbb{R}^{15}$ and the observer gain matrix $\mathbf{K}_{p5} \in \mathbb{R}^{15 \times 3}$ are of same structure as for the DP mode.

4.5.2 Controller Design

The control objectives are 1) to keep the vessel in a desired heading angle, ψ_d , and 2) to add damping in surge and/or sway. The latter is to ensure that the desired velocity in surge and sway $[u_d, v_d]^T = [0, 0]^T$, when resonant oscillatory motions happen due to environmental excitations.

4.6 Station Keeping – Transition from DP to PM and vice versa

The aim is to transit from DP to PM by smoothly switching off the surge and sway control while keeping the heading angle control. This can be done by weighting function as follows

$$\boldsymbol{\tau}_{q4}^{DP2PM} = \alpha_1(t - t_0) \boldsymbol{\tau}_{q3} + \alpha_2(t - t_0) \boldsymbol{\tau}_{q5} \quad (4.46)$$

where the weighting functions α_1 and α_2 are used to smoothly transform the controller from DP to PM mode, t is time, and t_0 is the time instant when the switching begins.

The process of connecting the mooring system and switching the controllers from DP to PM can be as follows:

1. Connect the mooring system to the vessel while the controller is in DP mode,
and
2. Smoothly transform the controller from DP to PM mode.

When the mooring system is connected to the vessel, but the operation is still in DP mode, the bias term in the observer automatically estimates the external loads including the mooring load. Therefore, the switching from DP to PM is stable.

The process of disconnecting the mooring system and switching the controllers from PM to DP can be as follows:

1. Smoothly transform the controller from PM to DP and also use reference model to force the vessel move from the set-point of PM mode to the set-point of DP mode while the mooring system is still connected, and
2. Disconnect the mooring system from the vessel.

Note that if on the contrary, the first stage of switching from PM to DP when the mooring system is disconnected from the vessel while the operation is still in PM mode, the observer will be unstable. The reason is that the estimation of the mooring loads from the observer (while the mooring is not there) may generate significant disturbance to the observer.

4.7 Experimental Results

In this section, the experiments for switching from DP to SPM and vice versa, and from STL to DP of a shuttle tanker are presented. The experiments were carried out using the model vessel, Cybership III (Appendix C), which in these tests was a 1:90 scaled model of a shuttle tanker having a mass of $m = 75$ kg, length of $L = 2.27$ m and breadth of $B = 0.4$ m (in full scale: $m = 54675$ ton, $L = 204.3$ m, $B = 36$ m).

4.7.1 Switching from DP Mode to SPM Mode

The SPM system is model by a mooring line. One end of the mooring line is connected to the fixed bridge; the other end is connected to the bow of the Cybership III (Figure 4.4). This mooring line acts as a linear spring since the restoring forces acting on the ship due to the whole SPM system is almost linear (Sørheim, 1981). There are six tests carried out for three mooring line configurations: namely, mooring line with low, medium and high stiffness under moderate and high seas. The low, medium and high stiffness values are $K_{moor} = 40.5, 56.7$, and 81 kN/m , respectively. The summary of the experiments are shown in Table 4.1. The vessel is subjected to JONSWAP distributed head waves with significant wave height (H_s) and peak period of wave (T_p) shown in Table 4.2.

Figures from 4.5a to 4.10a show the performance of the vessel and Figures from 4.5b to 4.10b show the control force and moment from control system during the switching procedure. The sequence of switching from DP to SPM and vice versa is as follows:

- Stage 1. DP mode. The vessel is kept in fixed position and heading by DP system.
- Stage 2. SPM with heading control. The vessel is connected to the SPM system. The heading control for SPM is turned on while DP is turned off.
- Stage 3. SPM with heading control and surge damping.
- Stage 4. Smooth switching from the SPM with heading control and surge damping to DP. The reference model provides the path from the existing position and heading of the vessel in SPM mode to the desired position and heading of the vessel in DP mode.
- Stage 5. DP mode. The vessel returns to DP mode, same as Stage 1.

Different modes of operation are summarized in Table 4.3. The five stages are shown with the numbers in Figures from 4.5a to 4.10b. The smooth transformation in (4.46) is used between Stage 1 and 2, and Stage 2 and 3.

4.7.2 Switching from STL Mode to DP Mode

The STL system is model by four mooring lines connected to the floating turret which can be connected and disconnected to the Cybership III. The turret can be freely rotated relative to the mooring system (Figure 4.11). There are six tests carried out in three water depths: shallow, medium and deep, under moderate and high seas. The mooring configurations corresponding to these three water depths are linear, moderately nonlinear and highly nonlinear mooring systems (Figure 4.12). The vessel was excited by JONSWAP distributed head waves with significant wave height and peak period of wave shown in Table 4.2. The summary of the experiments are shown in Table 4.4.

Figures from 4.13a to 4.18a show the performance of the vessel and Figures from 4.13b to 4.18b show the control force and moment from control system during the switching procedure. The sequence of switching from DP to STL and vice versa is as follows.

- Stage 1. STL with heading control.
- Stage 2. STL with heading control and surge damping.
- Stage 3. Smooth switch from the STL with heading control and surge damping to DP. The reference model provides the path from the existing position and heading of the vessel in STL mode to the desired position and heading of the vessel in DP mode.
- Stage 4. DP mode. The vessel is kept in fixed position and heading by DP system.

Different modes of operation are summarized in Table 4.5. The four stages are shown with the numbers in Figures from 4.13a to 4.18b. The smooth transformation in (4.46) is used between Stage 1 and 2.

4.7.3 Discussions

The experiments with the switching from PM to DP mode and vice versa in different sea conditions and different mooring system configurations show good performance. When the vessel is kept in a fixed heading, there may be oscillation in surge due to resonance (Stage 2 of experiments DP to SPM, and Stage 1 of experiments STL to DP). These oscillations as expected can be reduced considerably by adding surge damping (Stage 3 of experiments DP to SPM, and Stage 2 of experiments STL to DP). This hybrid control strategy shows the feasibility of designing an integrated control system extending the marine operation from transit speed to station keeping and vice versa.

4.8 Conclusions

This chapter presented the novel concept of hybrid marine control system integrating functions for DP, low speed maneuvering and transit operations into one hybrid control system. When the operator performs switching, weighting functions can be used to smoothly switch from one controller to another controller. The experiments with a model ship in the laboratory showed good performance of smooth switching from PM mode to DP mode and vice versa. The findings in this Chapter suggest that hybrid control using smooth switching involving the operator would have the ability to extend the marine vessel operation from/to transit to/from station keeping.

Table 4.1. Summary of experiments: switching from DP to SPM mode.

Test 1a	low stiffness mooring line, moderate sea
Test 2a	low stiffness mooring line, high sea
Test 3a	medium stiffness mooring line, moderate sea
Test 4a	medium stiffness mooring line, high sea
Test 5a	high stiffness mooring line, moderate sea
Test 6a	high stiffness mooring line, high sea

Table 4.2. Environmental conditions.

Tests	Sea state code	Hs (m)	Tp (s)
1, 3 and 5	Moderate sea	2.52	9.20
2, 4, and 6	High sea	3.96	10.44

Table 4.3. Summary of operation modes from SPM to DP.

Stage – Mode	Surge	Sway	Yaw	Reference set-point
1. DP	On	On	On	x_d, y_d, ψ_d
2. SPM – heading control	Off	Off	On	ψ_d
3. SPM – heading and surge damping	Damping	Off	On	ψ_d $u_d = 0$
4. Smooth switch to DP	Smooth switch from stage 3 to 5			
5. DP	On	On	On	x_d, y_d, ψ_d

Table 4.4. Summary of experiments: switching from STL to DP.

Test 1b	in shallow water, under moderate sea
Test 2b	in shallow water, under high sea
Test 3b	in deeper water, under moderate sea
Test 4b	in deeper water, under high sea
Test 5b	in deep water, under moderate sea
Test 6b	in deep water, under high sea

Table 4.5. Summary of operation modes from STL to DP.

Stage – Mode	Surge	Sway	Yaw	Reference setpoint
1. STL – heading control	Off	Off	On	ψ_d
2. STL – heading and surge damping	Damping	Off	On	ψ_d $u_d = 0$
3. Smooth switch to DP	Smooth switch from stage 2 to 4			
4. DP	On	On	On	x_d, y_d, ψ_d

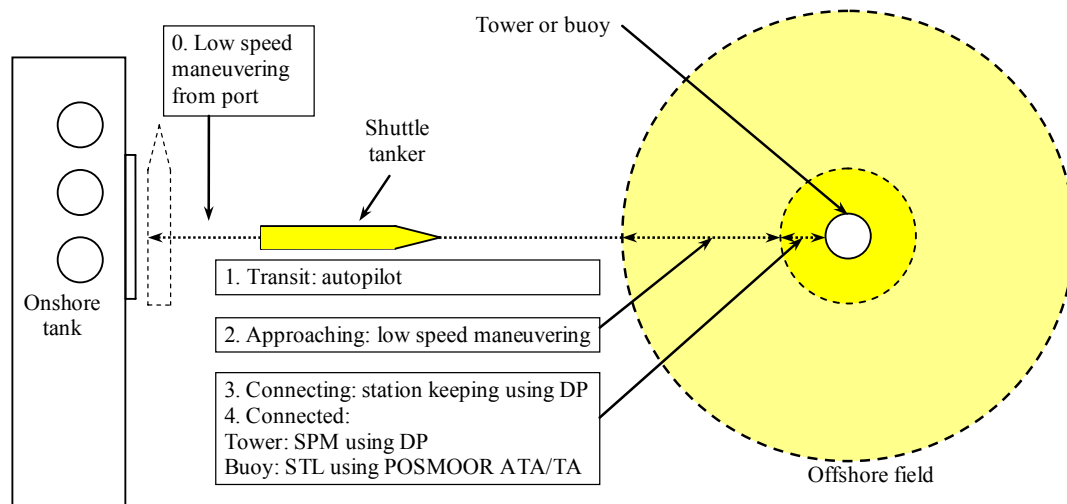


Figure 4.1. Various marine operations of a shuttle tanker.

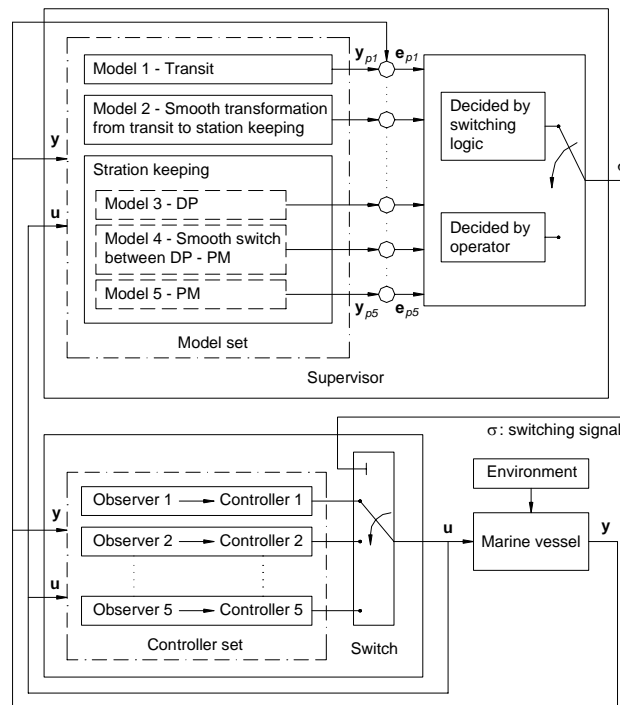


Figure 4.2. Concept of hybrid controller for marine operations from transit to station keeping.

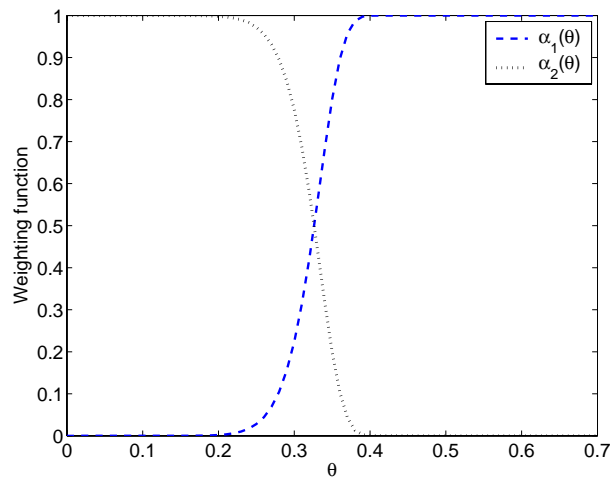


Figure 4.3. Weighting function α_1 and α_2 , with $q = 8$, $p = 2.5$, $r = 12$.

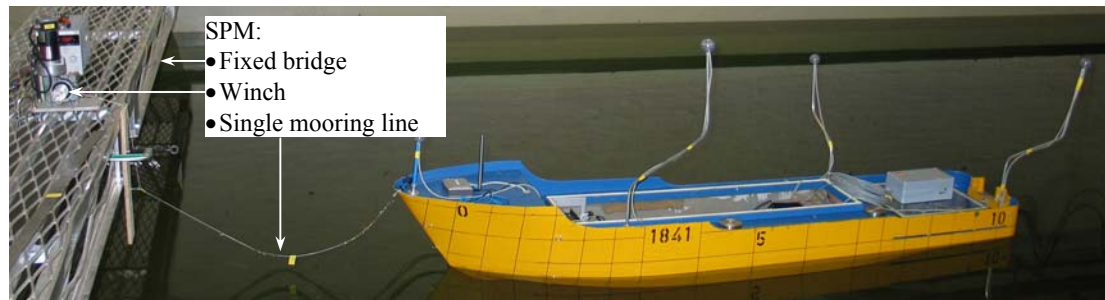


Figure 4.4. The Cybership III with SPM.

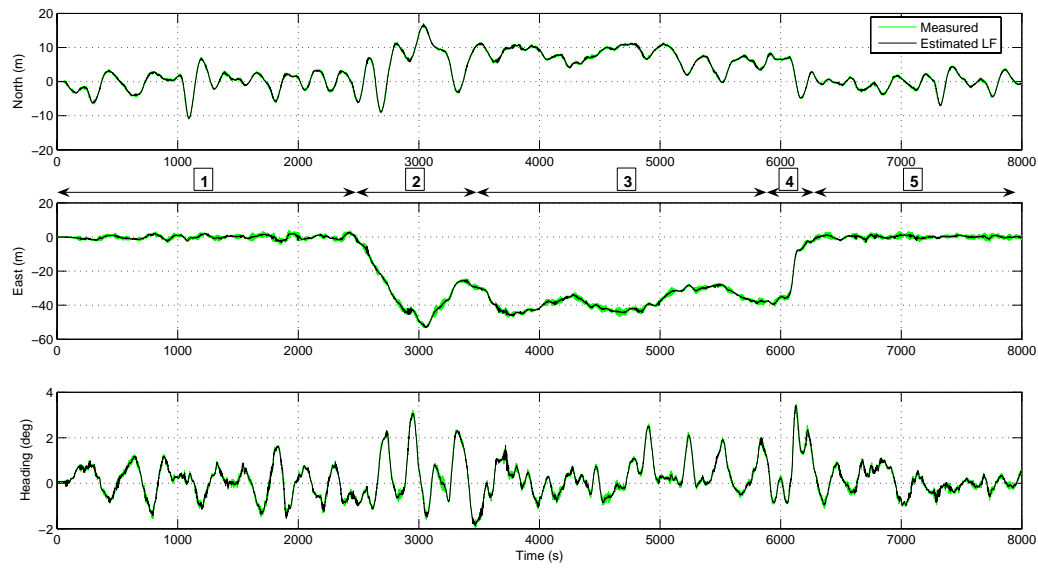


Figure 4.5a. Test 1a: performance of switching from DP to SPM mode and vice versa of the shuttle tanker: measured position and heading (solid) and their LF estimation (grey).

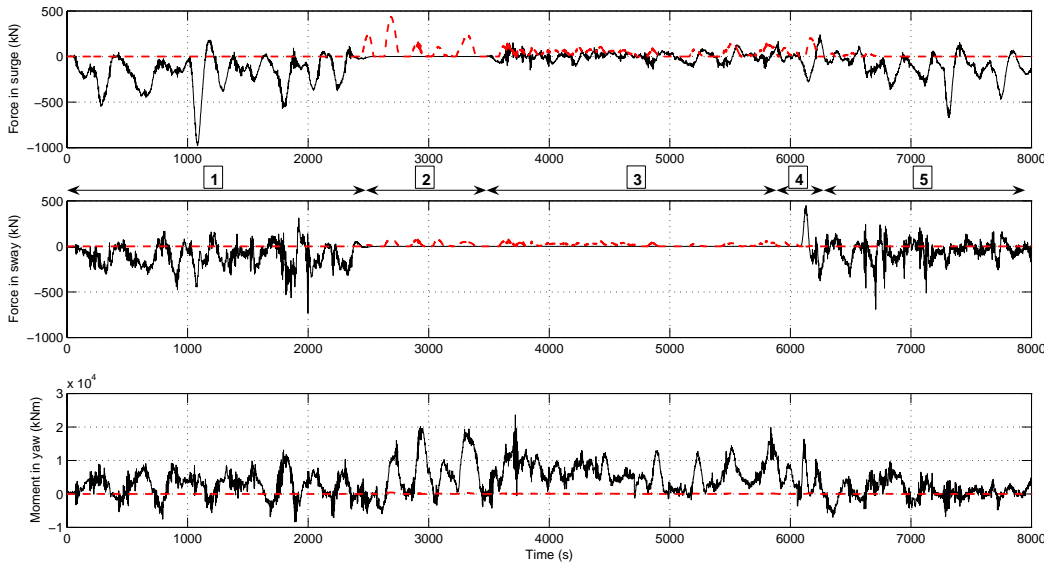


Figure 4.5b. Test 1a: control force and moment: force and moment produced by thrusters (solid), force and moment produced by the mooring system (dash).

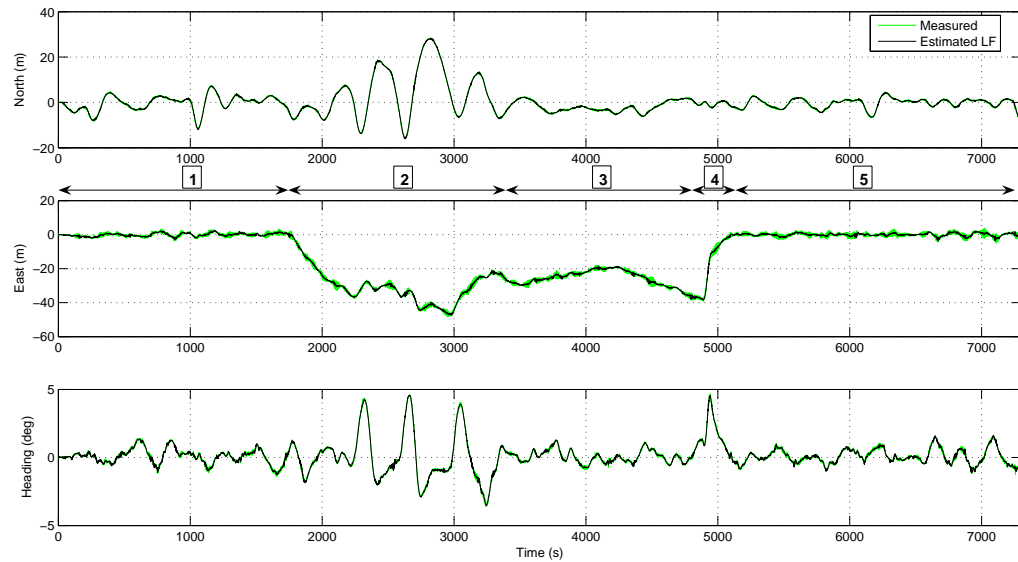


Figure 4.6a. Test 2a: performance of switching from DP to SPM mode and vice versa of the shuttle tanker: measured position and heading (solid) and their LF estimation (grey).

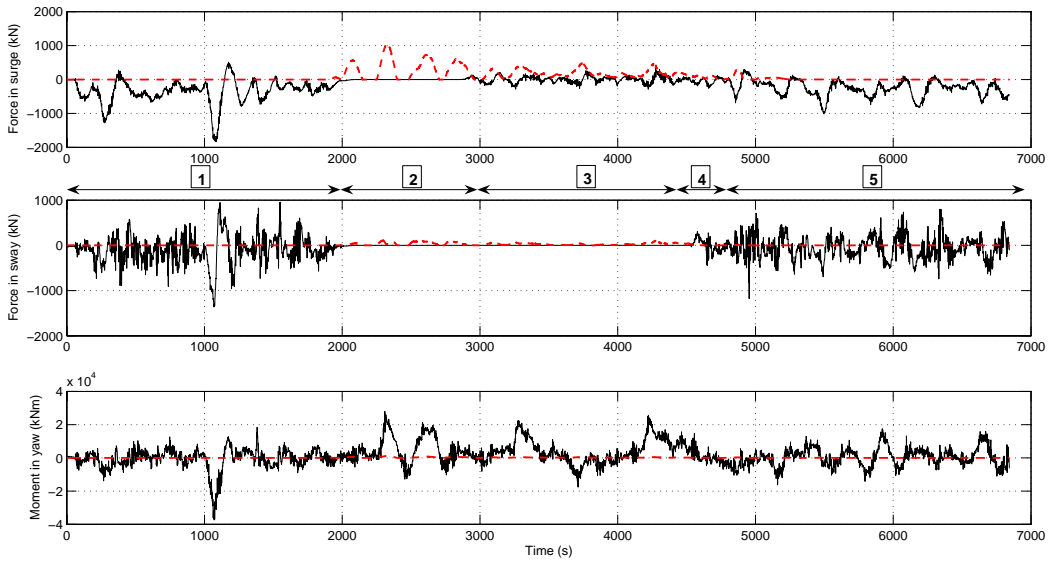


Figure 4.6b. Test 2a: control force and moment: force and moment produced by thrusters (solid), force and moment produced by the mooring system (dash).

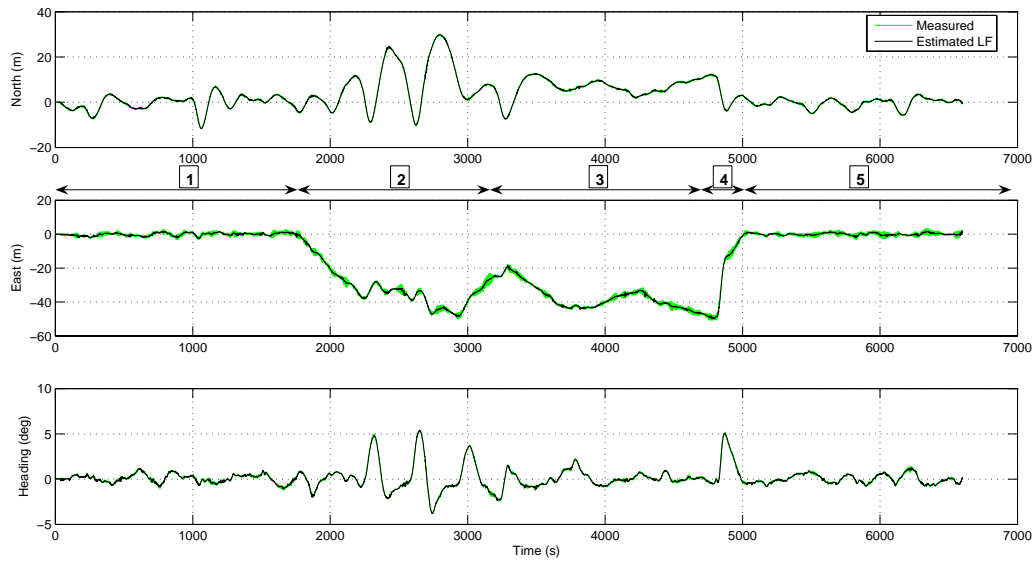


Figure 4.7a. Test 3a: performance of switching from DP to SPM mode and vice versa of the shuttle tanker: measured position and heading (solid) and their LF estimation (grey).

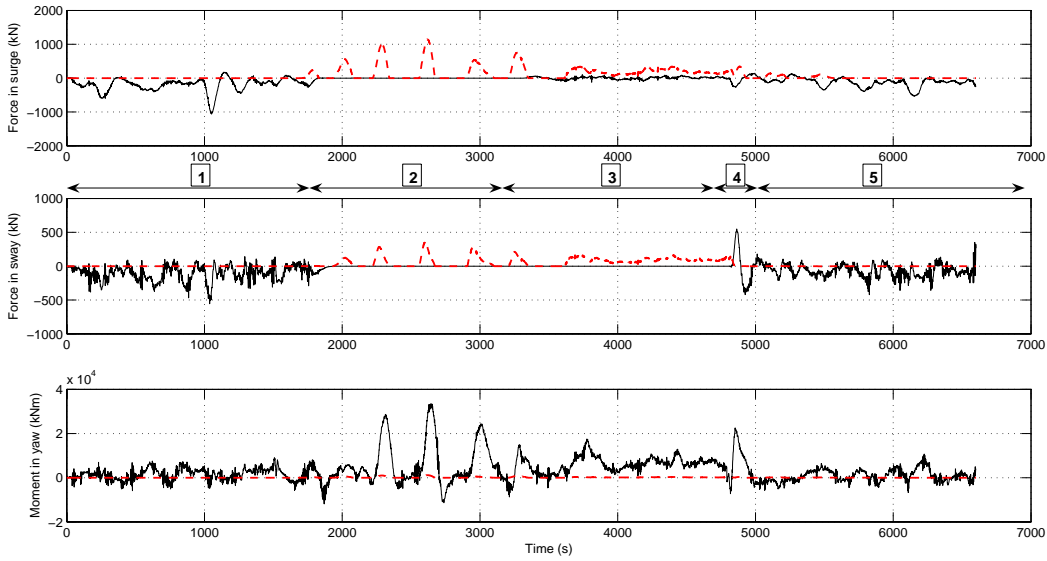


Figure 4.7b. Test 3a: control force and moment: force and moment produced by thrusters (solid), force and moment produced by the mooring system (dash).

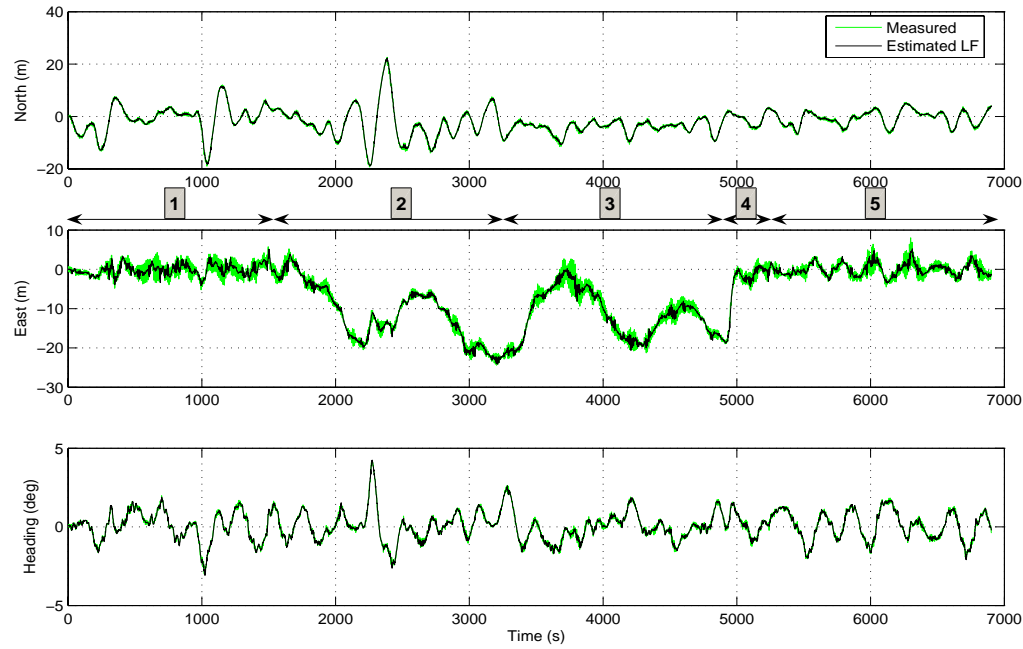


Figure 4.8a. Test 4a: performance of switching from DP to SPM mode and vice versa of the shuttle tanker: measured position and heading (solid) and their LF estimation (grey).

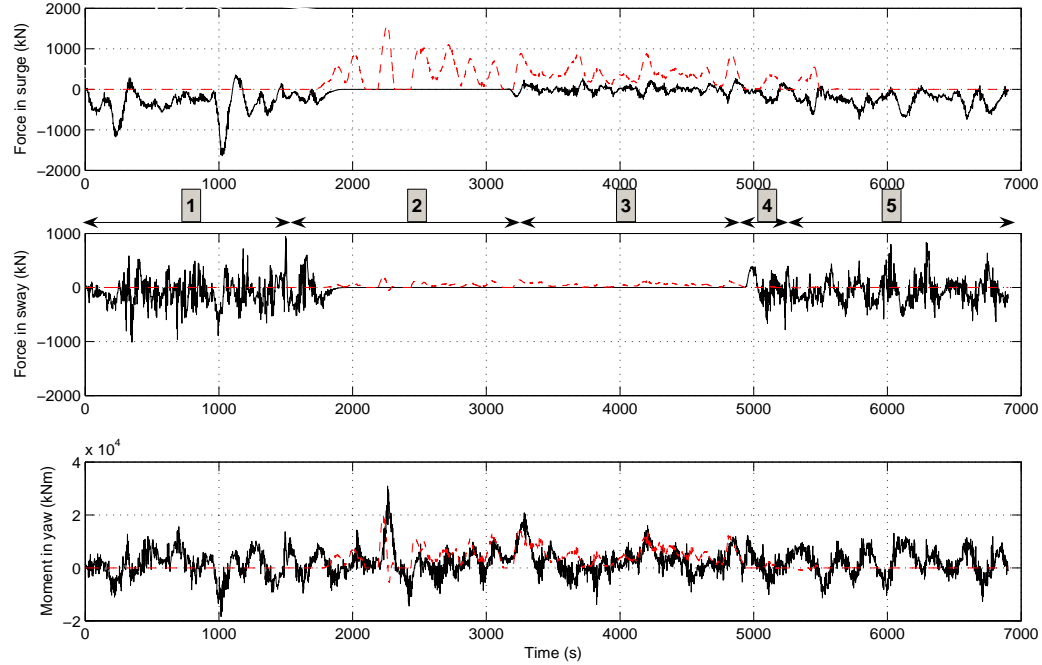


Figure 4.8b. Test 4a: control force and moment: force and moment produced by thrusters (solid), force and moment produced by the mooring system (grey).

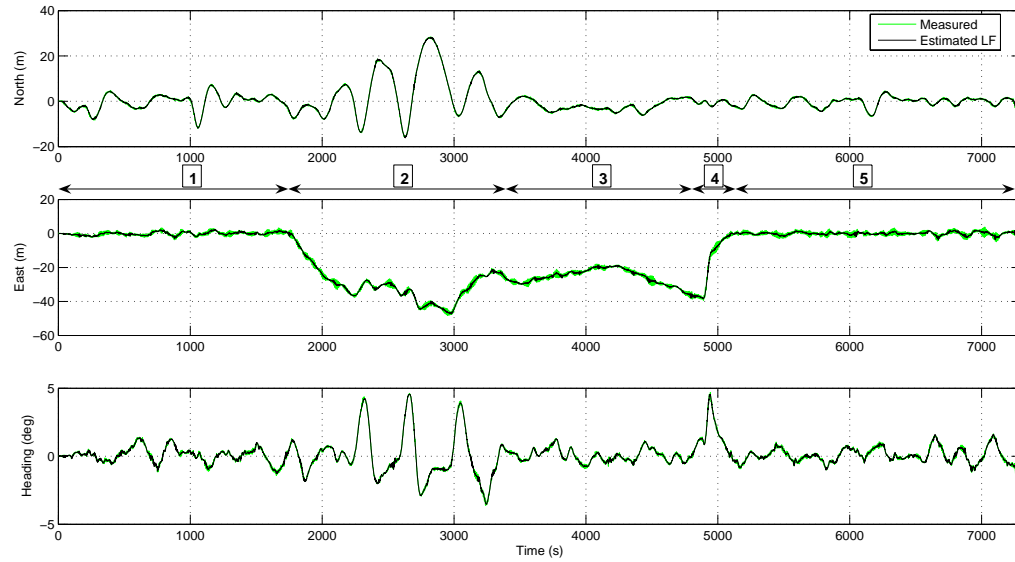


Figure 4.9a. Test 5a: performance of switching from DP to SPM mode and vice versa of the shuttle tanker: measured position and heading (solid) and their LF estimation (grey).

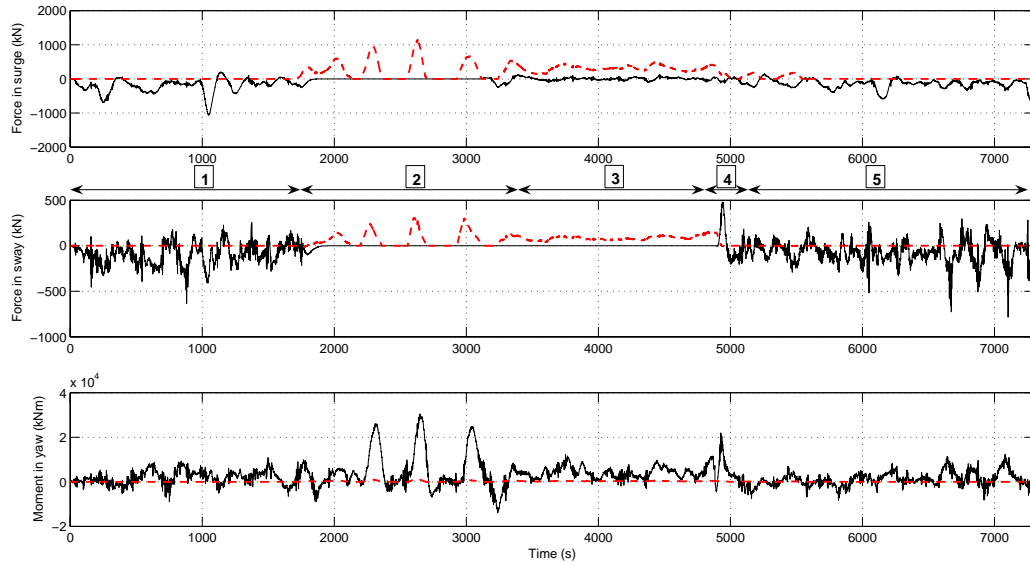


Figure 4.9b. Test 5a: control force and moment: force and moment produced by thrusters (solid), force and moment produced by the mooring system (dash).

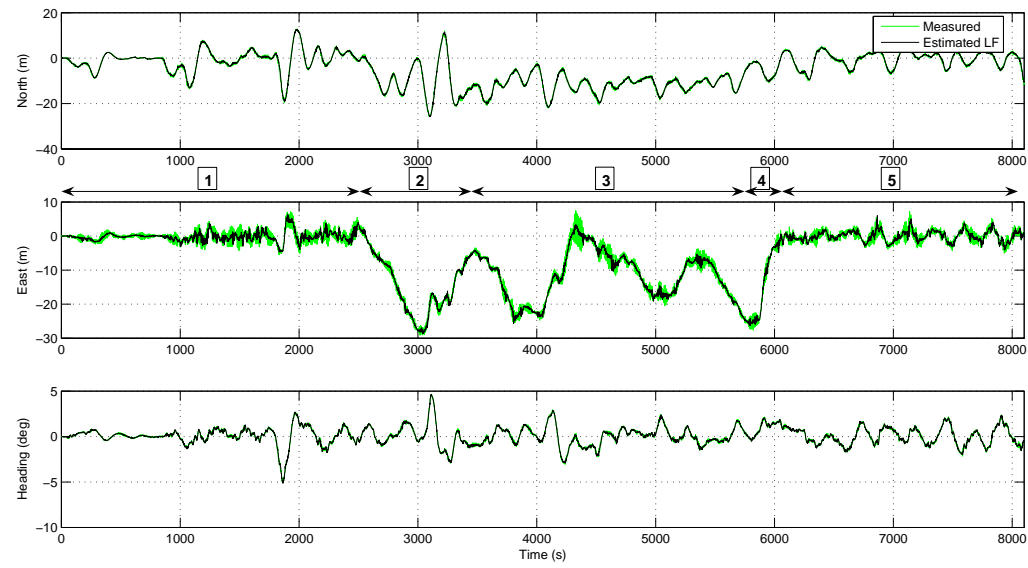


Figure 4.10a. Test 6a: performance of switching from DP to SPM mode and vice versa of the shuttle tanker: measured position and heading (solid) and their LF estimation (grey).

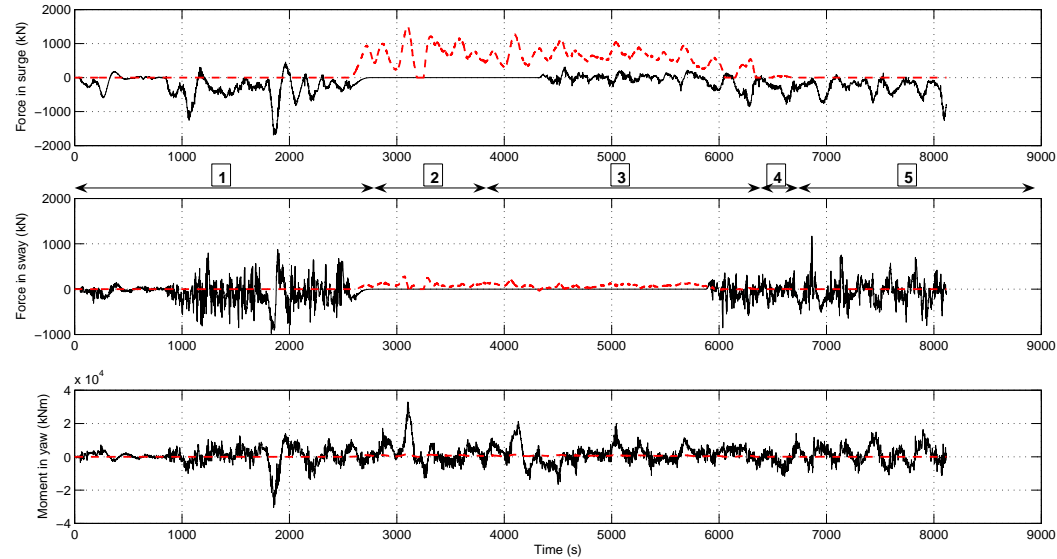


Figure 4.10b. Test 6a: control force and moment: force and moment produced by thrusters (solid), force and moment produced by the mooring system (dash).



Figure 4.11. STL model: four mooring lines connected to the floating turret which can be connected and disconnected to the bow of the Cybership III. The turret can be freely rotated relatively to the mooring system.

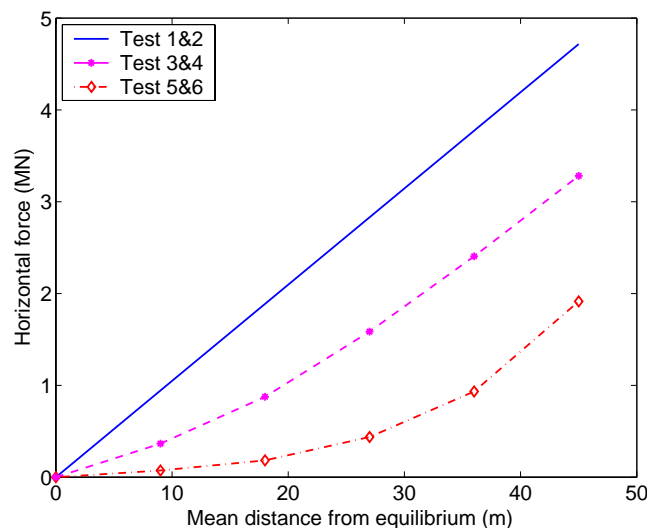


Figure 4.12. Three mooring system configurations.

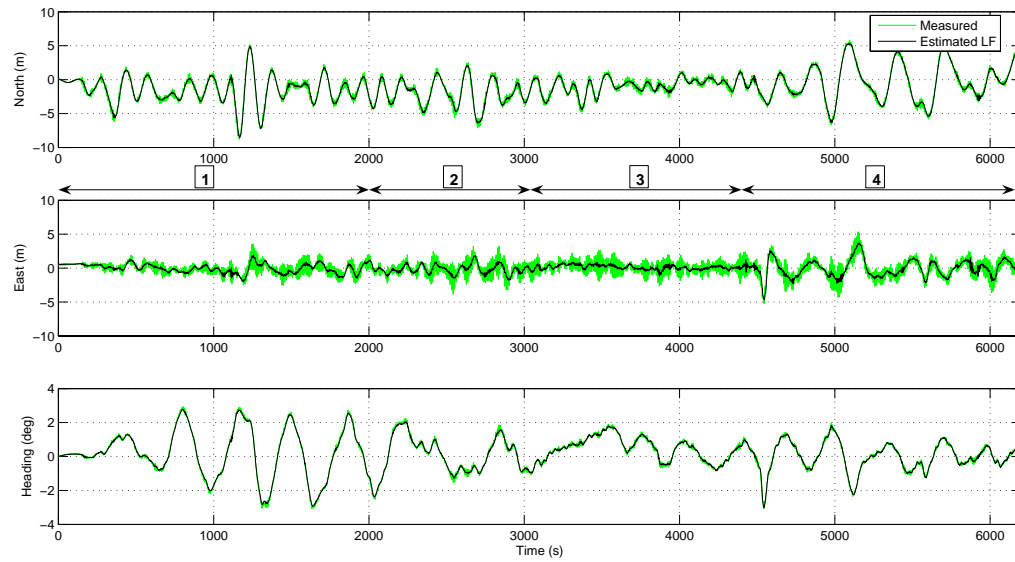


Figure 4.13a. Test 1b: performance of switching from STL to DP mode of the shuttle tanker: measured position and heading (solid) and their LF estimation (grey).

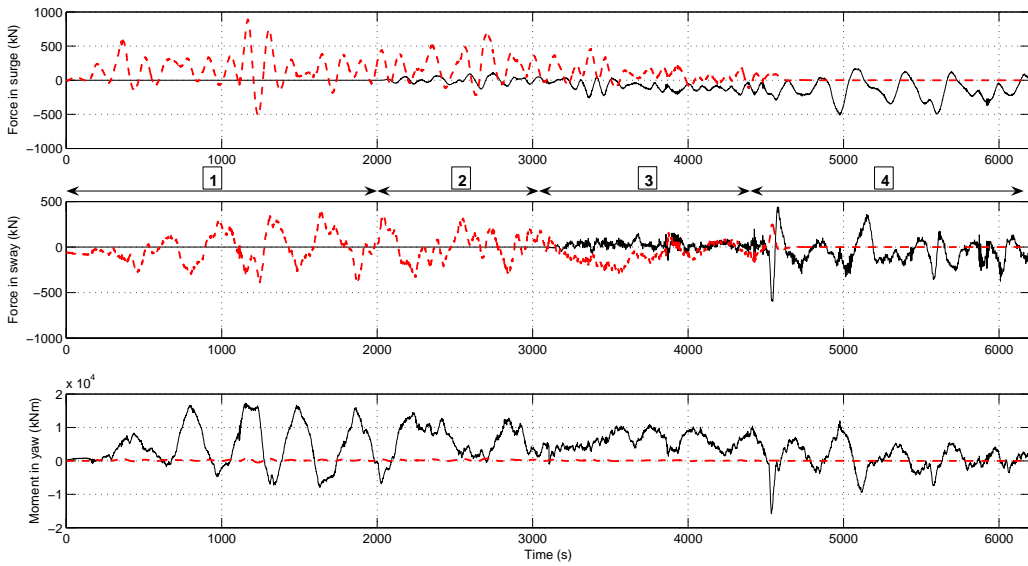


Figure 4.13b. Test 1b: control force and moment: force and moment produced by thrusters (solid), force and moment produced by the mooring system (dash).

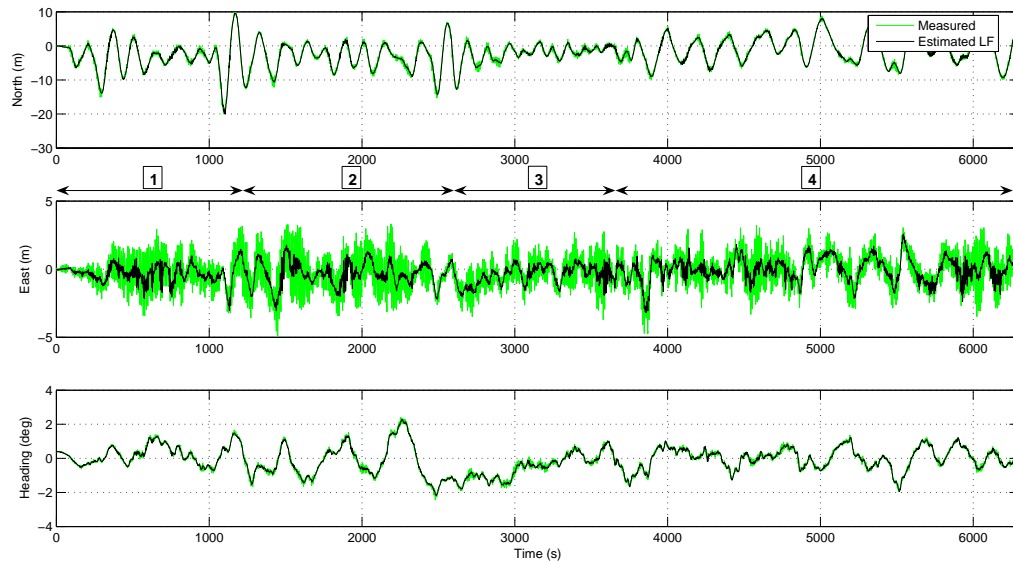


Figure 4.14a. Test 2b: performance of switching from STL to DP mode of the shuttle tanker: measured position and heading (solid) and their LF estimation (grey).

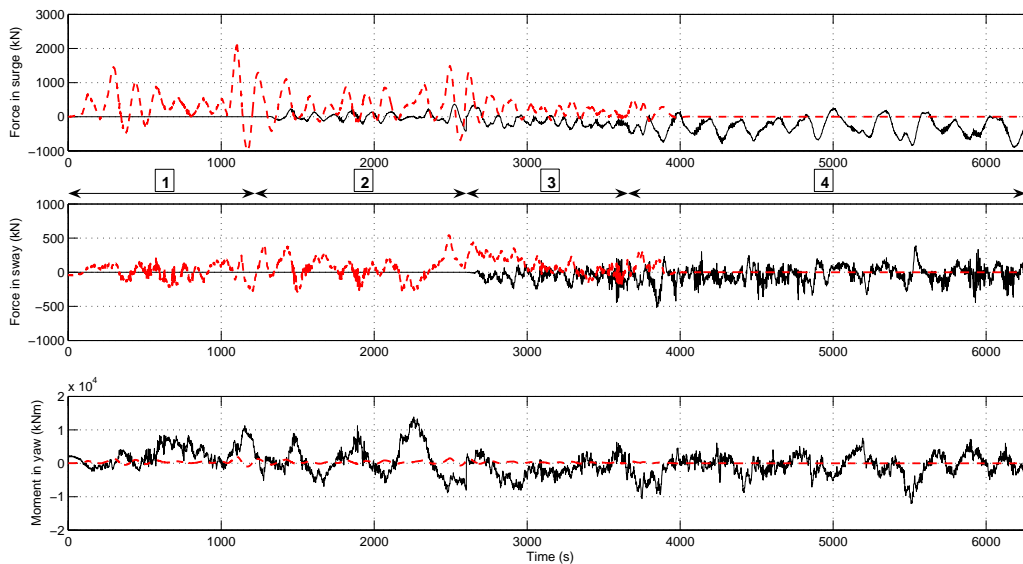


Figure 4.14b. Test 2b: control force and moment: force and moment produced by thrusters (solid), force and moment produced by the mooring system (dash).

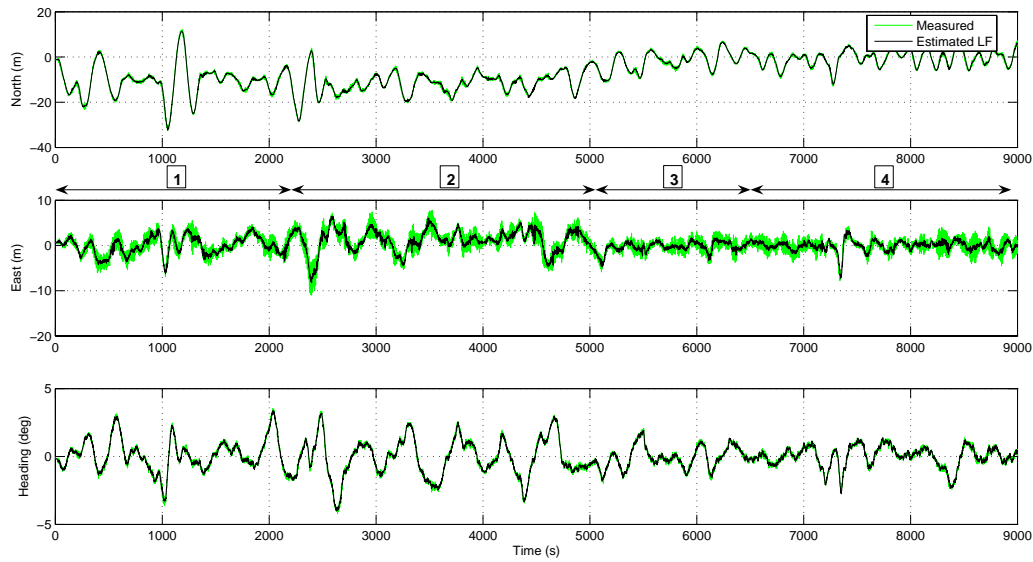


Figure 4.15a. Test 3b: performance of switching from STL to DP mode of the shuttle tanker: measured position and heading (solid) and their LF estimation (grey).

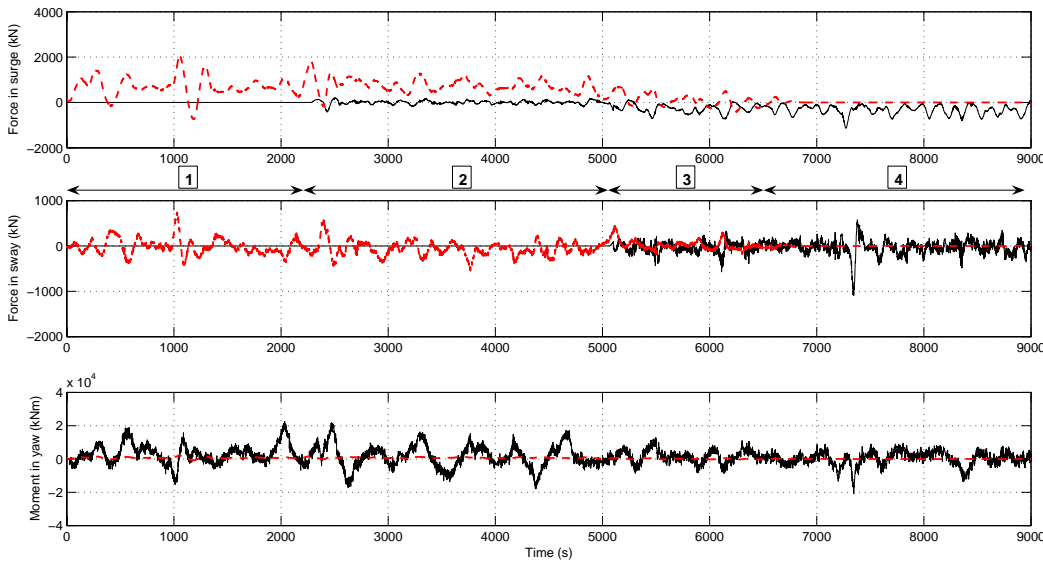


Figure 4.15b. Test 3b: control force and moment: force and moment produced by thrusters (solid), force and moment produced by the mooring system (dash).

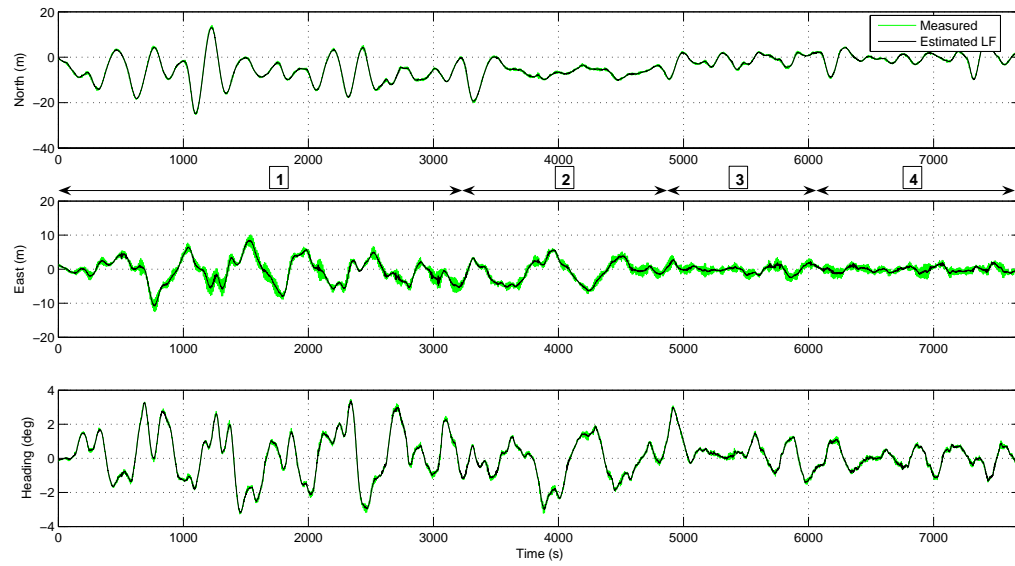


Figure 4.16a. Test 4b: performance of switching from STL to DP mode of the shuttle tanker: measured position and heading (solid) and their LF estimation (grey).

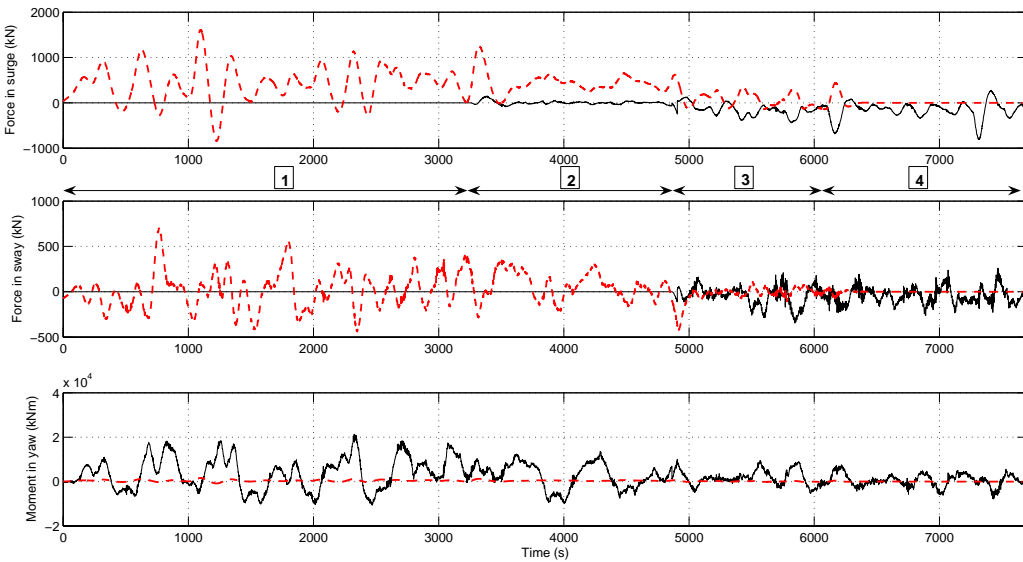


Figure 4.16b. Test 4b: control force and moment: force and moment produced by thrusters (solid), force and moment produced by the mooring system (dash).

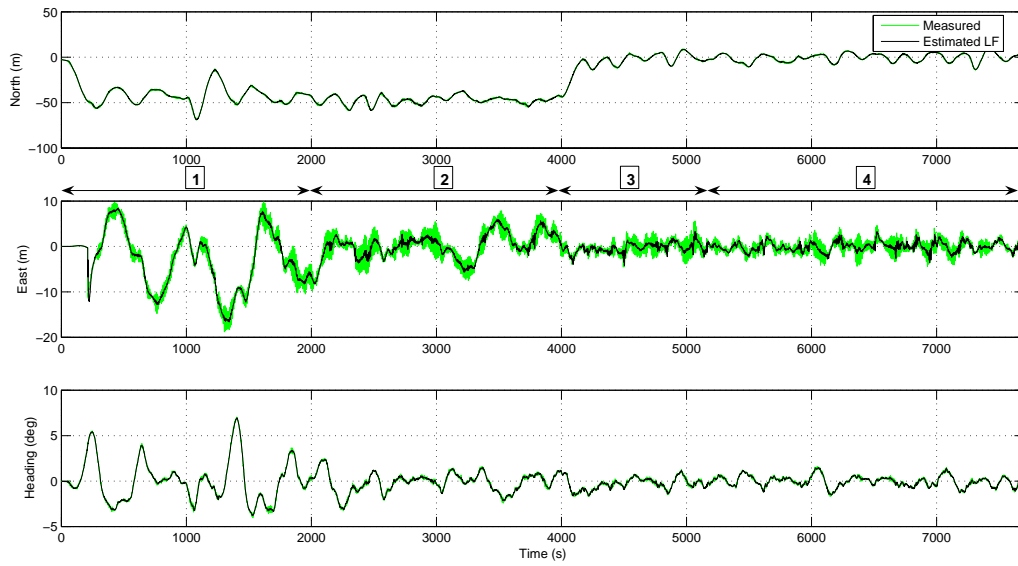


Figure 4.17a. Test 5b: performance of switching from STL to DP mode of the shuttle tanker: measured position and heading (solid) and their LF estimation (grey).

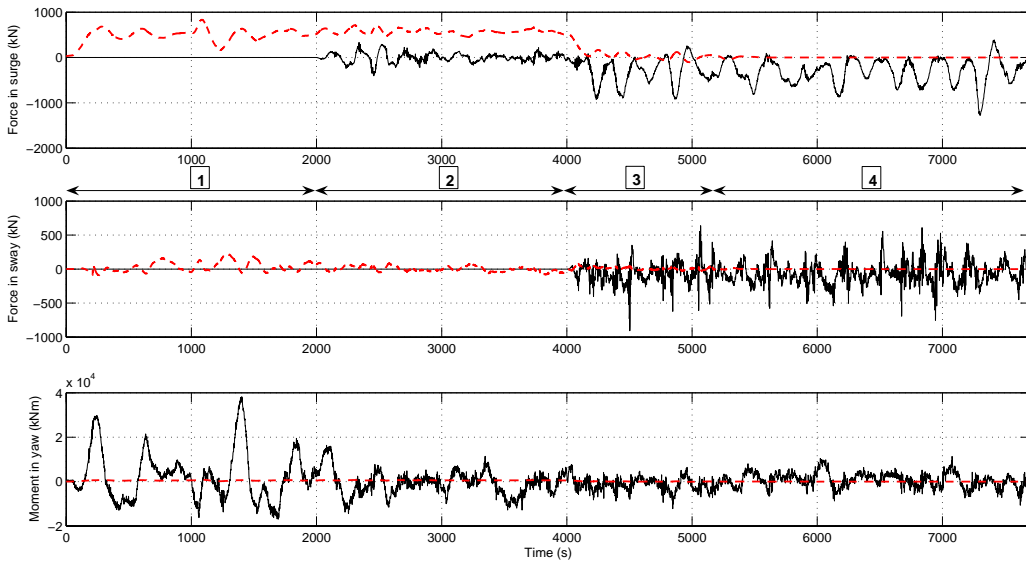


Figure 4.17b. Test 5b: control force and moment: force and moment produced by thrusters (solid), force and moment produced by the mooring system (dash).

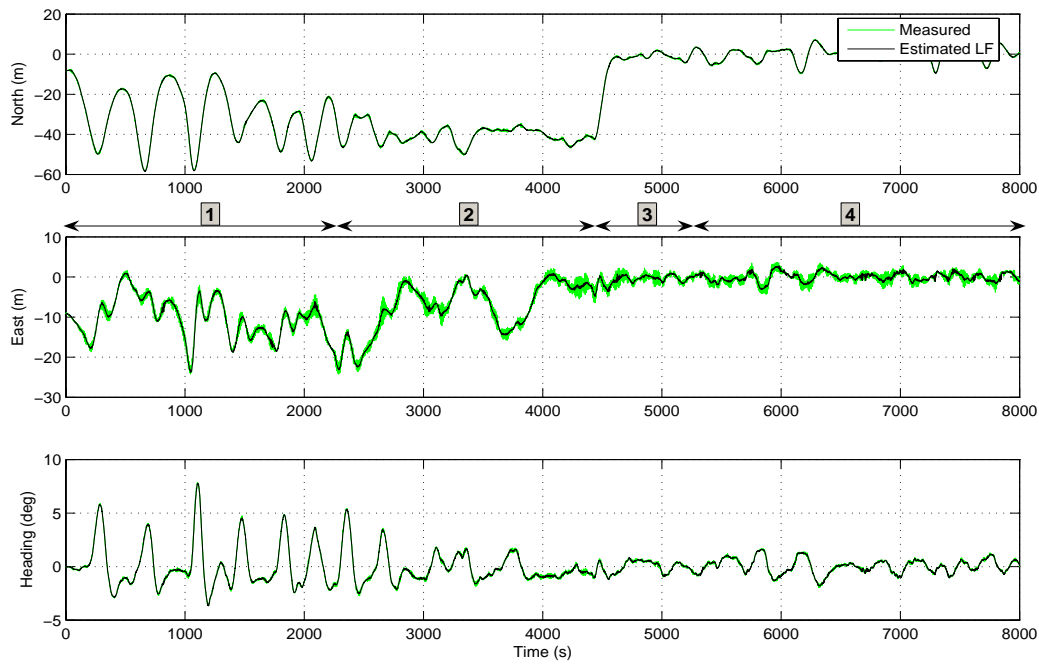


Figure 4.18a. Test 6b: performance of switching from STL to DP mode of the shuttle tanker: measured position and heading (solid) and their LF estimation (grey).

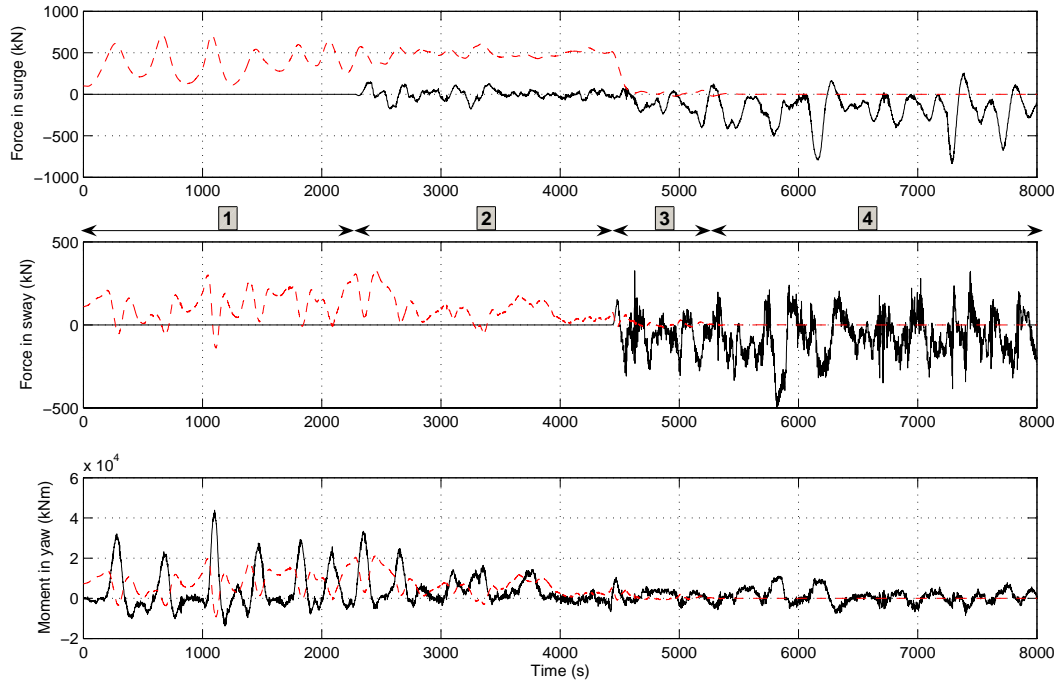


Figure 4.18b. Test 6b: control force and moment: force and moment produced by thrusters (solid), force and moment produced by the mooring system (grey).

Chapter 5 Design of Observer and Controller for Dynamic Positioning in Moderate and Extreme Seas

5.1 Introduction

Most of the current DP systems have been designed to operate up to a certain limit of weather condition (Balchen et al., 1976; Balchen et al., 1980; Sørensen et al., 1996; Fossen and Strand, 1999; Strand and Fossen, 1999; Sørensen and Strand, 2000; Sørensen et al., 2001; Fossen and Strand, 2001; and Fossen, 2002). These DP systems at plant control level contain basically of one observer and controller often with adaptive wave frequency tracking and gain scheduling to cope with varying sea states and bandwidth requirements. The latter is implemented as human operator defined gain inputs from low to high gains. The observer is used to estimate the unmeasured states and filter the measurements. The states are then used by the output controller.

In low to moderate sea, the WF motion is of high frequency and with increasing intensity; therefore it is neither needed nor impossible to compensate this motion by the DP system. To reduce unnecessary high frequency thruster modulations resulting in increased wear and tear and fuel consumption, the DP system should counteract the LF motions rather than the WF motions. The conventional observer filters out the WF motions from the measured position, and estimates the LF position and velocity. In the early studies, Balchen et al. (1976, 1980) and Sørensen et al. (1996) used the Kalman filter in the observer to filter the WF motion. Later, Fossen and Strand (1999) introduced the nonlinear passive observer. Strand and Fossen (1999) improved the nonlinear passive observer with recursively adaptive WF filtering. The disadvantage of the recursively adaptive observer is the difficulty in tuning, resulting in limited industrial applications. The use of a parametrically adaptive observer makes it easier

to filter the WF motion. This observer has been theoretical and numerically simulated by Torsetnes (2004) and Nguyen et al. (2004). However, it has not been experimentally examined.

The common controller for DP in moderate sea is the PID controller. The PD controller is used to counteract the oscillatory environmental loads. The integral controller is used to counteract the mean environmental loads, and therefore cancels the steady state deviation from desired values.

In low to moderate sea states, the observer with WF filtering and PID controller work quite well. However, in extreme seas when the WF motions are of low frequency and within the LF domain, separation of WF and LF motions is not evident (Sørensen et al., 2002). The observer for DP in extreme seas should estimate total motion, instead of filtering out the WF motion. In addition, the motion of the vessel is of large amplitude then PID controller may not be adequate to compensate the environmental loads in extreme seas. It was shown that the acceleration feedback in combination with PID controller will improve the performance of the DP vessel (Lindegård, 2003). This controller, in short AFB, adds virtual mass to physical mass of the vessel; therefore, the vessel is influenced to a lesser extent by the environmental excitations. However, the observer without WF filtering has not been experimentally studied and the AFB has not been studied for harsh seas.

The objectives of the research presented in this chapter are to:

- (1) study the observer with adaptive WF filtering where the peak frequency of wave is estimated via spectral analysis of the measured responses (Section 5.2),
- (2) study the observer without WF filtering for extreme seas as proposed by Sørensen et al. (2002) (Section 5.3), and
- (3) study the effectiveness of AFB in extreme sea (Section 5.4).

5.2 Observer with Parametrically Adaptive WF Filtering

In moderate sea, the observer with WF filtering has been designed for DP system; for example, Balchen (1976) used a Kalman filter observer whereas Fossen and Strand (1999) employed a nonlinear passive observer. It should be noted that the two types of observers are based on the *a priori* knowledge of the sea state to filter the WF motions; this means ω_p is assumed to be known. However, over a longer time frame, the sea state may change, and therefore ω_p in general is not known. For efficient wave filtering, an adaptive observer is proposed here to capture the varying sea states.

The peak frequency of wave (PFW), ω_p , which is used to address the dominating frequency of a wave spectrum, is assumed to be an unknown slowly-varying parameter. By performing spectral analysis of the position (surge, sway) and heading (yaw) measurements, the dominating wave-response frequencies of these three modes can be found, denoted as $\hat{\omega}_1$, $\hat{\omega}_2$ and $\hat{\omega}_3$. The estimated PFW, $\hat{\omega}_p$, may be taken as the median value of $\hat{\omega}_1$, $\hat{\omega}_2$ and $\hat{\omega}_3$, that is $\hat{\omega}_p \approx \text{median}(\hat{\omega}_1, \hat{\omega}_2, \hat{\omega}_3)$ as shown in Figure 5.1, although in practice, the estimated PFW has been set as one of the three values of $\hat{\omega}_i$ or as the average of three values.

The estimation of PFW based on spectral analysis of measured surge, sway and yaw, in some cases such as calm and moderate sea states, may be difficult to determine. The main reason is that the vessel generally acts as a low pass filter since the high frequency motion has virtually no effect on the vessel due to its large mass. Hence, the signal is not strong and easily overwhelmed by noise making spectral analysis prone to error. Depending on the condition of the developed sea, it may also be difficult to find only one single peak frequency. The response frequency band may be broader than that of fully wind developed seas, which have a distinct peak value. In

the case of swell, in addition to wind generated seas, it may be difficult to distinguish the WF of wind developed sea from that of swell.

Although the roll and pitch measurements may be more sensitive to calm and moderate seas and hence conducive for spectral analysis, the drawback is that their frequencies are close to the natural frequencies (resonances) of floating structures that determining PFW can be problematic. Wind measurements may also be a good indication of the sea state, based on the assumption that the seas is wind generated and that the fetch length is long enough.

In this thesis, the PFW is updated by the estimated dominating wave-response frequencies of the surge, sway and yaw measurements. This estimated PFW will be used in the nonlinear passive observer with parametrically adaptive WF filtering which is numerically and experimentally studied in the following subsections. The stability analysis for observer with parametrically adaptive WF filtering using contraction theory was provided by Torsetnes (2004).

5.2.1 Formulation

The control plant model in Fossen and Strand (1999) is derived by simplifying the process plant model, (2.7), (2.8), (2.47) and (2.48), resulting in the following

$$\dot{\mathbf{p}}_w = \mathbf{A}_{pw}\mathbf{p}_w + \mathbf{E}_{pw}\mathbf{w}_{pw}, \quad (5.1)$$

$$\dot{\mathbf{b}} = \mathbf{E}_b\mathbf{w}_b, \quad (5.2)$$

$$\mathbf{M}\dot{\mathbf{v}} = -\mathbf{D}\mathbf{v} + \mathbf{R}^T(\psi)\mathbf{b} + \boldsymbol{\tau}_{thr}, \quad (5.3)$$

$$\dot{\boldsymbol{\eta}} = \mathbf{R}(\psi)\mathbf{v}, \quad (5.4)$$

$$\mathbf{y} = \boldsymbol{\eta} + \mathbf{C}_w\mathbf{p}_w + \mathbf{v}, \quad (5.5)$$

where $\mathbf{p}_w \in \mathbb{R}^6$ are the WF state variables; \mathbf{w}_w , \mathbf{w}_b and $\mathbf{v} \in \mathbb{R}^3$ are the zero-mean Gaussian white noise vectors; $\mathbf{b} \in \mathbb{R}^3$ is the bias vector accounting for both slowly

varying disturbances and unmodelled dynamics; $\mathbf{E}_b = \text{diag}(e_{b1}, e_{b2}, e_{b3})$ is a diagonal scaling matrix, $\tau \in \mathbb{R}^3$ is the control vector. The WF motion is modelled by a second-order model (5.1) and (5.5), where

$$\mathbf{A}_{pw} = \begin{bmatrix} \mathbf{0} & \mathbf{I} \\ -\boldsymbol{\Omega}^2 & -2\boldsymbol{\lambda}\boldsymbol{\Omega} \end{bmatrix}, \quad (5.6)$$

$$\mathbf{C}_w = [\mathbf{0} \ \mathbf{I}], \quad (5.7)$$

$$\mathbf{E}_w = \begin{bmatrix} \mathbf{0} \\ \mathbf{K}_w \end{bmatrix}, \quad (5.8)$$

in which $\boldsymbol{\Omega} = \text{diag}(\omega_1, \omega_2, \omega_3)$ is a diagonal matrix containing the dominating wave response frequencies, $\boldsymbol{\lambda} = \text{diag}(\zeta_1, \zeta_2, \zeta_3)$ is a diagonal matrix of damping ratios (ζ_i is often set between 0.1 and 0.5), and $\mathbf{K}_w = \text{diag}(k_{w1}, k_{w2}, k_{w3})$ is a diagonal scaling matrix.

The resulting observer model is found by copying the control plant model of (5.1)-(5.5) such that

$$\dot{\hat{\mathbf{p}}}_w = \mathbf{A}_{pw}\hat{\mathbf{p}}_w + \mathbf{K}_1\tilde{\mathbf{y}}, \quad (5.9)$$

$$\dot{\hat{\mathbf{b}}} = \mathbf{K}_3\tilde{\mathbf{y}}, \quad (5.10)$$

$$\dot{\hat{\mathbf{v}}} = -\mathbf{D}\hat{\mathbf{v}} + \mathbf{R}^T(\psi_y)\hat{\mathbf{b}} + \tau_{thr} + \mathbf{R}^T(\psi_y)\mathbf{K}_4\tilde{\mathbf{y}}, \quad (5.11)$$

$$\dot{\hat{\boldsymbol{\eta}}} = \mathbf{R}(\psi_y)\hat{\mathbf{v}} + \mathbf{K}_2\tilde{\mathbf{y}}, \quad (5.12)$$

$$\hat{\mathbf{y}} = \underbrace{\hat{\boldsymbol{\eta}}}_{LF} + \underbrace{\mathbf{C}_w\hat{\mathbf{p}}_w}_{WF}, \quad (5.13)$$

where $\tilde{\mathbf{y}} = \mathbf{y} - \hat{\mathbf{y}}$ is the estimation error.

The observer gain matrices is given by Fossen and Strand (1999) as

$$\mathbf{K}_1 = \begin{bmatrix} \text{diag}(k_1, k_2, k_3) \\ \text{diag}(k_4, k_5, k_6) \end{bmatrix}, \quad (5.14)$$

$$\mathbf{K}_2 = \text{diag}(k_7, k_8, k_9), \quad (5.15)$$

$$\mathbf{K}_3 = \text{diag}(k_{10}, k_{11}, k_{12}), \quad (5.16)$$

$$\mathbf{K}_4 = \text{diag}(k_{13}, k_{14}, k_{15}). \quad (5.17)$$

The tuning of these gains is based on the passivity in the observer and is proposed as

$$k_i = -2(\zeta_n - \zeta)(\omega_c/\omega_p) \quad i = 1, 2, 3, \quad (5.18)$$

$$k_i = 2\omega_p(\zeta_n - \zeta), \quad i = 4, 5, 6, \quad (5.19)$$

$$k_i = \omega_c, \quad i = 7, 8, 9, \quad (5.20)$$

where $\omega_c > \omega_p$ is the filter cut-off frequency. $\zeta_n > \zeta$ is a tuning parameter to be set between 0.5-1.0. $k_{10} - k_{12}$ should be sufficiently high to ensure proper bias estimation.

5.2.2 Simulation and Experimental Results

A model of a supply vessel (Table C.1) was used in the simulation to demonstrate the performance of the DP vessel using adaptive observer in moderate sea. The model ship (Cybership III – Appendix C) in the experiment is the 1:30 scaled vessel in the simulation. The vessel was exposed to the JONSWAP distributed waves with significant wave height (H_s) = 2.7 m and peak period of wave (T_p) = 8.22 s corresponding to PWF (ω_p) = 0.76 rad/s.

Figures 5.2 and 5.4 show the estimated PWF from simulation and experiment, respectively. At Stage 1, the PWF was unknown and assumed initially to be 0.86 rad/s. At Stage 2, the PWF updated from spectral analysis to approximately 0.761 rad/s based on simulation data (Figure 5.2) and 0.762 rad/s based on experiment data (Figure 5.4) which captured quite well the real sea state with $\omega_p = 0.76$ rad/s. The measured position and heading with corresponding estimated LF motion are shown in Figure 5.3 from simulation and Figure 5.5 from experiment. As shown in these two figures, while the estimated LF motion in Stage 1 was not good due to incorrect PWF input, the estimated LF in Stage 2 was quite good in terms of filtering out efficiently

WF motion. This indicates that the observer with parametrically adaptive observer works quite well. The results are similar to those of Strand and Fossen (1999).

5.3 Observer without WF Filtering

As sea state increases, the PFW shift to the low frequency range. This motivates the design of observer without WF filtering (Sørensen et al., 2002). This section investigates the observer without WF filtering for extreme sea condition. The formulation of observer without WF filtering is presented in Sub-section 5.3.1, followed by simulation and experimental results in Sub-sections 5.3.2 and 5.3.3, respectively.

5.3.1 Formulation

The nonlinear passive observer without wave filter for use in extreme seas is proposed by Sørensen (2002), given by

$$\dot{\hat{\eta}}_T = \mathbf{R}(\psi_y) \hat{\mathbf{v}}_T + \mathbf{K}_{2T} \tilde{\mathbf{y}}, \quad (5.21)$$

$$\dot{\hat{\mathbf{b}}}_T = -\mathbf{T}_b \mathbf{b}_T + \mathbf{K}_{3T} \tilde{\mathbf{y}}, \quad (5.22)$$

$$\dot{\hat{\mathbf{M}}\hat{\mathbf{v}}}_T = -\mathbf{D}\hat{\mathbf{v}}_T + \mathbf{R}^T(\psi_y) \hat{\mathbf{b}} + \boldsymbol{\tau}_{thr} + \mathbf{R}^T(\psi_y) \mathbf{K}_{4T} \tilde{\mathbf{y}}, \quad (5.23)$$

$$\hat{\mathbf{y}} = \underbrace{\hat{\eta}_T}_{\text{Total motions}}, \quad (5.24)$$

where the subscript T denotes total motion which is assumed to be of low frequency.

The stability analysis of this observer is shown in Appendix A.2.

5.3.2 Simulation Results

A model of a supply vessel (Table C.1) was used in the simulation to demonstrate the performance of the DP vessel using an observer with WF filtering under increasing sea states: $H_s = 1$ m, $T_p = 7.56$ s; $H_s = 2$ m, $T_p = 8.78$ s; $H_s = 3$ m, $T_p = 9.73$ s; $H_s = 4$ m, $T_p = 10.55$; $H_s = 4.2$ m, $T_p = 10.70$ s; and $H_s = 4.5$ m, $T_p = 10.92$ s.

Figure 5.6 shows the standard deviation of position and control force in increasing sea states. The DP vessel using observer with WF filtering became unstable in the sea state of $H_s = 4.5$ m. In this sea state, $T_p = 10.92$ s which is getting closer to the natural frequency of the DP vessel of ~ 15 s.

5.3.3 Experimental Results

Experiments with Cybership III (a 1:30 scaled model of the supply ship in simulation, see Appendix C) were carried out in this section to investigate the stability and performance of DP vessel using nonlinear passive observer with perfect adaptive WF filtering (Test 1a) and nonlinear observer without WF filtering (Test 1b using output PID and Test 1c using output AFB). The model ship was exposed to heading regular waves with $H_s = 1.2$ m and $T_p = 30$ s corresponding to $\omega_p = 0.21$ rad/s.

In order to compare the performances and control forces and moments of the three tests, the normalized statistical data obtained from the surge measurement and control force in surge direction are tabulated in Table 5.1. The performance indicators are standard deviation of surge, sway and yaw (s_x , s_y , and s_ψ); and the consumed energy indicators are those of control force in surge, sway and yaw ($s_{\tau 1}$, $s_{\tau 2}$, and $s_{\tau 3}$).

As shown in columns (2) – (4) of Table 5.1, and comparing Figures 5.7, 5.8, and 5.9, the performances of DP vessel using observer without WF filtering (Test 1b and 1c) were better than the performances of DP vessel using observer with perfect filtering (Test 1a). This indicates that the use of observer without WF filtering should improve and stabilize the performance of DP vessel in extreme sea.

Columns (6) and (7) of Table 5.1 show significant reduction of control force and moment needed in sway and yaw in the case of observer without WF filtering. This is explained by the fact that the observer with WF filtering almost destabilized and the observer without WF filtering stabilized the performance of the DP vessel. Column (1)

of Table 5.1 shows slight increase of control force needed in the case of observer without WF filtering comparing to the case of observer with WF filtering. This is expected because the vessel was exposed to heading wave and the DP system compensated both WF and LF motions in the case of observer without WF filtering rather than only LF motion in the case of observer with WF filtering.

Furthermore, the performance of DP vessel using AFB (Test 1c) was better than the performance of DP vessel using PID (Test 1b). As Tests 1b and 1c were conducted in long waves but small wave height, the effectiveness of AFB in terms of improved performance in the real harsh environments (both long and high waves) may be observed clearer. The experiments in the next Section will investigate the effectiveness of AFB in harsh environments.

5.4 Experiments with AFB in different sea states

5.4.1 Overview of Experiments

The experiments in this section were carried out to investigate and verify the effects of AFB proposed by Lindegaard (2003) in different sea states (i.e. for different significant wave heights). In order to investigate the effects of AFB in different sea states, experiments with output AFB and with purely output PID were carried out in 3 sea states as shown in Table 5.2. The model ship (Cybership III in Appendix C) in the experiments was exposed to head waves, so AFB was only implemented in surge.

5.4.2 Results and Discussions

Figures 5.10, 5.12, and 5.14 show graphical illustration for the performances of DP vessel using PID in different sea states. Figures 5.11, 5.13, and 5.15 show performances of DP vessel using AFB in corresponding sea states. In order to compare the performance and consumed energy of AFB with those of conventional PID in

different sea states, the normalized statistical data obtained from the surge measurement and control force in surge direction are tabulated in Table 5.3. The performance indicators are standard deviation of surge (s_x) and RMS-norm (RMS denotes root mean square) of surge ($\|x\|_{RMS}$) whereas the consumed energy indicators are those of control force in surge direction (s_{rl} and $\|\tau_1\|_{RMS}$, respectively).

By comparing Figure 5.11 against Figure 5.10, Figure 5.13 against Figure 5.12, and Figure 5.15 against Figure 5.14, we can observe that the surge motions of DP vessel using AFB were less oscillatory than those using PID controller. From Table 5.3, the standard deviation of position and control force in surge in the case of AFB controller (last 3 rows) were less than those in the case of PID controller (row 1). This is consistent with the result of the previous study (Lindegard, 2003) suggesting that AFB should improve the performance of DP vessel.

In addition, the performance of AFB in moderately rough sea (Test 2b) was better than in moderate sea (Test 2a) in terms of reducing the standard deviation of position and control force in surge as shown in Table 5.3. This indicates that the level of improved performance of AFB may increase in slightly harsher environment. This has not been shown in experiments of Lindegard (2003) since the hull of the model vessel in his experiments (Cybership II) was not designed for high waves. The increased effectiveness of AFB in higher sea states is expected. The phase of AFB is the same as the phase of disturbance forces. That means AFB directly cancels the effect of disturbance forces. AFB is better than position and velocity feedbacks because the phase of acceleration is earlier than the phase of position by 180° and the phase of velocity by 90° , e.g. if disturbance force is $A \sin \omega t$, then acceleration of ship is $\omega^2 A \sin(\omega t + 180^\circ)$, velocity is $\omega A \cos \omega t = \omega A \sin(\omega t + 90^\circ)$, and position is $A \sin \omega t$, where A and A_1 is the amplitude of disturbance force and response, respectively. In

addition, the acceleration measurement used in AFB is more accurate than position measurement since the acceleration measurement does not depend on the reference frame whereas position measurement does.

The last row of Table 5.3 shows the performance of DP vessel using AFB in rough sea. The position and control force were higher than those for moderately rough sea and slightly higher than those for moderate sea. The data suggest that the level of improved performance of AFB in rough sea may not be so evident. The reasons could be:

- In rough sea, tunnel thruster and main thrusters usually go in-and-out of water which is associated with severe *thrust loss*. The thruster control of Cybership III in these experiments was sharp speed control which may not be appropriate for thrust loss conditions. To reduce the effect of this problem, more sophisticated thruster control strategy, such as combined torque and power control or anti-spin control with thrust loss estimation (Smogeli et al., 2004 and 2005) should be used. Nevertheless, the real power and thrust capacity including losses will be a hard constraint for the DP capability of the vessel.
- The change of environment was done by turning off and on the wave maker. When turning on the wave maker, the *integral controller* must take some time to get a proper value. During this period (about 20 seconds or 1-2 period(s) of DP vessel), one may not see the improvement of AFB (in terms of reducing maximum position).

5.5 Conclusions

The purposes of this Chapter were to improve the observer with parametrically adaptive WF filtering for moderate seas and to develop the observer without WF

filtering and AFB for extreme seas. Both simulation and experiment showed that the observer with adaptive observer captured quite well the peak frequency of wave and therefore filtered more efficiently the WF motion. However, the use of observer with WF filtering led to the instability of the DP vessel in extreme conditions because the notch effect of this observer unintentionally filter out the LF motions. The observer without WF filtering was proposed to stabilize the DP vessel and improve its performances in extreme seas. Both simulation and experiment showed that the DP vessel using the observer without WF filtering performed much better the DP vessel using observer with WF filtering. These findings indicate that the observer with adaptive WF filtering should be used in moderate seas, and observer without WF filtering should be used in extreme seas. In the search of a better controller for the DP vessel in extreme conditions, both simulation and experiment were conducted to verify the efficiency of the AFB controller in harsh environments. They showed that the AFB controller was more effective under increasingly severe sea states. The simulation and experimental results suggest that the AFB controller should be used in extreme seas.

Based on the findings in this Chapter, the observer with and without adaptive WF filtering and the PID with and without acceleration feedback will be integrated into the hybrid DP control system making it possible for the DP vessel to operate from calm to extreme seas, to be presented in the next Chapter.

Table 5.1. Performance and consumed energy indicators (standard deviation values) normalized with respect to value obtained by Test 1.

	s_x	s_y	s_{ψ}	s_{τ_1}	s_{τ_2}	s_{τ_3}
(1)	(2)	(3)	(4)	(5)	(6)	(7)
Test 1a	1	1	1	1	1	1
Test 1b	0.93	0.06	0.05	1.35	0.19	0.18
Test 1c	0.91	0.06	0.05	1.32	0.17	0.17

Table 5.2. Experiments to investigate effects of AFB.

	Sea state	H_s (m)	T_p (s)
Test 2a	Moderate	2.5 m	9.3 s
Test 2b	Moderately rough	3.0 m	9.6 s
Test 2c	Rough	3.6 m	8.9 s

Table 5.3. Empirical performance indicators (standard deviation and RMS values) normalized with respect to values obtained by conventional PID-control.

	s_x	$\ x\ _{RMS}$	s_n	$\ \tau_1\ _{RMS}$
Standard PID	1	1	1	1
AFB1 – Test 2a	0.95	0.95	0.78	0.86
AFB2 – Test 2b	0.85	0.86	0.68	0.78
AFB3 – Test 2c	0.96	0.96	0.80	0.90

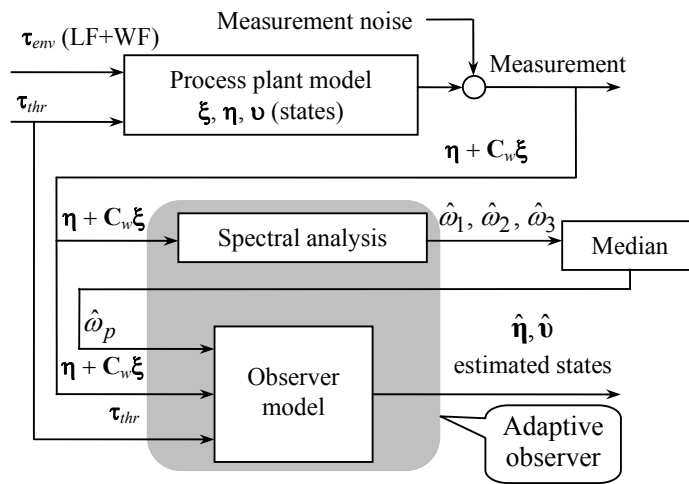


Figure 5.1. Concept of adaptive observer

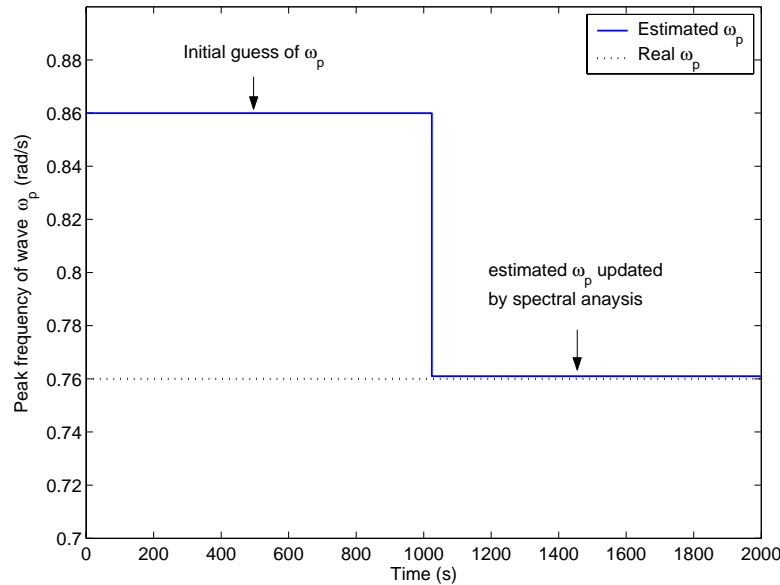


Figure 5.2. Estimated peak frequency of wave from observer with parametrically adaptive WF filtering – simulation result.

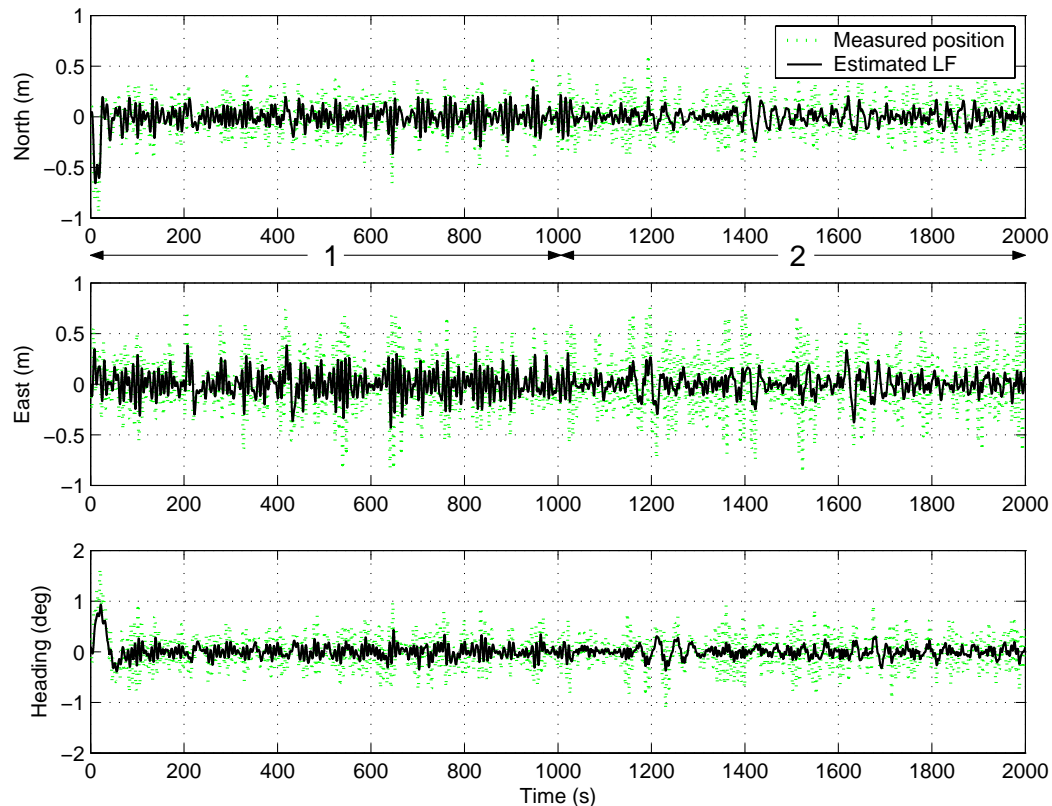


Figure 5.3. Measured position and heading (grey) and corresponding LF (black) estimates from observer with parametrically adaptive WF filtering – simulation result.

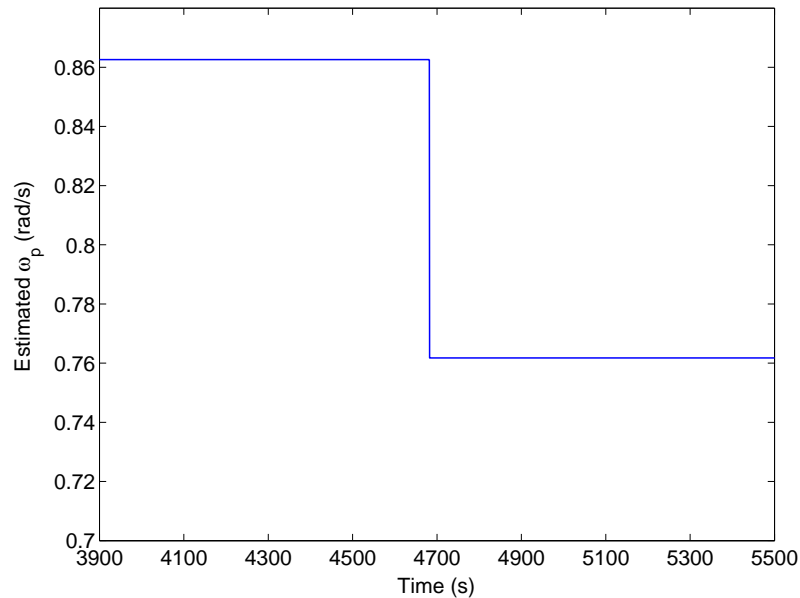


Figure 5.4. Estimated peak frequency of wave from observer with parametrically adaptive WF filtering – experimental result.

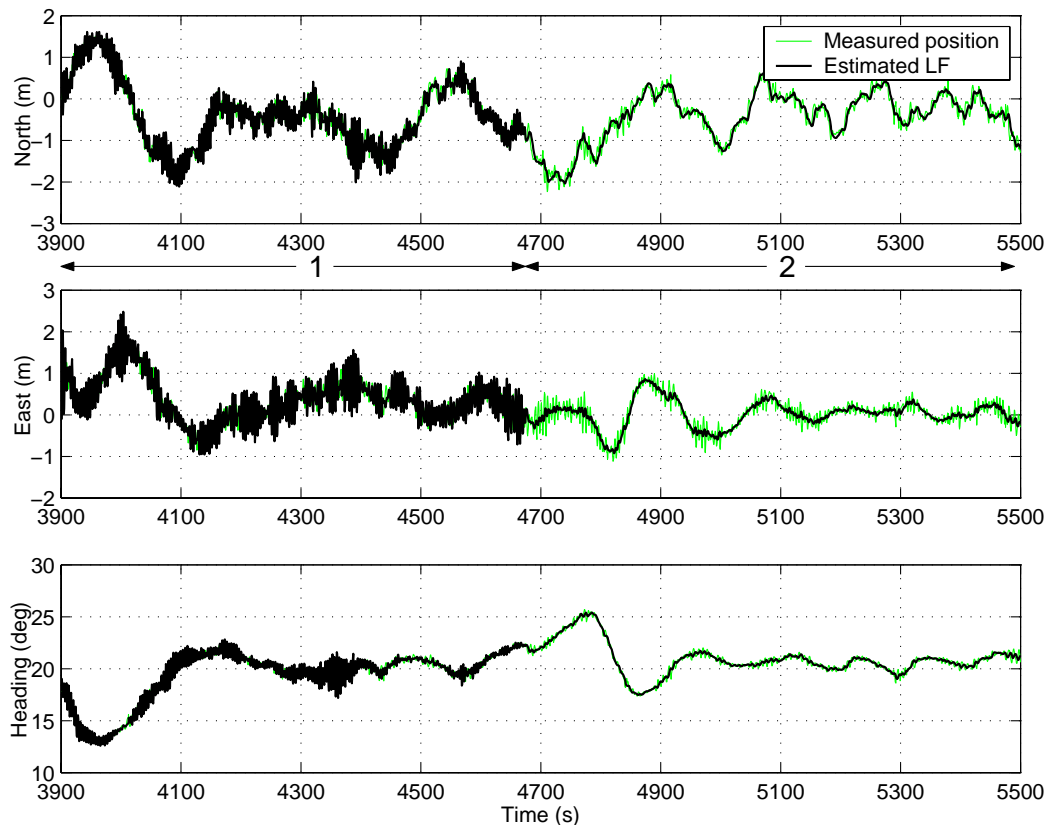


Figure 5.5. Measured position and heading (grey) and corresponding LF (black) estimates from observer with parametrically adaptive WF filtering – experimental result.

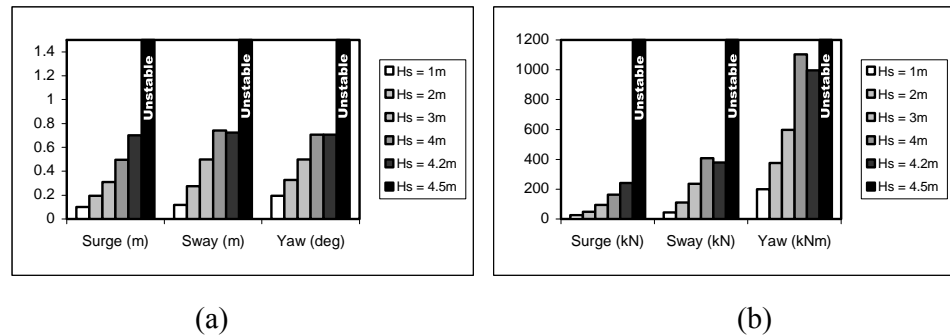


Figure 5.6. Standard deviation of (a) position; and (b) commanded control force and moment, in increasing sea states of the DP vessel using observer with WF filtering.

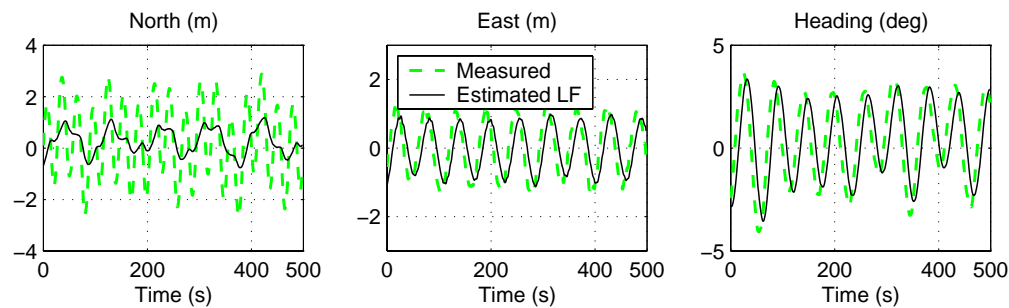


Figure 5.7. Performance of DP vessel using observer with WF filtering and output PID in extreme sea (Test 1a).

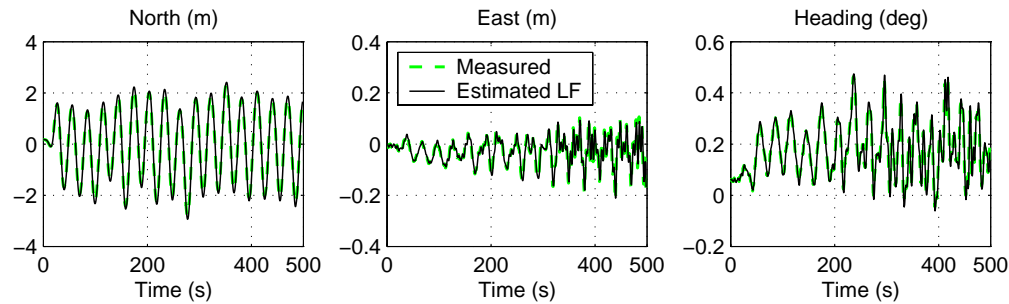


Figure 5.8. Performance of DP vessel using observer without WF filtering and output PID in extreme sea (Test 1b).

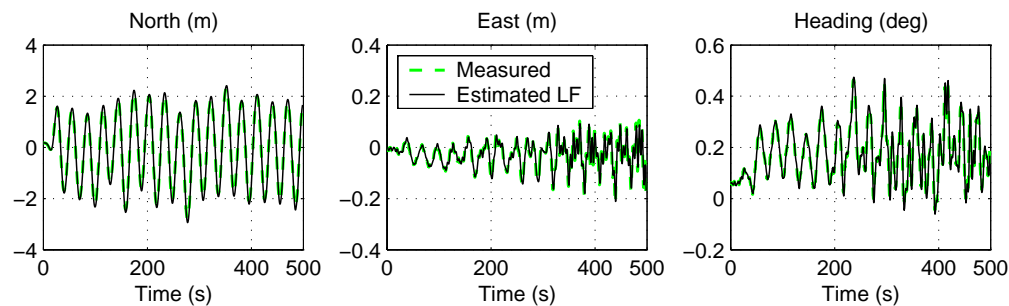


Figure 5.9. Performance of DP vessel using observer without WF filtering and output AFB in extreme sea (Test 1c).

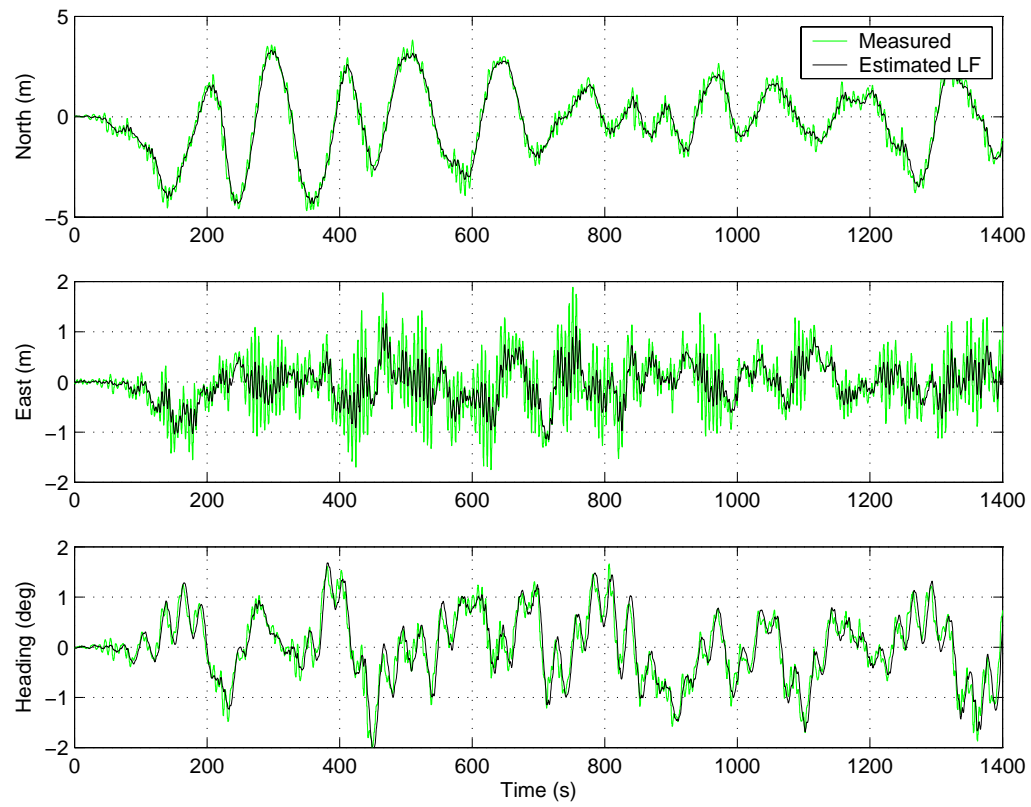


Figure 5.10. Performance of PID in moderate sea, Test 2a.

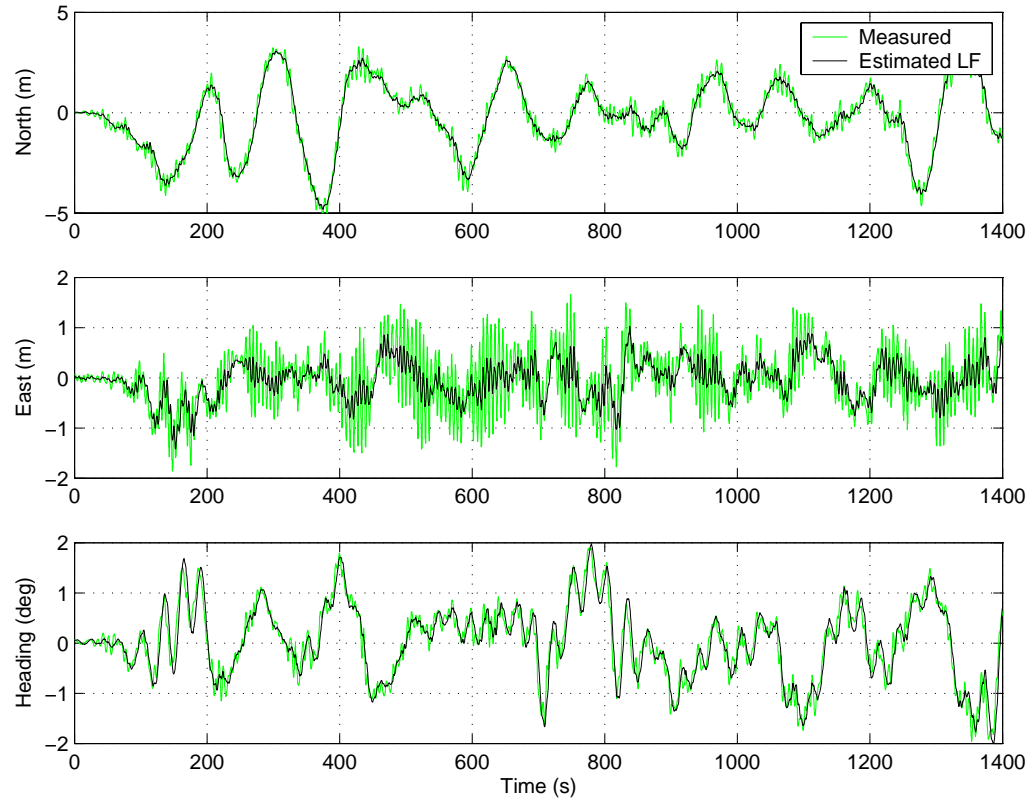


Figure 5.11. Performance of AFB in moderate sea, Test 2a.

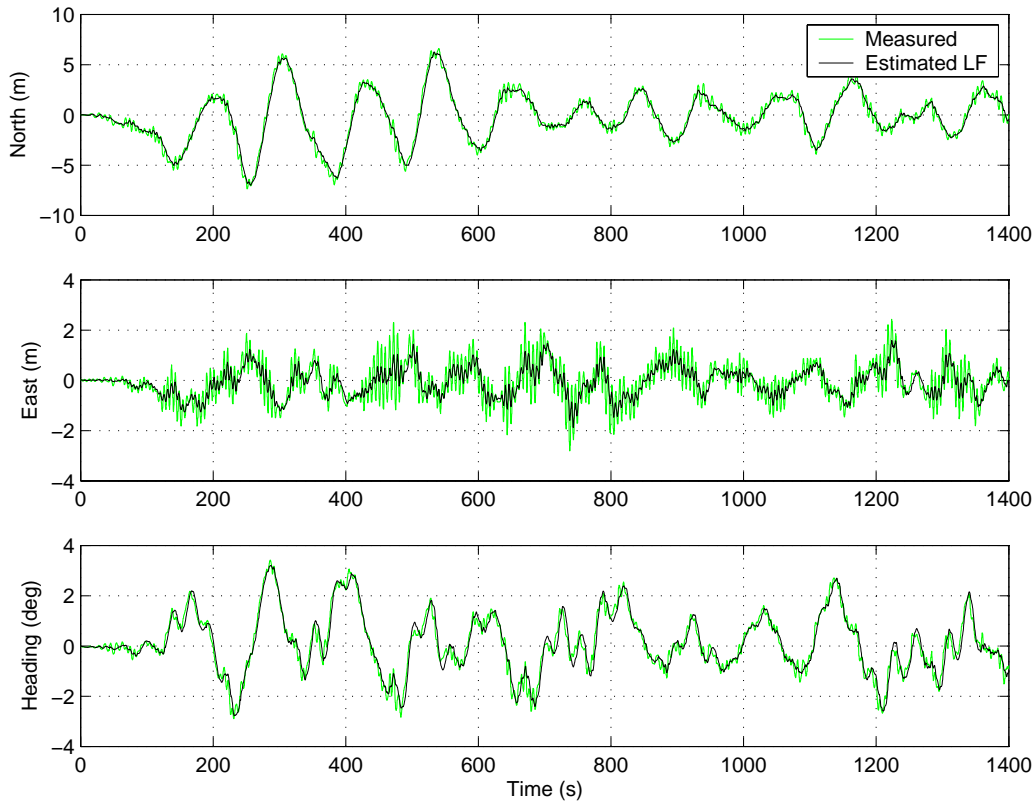


Figure 5.12. Performance of PID in moderately rough sea, Test 2b.

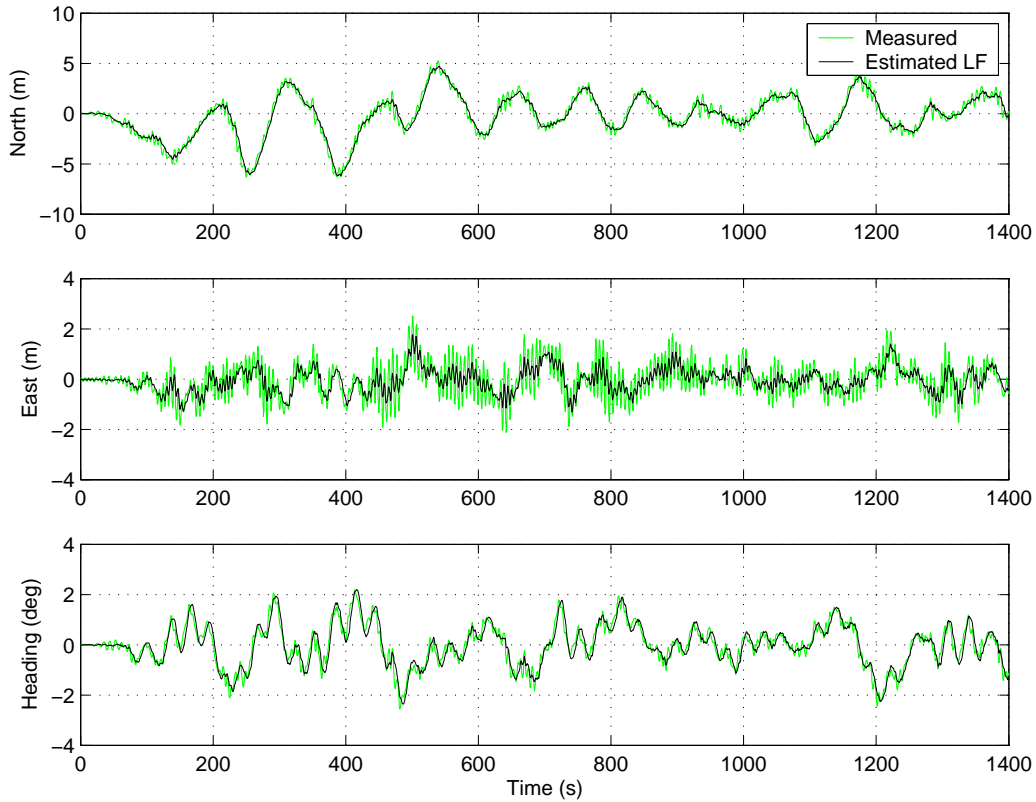


Figure 5.13. Performance of AFB in moderately rough sea, Test 2b.

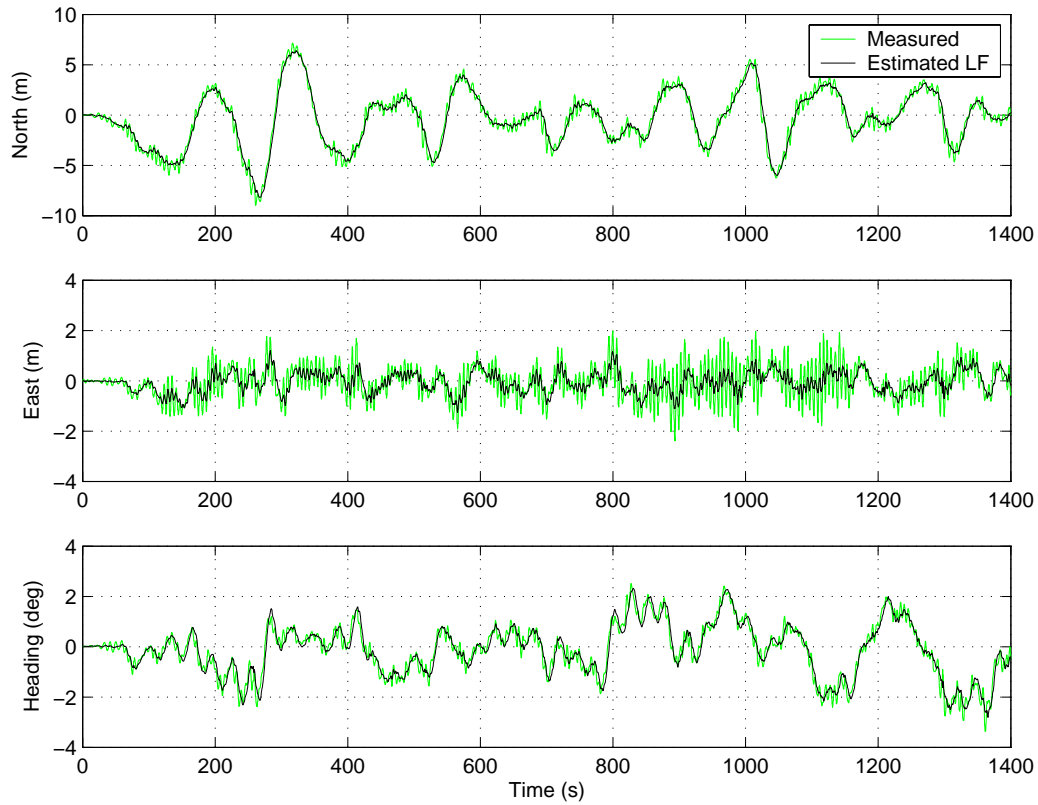


Figure 5.14. Performance of PID in rough sea, Test 2c.

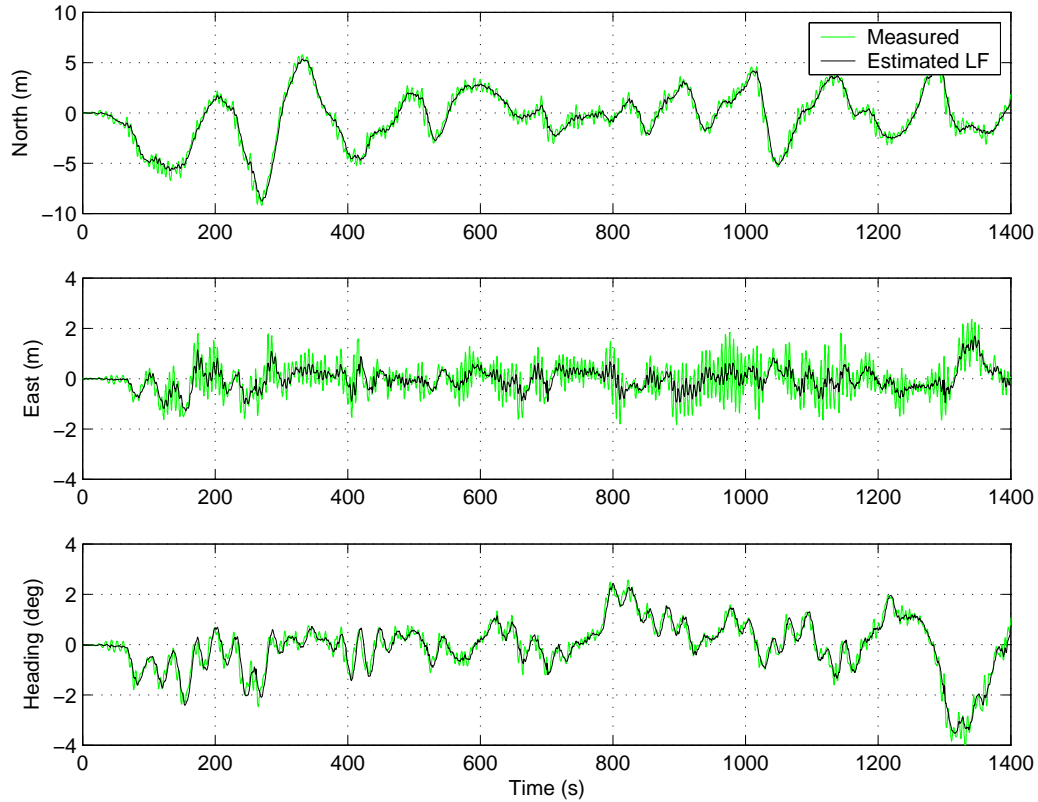


Figure 5.15. Performance of AFB in rough sea, Test 2c.

Chapter 6 Design of Hybrid Controller for Dynamic Positioning from Calm to Extreme Seas

6.1 Introduction

The main objective of this Chapter is to integrate appropriate controllers at the plant control level into a hybrid DP system capable of operating under varying conditions from calm to extreme seas. The hybrid control system consists of continuous state multi-controllers and discrete state logics that allow smooth switching among the various controllers for the particular operations and functions. To facilitate automatic smooth switching, an estimator-based supervisory control is employed here.

The proposed hybrid DP systems adopt the supervisory switching control of Hespanha (2001) employing scale-independent hysteresis switching logic to guarantee stability of the system. Two types of hybrid-controller DP system are investigated: hybrid-controller DP system using multi-PID controllers with position measurements as input to observer (Section 6.2), and hybrid-controller DP system using multi-PID and AFB controllers with position and acceleration measurements (Section 6.3).

By tracking the PFW (Section 5.2) using the spectral analysis of surge, sway and yaw measurements, the sea states can be detected. The definitions of sea states with associated ranges of wave heights and PFW (Price and Bishop, 1974) are shown in Table 6.1. These values are only indicative. In the Barents Sea, experiences by vessel contractors/operators indicated that the PFW associated with the corresponding significant wave height may be even lower than what are shown in the Table.

In order to validate the proposed hybrid DP system, stability analysis, numerical simulations and experiments are provided in Sections 6.4, 6.5 and 6.6, respectively. Finally, Section 6.7 provides the conclusions to this Chapter.

6.2 Hybrid Controller DP System Using Multi-output PID Controllers with Position Measurement

Based on Table 6.1 and using the concept of hybrid controller, four environmental conditions are considered and denoted as 1, 2, 3 and 4 for calm, moderate, high and extreme seas, respectively. Table 6.2 shows definition of sea conditions associated with a particular supply vessel (Table C.1), the process switching signal, ρ , and the switching signal, σ , according to the PFW. Figure 6.1 shows the structure of the proposed hybrid controller. The model set comprises four models and the controller set comprises four controllers corresponding to the four sea conditions.

In this section, adaptive WF filtering observer and output feedback PID controller are used in calm and moderate seas corresponding to model 1 and 2, respectively. An observer without WF filtering and an output feedback PID controller are used in extreme seas corresponding to model 4. Observers and controllers facilitating smooth transformation from moderate to extreme seas are used in high seas corresponding to model 3.

Controller 3 is introduced in the transition regime between moderate and extreme seas but not in the transition regime between calm and moderate seas, since there is significant change of observer and controller structure between moderate and extreme seas. In addition, this controller provides freedom in selecting the value of PFW to define “extreme” and “moderate” seas, since it is dependent on vessel size. Hence, the limits of PFW to disable and enable WF filtering are different for different type of vessel.

6.2.1 Output PID Controller for Calm and Moderate Seas (Models 1 and 2)

6.2.1.1 Observer design

The control plant model in Fossen and Strand (1999) is extended in this Chapter to include a PFW model such that

$$\dot{\mathbf{p}}_w = \mathbf{A}_{pw} \mathbf{p}_w + \mathbf{E}_{pw} \mathbf{w}_{pw}, \quad (6.1)$$

$$\dot{\boldsymbol{\eta}} = \mathbf{R}(\psi) \mathbf{v}, \quad (6.2)$$

$$\dot{\mathbf{b}} = -\mathbf{T}_b \mathbf{b} + \mathbf{E}_b \mathbf{w}_b, \quad (6.3)$$

$$\mathbf{M} \dot{\mathbf{v}} = -\mathbf{D}_L \mathbf{v} + \mathbf{R}^T(\psi) \mathbf{b} + \boldsymbol{\tau}_q, \quad (6.4)$$

$$\dot{\omega}_p = 0, \quad (6.5)$$

$$\mathbf{y} = \begin{bmatrix} (\boldsymbol{\eta} + \mathbf{C}_{pw} \mathbf{p}_w)^T & \omega_p \end{bmatrix}^T, \quad (6.6)$$

where $\omega_p \in \mathbb{R}$ is the PFW. The assumption $\dot{\omega}_p = 0$ is valid for slowly-varying sea state. Assume that the second-order linear model is sufficient to describe the first-order wave-induced motion (Fossen, 2002), then $\mathbf{p}_w \in \mathbb{R}^6$, is the state of WF model. $\mathbf{A}_{pw} \in \mathbb{R}^{6 \times 6}$ is assumed Hurwitz and describes the first-order wave-induced motion as a mass-damper-spring system. $\mathbf{w}_{pw} \in \mathbb{R}^3$ is a zero-mean Gaussian white noise vector. \mathbf{y} is the measurement vector. The WF measurement matrix $\mathbf{C}_{pw} \in \mathbb{R}^{3 \times 6}$ and the disturbance matrix $\mathbf{E}_{pw} \in \mathbb{R}^{6 \times 3}$ are formulated as

$$\mathbf{C}_{pw} = [\mathbf{0}_{3 \times 3} \quad \mathbf{I}_{3 \times 3}], \quad \mathbf{E}_{pw}^T = [\mathbf{0}_{3 \times 3} \quad \mathbf{K}_w^T]^T. \quad (6.7)$$

Here, a 3-DOF model is assumed adopting the notation in (2.6) where $\boldsymbol{\eta} \in \mathbb{R}^3$ and $\mathbf{v} \in \mathbb{R}^3$ are LF position vector in the Earth-fixed frame and LF velocity vector in the body-fixed frame, respectively. $\mathbf{M} \in \mathbb{R}^{3 \times 3}$ and $\mathbf{D}_L \in \mathbb{R}^{3 \times 3}$ are the body mass matrix including hydrodynamic added mass and linear damping matrix, respectively. The

bias term $\mathbf{b} \in \mathbb{R}^3$ is modelled as Markov processes with positive semi-definite diagonal matrix $\mathbf{T}_b \in \mathbb{R}^{3 \times 3}$ of time constants. $\mathbf{w}_b \in \mathbb{R}^3$ is a bounded disturbance vector, and $\mathbf{E}_b \in \mathbb{R}^{3 \times 3}$ is a disturbance scaling matrix. τ_q is the control force. Details can be found in Fossen (2002), Sørensen (2005a), and the references therein.

It is noted that the above control plant model in this Section is derived for both calm and moderate seas. The reason is that the state-space equations of model set and controller set for calm seas are same as those for moderate seas. However, the observer and controller gains can be different for the various seas. Hence, the subscript i is used here, where $i = 1$ denotes equations for calm seas and $i = 2$ for moderate seas.

By collecting the state $\mathbf{z}_i \in \mathbb{R}^{16}$, and the disturbance $\mathbf{w}_i \in \mathbb{R}^6$ according to

$$\mathbf{z}_i = \begin{bmatrix} \mathbf{p}_w^T & \boldsymbol{\eta}^T & \mathbf{b}^T & \mathbf{v}^T & \boldsymbol{\omega}_p^T \end{bmatrix}^T, \quad (6.8)$$

$$\mathbf{w}_i = \begin{bmatrix} \mathbf{w}_{pw}^T & \mathbf{w}_b^T \end{bmatrix}^T, \quad (6.9)$$

the control plant model can be compactly written as

$$\begin{aligned} \dot{\mathbf{z}}_i &= \mathbf{T}_{pi}^T(\psi) \mathbf{A}_{pi} \mathbf{T}_{pi}(\psi) \mathbf{z}_i + \mathbf{B}_{qi} \boldsymbol{\tau}_{qi} + \mathbf{E}_i \mathbf{w}_i, \\ \mathbf{y}_i &= \mathbf{C}_{pi} \mathbf{z}_i. \end{aligned} \quad (6.10)$$

The transformation matrix $\mathbf{T}_{pi} \in \mathbb{R}^{16 \times 16}$ is given by

$$\mathbf{T}_{pi}(\psi) = \text{diag}(\mathbf{R}^T(\psi), \dots, \mathbf{R}^T(\psi), \mathbf{I}_{33}, 1). \quad (6.11)$$

The system matrices $\mathbf{A}_{pi} \in \mathbb{R}^{16 \times 16}$ and $\mathbf{B}_{qi} \in \mathbb{R}^{16 \times 3}$, and $\mathbf{E}_i \in \mathbb{R}^{16 \times 6}$ are given by

$$\mathbf{A}_{pi} = \begin{bmatrix} \mathbf{A}_{pw} & \mathbf{0}_{6 \times 10} \\ \mathbf{0}_{10 \times 6} & \mathbf{A}_{LF} \end{bmatrix}, \quad \mathbf{B}_{qi} = \begin{bmatrix} \mathbf{0}_{6 \times 3} \\ \mathbf{B}_{LF} \end{bmatrix}, \quad \mathbf{E}_i = \begin{bmatrix} \mathbf{E}_{pw} & \mathbf{0}_{6 \times 3} \\ \mathbf{0}_{10 \times 3} & \mathbf{E}_{LF} \end{bmatrix}. \quad (6.12)$$

The subscripts denoting the dimension of zero and identity matrices can be abbreviated to save space, i.e. $\mathbf{0}_{i \times j} \triangleq \mathbf{0}_{ij}$. Then, the LF system matrices $\mathbf{A}_{LF} \in \mathbb{R}^{10 \times 10}$ and $\mathbf{B}_{LF} \in \mathbb{R}^{10 \times 3}$, and $\mathbf{E}_{LF} \in \mathbb{R}^{10 \times 3}$ are found to be

$$\mathbf{A}_{LF} = \begin{bmatrix} \mathbf{0}_{33} & \mathbf{0}_{33} & \mathbf{I}_{33} & \mathbf{0}_{31} \\ \mathbf{0}_{33} & -\mathbf{T}_b^{-1} & \mathbf{0}_{33} & \mathbf{0}_{31} \\ \mathbf{0}_{33} & \mathbf{0}_{33} & -\mathbf{M}^{-1}\mathbf{D}_L & \mathbf{0}_{31} \\ \mathbf{0}_{13} & \mathbf{0}_{13} & \mathbf{0}_{13} & 0 \end{bmatrix}, \quad \mathbf{B}_{LF} = \begin{bmatrix} \mathbf{0}_{33} \\ \mathbf{0}_{33} \\ \mathbf{M}^{-1} \end{bmatrix}, \quad \mathbf{E}_{LF} = \begin{bmatrix} \mathbf{0}_{33} \\ \mathbf{E}_b \\ \mathbf{0}_{33} \\ \mathbf{0}_{13} \end{bmatrix}. \quad (6.13)$$

As the measurements are positions and PFW, the projection $\mathbf{C}_{pi} \in \mathbb{R}^{4 \times 16}$ is

$$\mathbf{C}_{pi} = \begin{bmatrix} \mathbf{C}_{pw} & \mathbf{I}_{33} & \mathbf{0}_{33} & \mathbf{0}_{33} & \mathbf{0}_{31} \\ \mathbf{0}_{16} & \mathbf{0}_{13} & \mathbf{0}_{13} & \mathbf{0}_{13} & 1 \end{bmatrix}. \quad (6.14)$$

By copying the control plant model in (6.10), the passive nonlinear observer proposed by Fossen and Strand (1999) is extended to include PFW estimation. The estimator for $i = 1$ and 2 is then found to be

$$\begin{aligned} \dot{\mathbf{z}}_{pi} &= \mathbf{T}_{pi}^T(\psi_y)\mathbf{A}_{pi}\mathbf{T}_{pi}(\psi_y)\mathbf{z}_{pi} + \mathbf{B}_{qi}\boldsymbol{\tau}_{qi} + \mathbf{K}_{pi}(\mathbf{y}_i - \mathbf{y}_{pi}), \\ \mathbf{y}_{pi} &= \mathbf{C}_{pi}\mathbf{z}_{pi}. \end{aligned} \quad (6.15)$$

The state vector for observer $\mathbf{z}_{pi} \in \mathbb{R}^{16}$ is written as

$$\mathbf{z}_{pi} = \begin{bmatrix} \hat{\mathbf{p}}_w^T & \hat{\mathbf{n}}^T & \hat{\mathbf{b}}^T & \hat{\mathbf{v}}^T & \hat{\omega}_p \end{bmatrix}^T, \quad (6.16)$$

where $\hat{\omega}_p \in \mathbb{R}$ is the estimated PFW calculated by the spectral analysis.

The observer gain $\mathbf{K}_{pi} \in \mathbb{R}^{16 \times 4}$ is given by

$$\mathbf{K}_{pi} = \begin{bmatrix} \mathbf{K}_{1pi} & \mathbf{0}_{61} \\ \mathbf{K}_{LFPi} & \mathbf{0}_{10 \times 1} \end{bmatrix}, \quad (6.17)$$

where the observer gain for LF motion is given as

$$\mathbf{K}_{LFPi} = \begin{bmatrix} \mathbf{K}_{2pi}^T & \mathbf{K}_{3pi}^T & \mathbf{K}_{4pi}^T & \mathbf{0}_{31} \end{bmatrix}^T. \quad (6.18)$$

The tuning of the observer gain matrices $\mathbf{K}_{1pi} \in \mathbb{R}^{6 \times 3}$, $\mathbf{K}_{2pi} \in \mathbb{R}^{3 \times 3}$, $\mathbf{K}_{3pi} \in \mathbb{R}^{3 \times 3}$, and $\mathbf{K}_{4pi} \in \mathbb{R}^{3 \times 3}$ is based on the passivity requirements (Fossen and Strand, 1999).

6.2.1.2 Controller design

The nonlinear output-feedback PID control law for model 1 and 2 can be written

as

$$\dot{\xi}_{qi} = \hat{\eta}, \quad (6.19)$$

$$\hat{\tau}_{qi} = -\mathbf{K}_{ii}\mathbf{R}^T(\psi_y)\xi_{qi} - \mathbf{K}_{pi}\mathbf{R}^T(\psi_y)\hat{\eta} - \mathbf{K}_{di}\hat{\mathbf{v}}, \quad (6.20)$$

where $\mathbf{K}_{pi} \in \mathbb{R}^{3 \times 3}$, $\mathbf{K}_{ii} \in \mathbb{R}^{3 \times 3}$, and $\mathbf{K}_{di} \in \mathbb{R}^{3 \times 3}$ are the non-negative P, I, and D controller gain matrices, respectively.

6.2.2 Output PID Controller for Extreme Seas (Model 4)

6.2.2.1 Observer design

According to Sørensen et al. (2002), the state space equation of the control plant model for extreme seas is based on the control plant model for moderate sea in Sub-section 6.2.1 and excludes the WF motion, i.e. (6.1), such that

$$\dot{\eta}_T = \mathbf{R}(\psi)\mathbf{v}_T, \quad (6.21)$$

$$\dot{\mathbf{b}}_T = -\mathbf{T}_b\mathbf{b}_T + \mathbf{E}_b\mathbf{w}_b, \quad (6.22)$$

$$\mathbf{M}\dot{\mathbf{v}}_T = -\mathbf{D}_L\mathbf{v}_T + \mathbf{R}^T(\psi)\mathbf{b}_T + \boldsymbol{\tau}_q, \quad (6.23)$$

$$\dot{\omega}_p = 0, \quad (6.24)$$

The measurement vector $\mathbf{y}_4 \in \mathbb{R}^4$ includes the positions and PFW such that

$$\mathbf{y}_4 = [\eta_T^T \quad \omega_p]^T. \quad (6.25)$$

By collecting the state $\mathbf{z}_4 \in \mathbb{R}^{10}$, and the disturbance $\mathbf{w}_4 \in \mathbb{R}^3$ accordingly as

$$\mathbf{z}_4 = [\eta_T^T \quad \mathbf{b}_T^T \quad \mathbf{v}_T^T \quad \omega_p]^T, \quad (6.26)$$

$$\mathbf{w}_4 = \mathbf{w}_b, \quad (6.27)$$

where the superscript T denotes total motion which is assumed to be of low frequency, the control plant model can be compactly written as

$$\begin{aligned} \dot{\mathbf{z}}_4 &= \mathbf{T}_{p4}^T(\psi)\mathbf{A}_{p4}\mathbf{T}_{p4}(\psi)\mathbf{z}_4 + \mathbf{B}_{q4}\boldsymbol{\tau}_{q4} + \mathbf{E}_4\mathbf{w}_4, \\ \mathbf{y}_4 &= \mathbf{C}_{p4}\mathbf{z}_4. \end{aligned} \quad (6.28)$$

The transformation matrix $\mathbf{T}_{p4} \in \mathbb{R}^{10 \times 10}$ is given by

$$\mathbf{T}_{p4}(\psi) = \text{diag}(\mathbf{R}^T(\psi), \mathbf{R}^T(\psi), \mathbf{I}_{33}, 1). \quad (6.29)$$

The system matrices $\mathbf{A}_{p4} \in \mathbb{R}^{10 \times 10}$, $\mathbf{B}_{q4} \in \mathbb{R}^{10 \times 3}$ and $\mathbf{E}_4 \in \mathbb{R}^{10 \times 6}$ are same as \mathbf{A}_{LF} , \mathbf{B}_{LF} , and \mathbf{E}_{LF} found in (6.13), respectively.

As the measurements are positions and the PFW, the projection $\mathbf{C}_{p4} \in \mathbb{R}^{4 \times 10}$ is

$$\mathbf{C}_{p4} = \begin{bmatrix} \mathbf{I}_{33} & \mathbf{0}_{33} & \mathbf{0}_{33} & \mathbf{0}_{31} \\ \mathbf{0}_{13} & \mathbf{0}_{13} & \mathbf{0}_{13} & 1 \end{bmatrix}, \quad (6.30)$$

By copying the control plant model in (6.28), the passive nonlinear observer proposed by Sørensen (2002) is extended to include the PFW model. The estimator in extreme seas is then found to be

$$\begin{aligned} \dot{\mathbf{z}}_{p4} &= \mathbf{T}_{p4}^T(\psi_y) \mathbf{A}_{p4} \mathbf{T}_{p4}(\psi_y) \mathbf{z}_{p4} + \mathbf{B}_{q4} \boldsymbol{\tau}_{q4} + \mathbf{K}_{p4} (\mathbf{y}_4 - \mathbf{y}_{p4}) \\ \mathbf{y}_{p4} &= \mathbf{C}_{p4} \mathbf{z}_{p4} \end{aligned} \quad (6.31)$$

$$\text{where } \mathbf{z}_{p4} = \begin{bmatrix} \hat{\mathbf{q}}_T^T & \hat{\mathbf{b}}_T^T & \hat{\mathbf{v}}_T^T & \hat{\omega}_p \end{bmatrix}^T \in \mathbb{R}^{10}, \quad (6.32)$$

The observer gain matrix $\mathbf{K}_{p4} \in \mathbb{R}^{10 \times 4}$ becomes

$$\mathbf{K}_{p4} = \begin{bmatrix} \mathbf{K}_{LFp4} & \mathbf{0}_{10 \times 1} \end{bmatrix}. \quad (6.33)$$

The tuning rules for $\mathbf{K}_{2p4} \in \mathbb{R}^{3 \times 3}$, $\mathbf{K}_{3p4} \in \mathbb{R}^{3 \times 3}$, and $\mathbf{K}_{4p4} \in \mathbb{R}^{3 \times 3}$ are similar to \mathbf{K}_{2p1} , \mathbf{K}_{3p1} , and \mathbf{K}_{4p1} as given in (6.18), respectively.

6.2.2.2 Controller design

The PID controller design is same as (6.19) and (6.20) with $\hat{\mathbf{q}}_T$ and $\hat{\mathbf{v}}_T$ as estimated state vectors, such that

$$\dot{\xi}_{q4} = \hat{\mathbf{q}}_T, \quad (6.34)$$

$$\hat{\boldsymbol{\tau}}_{q4} = -\mathbf{K}_{i4} \mathbf{R}^T(\psi_y) \xi_{q4} - \mathbf{K}_{p4} \mathbf{R}^T(\psi_y) \hat{\mathbf{q}}_T - \mathbf{K}_{d4} \hat{\mathbf{v}}_T, \quad (6.35)$$

where $\mathbf{K}_{p4} \in \mathbb{R}^{3 \times 3}$, $\mathbf{K}_{i4} \in \mathbb{R}^{3 \times 3}$, and $\mathbf{K}_{d4} \in \mathbb{R}^{3 \times 3}$ are the non-negative P, I, and D controller gain matrices, respectively, designed for extreme sea.

6.2.3 Output PID for Transition Regime between Moderate and Extreme Seas (Model 3)

The controller in high seas is obtained by combining the controllers in moderate and extreme seas through weighting-like functions to effect a smooth transition, such that

$$\begin{aligned}\hat{\mathbf{\tau}}_{q3} &= \alpha_1(\hat{\omega}_p)\hat{\mathbf{\tau}}_{q2} + \alpha_2(\hat{\omega}_p)\hat{\mathbf{\tau}}_{q4} \\ &= -\left[\alpha_1(\hat{\omega}_p)\mathbf{K}_{i2}\mathbf{R}^T(\psi)\xi_{q2} + \alpha_2(\hat{\omega}_p)\mathbf{K}_{i4}\mathbf{R}^T(\psi)\xi_{q4}\right] \\ &\quad -\left[\alpha_1(\hat{\omega}_p)\mathbf{K}_{p2}\mathbf{R}^T(\psi)\hat{\mathbf{n}} + \alpha_2(\hat{\omega}_p)\mathbf{K}_{p4}\mathbf{R}^T(\psi)\hat{\mathbf{n}}_T\right] \\ &\quad -\left[\alpha_1(\hat{\omega}_p)\mathbf{K}_{d2}\hat{\mathbf{v}} + \alpha_2(\hat{\omega}_p)\mathbf{K}_{d4}\hat{\mathbf{v}}_T\right],\end{aligned}\tag{6.36}$$

where the weighting functions α_1 and α_2 are used to smoothly transform the controller from moderate to extreme seas and vice versa. This will prevent sudden change of control loads, especially when the sea state is at the marginal conditions. The weighting functions are assumed to have the following properties:

- $\alpha_i \rightarrow 1$ when the sea state is close to the i th condition;
- $\alpha_1(\omega) + \alpha_2(\omega) = 1, \forall \omega$;
- α_i is slowly varying such that $\frac{d\alpha_i}{dt} = \dot{\alpha}_i \approx 0$.

Examples of appropriate α_1 and α_2 are shown in (4.39), (4.40), and Figure 6.2.

$$\alpha_1(\omega_p) = 1 - \exp\left[-8(2.5\omega_p)^{12}\right]\tag{6.37}$$

$$\alpha_2(\omega_p) = \exp\left[-8(2.5\omega_p)^{12}\right]\tag{6.38}$$

6.3 Hybrid Controller DP System Using Multi-output PID and AFB Controllers with Position and Acceleration Measurements

The difference between this hybrid controller and the previous is the introduction of AFB in extreme seas (for model 4). The modification of AFB proposed by

Lindegaard (2003) is adopted instead of only using output feedback PID controller in harsh environments.

For calm and moderate seas (models 1 and 2), the observer design and the controller design are similar to those in Sub-section 6.2.1.

6.3.1 Output AFB Controller for Extreme Seas (Model 4)

6.3.1.1 Observer design

The control plant model in extreme seas is the same as (6.21)-(6.24). The measurement vector $\mathbf{y}_4 \in \mathbb{R}^6$ includes positions, accelerations, and PFW according to

$$\mathbf{y}_4 = \begin{bmatrix} \mathbf{y}_{14} \\ \mathbf{y}_{24} \\ \mathbf{y}_{34} \end{bmatrix} = \begin{bmatrix} \boldsymbol{\eta}_T \\ \Upsilon_3 \dot{\mathbf{v}}_T \\ \omega_p \end{bmatrix} = \begin{bmatrix} \boldsymbol{\eta}_T \\ \Upsilon_3 \mathbf{M}^{-1}(-\mathbf{D}_L \mathbf{v}_T + \mathbf{R}^T \mathbf{b} + \boldsymbol{\tau}_c) \\ \omega_p \end{bmatrix}, \quad (6.39)$$

where Υ_3 is the projection matrix extracting the acceleration measurements from the actual 3-DOF acceleration vector. Since angular acceleration is not easy to measure, the typical projection matrix is

$$\Upsilon_3 = \begin{bmatrix} 1 & 0 & 0 \\ 0 & 1 & 0 \end{bmatrix}. \quad (6.40)$$

The control plant model can be compactly written as

$$\begin{aligned} \dot{\mathbf{z}}_4 &= \mathbf{T}_{p4}^T(\psi) \mathbf{A}_{p4} \mathbf{T}_{p4}(\psi) \mathbf{z}_4 + \mathbf{B}_{q4} \boldsymbol{\tau}_{q4} + \mathbf{E}_4 \mathbf{w}_4, \\ \mathbf{y}_4 &= \mathbf{C}_{p4} \mathbf{z}_4 + \mathbf{D}_{p4} \boldsymbol{\tau}_{q4}, \end{aligned} \quad (6.41)$$

where $\mathbf{T}_{p4} \in \mathbb{R}^{10 \times 10}$, $\mathbf{A}_{p4} \in \mathbb{R}^{10 \times 10}$, $\mathbf{B}_{q4} \in \mathbb{R}^{10 \times 3}$ and $\mathbf{E}_4 \in \mathbb{R}^{10 \times 6}$ are same as those in Sub-section 6.2.2, and

$$\begin{aligned} \mathbf{C}_{p4}(\psi_y) &= \begin{bmatrix} \mathbf{I}_{33} & \mathbf{0}_{33} & \mathbf{0}_{33} & \mathbf{0}_{31} \\ \mathbf{0}_{33} & \Upsilon_3 \mathbf{M}^{-1} \mathbf{R}^T(\psi_y) & -\Upsilon_3 \mathbf{M}^{-1} \mathbf{D}_L & \mathbf{0}_{31} \\ \mathbf{0}_{13} & \mathbf{0}_{13} & \mathbf{0}_{13} & 1 \end{bmatrix}, \\ \mathbf{D}_{p4} &= \begin{bmatrix} \mathbf{0}_{33} & \mathbf{0}_{33} & \mathbf{M}^{-T} \Upsilon_3^T & \mathbf{0}_{31} \end{bmatrix}^T. \end{aligned} \quad (6.42)$$

Here, the proposed nonlinear observer for acceleration feedback can be considered as the estimator in extreme seas

$$\begin{aligned}\dot{\hat{\mathbf{a}}}_f &= \mathbf{T}_f^{-1} \left[-\hat{\mathbf{a}}_f + (\mathbf{y}_{24} - \mathbf{y}_{2p4}) \right], \\ \dot{\mathbf{z}}_{p4} &= \mathbf{T}_{p4}^T(\psi_y) \mathbf{A}_{p4} \mathbf{T}_{p4}(\psi_y) \mathbf{z}_{p4} + \mathbf{B}_{q4} \boldsymbol{\tau}_{q4} + \mathbf{K}_{p4} (\mathbf{y}_4 - \mathbf{y}_{p4}) + \mathbf{K}_f \hat{\mathbf{a}}_f, \\ \mathbf{y}_{p4} &= \mathbf{C}_{p4} \mathbf{z}_{p4} + \mathbf{D}_{q4} \boldsymbol{\tau}_{q4}.\end{aligned}\quad (6.43)$$

The observer gain matrices $\mathbf{K}_{p4} \in \mathbb{R}^{10 \times 6}$, and $\mathbf{K}_f \in \mathbb{R}^{10 \times 3}$ becomes

$$\mathbf{K}_{p4} = \begin{bmatrix} \mathbf{K}_{LFp4} & \mathbf{0}_{10 \times 3} \end{bmatrix}, \quad (6.44)$$

$$\mathbf{K}_f = \begin{bmatrix} \mathbf{0}_{33} & \mathbf{0}_{33} & \mathbf{K}_a^T & \mathbf{0}_{31} \end{bmatrix}^T. \quad (6.45)$$

The low-pass filter, $\hat{\mathbf{a}}_f \in \mathbb{R}^2$, between acceleration innovation $\mathbf{y}_{24} \in \mathbb{R}^2$ and $\mathbf{y}_{2p4} \in \mathbb{R}^2$ takes care of the roll-off at high frequencies; and $\mathbf{T}_f \in \mathbb{R}^{2 \times 2}$ are the filter constants.

The tuning rule for $\mathbf{K}_{2p4} \in \mathbb{R}^{3 \times 3}$, $\mathbf{K}_{3p4} \in \mathbb{R}^{3 \times 3}$, and $\mathbf{K}_{4p4} \in \mathbb{R}^{3 \times 3}$ is similar to \mathbf{K}_{2p1} , \mathbf{K}_{3p1} , and \mathbf{K}_{4p1} , as given in (6.18), respectively.

6.3.1.2 Controller design

The proposed nonlinear output-feedback PID control law extended to include acceleration feedback for model 4 can be formulated as

$$\dot{\xi}_{q4} = \hat{\mathbf{n}}_T, \quad (6.46)$$

$$\dot{\hat{\mathbf{a}}}_f = \mathbf{A}_f \mathbf{a}_f + \mathbf{B}_f \Upsilon_3 \hat{\mathbf{v}}, \quad (6.47)$$

$$\hat{\boldsymbol{\tau}}_{q4} = -\mathbf{K}_{i4} \mathbf{R}^T(\psi_y) \xi_{q4} - \mathbf{K}_{p4} \mathbf{R}^T(\psi_y) \hat{\mathbf{n}}_T - \mathbf{K}_{d4} \hat{\mathbf{v}}_T - \mathbf{K}_a^{PID} \mathbf{a}_f, \quad (6.48)$$

where $\mathbf{K}_a^{PID} \in \mathbb{R}^{3 \times 2}$ is the non-negative gain matrix for the acceleration feedback.

The matrices $\mathbf{A}_f \in \mathbb{R}^{2 \times 2}$ and $\mathbf{B}_f \in \mathbb{R}^{2 \times 2}$ are used to remove the high-frequency noise components from the acceleration measurements,

$$\mathbf{A}_f = -\mathbf{B}_f = \text{diag}(-1/T_f, -1/T_f). \quad (6.49)$$

The filter constant is selected to be small

$$T_f \ll \min\left(\frac{m_{11}}{d_{11}}, \frac{m_{22}}{d_{22}}\right). \quad (6.50)$$

where m_{ii} and d_{ii} are the mass and damping coefficients in surge and sway, respectively.

It should be noted that \mathbf{a}_f in (6.47) is different from $\hat{\mathbf{a}}_f$ in (6.43). The former is used to update $\dot{\hat{\mathbf{v}}}$, while the latter is the low-pass filtered acceleration. Detailed information on acceleration feedback with WF filtering can be found in Fossen (2002) and Lindegaard (2003).

6.3.2 Output PID and AFB for Transition Regime between Moderate and Extreme Seas (Model 3)

In order to have a smooth transition of control forces from moderate (output feedback PID controller) to extreme seas (output acceleration feedback controller), weighting-like functions are employed to combine the two controllers such that

$$\hat{\tau}_{q3} = \alpha_1(\hat{\omega}_p)\hat{\tau}_{q2} + \alpha_2(\hat{\omega}_p)\hat{\tau}_{q4}, \quad (6.51)$$

The weighting functions α_1 and α_2 are the same as those in (6.37)-(6.38).

A summary of multi-controllers for hybrid DP system using multi output PID and multi output PID + AFB is shown in Table 6.3.

6.4 Hybrid Controller DP System Using Multi-output PID and AFB Controllers with Position, Velocity and Acceleration Measurements

The difference between this hybrid controller and the previous one is the additional measurement of velocities. Although this measurement can improve the performance of the overall filter, the problem is that the velocity measurement units using e.g. GPS is not accurate enough to be used in station keeping operations with

low velocities. Using precise inertial motion units (IMU) for AFB may also be combined with GPS and hydroacoustics position reference systems to improve the accuracy of velocity measurements. However, at currently precise IMU may be costly with limited commercial availability.

6.4.1 Output PID Controller for Calm and Moderate Seas (Model 1 and 2)

6.4.1.1 Observer design

The control plant model proposed by Lindegaard (2003) is extended to include the wave peak frequency model. The estimator is then found to be

$$\dot{\mathbf{p}}_w = \mathbf{A}_{pw}\mathbf{p}_w + \mathbf{E}_{pw}\mathbf{w}_{pw}, \quad (6.52)$$

$$\dot{\mathbf{v}}_w = \mathbf{A}_{vw}\mathbf{v}_w + \mathbf{E}_{vw}\mathbf{w}_{vw}, \quad (6.53)$$

$$\dot{\boldsymbol{\eta}} = \mathbf{R}(\psi)\mathbf{v}, \quad (6.54)$$

$$\dot{\mathbf{b}} = -\mathbf{T}_b\mathbf{b} + \mathbf{E}_b\mathbf{w}_b, \quad (6.55)$$

$$\mathbf{M}\dot{\mathbf{v}} = -\mathbf{D}_L\mathbf{v} + \mathbf{R}^T(\psi)\mathbf{b} + \boldsymbol{\tau}_{qi}, \quad (6.56)$$

$$\dot{\omega}_p = 0, \quad (6.57)$$

$$\mathbf{y}_i = \begin{bmatrix} (\boldsymbol{\eta} + \mathbf{C}_{pw}\mathbf{p}_w)^T & (\mathbf{v} + \mathbf{C}_{vw}\mathbf{v}_w)^T & \omega_p \end{bmatrix}^T. \quad (6.58)$$

It should be noted that the additional model here in comparison to control plant model in Section 6.2 is the WF model for velocity represented by (6.53). Assume that the second-order linear model is sufficient to describe the first-order wave-induced motion as a mass-damper-spring system, then $\mathbf{v}_w \in \mathbb{R}^6$ is the state of first-order wave-induced velocity model. $\mathbf{A}_{vw} \in \mathbb{R}^{6 \times 6}$ is assumed Hurwitz and describes the first-order wave-induced motion. $\mathbf{w}_{vw} \in \mathbb{R}^3$ is a zero-mean Gaussian noise vector. The measurement matrix $\mathbf{C}_{vw} \in \mathbb{R}^{3 \times 6}$ and the disturbance matrix $\mathbf{E}_{vw} \in \mathbb{R}^{6 \times 3}$ are formulated as

$$\mathbf{C}_{vw} = \begin{bmatrix} \mathbf{0}_{3 \times 3} & \mathbf{I}_{3 \times 3} \end{bmatrix}, \quad \mathbf{E}_{vw} = \begin{bmatrix} \mathbf{0}_{3 \times 3} \\ \mathbf{K}_{vw} \end{bmatrix}. \quad (6.59)$$

By collecting the state $\mathbf{z}_1 \in \mathbb{R}^{22}$, $\mathbf{w}_1 \in \mathbb{R}^9$ accordingly as

$$\mathbf{z}_i = \begin{bmatrix} \mathbf{p}_w^T & \mathbf{\eta}^T & \mathbf{b}^T & \mathbf{v}_w^T & \mathbf{v}^T & \omega_p \end{bmatrix}^T, \quad (6.60)$$

$$\mathbf{w}_i = \begin{bmatrix} \mathbf{w}_{pw}^T & \mathbf{w}_b^T & \mathbf{w}_{vw}^T \end{bmatrix}^T, \quad (6.61)$$

the control plant can be compactly written as

$$\begin{aligned} \dot{\mathbf{z}}_i &= \mathbf{T}_{pi}^T(\psi) \mathbf{A}_{pi} \mathbf{T}_{pi}(\psi) \mathbf{z}_i + \mathbf{B}_{qi} \boldsymbol{\tau}_{qi} + \mathbf{E}_i \mathbf{w}_i, \\ \mathbf{y}_i &= \mathbf{C}_{pi} \mathbf{z}_i. \end{aligned} \quad (6.62)$$

The transformation matrix $\mathbf{T}_{pi} \in \mathbb{R}^{22 \times 22}$, system matrices $\mathbf{A}_{pi} \in \mathbb{R}^{22 \times 22}$, $\mathbf{B}_{qi} \in \mathbb{R}^{22 \times 3}$ and $\mathbf{E}_i \in \mathbb{R}^{22 \times 9}$ are given by

$$\mathbf{T}_{pi}(\psi) = \text{diag}(\mathbf{R}^T(\psi), \dots, \mathbf{R}^T(\psi), \mathbf{I}_{33}, 1), \quad (6.63)$$

$$\begin{aligned} \mathbf{A}_{pi} &= \begin{bmatrix} \mathbf{A}_{pw} & \mathbf{0}_{63} & \mathbf{0}_{63} & \mathbf{0}_{66} & \mathbf{0}_{63} & \mathbf{0}_{61} \\ \mathbf{0}_{36} & \mathbf{0}_{33} & \mathbf{0}_{33} & \mathbf{0}_{36} & \mathbf{I}_{33} & \mathbf{0}_{31} \\ \mathbf{0}_{36} & \mathbf{0}_{33} & -\mathbf{T}_b^{-1} & \mathbf{0}_{36} & \mathbf{0}_{33} & \mathbf{0}_{31} \\ \mathbf{0}_{66} & \mathbf{0}_{63} & \mathbf{0}_{63} & \mathbf{A}_{vw} & \mathbf{0}_{63} & \mathbf{0}_{61} \\ \mathbf{0}_{36} & \mathbf{0}_{33} & \mathbf{0}_{33} & \mathbf{0}_{36} & -\mathbf{M}^{-1} \mathbf{D}_L & \mathbf{0}_{31} \\ \mathbf{0}_{16} & \mathbf{0}_{13} & \mathbf{0}_{13} & \mathbf{0}_{16} & \mathbf{0}_{13} & 0 \end{bmatrix}, \\ \mathbf{B}_{qi} &= \begin{bmatrix} \mathbf{0}_{63} \\ \mathbf{0}_{33} \\ \mathbf{0}_{33} \\ \mathbf{0}_{63} \\ \mathbf{M}^{-1} \\ \mathbf{0}_{33} \end{bmatrix}, \quad \mathbf{E}_i = \begin{bmatrix} \mathbf{E}_{pw} & \mathbf{0}_{63} & \mathbf{0}_{63} \\ \mathbf{0}_{33} & \mathbf{0}_{33} & \mathbf{0}_{33} \\ \mathbf{0}_{33} & \mathbf{E}_b & \mathbf{0}_{33} \\ \mathbf{0}_{63} & \mathbf{0}_{63} & \mathbf{E}_{vw} \\ \mathbf{0}_{33} & \mathbf{0}_{33} & \mathbf{0}_{33} \\ \mathbf{0}_{13} & \mathbf{0}_{13} & \mathbf{0}_{13} \end{bmatrix}. \end{aligned} \quad (6.64)$$

As positions and velocities are measured, the projection $\mathbf{C}_{pi} \in \mathbb{R}^{7 \times 22}$ is

$$\mathbf{C}_{pi} = \begin{bmatrix} \mathbf{C}_{pw} & \mathbf{I}_{33} & \mathbf{0}_{33} & \mathbf{0}_{36} & \mathbf{0}_{33} & \mathbf{0}_{31} \\ \mathbf{0}_{36} & \mathbf{0}_{33} & \mathbf{0}_{33} & \mathbf{C}_{vw} & \mathbf{I}_{33} & \mathbf{0}_{31} \\ \mathbf{0}_{16} & \mathbf{0}_{13} & \mathbf{0}_{13} & \mathbf{0}_{36} & \mathbf{0}_{13} & 1 \end{bmatrix}. \quad (6.65)$$

By copying the control plant model (6.52)-(6.58), the passive nonlinear observer proposed by Lindegaard (2003) is extended to include the wave peak frequency model. The estimator is then found to be

$$\begin{aligned}\dot{\mathbf{z}}_{pi} &= \mathbf{T}_{pi}^T(\psi_y) \mathbf{A}_{pi} \mathbf{T}_{pi}(\psi_y) \mathbf{z}_{pi} + \mathbf{B}_{qi} \boldsymbol{\tau}_{qi} + \mathbf{K}_{pi} (\mathbf{y}_i - \mathbf{y}_{pi}), \\ \mathbf{y}_{pi} &= \mathbf{C}_{pi} \mathbf{z}_{pi},\end{aligned}\quad (6.66)$$

where $\mathbf{z}_{pi} = [\hat{\mathbf{p}}_w^T \quad \hat{\mathbf{n}}^T \quad \hat{\mathbf{b}}^T \quad \hat{\mathbf{v}}_w^T \quad \hat{\mathbf{v}}^T \quad \hat{\omega}_p]^T \in \mathbb{R}^{22}$, and

$$\text{the observer gain } \mathbf{K}_{pi} = \begin{bmatrix} \mathbf{K}_{1pi} & \mathbf{0}_{63} & \mathbf{0}_{61} \\ \mathbf{K}_{2pi} & \mathbf{0}_{33} & \mathbf{0}_{31} \\ \mathbf{K}_{3pi} & \mathbf{0}_{33} & \mathbf{0}_{31} \\ \mathbf{0}_{63} & \mathbf{K}_{1pi} & \mathbf{0}_{61} \\ \mathbf{K}_{4pi} & \mathbf{K}_{2pi} & \mathbf{0}_{31} \end{bmatrix} \in \mathbb{R}^{27 \times 7}. \quad (6.68)$$

The observer gain matrices $\mathbf{K}_{1pi} \in \mathbb{R}^{6 \times 3}$, $\mathbf{K}_{2pi} \in \mathbb{R}^{3 \times 3}$, $\mathbf{K}_{3pi} \in \mathbb{R}^{3 \times 3}$, and $\mathbf{K}_{4pi} \in \mathbb{R}^{3 \times 3}$ are similar to those in Sub-section 6.2.1.

6.4.1.2 Controller design

The controller design is similar to section 6.2.1.2.

6.4.2 *Output AFB Controller for Extreme Seas (Model 4)*

6.4.2.1 Observer design

The control plant model in extreme seas is described by

$$\dot{\mathbf{q}}_T = \mathbf{R}(\psi) \mathbf{v}_T, \quad (6.69)$$

$$\dot{\mathbf{b}}_T = -\mathbf{T}_b \mathbf{b}_T + \mathbf{E}_b \mathbf{w}_b, \quad (6.70)$$

$$\mathbf{M} \dot{\mathbf{v}}_T = -\mathbf{D} \mathbf{v}_T + \mathbf{R}^T(\psi) \mathbf{b} + \boldsymbol{\tau}_{q4}, \quad (6.71)$$

$$\dot{\omega}_p = 0. \quad (6.72)$$

The measurements vector $\mathbf{y}_4 \in \mathbb{R}^9$ comprises positions, velocities, accelerations, and wave peak frequency, given by

$$\mathbf{y}_4 = \begin{bmatrix} \mathbf{y}_{14} \\ \mathbf{y}_{24} \\ \mathbf{y}_{34} \\ y_{44} \end{bmatrix} = \begin{bmatrix} \mathbf{\eta}_T \\ \mathbf{v}_T \\ \Upsilon_3 \dot{\mathbf{v}}_T \\ \omega_p \end{bmatrix} = \begin{bmatrix} \mathbf{\eta}_T \\ \mathbf{v}_T \\ \Upsilon_3 \mathbf{M}^{-1}(-\mathbf{D}\mathbf{v}_T + \mathbf{R}^T \mathbf{b} + \boldsymbol{\tau}_c) \\ \omega_p \end{bmatrix}, \quad (6.73)$$

where Υ_3 was defined in (6.40).

By collecting the state $\mathbf{z}_4 \in \mathbb{R}^{10}$, $\mathbf{w}_4 \in \mathbb{R}^3$ accordingly as

$$\mathbf{z}_4 = [\mathbf{\eta}_T^T \quad \mathbf{b}_T^T \quad \mathbf{v}_T^T \quad \omega_p]^T, \quad (6.74)$$

$$\mathbf{w}_4 = \mathbf{w}_b, \quad (6.75)$$

the control plant can be compactly written as

$$\begin{aligned} \dot{\mathbf{z}}_4 &= \mathbf{T}_{p4}^T(\psi_y) \mathbf{A}_{p4} \mathbf{T}_{p4}(\psi_y) \mathbf{z}_4 + \mathbf{B}_{q4} \boldsymbol{\tau}_{q4} + \mathbf{E}_4 \mathbf{w}_4, \\ \mathbf{y}_4 &= \mathbf{C}_{p4} \mathbf{z}_4 + \mathbf{D}_{p4} \boldsymbol{\tau}_{q4}, \end{aligned} \quad (6.76)$$

where $\mathbf{T}_{p4} \in \mathbb{R}^{10 \times 10}$, $\mathbf{A}_{p4} \in \mathbb{R}^{10 \times 10}$, $\mathbf{B}_{q4} \in \mathbb{R}^{10 \times 3}$ and $\mathbf{E}_4 \in \mathbb{R}^{10 \times 6}$ are the same as those in

Sub-section 6.2.2. $\mathbf{C}_{p4} \in \mathbb{R}^{10 \times 10}$ and $\mathbf{D}_{p4} \in \mathbb{R}^{10 \times 3}$ are given by

$$\mathbf{C}_{p4}(\psi_y) = \begin{bmatrix} \mathbf{I}_{33} & \mathbf{0}_{33} & \mathbf{0}_{33} & \mathbf{0}_{31} \\ \mathbf{0}_{33} & \mathbf{0}_{33} & \mathbf{I}_{33} & \mathbf{0}_{33} \\ \mathbf{0}_{33} & \Upsilon_3 \mathbf{M}^{-1} \mathbf{R}^T(\psi_y) & -\Upsilon_3 \mathbf{M}^{-1} \mathbf{D}_L & \mathbf{0}_{31} \\ \mathbf{0}_{13} & \mathbf{0}_{13} & \mathbf{0}_{13} & 1 \end{bmatrix}, \quad (6.77)$$

$$\mathbf{D}_{p4} = [\mathbf{0}_{33} \quad \mathbf{0}_{33} \quad \mathbf{M}^{-T} \Upsilon_3^T \quad \mathbf{0}_{31}]^T. \quad (6.78)$$

Here, the proposed nonlinear observer for acceleration feedback can be considered as the estimator in extreme seas, that is,

$$\begin{aligned} \dot{\hat{\mathbf{a}}}_f &= \mathbf{T}_f^{-1} [-\hat{\mathbf{a}}_f + (\mathbf{y}_{34} - \mathbf{y}_{3p4})], \\ \dot{\mathbf{z}}_{p4} &= \mathbf{T}_{p4}^T(\psi_y) \mathbf{A}_{p4} \mathbf{T}_{p4}(\psi_y) \mathbf{z}_{p4} + \mathbf{B}_{q4} \boldsymbol{\tau}_{q4} + \mathbf{K}_{p4} (\mathbf{y}_4 - \mathbf{y}_{p4}) + \mathbf{K}_f \hat{\mathbf{a}}_f, \\ \mathbf{y}_{p4} &= \mathbf{C}_{p4} \mathbf{z}_{p4} + \mathbf{D}_{q4} \boldsymbol{\tau}_{q4}. \end{aligned} \quad (6.79)$$

where $\mathbf{y}_{34} \in \mathbb{R}^2$ is the acceleration innovation, $\mathbf{y}_{3p4} \in \mathbb{R}^2$ is the estimated accelerations which is one of the element of the measurements

$$\mathbf{y}_{p4} = [\mathbf{y}_{1p4}^T \quad \mathbf{y}_{2p4}^T \quad \mathbf{y}_{3p4}^T \quad y_{4p4}]^T$$

$$= \begin{bmatrix} \hat{\mathbf{n}}_T^T & \hat{\mathbf{v}}_T^T & \left(\Upsilon_3 \hat{\mathbf{v}}_T \right)^T & \hat{\omega}_p \end{bmatrix}^T. \quad (6.80)$$

The estimated states are

$$\mathbf{z}_{p4} = \begin{bmatrix} \hat{\mathbf{n}}_T^T & \hat{\mathbf{b}}_T^T & \hat{\mathbf{v}}_T^T & \hat{\omega}_p \end{bmatrix}^T \in \mathbb{R}^{10}. \quad (6.81)$$

The observer gains are

$$\mathbf{K}_{p4} = \begin{bmatrix} \mathbf{K}_{2p4} & \mathbf{0}_{33} & \mathbf{0}_{32} & \mathbf{0}_{31} \\ \mathbf{K}_{3p4} & \mathbf{0}_{33} & \mathbf{0}_{32} & \mathbf{0}_{31} \\ \mathbf{0}_{33} & \mathbf{K}_{2p4} & \mathbf{0}_{32} & \mathbf{0}_{31} \\ \mathbf{K}_{4p4} & \mathbf{0}_{33} & \mathbf{0}_{32} & \mathbf{0}_{31} \end{bmatrix} \in \mathbb{R}^{12 \times 9}; \text{ and} \quad (6.82)$$

$$\mathbf{K}_f = \begin{bmatrix} \mathbf{0}_{33} & \mathbf{0}_{33} & \mathbf{K}_a^T & \mathbf{0}_{31} \end{bmatrix}^T \in \mathbb{R}^{10 \times 3}. \quad (6.83)$$

6.4.2.2 Controller design

The controller design is similar to Sub-section 6.3.2.2.

6.4.3 Output PID and AFB for Transition Regime between Moderate and Extreme Seas (Model 3)

The controller design is similar to Sub-section 6.3.3.

6.5 Stability Analysis

In this section, the stability analysis of high level hybrid-controller DP system using multi-output PID and AFB controllers with position and acceleration measurements is examined. The stability analysis for the other types of hybrid DP system is similar and not shown here.

6.5.1 Multi-output PID and AFB Controllers, with Position and Acceleration Measurements

The switched system should satisfy four properties, namely, matching, detectability, small error, and non-destabilization (Hespanha, 2001).

Matching property: Passive nonlinear observer/estimator for calm and moderate seas was proven to be exponentially stable (Fossen and Strand, 1999), i.e. the error dynamics vector converges to zero exponentially. Consequently, the matching property is satisfied (Hespanha, 2001). In addition, uniformly locally exponential stability (ULES) and uniformly globally exponential stability (UGES) of the observer for extreme seas can be proven similar to that for calm and moderate seas, and is shown in Appendix A.3.

Detectability property: For a fixed pair of ρ and σ , the input to the injected system is $\mathbf{v} = \mathbf{e}_\rho := \mathbf{y}_\rho - \mathbf{y}$; and outputs are control τ_q and estimated \mathbf{y}_ρ . The injected system (Figure 3.4) contains the selected estimator and controller; and its state-space model is

$$\dot{\mathbf{x}} = \mathbf{A}_{\rho\sigma}(\mathbf{x}, \mathbf{v}), \quad \tau_q = \mathbf{F}_{\rho\sigma}(\mathbf{x}, \mathbf{v}), \quad \mathbf{y}_p = \mathbf{C}_p(\mathbf{x}), \quad p \in \mathcal{P}. \quad (6.84)$$

The simplest mechanism to make the switched system detectable is to ensure that the injected system is stable. The following theorem from Hespanha (2001) is provided for this purpose.

Theorem 1 (Certainty Equivalent Stabilization – Hespanha, 2001). *Suppose that the process is detectable and take a fixed $\rho = p \in \mathcal{P}$ and $\sigma = q \in \mathcal{Q}$. Then if the injected system is input-to-state stable (ISS), then the switched system is detectable.*

Proof, see Hespanha, (2001).

The following proposition is adopted from Theorem 1 to achieve detectability of the hybrid-controller DP system.

Proposition 1 (Certainty Equivalent Stabilization for hybrid DP system). *Suppose that the process of DP vessel is detectable and take a fixed $\rho = p \in \mathcal{P}$ and $\sigma = q \in \mathcal{Q}$, then*

- *The injected system is ISS; and*

- The switched system is detectable.

Proof. The proof is divided into two parts: the ISS of the injected system and the detectability of the switched system. If the former is satisfied, the latter is straightforward by using Theorem 1. The proof of the ISS of the injected system is given in Appendix A.4.

Small Error Property and Non-destabilization Property:

The scale-independent hysteresis switching logic guarantees the non-destabilization of the switching and the small error properties by the following theorem.

Theorem 2 (Scale-Independent Hysteresis Switching – Hespanha, 2001). Let $N_\sigma(\tau, t)$, $t > \tau \geq 0$, be the number of discontinuities of σ in the open interval (τ, t) . Let \mathcal{P} be a finite set with m elements. For any $p \in \mathcal{P}$ we have that

$$N_\sigma(\tau, t) \leq 1 + m + \frac{m \log \left(\frac{\mu_p(t)}{\varepsilon + e^{-\lambda t} \varepsilon_0} \right)}{\log(1+h)} + \frac{m\lambda(t-\tau)}{\log(1+h)}, \quad (6.85)$$

and

$$\int_0^t e^{-\lambda(t-\tau)} \gamma_\rho (\|e_\rho(\tau)\|) dt \leq (1+h)m\mu_p(t). \quad (6.86)$$

Equation (6.85) guarantees the non-destabilization of switching and (6.86) guarantees the small error properties.

Proof. See Hespanha (2001).

6.5.2 Tuning for Supervisory Control

The hysteresis parameter h is chosen positive to prevent chattering. However, if h is too large, the switching procedure will be frozen at previous operating regimes.

For the proposed hybrid DP system, the estimated PFW is kept unchanged due to data collection requirement for spectral analysis. Hence, the update rate of this estimation also affects the switching, specifically how fast the model switches to the current operating regime.

According to Böling et al. (2005), the forgetting factor λ is chosen such that the monitoring signal, μ_p , is neither too sluggish nor aggressive.

6.6 Numerical Simulation Results

6.6.1 Overview of Simulation

A model of a supply vessel (Table C.1) is used in the simulations to demonstrate the performance of the hybrid-controller DP vessel subject to varying sea states. The simulations are performed using Marine Systems Simulator (MSS) developed by the Norwegian University of Science and Technology (see Appendix D).

The environmental conditions from calm to extreme states are simulated by considering only JONSWAP distributed wave excitations. As shown in Table 6.4, the sea condition is calm sea during the first 2000s. Subsequently, it changes from calm to extreme seas over 11500s before dwelling in the extreme sea for 2500s. The ship is maintained in the desired position and heading $\eta_d = [0, 0, 0]^T$ while it is exposed to irregular head waves.

Simulations with the hybrid-controller DP vessel were performed to compare with the same vessel using the single-controller DP system subject to changes of sea states. Table 6.5 summarized the various cases of numerical simulations studied. In all cases, the estimated PFW is calculated by spectral analysis from surge, sway and yaw measurements. In Cases 2 and 3, the supervisory control will activate the appropriate model corresponding to the particular sea condition, signified by the signal

ρ . The mapping from signal ρ to switching signal σ is given in Table 6.2. In Case 3, acceleration feedback was implemented for surge and sway.

6.6.2 Results

The simulated performances of hybrid DP vessel for Cases from 1, 2 and 3 were shown in Figures 6.3, 6.5 and 6.7, respectively. Here, North, East, and Heading correspond to surge, sway, and yaw, respectively. Figures 6.4, 6.6 and 6.8 show the estimated PFWs for Cases 1, 2, and 3 and the switching signal σ for Cases 2 and 3.

As expected, the vessel in Case 1 becomes unstable when sea condition approaches higher sea states (Figures 6.3 and 6.4), while it is stable in Cases 2 and 3 from calm to extreme seas (Figures from 6.5 to 6.8). Thus, it is relevant to only compare the performance and consumed energy between Cases 2 and 3 in detail. The normalized statistical data obtained from position and heading measurement in Cases 2 and 3 are tabulated in Table 6.6. The performance indicators are standard deviations of position and heading, whereas the consumed energy indicators are those of control forces and moment.

6.6.3 Discussions

As shown in Case 1, a single output PID controller designed for moderate seas performs quite well in calm and moderate sea. However, in extreme seas, this controller shows poor performance in terms of instability. This is similar to the results presented in Sørensen et al. (2002). The notch effect of the adaptive observer unintentionally filters out the LF motions when the PFW enters the bandwidth of the controller (from 14500s onward). By using hybrid controller in Cases 2 and 3, the weather operation window is extended in terms of performance and stability. The simulations show that the switching among controllers does not affect the stability and performance of the whole system.

In Table 6.6, the performance indicators are standard deviation of surge, sway and yaw (s_x , s_y , and s_ψ , respectively), whereas the consumed energy indicators are those of control force in surge, sway and yaw ($s_{\tau 1}$, $s_{\tau 2}$, and $s_{\tau 3}$, respectively). Table 6.6 shows that the hybrid control using AFB gave better performance and consumed less energy than hybrid control using output PID. Thus, it is recommended that AFB should be used in harsh environment.

6.7 Experimental Results

6.7.1 Overview of Experiments

The experiments in this section were carried out to verify and validate the proposed hybrid control at plant control level from calm to extreme seas. Experiments were performed to compare hybrid control with single output PID controller at plant control level. Due to the limitation of the wave maker, it is not possible to generate high and long wave simultaneously; therefore, the experiments were carried out in two varying environmental conditions as follows:

- First set of tests (Tests 1a, 1b and 1c in Table 6.7) was carried out under changes of sea conditions from short to long waves, corresponding to calm to extreme seas in terms of wave frequency, but with constant wave height; and
- Second set of tests (Tests 2a, 2b and 2c in Table 6.8) was carried out under changes of sea conditions from calm to rough seas, according to the definition of Sea State codes (Price and Bishop, 1974).

While the purpose of the first set of tests is to investigate the effects of observer with or without WF filtering, the purpose of the second set is to study effects of both observer with or without WF filtering and AFB. It should be noted that all the data in this section are converted into equivalent full scale values.

The experiments were carried out using the model vessel, Cybership III (Appendix C). The Cybership III was exposed to head waves, so AFB was only implemented in surge.

6.7.2 Results and Discussions

The performances of single output PID controller (Test 1a) and hybrid controller (Tests 1b and 1c) in varying sea condition from short to long waves are shown in Figures 6.9, 6.11 and 6.13, respectively. The performances of single output PID controller (Test 2a) and hybrid controller (Test 2b and 2c) in varying sea condition from calm to rough seas are shown in Figures 6.15, 6.18 and 6.21, respectively. It should be noted that North, East and Heading correspond to surge, sway and yaw, respectively, of the vessel. The corresponding normalized statistical data are tabulated in Tables 6.9 and 6.10 in order to demonstrate the improved performance and efficiency of consumed energy of the proposed hybrid control as compared with those of single output PID. The performance indicators are standard deviation of surge, sway and yaw (s_x , s_y , and s_ψ , respectively), whereas the consumed energy indicators are those of control force in surge, sway and yaw ($s_{\tau 1}$, $s_{\tau 2}$, and $s_{\tau 3}$, respectively). Figures 6.10 and 6.16 show the estimated PFW of Test 1a and Test 2a, respectively.

In Test 1a, the deterioration of performance can be seen from the large deviation of sway and yaw when the PFW entered low frequencies corresponding to high and extreme seas (Figures 6.9 and 6.10). While extreme sea in reality involves both high and long waves, the extreme sea in this Test could be generated only with long wave of small wave height due to the limitation of the wave generator. This explains why the ship in Test 1a did not lose its stability, unlike that in the numerical simulation (Case 1), although its performance did indeed deteriorate significantly, particularly in sway and yaw. These experimental results are similar to the simulation results in Section 6.6.

In these simulations, the DP vessel using single output PID controller in varying environmental conditions from calm to extreme seas starts to be unstable in sway and yaw first and then later in surge when the sea state approaches extreme sea. The deteriorated performance of DP vessel using single output PID can be explained by the fact that the single output PID controller can only work well in moderate sea but not in high and extreme seas.

In Tests 1b and 1c, the performance in sway and yaw improved considerably as shown in Figures 6.11 and 6.13 and in columns (3), (4), (6) and (7) of Table 6.9. This can be explained by the fact that the DP system switched to the appropriate controller designed for the particular operating condition. Specifically, the observer with adaptive WF filtering is designed for calm and moderate seas while the observer without WF filtering is designed for extreme sea. The improved performance of DP vessel using observer without WF filtering has been shown in Chapter 5. The hybrid control obviously stabilizes and improves the performance of the DP vessel subject to change of environmental condition from calm to extreme seas; hence the hybrid control can indeed expand the weather window for DP vessel. These results are in tandem with the simulation results. Tests 1b and 1c showed no improvement in surge (columns (2) of Table 6.9). One reason is that the controller gains of hybrid DP system in Tests 1b and 1c, which were designed for extreme sea, may be too high for very long wave but small wave height in these cases. Therefore, improper tuning may result in aggressive thrust loads. In addition, small motions of the ship due to the small wave heights are difficult to measure accurately.

In the test of the single output controller performing in changing of sea state from calm to rough sea (Test 2a), the deterioration was not easy to visually observe

(see Figure 6.15) as the PFW only approaches the value of rough sea rather than the value of extreme sea.

The hybrid control (Tests 2b and 2c) performed better than the single output controller (Test 2a) in terms of reduction of standard deviation of surge, comparing Figures 6.18 and 6.21 against Figure 6.15, and column (2) of Table 6.10. However, the drawback is the slight increase of thrust in surge direction as shown in column (5) of Table 6.10. In this case, the sea state was ramped up to the rough sea rather than extreme sea; therefore, the supervisory control at the final stage switched to Controller 3. This controller is the smooth transformation of the observer with WF filtering and without WF filtering; thus, part of WF motion was in the closed loop. The slight increase of thrust in surge direction is expected because the controller compensates for both LF and WF motions in Tests 2b and 2c rather than only LF motion as in Test 2a. Although observer without WF filtering may result in a slight increase in control force needed, it is necessary to improve and most importantly stabilize the DP vessel in rough and extreme seas. This has been also shown in Section 5.3.

Tests 2b and 2c also showed improvement in sway and yaw in terms of reduction of standard deviation of surge (columns (3) and (4) of Table 6.10) and control force and moment (columns (6) and (7) of Table 6.10). This is similar to the results of Tests 1b and 1c.

The hybrid control using multi-PID and AFB controllers (Test 1c and Test 2c) performed better than hybrid control using multi-PID controller (Test 1b and Test 2b) as shown in Table 6.9 and Table 6.10. This is consistent with the results of Lindegaard (2003) and Section 5.4. It should be noted that acceleration feedback was applied for both surge and sway in simulations while it was applied only for surge in experiments. Hence, improved performances can be observed in both surge and sway from

simulations, but the improvements are only in surge from experiments. Here, the improved performance was the reduction of both standard deviations of position and control forces (including moment).

In Figures 6.11, 6.13, 6.18 and 6.21, the performances of the hybrid DP vessel did not show instability when the hybrid control systems performed switching. This suggests that the switching may not have a negative effect on the stability of the whole system. The supervisory control seems to work quite well by automatically tracking the PFW and switching to pre-defined models as shown in Figures 6.12, 6.14, 6.19 and 6.22.

6.8 Conclusions

This chapter presented the development of the hybrid DP system at high level control extending the operability and performance of DP system from calm to extreme seas. Three types of hybrid DP systems were developed: (a) multi-output PID controllers with position measurement, (b) multi-output PID + AFB controllers with position and acceleration measurements, and (c) multi-output PID + AFB with position, velocity and acceleration measurements. However, only the stability analysis of hybrid DP system using multi-output PID + AFB controllers with position and acceleration measurements were provided since the stability analysis of other types of hybrid DP system is similar.

Both simulation and experiment showed that the hybrid DP systems stabilized the vessel while the single-output controller DP system destabilized the vessel. The hybrid DP system using multi-output PID + AFB controllers performed better than the hybrid DP system using multi-output PID controllers. These findings indicate that the hybrid DP system using multi-output PID + AFB controllers can be used to expand the weather operation window from calm to extreme seas.

Table 6.1. Definition of Sea State codes (Price and Bishop, 1974).

Sea state code	Sea states	Wave height H_s (m)	PFW ω_p (rad/s)
0	Calm (glassy)	0	1.29
1	Calm (ripples)	0-0.1	1.29-1.11
2	Smooth (wavelets)	0.1-0.5	1.11-0.93
3	Slight	0.5-1.25	0.93-0.79
4	Moderate	1.25-2.5	0.79-0.68
5	Rough	2.5-4.0	0.68-0.60
6	Very Rough	4.0-6.0	0.60-0.53
7	High	6.0-9.0	0.53-0.46
8	Very high	9.0-14.0	0.46-0.39
9	Phenomenal (Extreme)	Over 14.0	< 0.39

Table 6.2. Sea state definition based on PFW.

	PFW ω_p (rad/s)	Process switching signal, ρ	Switching signal, σ
Calm seas	> 0.79	1	1
Moderate seas	0.79 – 0.67	2	2
High seas	0.67 – 0.45	3	3
Extreme seas	< 0.45	4	4

Table 6.3. Observers and controllers for proposed hybrid DP system using multi-PID and multi-PID + AFB

	Model 1 and 2	Model 3	Model 4
(a) Multi-PID controllers			
Observer	LF + WF state estimation with adaptive WF filtering	Smooth transformation between observers 2 and 4	State estimation without WF filtering
Controller	Output PID _i ($i=1, 2$)	Smooth transformation between PID ₂ and PID ₄	Output PID ₄
(b) Multi-PID and AFB controllers			
Observer	LF + WF state estimation with adaptive WF filtering	Smooth transformation between observers 2 and 4	State estimation without WF filtering
Controller	Output PID _i ($i=1, 2$)	Smooth transformation between PID ₂ and AFB	Output AFB

Table 6.4. Environmental conditions

Time start	Time end	Significant wave height, H_s (m)	PFW, ω_p (rad/s)
0	2000	1.2	0.79
2000	13500	varies from 1.2 to 13.5	from 0.79 to 0.18
13500	16000	13.5	0.18

Table 6.5. Simulation and experimental setup

Case 1	Single output PID controller from calm to extreme seas
Case 2	Hybrid controller using multi output PID controller with position measurement from calm to extreme seas
Case 3	Hybrid controller using multi output PID and AFB with position and acceleration measurements from calm to extreme seas

Table 6.6. Performance and consumed energy indicators (standard deviation values) normalized with respect to value obtained by Case 2.

	s_x	s_y	s_ψ	s_{τ_1}	s_{τ_2}	s_{τ_3}
Case 2	1	1	1	1	1	1
Case 3	0.96	0.97	0.99	0.95	0.96	0.99

Table 6.7. Experiments with hybrid control for DP vessel under changes of environmental conditions from short to long waves (constant H_s).

(a) Experiment summary					
Test 1a	Single output PID controller				
Test 1b	Hybrid controller using multi output PID controller				
Test 1c	Hybrid controller using multi output PID and AFB				
(b) Environmental conditions					
Time start (s)	Time end (s)	H_s (m)	T_p (s)	Sea state codes (corresponding to wave frequency)	
0	2000	1.2	7.9	Calm	
2000	13500	1.2	from 7.9 to 35	Calm to extreme	
13500	16000	1.2	35	Extreme	

Table 6.8. Experiments with hybrid control for DP vessel under changes of environmental conditions from calm to rough seas (varying H_s).

(a) Experiment summary					
Test 2a	Single output PID controller				
Test 2b	Hybrid controller using multi output PID controller				
Test 2c	Hybrid controller using multi output PID and AFB				
(b) Environmental conditions					
Time start (s)	Time end (s)	Duration (s)	H_s (m)	T_p (s)	Sea state codes
0	930	930	0.1	5.6	Calm
930	2000	1070	0.5	6.7	Smooth
2000	3260	1260	1.25	7.9	Slight
3260	4640	1380	2.5	9.2	Moderate
4640	6220	1580	3.0	9.7	-
6220	7940	1720	3.3	9.9	-
7940	9680	1740	3.6	10.2	Rough

Table 6.9. Performance and consumed energy indicators (standard deviation values) normalized with respect to value obtained by single output PID control (constant H_s).
Experiments with varying environmental conditions from short to long waves.

	s_x	s_y	s_ψ	s_{τ_1}	s_{τ_2}	s_{τ_3}
(1)	(2)	(3)	(4)	(5)	(6)	(7)
Test 1a	1	1	1	1	1	1
Test 1b	1.23	0.70	0.14	1.42	0.30	0.04
Test 1c	1.03	0.68	0.14	1.36	0.41	0.05

Table 6.10. Performance and consumed energy indicators (standard deviation values) normalized with respect to value obtained by single output PID control (varying H_s).
Experiments with varying environmental conditions from calm to rough sea.

	s_x	s_y	s_ψ	s_{τ_1}	s_{τ_2}	s_{τ_3}
(1)	(2)	(3)	(4)	(5)	(6)	(7)
Test 2a	1	1	1	1	1	1
Test 2b	0.90	0.84	0.89	1.18	0.81	0.87
Test 2c	0.85	0.80	0.81	1.13	0.76	0.80

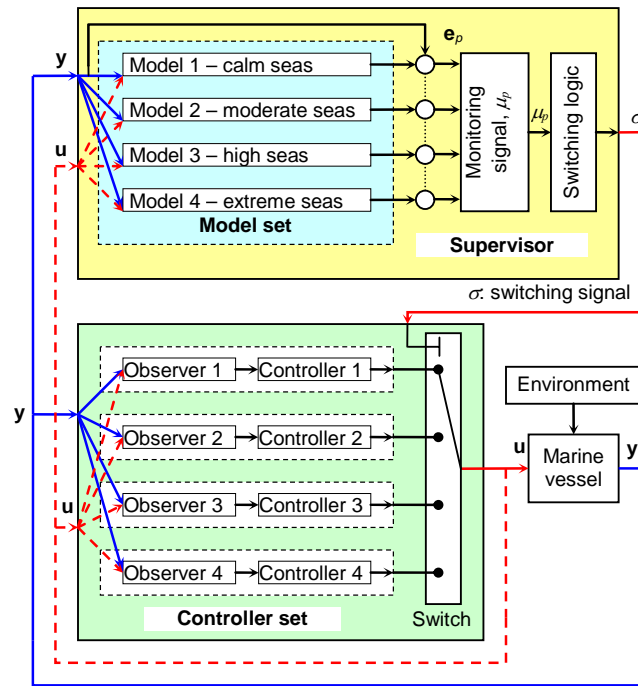


Figure 6.1. Concept of hybrid controller DP system using discrete switching signal.

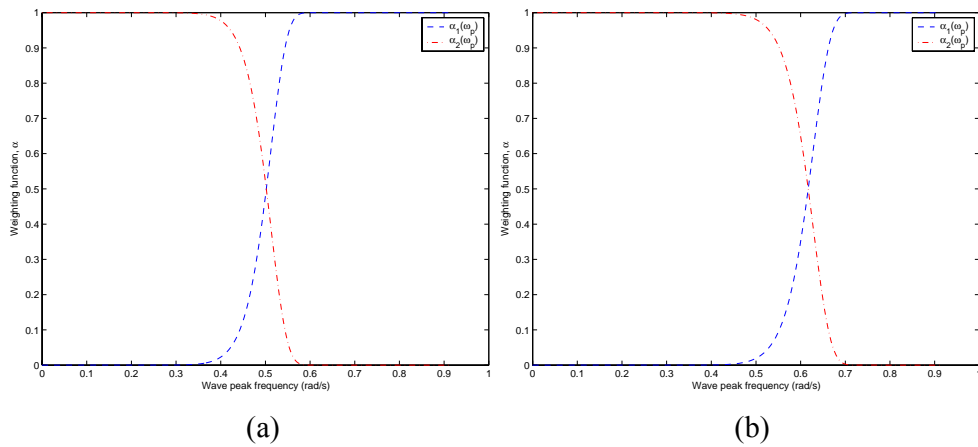


Figure 6.2. Weighting function in (a) test 1b and 1c, (b) test 2b and 2c.

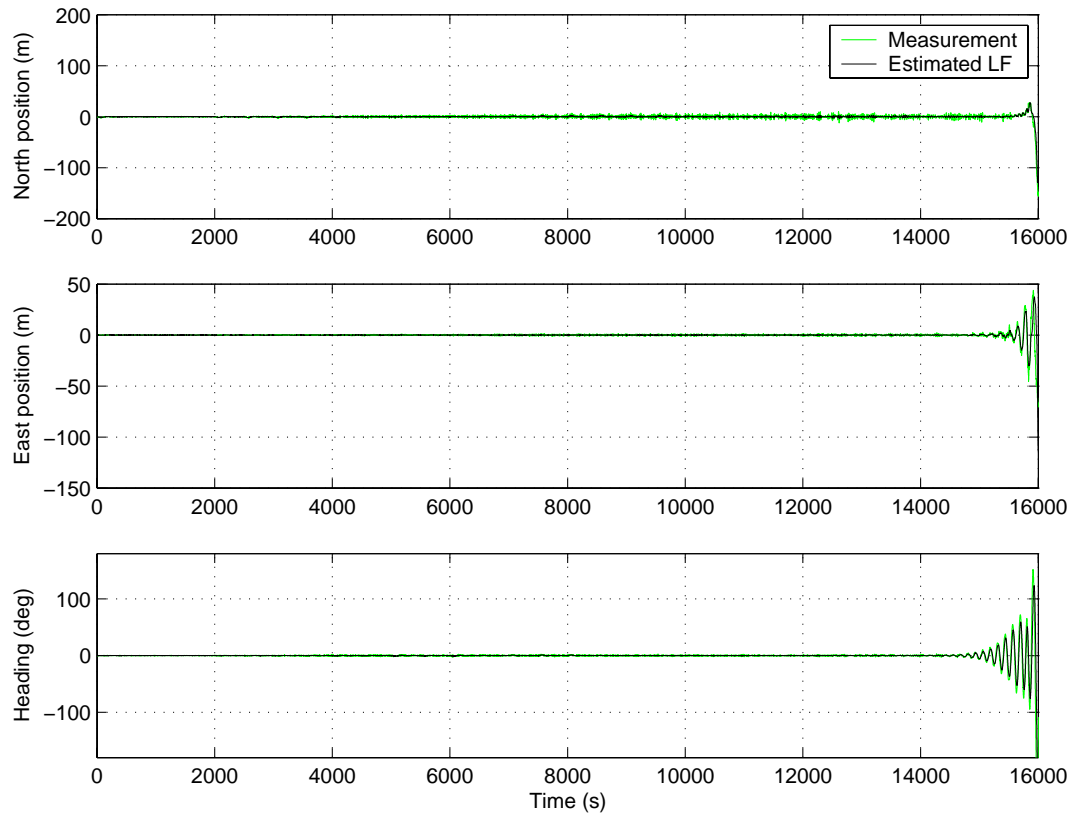


Figure 6.3. Position and heading of DP vessel in Case 1 using single output PID.

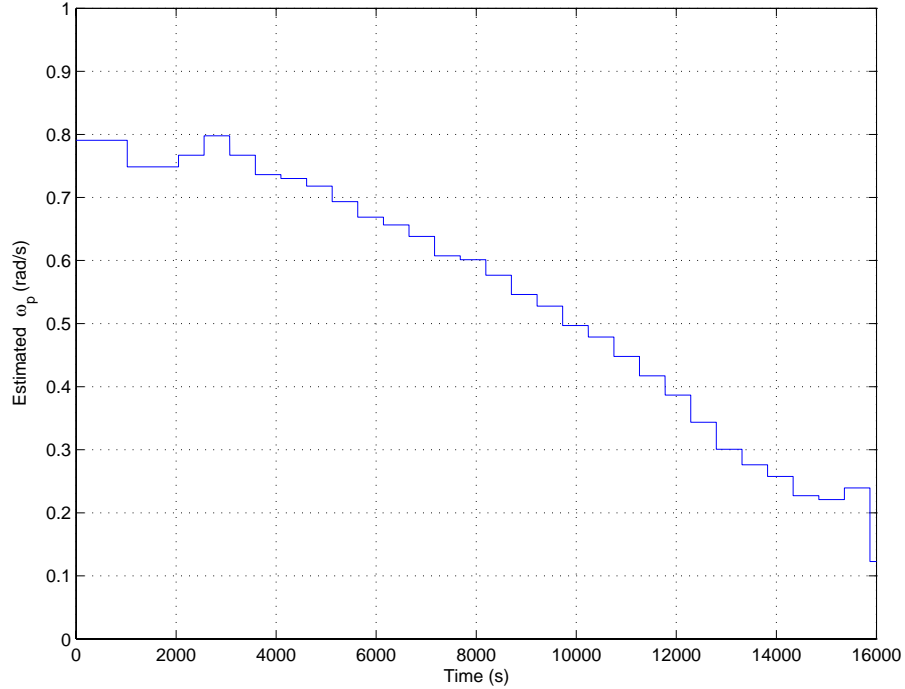


Figure 6.4. Estimated PFW in Case 1.

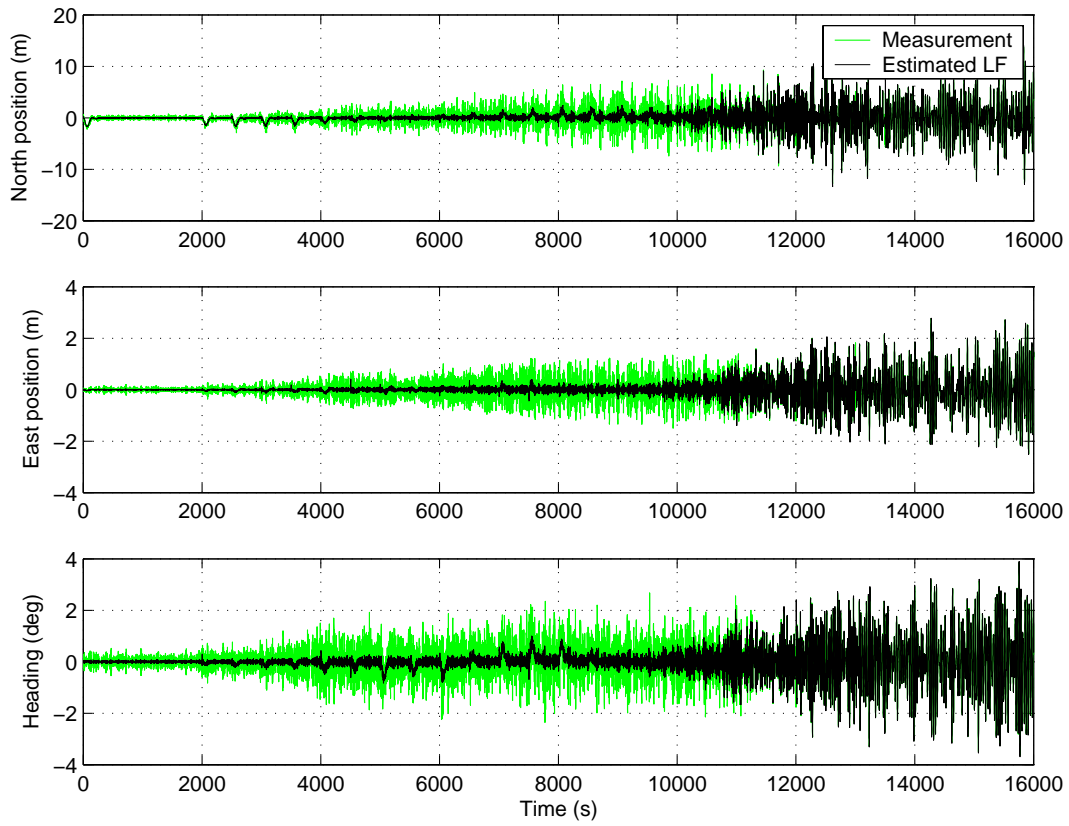


Figure 6.5. Position and heading of DP vessel in Case 2 with hybrid controller using multi-output PID.

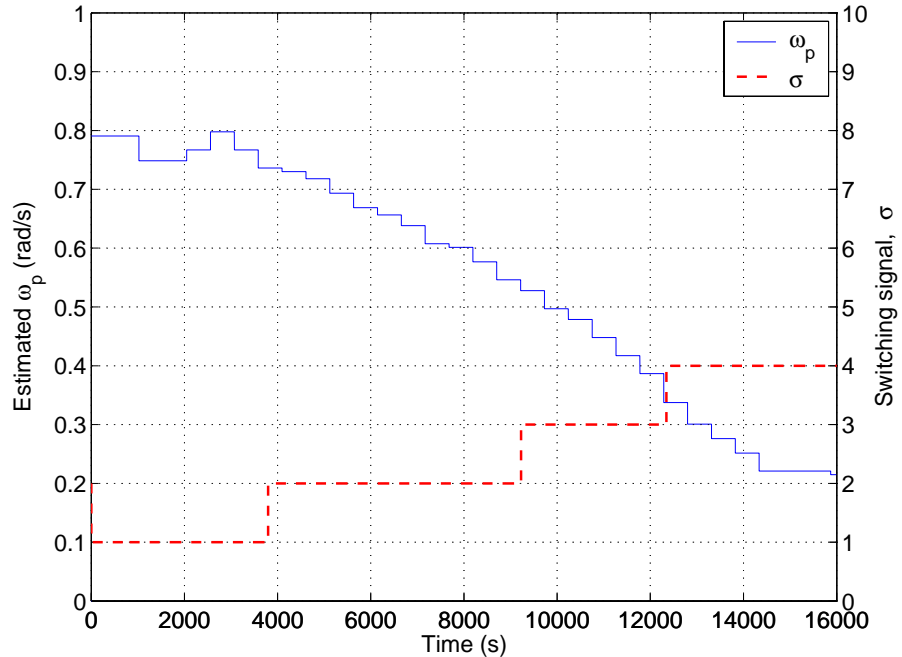


Figure 6.6. Estimated PFW and switching signal, σ , in Case 2.

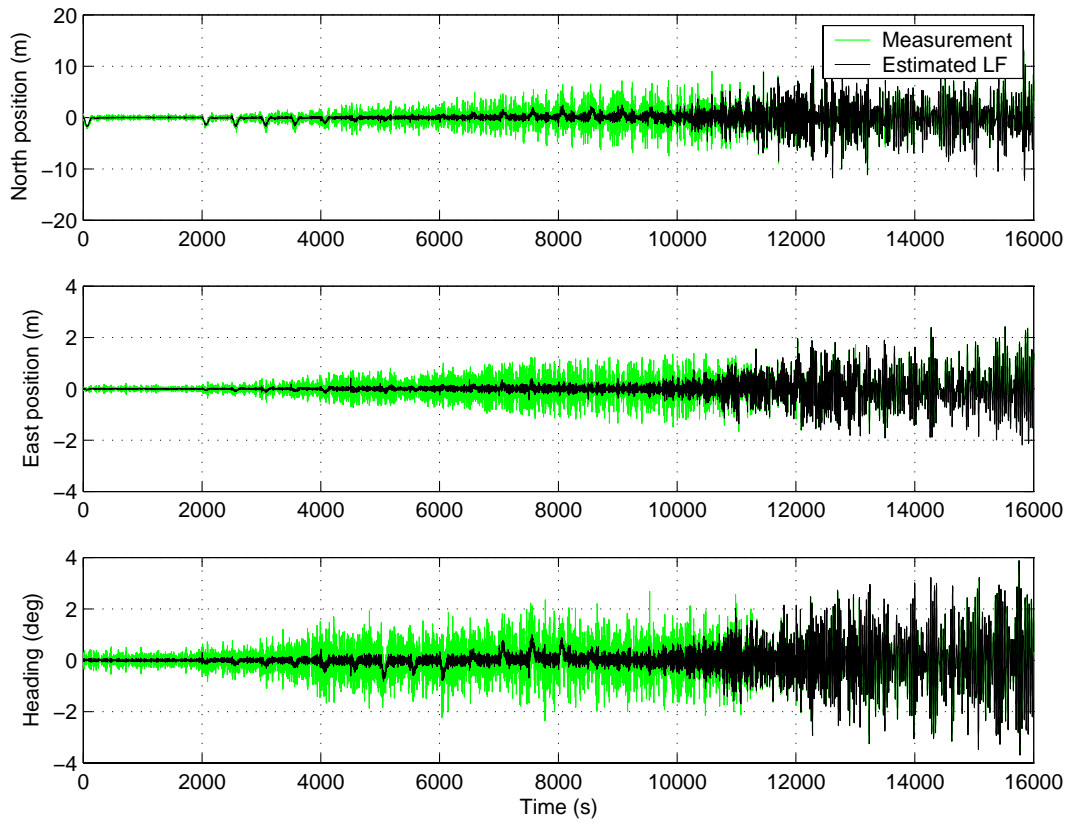


Figure 6.7. Performance of DP vessel in Case 3 with hybrid controller using multi-output PID and AFB.

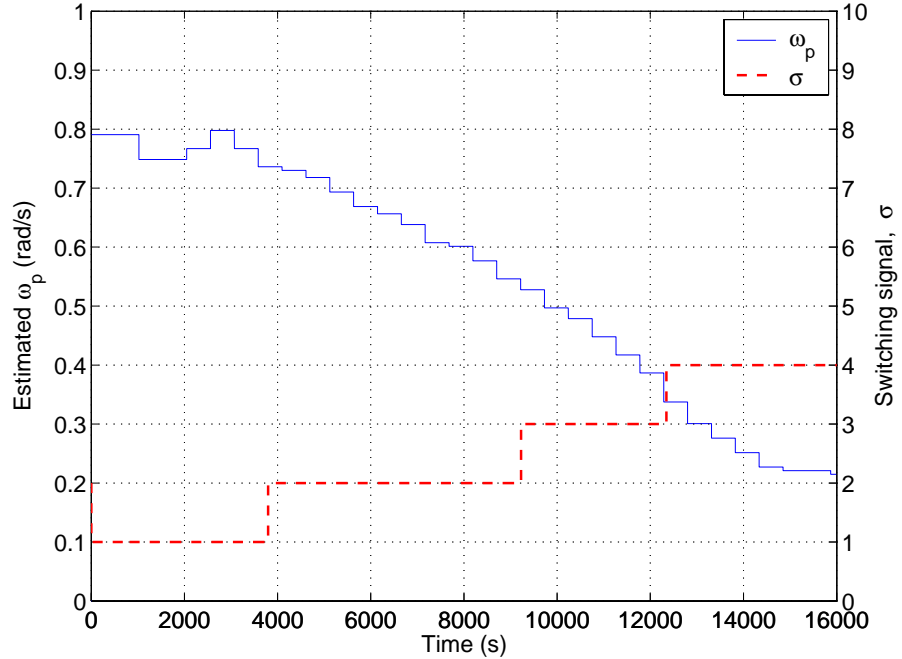


Figure 6.8. Estimated PFW and switching signal, σ , in Case 3.

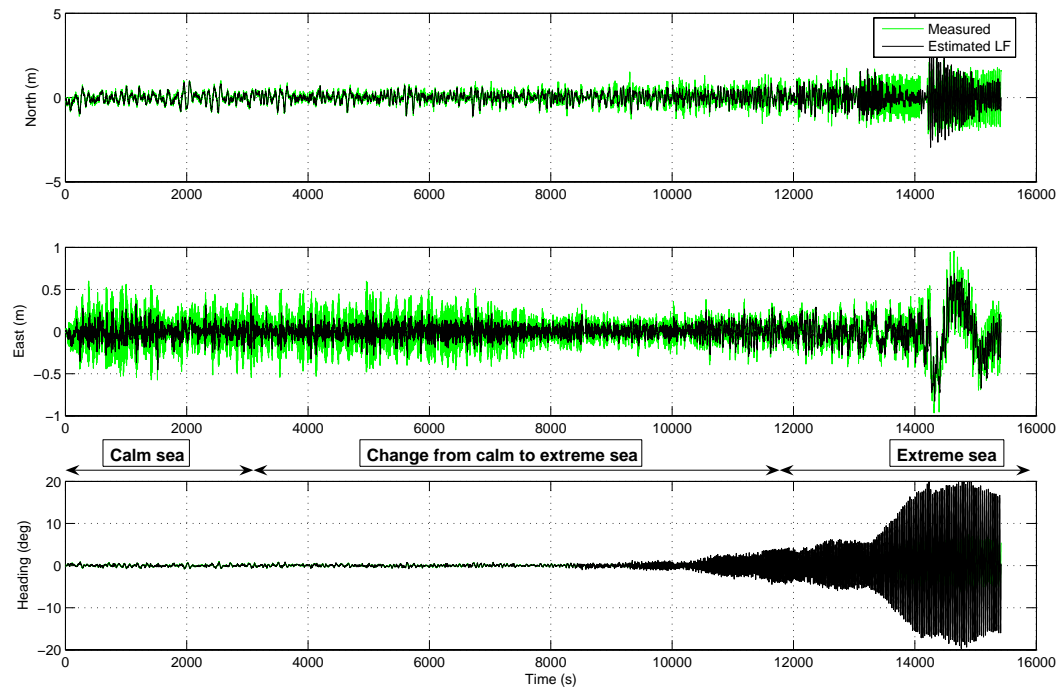


Figure 6.9. Performance of DP vessel in Test 1a using single output PID controller from short to long waves.

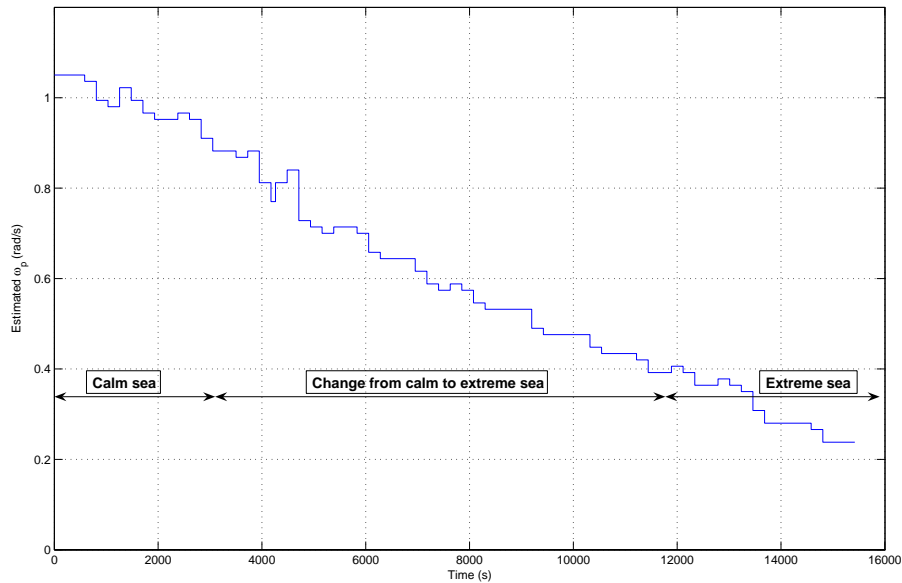


Figure 6.10. Estimated PFW in Test 1a.

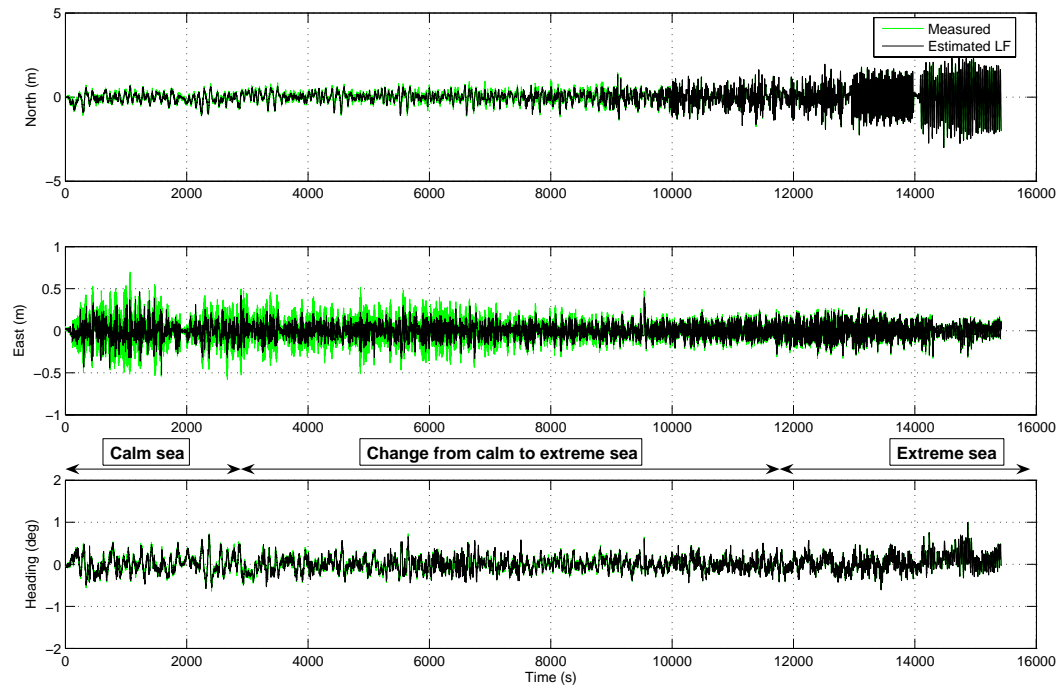


Figure 6.11. Performance of DP vessel in Test 1b with hybrid controller using multi-PID controller.

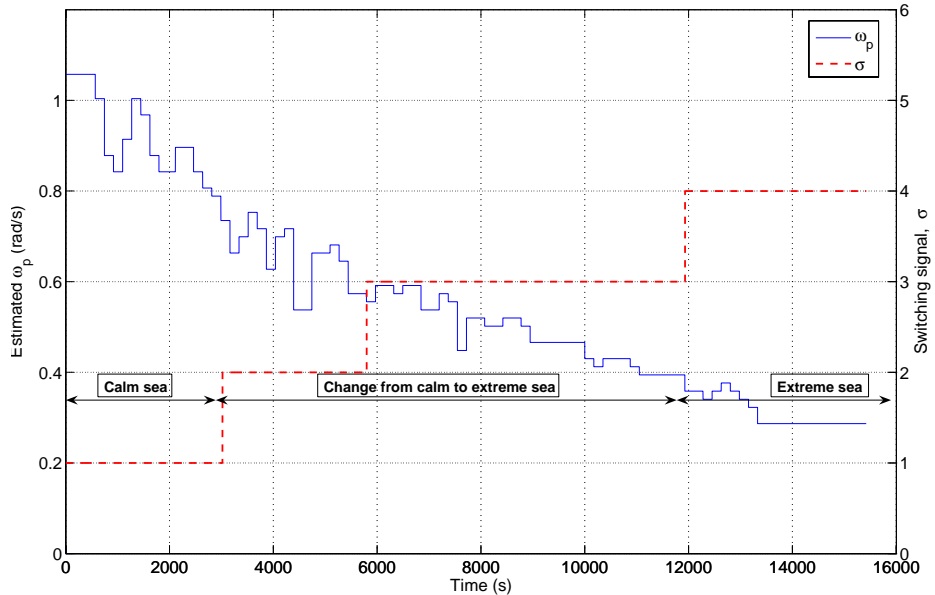


Figure 6.12. Estimated PFW and switching signal, σ , in Test 1b.

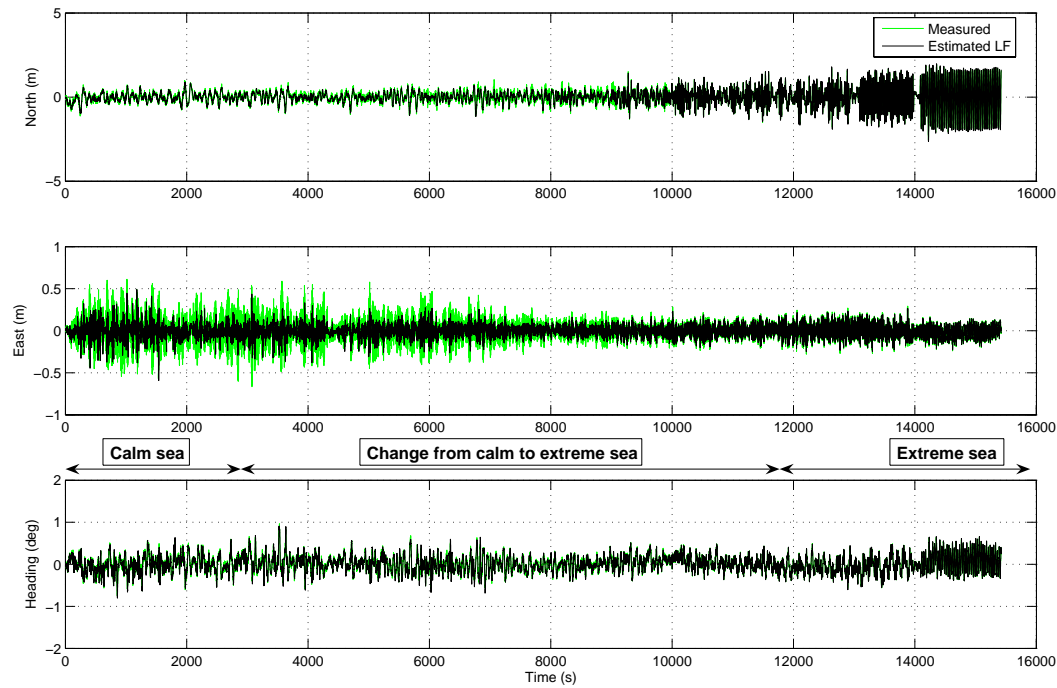


Figure 6.13. Performance of DP vessel in Test 1c with hybrid controller using multi output PID and AFB.

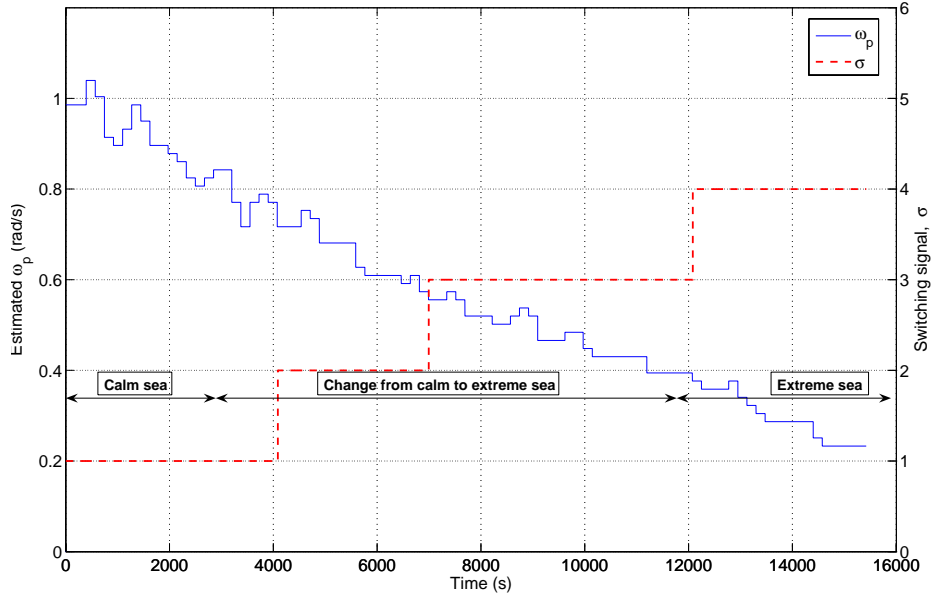


Figure 6.14. Estimated PFW and switching signal, σ , in Test 1c.

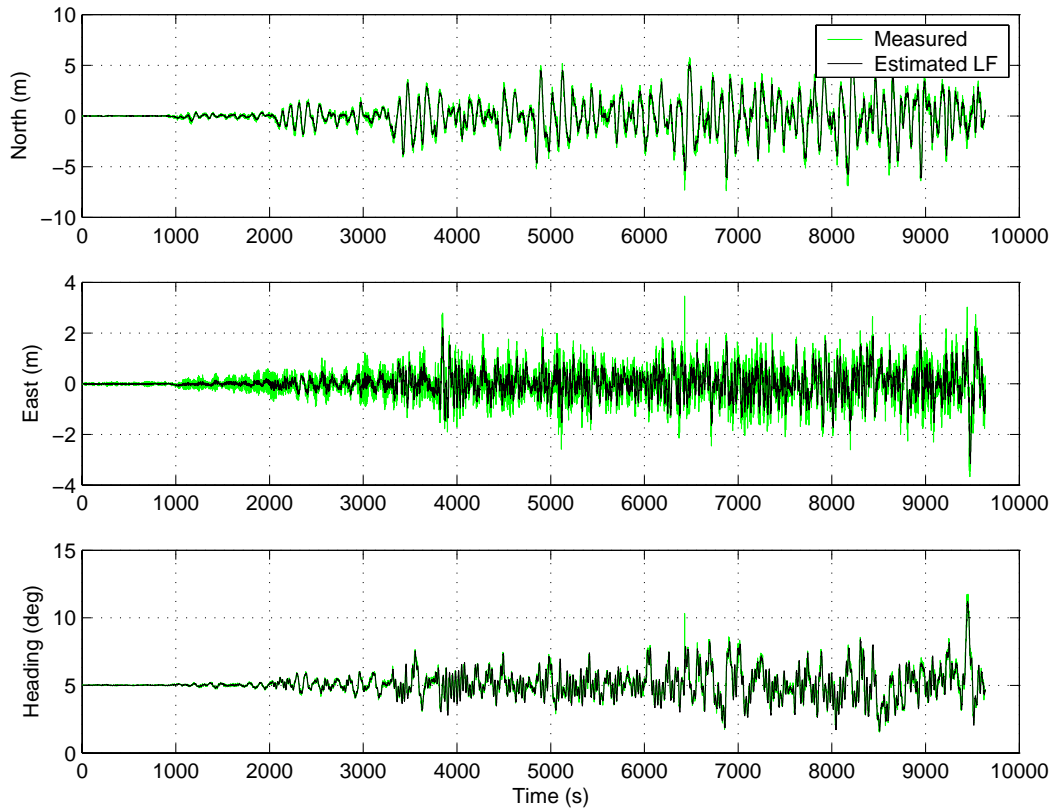


Figure 6.15. Performance of DP vessel in Test 2a with single output PID controller from calm to rough sea.

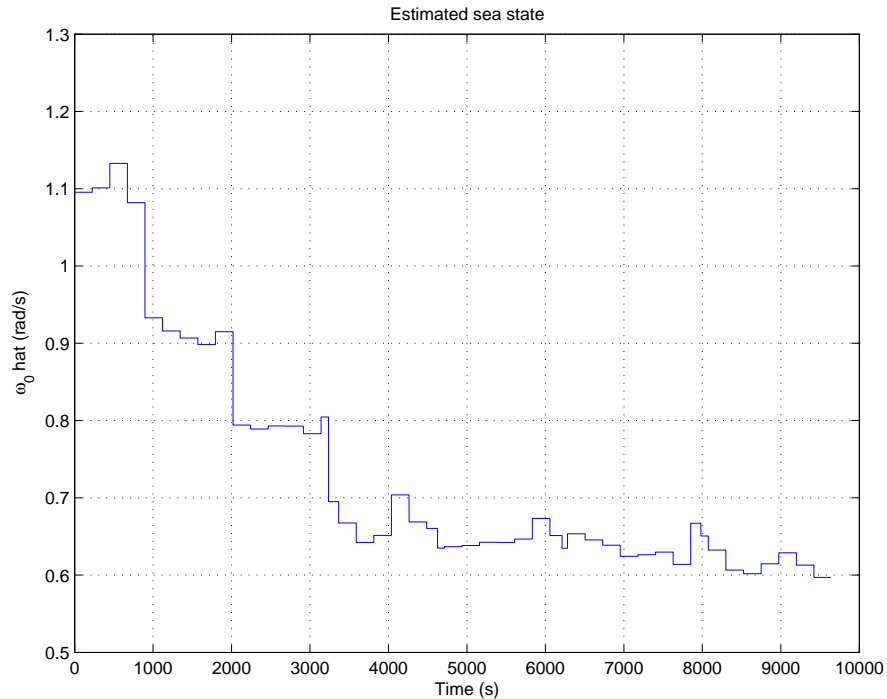


Figure 6.16. Estimated PFW in Test 2a.

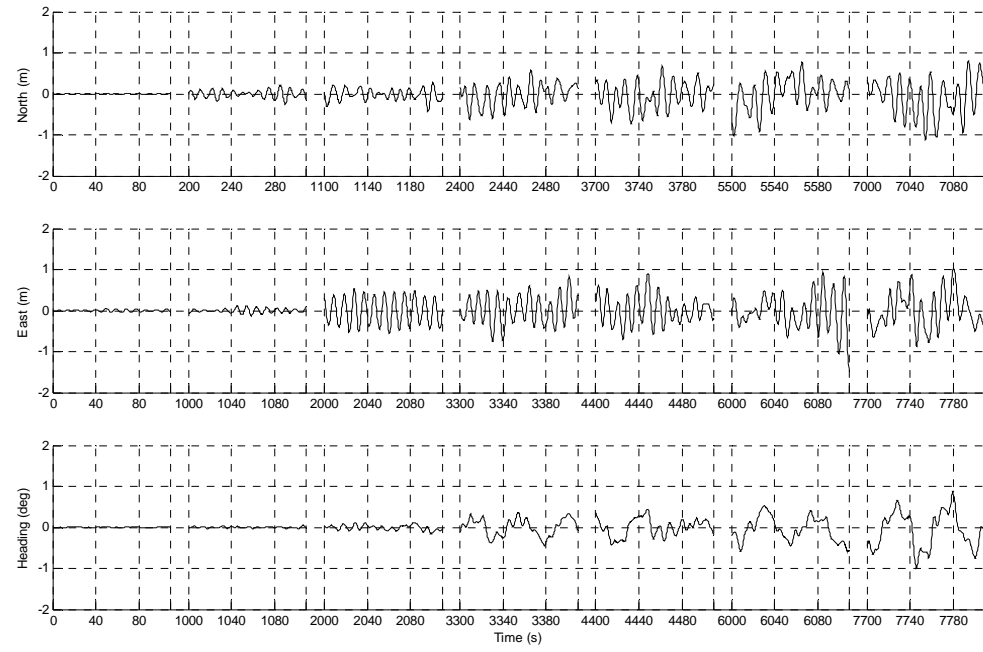


Figure 6.17. Estimated WF motion in 7 sea states (Test 2a).

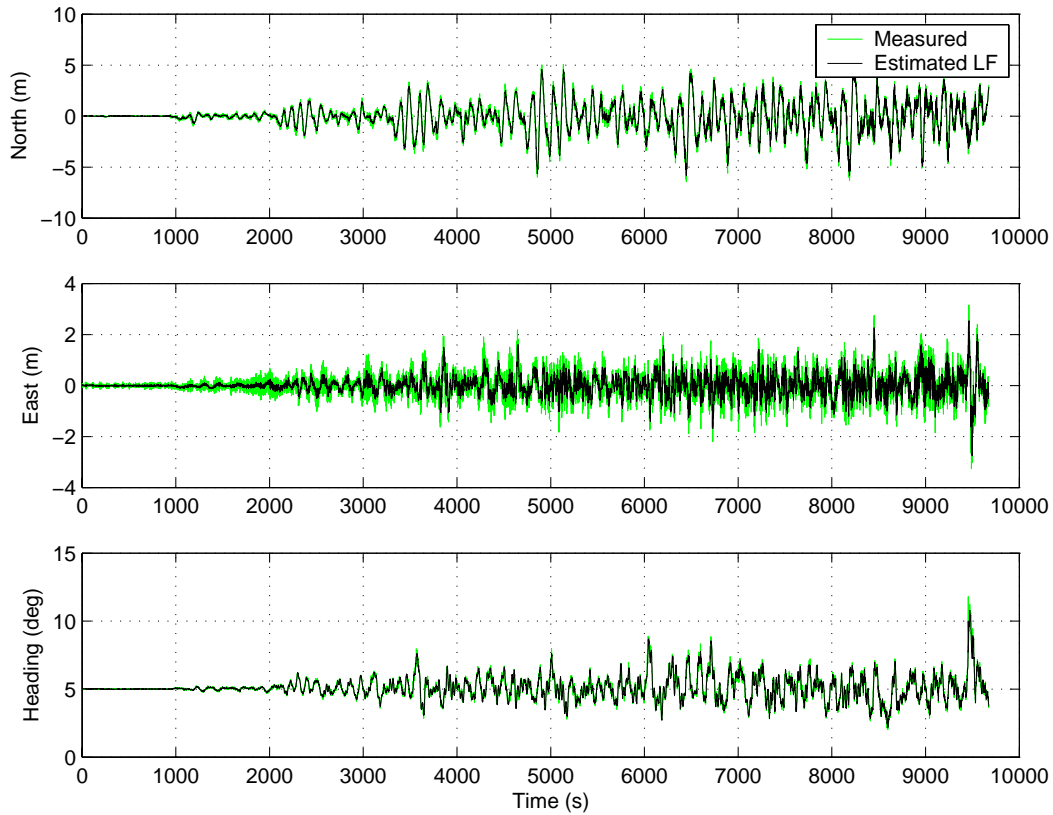


Figure 6.18. Performance of DP vessel in Test 2b with hybrid controller using multi-PID controller.

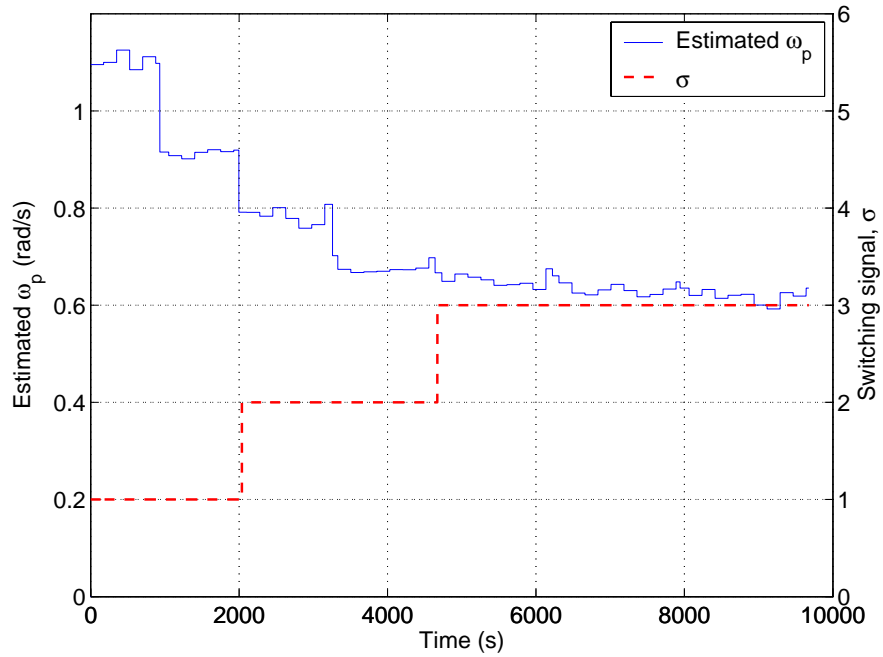


Figure 6.19. Estimated PFW and switching signal, σ , in Test 2b.

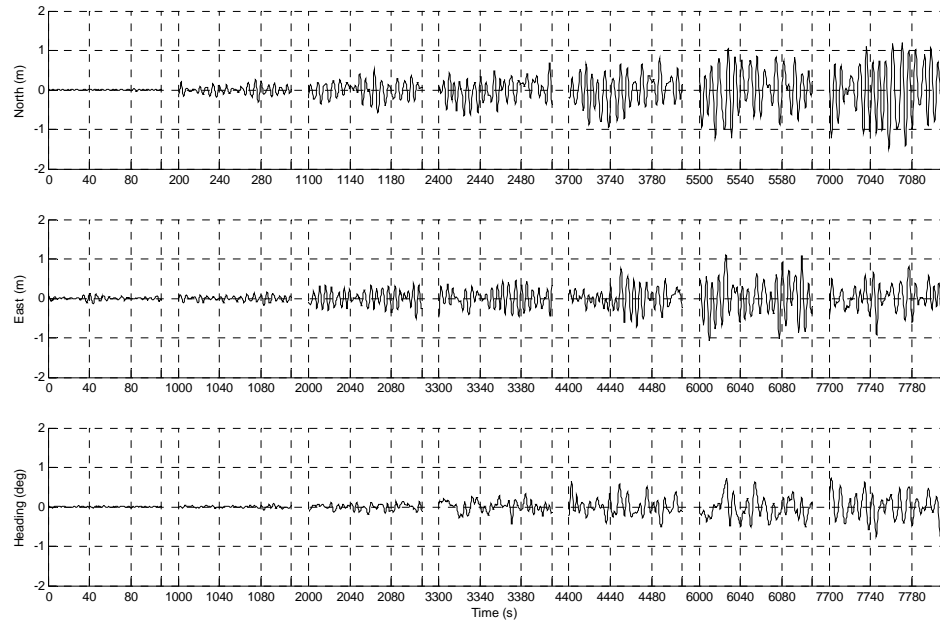


Figure 6.20. Estimated WF motion in 7 sea states (Test 2b).

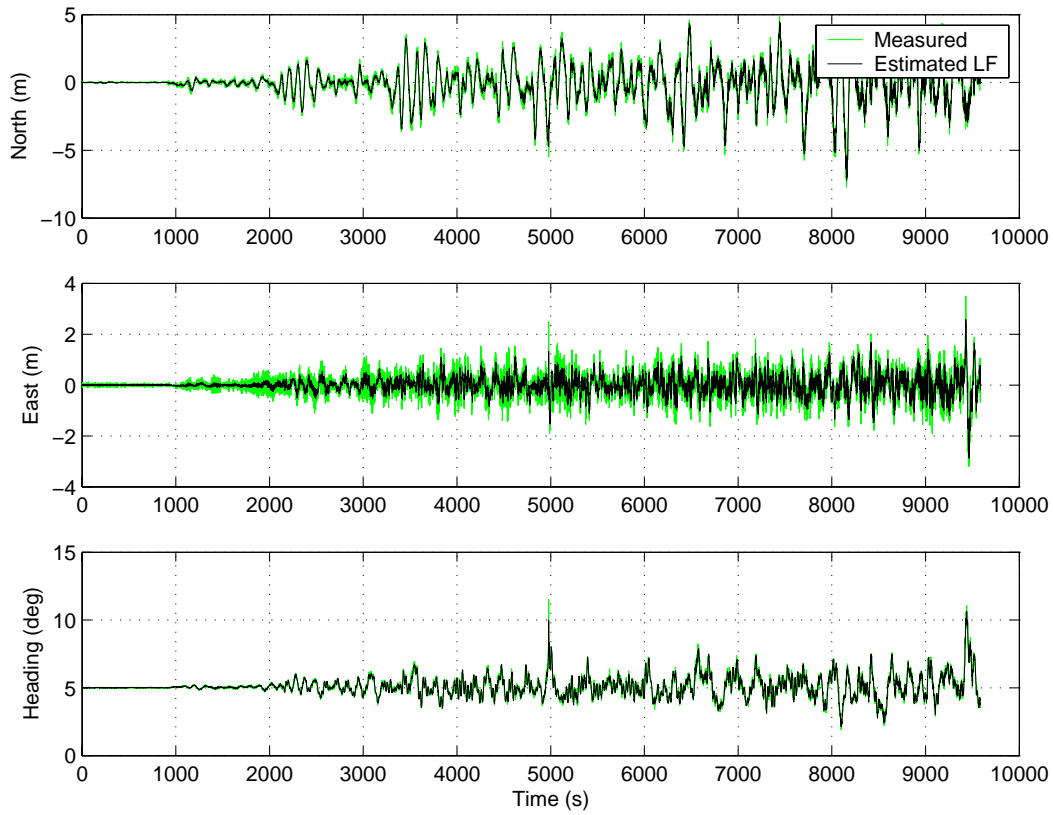


Figure 6.21. Performance of DP vessel in Test 2c with hybrid controller using multi output PID and AFB.

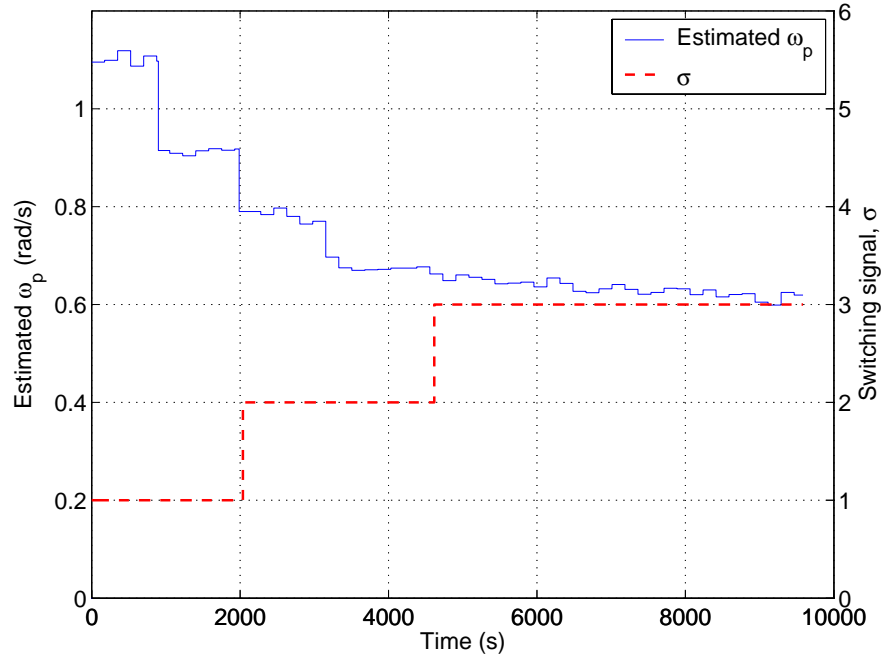


Figure 6.22. Estimated PFW and switching signal, σ , in Test 2c.

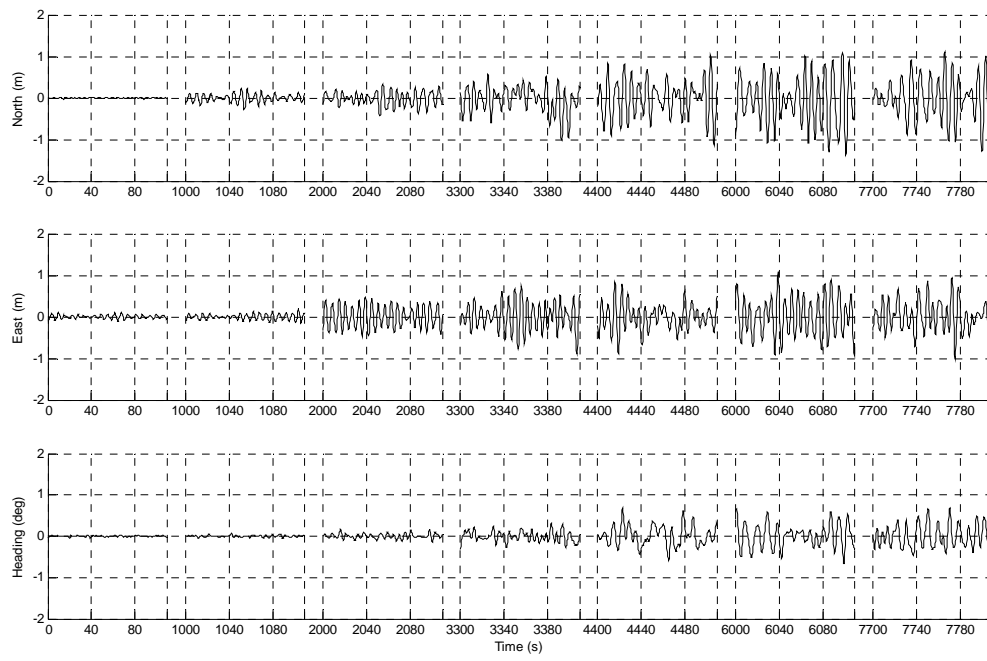


Figure 6.23. Estimated WF motion in 7 sea states (Test 2c).

Chapter 7 Conclusions and Recommendations for Further Work

The main purpose of this thesis is to provide a framework for hybrid control marine systems and in particular, to develop a hybrid control strategy for DP system handling from calm to extreme seas. The modeling of vessels was presented in the first part of the thesis (Chapter 2). The second part discussed the feasibilities of developing the hybrid control for marine control system and provided an example of hybrid control for marine operation from transit to station keeping (Chapters 3 and 4). In the third part, a hybrid control strategy was developed for DP system handling changes of environmental conditions from calm to extreme seas (Chapters 5 and 6).

In this chapter, the conclusions and summary on the results will be presented. The chapter ends with recommendations for further work.

7.1 Conclusions

The significant findings in this thesis can be summarized as follows:

1. The investigation on the feasibilities of developing hybrid control showed that controllers in marine control system can be integrated under three major domains in terms of functions, environments and speed regimes. Another dimension which can be treated separately is fault-tolerant control. In addition, the human operator interacting with the control system may be the fifth dimension. Changes in these domains will result in changes in control objectives, constraints, dynamic responses and disturbance characteristics. Although marine vessels nowadays usually operate in response to the changes of functions, environments and speed regimes, literature reviews showed that the current marine control system contains separate controllers which do not handle these changes in an integrated manner. The requirements of current marine operations and the

literature reviews indicate that it is feasible to develop the hybrid marine control system which can handle these changes by switching among multiple controllers.

Two main types of hybrid control are one in which switching was performed manually by the operator and one which adopted supervisory control such that switching was performed automatically via a switching logic.

2. The novel concept of hybrid marine control system integrating functions for DP, low speed maneuvering and transit operations into one hybrid control system in which the switching was performed by the operator was developed. As the purpose of this part was to show the feasibility of the hybrid control, numerical simulation was not performed. Instead, experiments with a model ship were conducted for operation from DP to PM and vice versa. The experiments showed good performances in terms of smooth transformation from one controller to another controller although the switching signal determined by the operator was discrete. The experiments for the transit operation of the model ship, Cybership III, could not be carried out since the tank is not large enough. The experiment data suggest that hybrid control can smoothly switch among several controllers for marine operation from transit to station keeping automatically, as opposed to the conventional manual operation which needs experience, concentration and is time-consuming.
3. The numerical simulations for DP vessel in extreme seas showed that nonlinear passive observer without WF filtering stabilized the DP vessel and performed better than nonlinear passive observer with WF filtering which is designed for DP in moderate seas. Although the experiments could not be conducted in extreme conditions due to the limitation of the wave maker, the experimental results for observer without WF filtering in high sea (approaching extreme sea)

and in very long waves showed similar conclusions to those from simulations. It may be inferred that when the sea state increases, the WF motion may be of low frequencies and therefore the DP system should compensate both LF and WF motions in extreme conditions rather than only LF motions.

4. The experiments with a model vessel under three sea states, i.e. moderate, moderately rough and rough seas, showed that AFB controller improved the performance of DP vessel compared with that using PID controller only, where the latter is usually designed for DP in moderate seas. The experimental results were similar to those in Lindegaard (2003). In addition, the experimental results showed that the level of improvement seems to increase with increasing sea states. The increased effectiveness of AFB in higher sea states is expected since AFB counteracts the excitations in the phase of acceleration which is earlier than the phase of position. In addition, the acceleration measurement used in AFB is more accurate than position measurement as acceleration measurement does not depend on the reference frame, unlike that for position measurement. The experiments confirmed that the AFB controller will improve the positioning performance in extreme conditions.
5. The hybrid control for DP system from calm to extreme sea was developed by adopting the concept of supervisory switching. This hybrid control strategy has the ability to automatically switch to the controller designed for the particular regime under which the vessel is operating at that point in time. Stability analysis, numerical simulations and experiments for the proposed hybrid control using supervisory control were provided. The performances of the DP vessel in simulations and experiments did not show instability when the hybrid control systems performed switching. This suggests that the switching may not have a

negative effect on the stability of the whole system. This was probably due to the use of hysteresis switching logic which slowed down the switching process and thus prevented chattering. The simulations and experiments showed that the multi-controller integrated into the hybrid control system performed better than the single controller when the vessel was exposed to changes of environmental conditions. The simulation and experimental results confirmed that by implementing hybrid control concept, the weather window for DP system can be expanded to extreme conditions.

7.2 Recommendations for Further Work

Based on the findings presented above, the study of hybrid marine control system can be extended to widen their applicability. Some recommendations for future work are listed below:

1. The switching among controllers in different speed regimes should be further studied. The choice of controllers to be switched can be different from those in this thesis. For example, the low speed maneuvering control proposed by Skjetne et al. (2005) can be set between DP controller and autopilot if the marine vessel requires speed maneuvering. Furthermore, the DP and low speed maneuvering controllers can be replaced by the unified controller for station keeping and low speed maneuvering proposed by Fossen (2005), and therefore the switching among controllers could be less frequent. Numerical simulations and case study from industry may also be included to verify the validity of this hybrid control approach.
2. The observer without WF filtering and AFB controller can also be implemented for PM at plant control level to improve and stabilize the performance of vessel in extreme conditions. Other aspects, such as set-point chasing, mooring system

configurations, and nonlinearity of observer due to mooring system need to be studied for PM to handle extreme conditions.

3. The hybrid control for PM vessels subjected to change of environmental conditions can be developed. Partly moored structures like single point mooring (SPM) of shuttle tankers should also be addressed.
4. The fault tolerance issue should be included in hybrid marine system control in addition to the changes of environmental conditions, speeds and functions. Fault tolerance refers to the ability of the control system to handle the failure of actuators, e.g. the failure of one thruster of DP system or failure of one cable of PM system. These failures may affect the performance and stability of the system. The supervisory control can be modified to facilitate fault-tolerant control since it can handle a large number of candidate controllers.
5. The present investigation on the feasibility of developing the hybrid control for marine vessel showed potential for a significant number of applications. The hybrid control concept can be implemented at other levels of marine control system. For example, the hybrid control at actuator level can be developed by integrating shaft speed control, torque control, power control and anti-spin control to handle thruster control from calm to extreme conditions. In transit function, the hybrid control at actuator level is able to switch between that with and that without roll control. At guidance and navigation level, the hybrid control can be implemented to switch among various possible paths.

References

- [1] Aamo O. M. and T. I. Fossen (1999). Controlling Line Tension in Thruster Assisted Mooring Systems. *Proceeding of the 1999 IEEE, International Conference on Control Applications*, pp. 1104–1109, August.
- [2] Åström K. J. and B. Wittenmark (1995). *Adaptive Control*, 2nd edition. Addison-Wesley Publ Co.
- [3] Bailey P. A., W. G. Price and P. Temarel (1998). A Unified Mathematical Model Describing the Maneuvering of a Ship Travelling in a Seaway. *Trans. RINA*, Vol. 140, pp. 131–149.
- [4] Balchen J. G., N. A. Jenssen and S. Sælid (1976). Dynamic Positioning Using Kalman Filtering and Optimal Control Theory. *IFAC/IFIP Symposium on Automation in Offshore Oil Field Operation*, Amsterdam, the Netherlands, pp. 183–186.
- [5] Balchen J. G., N. A. Jenssen, E. Mathisen and S. Sælid (1980). A Dynamic Positioning System Based on Kalman Filtering and Optimal Control. *Modeling, Identification and Control*, Vol. 1, Issue 3, pp. 135–163.
- [6] Berntsen P. I. B., O. M. Aamo, and A. J. Sørensen (2003). Modelling and Control of Single Point Moored Interconnected Structures. *In Proceedings of 6th Conference on Manoeuvring and Control of Marine Crafts (MCMC2003)*, Girona, Spain, September 16-19.
- [7] Berntsen P. I. B., B. J. Leira, O. M. Aamo and A. J. Sørensen (2004). Structural Reliability Criteria for Control of Large-Scale Interconnected Marine Structures. *In Proceedings of OMAE'04, paper OMAE2004-51350, 23rd International*

Conference on Offshore Mechanics and Arctic Engineering, June 20-25,
Vancouver, Canada.

- [8] Blanke M., M. Kinnaert, J. Lunze and M. Staroswiecki (2003). *Diagnostics and Fault-Tolerant Control*. Springer-Verlag, Berlin, Germany.
- [9] Böling J. M., D. Seborg, and J. Hespanha (2005). Multi-Model Control of a Simulated pH. *The 16th World Congress of Int. Federation of Automat. Control*.
- [10] Cummins W. E. (1962). The Impulse Response Function and Ship Motions. *Technical Report 1661*. David Taylor Model Basin. Hydromechanics Laboratory, USA.
- [11] El-Hawary F. (2001). *Ocean Engineering*. CRC Press.
- [12] Faltinsen O. M. and A. E. Løken (1979). Slow-drift Oscillations of a Ship in Irregular Wave. *Applied Ocean Research*, Vol. 1, Issue 1, pp. 21–31, June.
- [13] Faltinsen O. M. and R. Zhao (1989). Slow-drift Motions of a Moored Two-Dimensional Body in Irregular Waves. *Journal of Ship Research*, Vol. 33, Issue 2, pp. 93–106, June.
- [14] Faltinsen O. M. (1990). *Sea Loads on Ships and Offshore Structures*. Cambridge University Press.
- [15] Fossen T. I. (1994). *Guidance and Control of Ocean Vehicles*. John Wiley and Sons Ltd.
- [16] Fossen T. I. and J. P. Strand (1999). Passive Nonlinear Observer Design for Ships Using Lyapunov Methods: Full-scale experiments with a supply vessel. *Automatica*, Vol. 35, Issue 1, pp. 3–16.
- [17] Fossen T. I. and J. P. Strand (2001). Nonlinear Passive Weather Optimal Positioning Control (WOPC) System for Ships and Rigs: Experimental results. *Automatica*, Vol. 37, Issue 5, pp. 701-715.

- [18] Fossen T. I. (2002). *Marine Control Systems: Guidance Navigation and Control of Ships Rigs and Underwater Vehicles*. Marine Cybernetics, Trondheim, Norway.
- [19] Fossen T. I. (2005). A Nonlinear Unified State-Space Model for Ship Maneuvering and Control in a Seaway. *Journal of Bifurcation and Chaos* (ENOC'05 Plenary), to appear.
- [20] Fung P. T-K. and M. Grimble (1983). Dynamic Ship Positioning Using Self-Tuning Kalman Filter. *IEEE Transaction on Automatic Control*, Vol. 28, Issue 3, pp. 339–349.
- [21] Grimble M. J. (1978). Relationship between Kalman and Notch Filters Used in Dynamic Ship Positioning Systems. *Electronics Letters*. Vol. 14, Issue13, pp. 399-400.
- [22] Grimble M. J., R. J. Patton and D. A. Wise (1979). The Design of Dynamic Positioning Systems Using Extend Kalman Filtering Techniques. *Proceeding of OCEAN'79*, pp. 488-749.
- [23] Grimble M. J., R. J. Patton and D. A. Wise (1980a). The Design of Dynamic Positioning Systems Using Stochastic Optimal Control Theory. *Optimal Control Applications and Methods*. Vol. 1, pp. 167-202.
- [24] Grimble M. J., R. J. Patton and D. A. Wise (1980b). Use of Kalman Filtering Techniques in Dynamic Positioning Systems. *IEE Proceedings Vol. 127, Pt. D, No. 3*, pp. 93-102.
- [25] Grimble M. J. and M. A. Jonhson (1989). *Optimal Control and Stochastic Estimation. Theory and Applications*. John Wiley & Sons Ltd.

- [26] Hespanha J. P. (2001). Tutorial on Supervisory Control, Lecture Notes for the Workshop *Control using Logic and Switching for the 40th Conference on Decision and Control*, Orlando, Florida.
- [27] Hespanha J. P. and A. S. Morse (2002). Switching between Stabilizing Controllers. *Automatica*, Vol. 38, Issue 11, pp. 1905–1917.
- [28] Hespanha J. P., D. Liberzon and A. S. Morse (2003). Hysteresis-based Switching Algorithms for Supervisory Control of Uncertain Systems. *Automatica*, Vol. 39, Issue 2, pp. 263–272.
- [29] Hunt K. J., J. C. Kalkkuhl, H. Fritz and T. A. Johansen (1996a). Constructive Empirical modelling of Longitudinal Vehicle Dynamics Using Local Model Networks. *Control Engineering Practice*, Vol. 4, pp. 167–178.
- [30] Hunt K. J., R. Haas and J. C. Kalkkuhl (1996b). Local Controller Network for Autonomous Vehicle Steering. *Control Engineering Practice*, Vol. 4, pp. 1045–1051.
- [31] Hunt K. J., and T. A. Johansen (1997). Design and Analysis of Gain-Scheduled Control Using Local Controller Networks”, *Int. J. Control*, Vol. 66, Issue 5, pp. 619–651.
- [32] Isherwood M. A. (1972). Wind Resistance of Merchant Ships. *Trans. Inst. Naval Arch., RINA*, Vol. 115, pp. 327-338.
- [33] Leira, B. J., A. J. Sørensen and C. M. Larsen (2004). A Reliability-based Control Algorithm for Dynamic Positioning of Floating Vessels. *Structural Safety*, Elsevier Ltd., Vol. 26, pp. 1-28.
- [34] Liberzon D. and A. S. Morse (1999). Basic Problems in Stability and Design of Switched Systems. *IEEE Control Systems Magazine*, Vol. 19, No. 5, pp. 59-70, Oct. 1999.

- [35] Lindegaard K. P. W. (2003). *Acceleration Feedback in Dynamic Positioning*. PhD thesis, Department of Engineering Cybernetics, Norwegian University of Science and Technology, September.
- [36] Marine Cybernetic Laboratory (MCLab) www.itk.ntnu.no/marinkyb/MCLab/
- [37] Marine Systems Simulator (MSS), Norwegian University of Science and Technology, Trondheim <www.cesos.ntnu.no/mss>.
- [38] McLean D. (1990). Automatic Flight Control Systems. *Prentice Hall international series in systems and control engineering*. New York: Prentice Hall.
- [39] Newman J. N. (1974). Second-Order, Slowly-varying Forces on Vessels in Irregular Waves. *Proc. Int. Symp. Dynamics of Marine Vehicles and Structures in Waves*, Mechanical Engineering Publication Ltd., pp. 182-186, London.
- [40] Nilsen T. (2003). *Development of Cybership III*. Master thesis, Department of Marine Technology, Norwegian University of Science and Technology.
- [41] Nomoto K., T. Taguchi, K. Honda and S. Hirano (1957). On the Steering Qualities of Ships. *Technical report*. International Shipbuilding Progress, Vol. 4.
- [42] Norrbin N. H. (1963). On the Design and Analyses of the Zig-Zag Test on Base of Quasi Linear Frequency Response. *Technical Report B 104-3*. The Swedish State Shipbuilding Experimental Tank (SSPA). Gothenburg, Sweden.
- [43] Norrbin N. H. (1970). Theory and Observation on the Use of a Mathematical Model for Ship Maneuvering in Deep and Confined Waters. In *Proc. of the 8th Symposium on Naval Hydrodynamics*. Pasadena, California, pp. 807–904.
- [44] Oishi M. and C. Tomlin (1999). Switched Nonlinear Control of a VSTOL Aircraft. In *the Proceedings of the 38th IEEE Conference on Decision and Control*, Phoenix, December.

- [45] Oishi M. and C. Tomlin (2000). Switching in Nonminimum Phase Nonlinear Systems: Applications to a VSTOL Aircraft, *In the Proceedings of the American Control Conference*, Chicago, June.
- [46] Oishi M., I. Mitchell, A. Bayen, C. Tomlin and A. Degani (2002). Hybrid Verification of an Interface for an Automatic Landing. *In the Proceedings of the 41st IEEE Conference on Decision and Control*, Las Vegas, December.
- [47] Oosterom M. and R. Babuška (2005). Design of a Gain-scheduling Mechanism for Flight Control Laws by Fuzzy Clustering. *Control Engineering Practice*, May.
- [48] Perez T. and M. Blanke (2003). DCMV a Matlab/Simulink® Toolbox for Dynamics and Control of Marine Vehicles. *In: 6th IFAC Conference on Manoeuvring and Control of Marine Craft, MCMC'03*.
- [49] Perez, T., Ø. N. Smogeli, T. I. Fossen, and A. J. Sørensen (2005). An Overview of Marine Systems Simulator (MSS): A Simulink® Toolbox for Marine Control Systems. *Scandinavian Conference on Simulation and Modeling SIMS05*, Trondheim, Norway. October.
- [50] Pettersen K. Y. and E. Lefeber (2001). Way-point Tracking Control of Ships. *Proceedings of the 40th IEEE conference on decision & control*, pp. 940–945. IEEE, Orlando, FL, USA.
- [51] Price W. G. and R. E. D. Bishop (1974). *Probabilistic Theory of Ship Dynamics*. Chapman and Hall. London.
- [52] Reddy D.V. and M. Arockiasamy (1991). *Offshore Structures*. Krieger Publishing Company, Malabar, Florida.

- [53] Sælid S., N. A. Jessen and J. G. Balchen (1983). Design and Analysis of a Dynamic Positioning System Based on Kalman Filtering and Optimal Control. *IEEE Transaction on Automatic Control*, Vol. 28, Issue 3, pp. 331-339.
- [54] Skjetne R., T. I. Fossen, and P. V. Kokotovic (2004). Robust Output Maneuvering for a Class of Nonlinear Systems. *Automatica*, Vol. 40, Issue 3, pp. 373-383.
- [55] Skjetne R., T. I. Fossen, and P. V. Kokotovic (2005). Adaptive Output Maneuvering with Experiments for a Model Ship in a Marine Control Laboratory. *Automatica*, Vol. 41, Issue 4, pp. 289-298.
- [56] Skjetne R. (2005). *The Maneuvering Problem*. PhD thesis, Department of Engineering Cybernetics, Norwegian University of Science and Technology.
- [57] Smogeli Ø. N., Sørensen A. J. and Minsaas K. J. (2005). The Concept of Anti-Spin Thruster Control. *Submitted to Control Engineering Practice (CEP)*.
- [58] Smogeli Ø. N., L. Aarseth, E. S. Overå, A. J. Sørensen and K. J. Minsaas (2002). Anti-spin thruster control in extreme seas. In *Proceedings of 6th Conference on Manoeuvring and Control of Marine Crafts (MCMC2003)*, Girona, Spain, September 16-19.
- [59] Smogeli Ø. N, E. Ruth and A. J. Sørensen (2005). Experimental Validation of Power and Torque Thruster Control. *13th Mediterranean Conference on Control and Automation (MED'05)*, June 27-29, Limassol, Cyprus.
- [60] Smogeli Ø. N., A. J. Sørensen and T. I. Fossen (2004). Design of a Hybrid Power/torque Thruster controller with Thrust Loss Estimation. *Proceedings of the IFAC Conference on Control Applications in Marine Systems (CAMS'04)*, July 7-9, Ancona, Italy.

- [61] SNAME (1950). The Society of Naval Architects and Marine Engineers. Nomenclature for Treating the Motion of a Submerged Body through a Fluid. In: *Technical and Research Bulletin No. 1-5*.
- [62] Sørensen A. J. and A. K. Ådnanes (1997). High Performance Thrust Allocation Scheme in Positioning of Ships Based on Power and Torque Control. In the *Proc. of Dynamic Positioning Conference, Dynamic Positioning Committee, Marine Technology Society*, pp. 1-14, Session 9, Houston, Texas.
- [63] Sørensen A. J., S. I. Sagatun, and T. I. Fossen (1996). Design of a Dynamic Position System Using Model-based Control. *Control Engineering Practice*, Vol. 4, Issue 3, pp. 359–368.
- [64] Sørensen A. J. and J. P. Strand (1998). Positioning of Semi-submersible with Roll and Pitch Damping. *Proc. of the IFAC Conference on Control Applications in Marine Systems (CAMS'98)*. Fukuoka, Japan, pp. 67-73.
- [65] Sørensen A. J. and J. P. Strand (2000). Positioning of Small-Waterplane-Area Marine Constructions with Roll and Pitch Damping. *Journal of Control Engineering in Practice*, Vol. 8, Issue 2, pp. 205-213.
- [66] Sørensen A. J., J. P. Strand and H. Nyberg (2002). Dynamic of Ships and Floaters in Extreme Seas. *Proceedings of OCEANS'02 MTS/IEEE*, pp. 1849–1854.
- [67] Sørensen A. J., K. P. W. Lindegaard and E. D. D. Hansen (2002). Locally Multi-objective H_2 and H_∞ Control of Large-scale Interconnected Marine Structures. *Proceedings of CDC'02, 41st IEEE Conference on Decision and Control*, pp. 1849–1854.
- [68] Sørensen, A. J., E. Pedersen and Ø. Smogeli (2003). Simulation-Based Design and Testing of Dynamically Positioned Marine Vessels. In Proceedings of

International Conference on Marine Simulation and Ship Maneuverability,
MARSIM'03, August 25 - 28, Kanazawa, Japan.

- [69] Sørensen A. J. (2004). *Short Course on Marine Control Systems*. National University of Singapore, 3 – 5 May.
- [70] Sørensen, A. J. (2005a). Marine Cybernetics: Modelling and Control. *Lecture Notes, Fifth Edition, UK-05-76*, Department of Marine Technology, the Norwegian University of Science and Technology, Trondheim, Norway.
- [71] Sørensen, A. J. (2005b). Structural Issues in the Design and Operation of Marine Control Systems. *IFAC Journal of Annual Reviews in Control*, Vol. 29, Issue 1, pp. 125-149, Elsevier Ltd.
- [72] Sørheim H. R. (1981). *Dynamic Positioning in Single Point – A Theoretical Analysis of Motions, and Design and Evaluation of an Optimal Control System*. PhD thesis, Department of Engineering Cybernetics, the Norwegian Institute of Technology, the University of Trondheim, Norway.
- [73] Strand J. P., A. J. Sørensen and T. I. Fossen (1998). Modelling and control of thruster assisted positioning mooring system for ships. *Modelling, Identification and Control*, Vol. 19, Issue 2, pp. 65-71.
- [74] Strand, J. P. and T. I. Fossen (1999). Nonlinear Passive Observer for Ships with Adaptive Wave Filtering. *New Directions in Nonlinear Observer Design* (H. Nijmeijer and Fossen T.I., Eds.). Chap. I-7, pp. 113-134. Springer-Verlag, London.
- [75] Strand J. P. (1999). *Nonlinear Position Control Systems Design for Marine Vessels*. PhD thesis, Department of Engineering Cybernetics, Norwegian University of Science and Technology.

- [76] Torsethaugen K. (1996). Model for a Doubly Peaked Wave Spectrum. *Technical Report STF22A96204. SINTEF*. Trondheim, Norway, Prepared for Norsk Hydro.
- [77] Torsetnes G. (2004). Nonlinear Control and Observer Design for Dynamic Positioning using Contraction Theory. Master Thesis, Department of Engineering Cybernetics, Norwegian University of Science and Technology.
- [78] Triantafyllou M. S. (1990). *Cable Mechanics with Marine Applications*, Lecture Notes. Department of Ocean Engineering, Massachusetts Institute of Technology, Cambridge, MA 02139, USA, May.
- [79] Wang F. and V. Balakrishnan (2002). Improved Stability Analysis and Gain Synthesis for Parameter-Dependent Systems, *IEEE Transaction for Automatic Control* Vol. 47, Issue 5, pp. 720-734.

Appendix A Stability Analysis of Hybrid Control for DP System

A.1 Fundamental Stability Analysis

Theorem A.1 Consider the system

$$\dot{\mathbf{x}} = \mathbf{T}^T \mathbf{A} \mathbf{T} \mathbf{x} \quad (\text{A.1})$$

where \mathbf{T} is transformation matrix given by

$$\mathbf{T}(\psi) = \text{diag}(\mathbf{R}^T(\psi), \dots, \mathbf{R}^T(\psi), \mathbf{I}) \quad (\text{A.2})$$

Assume that

- 1) $|\dot{\psi}| \leq r_{\max}$ provided that r_{\max} is sufficiently small, and
- 2) \mathbf{A} is Hurwitz.

Then the origin \mathbf{x} of (A.1) is uniformly locally exponentially stable (ULES). If r_{\max} is larger than any physical upper limit for $|\dot{\psi}(t)|$, (A.1) is said to be uniformly globally exponentially stable (UGES).

Proof.

Define

$$\mathbf{z} = \mathbf{T}(\psi) \mathbf{x}, \quad (\text{A.3})$$

$$\frac{d\mathbf{T}(\psi)}{dt} = \dot{\mathbf{T}}(\psi) = \dot{\psi} \mathbf{S}_T \mathbf{T}(\psi). \quad (\text{A.4})$$

Then

$$\dot{\mathbf{z}} = \dot{\mathbf{T}} \mathbf{x} + \mathbf{T} \dot{\mathbf{x}} = \dot{\psi} \mathbf{S}_T \mathbf{T} \mathbf{x} + \mathbf{T} \mathbf{T}^T \mathbf{A}_c \mathbf{T} \mathbf{x} = (\dot{\psi} \mathbf{S}_T + \mathbf{A}_c) \mathbf{z}, \quad (\text{A.5})$$

where $\mathbf{S}_T = \text{diag}(\mathbf{S}^T, \dots, \mathbf{S}^T, \mathbf{0})$. The matrix \mathbf{S} appear in the differential of the rotation matrix, $\mathbf{R}(\psi) \in \mathbb{R}^{3 \times 3}$, given by

$$\dot{\mathbf{R}}(\psi) = \dot{\psi} \mathbf{S} \mathbf{R}(\psi), \quad (\text{A.6})$$

$$\text{where } \mathbf{S} = \begin{bmatrix} 0 & -1 & 0 \\ 1 & 0 & 0 \\ 0 & 0 & 0 \end{bmatrix}. \quad (\text{A.7})$$

If \mathbf{A} is Hurwitz, then there exists a $\mathbf{P} = \mathbf{P}^T > \mathbf{0}$ such that

$$\mathbf{PA}_c + \mathbf{A}_c^T \mathbf{P} = -\mathbf{Q}, \quad (\text{A.8})$$

for a given $\mathbf{Q} = \mathbf{Q}^T > 0$.

Consider a Lyapunov function candidate (LFC)

$$V(\mathbf{x}, \psi) = \mathbf{x}^T \mathbf{T}^T(\psi) \mathbf{P} \mathbf{T}(\psi) \mathbf{x} = \mathbf{z}^T \mathbf{P} \mathbf{z}, \quad (\text{A.9})$$

By differentiating along the trajectories, we get

$$\begin{aligned} \dot{V} &= \dot{\mathbf{z}}^T \mathbf{P} \mathbf{z} + \mathbf{z}^T \mathbf{P} \dot{\mathbf{z}} \\ &= \mathbf{z}^T \left(\mathbf{A}^T + \dot{\psi} \mathbf{S}_T^T \right) \mathbf{P} \mathbf{z} + \mathbf{z}^T \mathbf{P} \left(\mathbf{A} + \dot{\psi} \mathbf{S}_T \right) \mathbf{z} \\ &= \mathbf{z}^T \left(\mathbf{A}^T \mathbf{P} + \mathbf{P} \mathbf{A} + \left(\dot{\psi} \mathbf{S}_T^T \mathbf{P} + \dot{\psi} \mathbf{P} \mathbf{S}_T \right) \right) \mathbf{z} \\ &\leq -\mathbf{z}^T \mathbf{Q} \mathbf{z} + 2r_{\max} \lambda_{\max}(\mathbf{P}) |\mathbf{z}|^2 \\ &\leq -[\lambda_{\min}(\mathbf{Q}) - 2r_{\max} \lambda_{\max}(\mathbf{P})] |\mathbf{z}|^2, \end{aligned} \quad (\text{A.10})$$

which is negative definite provided that r_{\max} is sufficiently small.

This completes the proof.

A.2 Stability Analysis of Observer without WF Filtering for Output PID

Recall the control plant model of vessel in extreme sea:

$$\dot{\mathbf{n}}_T = \mathbf{R}(\psi) \hat{\mathbf{v}}_T, \quad (\text{A.11})$$

$$\dot{\mathbf{b}}_T = -\mathbf{T}_b \mathbf{b}_T + \mathbf{E}_b \mathbf{w}_b, \quad (\text{A.12})$$

$$\mathbf{M} \dot{\mathbf{v}}_T = -\mathbf{D}_L \mathbf{v}_T + \mathbf{R}^T(\psi) \mathbf{b}_T + \boldsymbol{\tau}_q, \quad (\text{A.13})$$

$$\mathbf{y} = \mathbf{n}_T, \quad (\text{A.14})$$

and the observer without WF filtering

$$\dot{\hat{\mathbf{n}}}_T = \mathbf{R}(\psi_y) \hat{\mathbf{v}}_T + \mathbf{K}_{2T} (\mathbf{y} - \hat{\mathbf{y}}), \quad (\text{A.15})$$

$$\dot{\hat{\mathbf{b}}}_T = -\mathbf{T}_b \mathbf{b}_T + \mathbf{K}_{3T} (\mathbf{y} - \hat{\mathbf{y}}), \quad (\text{A.16})$$

$$\dot{\mathbf{M}\hat{\mathbf{v}}}_T = -\mathbf{D}\hat{\mathbf{v}}_T + \mathbf{R}^T(\psi_y)\hat{\mathbf{b}} + \boldsymbol{\tau} + \mathbf{R}^T(\psi_y)\mathbf{K}_{4T}(\mathbf{y} - \hat{\mathbf{y}}), \quad (\text{A.17})$$

$$\hat{\mathbf{y}} = \hat{\mathbf{n}}_T. \quad (\text{A.18})$$

Define the estimation error as

$$\tilde{\mathbf{z}} = \begin{bmatrix} (\mathbf{n}_T - \hat{\mathbf{n}}_T)^T & (\mathbf{b}_T - \hat{\mathbf{b}}_T)^T & (\mathbf{v}_T - \hat{\mathbf{v}}_T)^T \end{bmatrix}^T, \quad (\text{A.19})$$

then the observer error-dynamics can be compactly written as

$$\dot{\tilde{\mathbf{z}}} = \mathbf{T}^T(\psi_y)\mathbf{A}^o\mathbf{T}(\psi_y)\tilde{\mathbf{z}} + \mathbf{E}\mathbf{w}, \quad (\text{A.20})$$

$$\tilde{\mathbf{y}} = \mathbf{C}\tilde{\mathbf{z}}. \quad (\text{A.21})$$

where $\mathbf{T} \in \mathbb{R}^{9 \times 9}$, the observer system matrix $\mathbf{A}^o \in \mathbb{R}^{9 \times 9}$ and $\mathbf{C} \in \mathbb{R}^{3 \times 9}$ is given as

$$\mathbf{T}(\psi) = \text{diag}(\mathbf{R}^T(\psi), \mathbf{R}^T(\psi), \mathbf{I}_{33}), \quad (\text{A.22})$$

$$\mathbf{A}^o = \begin{bmatrix} -\mathbf{K}_{2T} & \mathbf{0}_{33} & \mathbf{I}_{33} \\ -\mathbf{K}_{3T} & -\mathbf{T}_b^{-1} & \mathbf{0}_{33} \\ -\mathbf{K}_{4T} & \mathbf{M}^{-1} & -\mathbf{M}^{-1}\mathbf{D} \end{bmatrix}, \quad (\text{A.23})$$

$$\mathbf{C} = [\mathbf{I}_{33} \quad \mathbf{0}_{33} \quad \mathbf{0}_{33}]. \quad (\text{A.24})$$

(A.20) without disturbance can be written compactly as

$$\dot{\tilde{\mathbf{z}}} = \mathbf{T}^T(\psi_y)\mathbf{A}^o\mathbf{T}(\psi_y)\tilde{\mathbf{z}}, \quad (\text{A.25})$$

Theorem A.2 Consider the observer (A.15)-(A.17).

Assume that

1) $|\dot{\psi}_y| \leq r_{\max}$ provided that r_{\max} is sufficiently small, and

2) The observer gain matrices $\mathbf{K}_{2T} \in \mathbb{R}^{3 \times 3}$, $\mathbf{K}_{3T} \in \mathbb{R}^{3 \times 3}$ and $\mathbf{K}_{4T} \in \mathbb{R}^{3 \times 3}$ such that

\mathbf{A}^o in (A.20) is Hurwitz.

Then the nonlinear observer (A.15)-(A.17) is ULES. If r_{\max} is larger than any physical upper limit for $|\dot{\psi}_y(t)|$, (A.15)-(A.17) is said to be UGES.

Proof. If the two conditions in Theorem A.2 are satisfied, then the estimation error dynamics is ULES. Moreover, if the additional condition r_{\max} is larger than any physical upper limit for $|\dot{\psi}(t)|$, then the estimation error dynamics is UGES. The ULES and UGES of the estimation error dynamics are provided in Theorem A.1.

A.3 Stability Analysis of Observer without WF Filtering for Output AFB

Recall the observer without WF filtering

$$\begin{aligned}\dot{\mathbf{z}}_{p4} &= \mathbf{T}_{p4}^T(\psi_y) \mathbf{A}_{p4} \mathbf{T}_{p4}(\psi_y) \mathbf{z}_{p4} + \mathbf{B}_{q4} \boldsymbol{\tau}_{q4} + \mathbf{K}_{p4} (\mathbf{y}_4 - \mathbf{y}_{p4}) \\ \mathbf{y}_{p4} &= \mathbf{C}_{p4} \mathbf{z}_{p4}\end{aligned}\quad (\text{A.26})$$

Define the estimation error as

$$\tilde{\mathbf{z}}_4 = \mathbf{z}_4 - \mathbf{z}_{p4}. \quad (\text{A.27})$$

From the observer equation (A.26), the observer error-dynamics can be rewritten in the compact form

$$\begin{aligned}\dot{\tilde{\mathbf{z}}}_4 &= \mathbf{T}_{p4}^T(\psi_y) \mathbf{A}_{p4}^o \mathbf{T}_{p4}(\psi_y) \tilde{\mathbf{z}}_4 + \mathbf{K}_f \hat{\mathbf{a}}_f + \mathbf{E}_4 \mathbf{w}_4, \\ \dot{\hat{\mathbf{a}}}_f &= -\mathbf{T}_f^{-1} \hat{\mathbf{a}}_f + \mathbf{T}_f^{-1} \mathbf{C}_3 \mathbf{T}_{p4}(\psi_y) \tilde{\mathbf{z}}_4.\end{aligned}\quad (\text{A.28})$$

The observer system matrix $\mathbf{A}_{p4}^o \in \mathbb{R}^{10 \times 10}$ is given as

$$\mathbf{A}_{p4}^o = \begin{bmatrix} -\mathbf{K}_{2p4} & \mathbf{0}_{33} & \mathbf{I}_{33} & \mathbf{0}_{31} \\ -\mathbf{K}_{3p4} & -\mathbf{T}_b^{-1} & \mathbf{0}_{33} & \mathbf{0}_{31} \\ -\mathbf{K}_{4p4} & \mathbf{M}^{-1} & -\mathbf{M}^{-1} \mathbf{D} & \mathbf{0}_{31} \\ \mathbf{0}_{13} & \mathbf{0}_{13} & \mathbf{0}_{13} & 0 \end{bmatrix}, \quad (\text{A.29})$$

$$\mathbf{C}_3 = \begin{bmatrix} \mathbf{0}_{23} & \Upsilon_3 \mathbf{M}^{-1} & -\Upsilon_3 \mathbf{M}^{-1} \mathbf{D} & \mathbf{0}_{21} \end{bmatrix}. \quad (\text{A.30})$$

By collecting the state $\mathbf{z} \in \mathbb{R}^{12}$ according to

$$\mathbf{z} = \begin{bmatrix} \tilde{\mathbf{z}}_4^T & \hat{\mathbf{a}}_f^T \end{bmatrix}^T, \quad (\text{A.31})$$

(A.28) without disturbance can be written compactly as

$$\dot{\mathbf{z}} = \mathbf{T}_z^T(\psi_y) \mathbf{A}_z \mathbf{T}_z(\psi_y) \mathbf{z}, \quad (\text{A.32})$$

where $\mathbf{T}_z \in \mathbb{R}^{12 \times 12}$, $\mathbf{A}_z \in \mathbb{R}^{12 \times 12}$ are given as

$$\mathbf{T}_z = \text{diag}\left(\mathbf{T}_{p4}(\psi_y), \mathbf{I}_{22}\right), \quad (\text{A.33})$$

$$\mathbf{A}_z = \begin{bmatrix} \mathbf{A}_o & \mathbf{K}_f \\ \mathbf{T}_f^{-1} \mathbf{C}_3 & -\mathbf{T}_f^{-1} \end{bmatrix}. \quad (\text{A.34})$$

Theorem A.2 Consider the observer:

$$\begin{aligned} \dot{\hat{\mathbf{a}}}_f &= \mathbf{T}_f^{-1} \left[-\hat{\mathbf{a}}_f + (\mathbf{y}_{24} - \mathbf{y}_{2p4}) \right], \\ \dot{\mathbf{z}}_{p4} &= \mathbf{T}_{p4}^T(\psi_y) \mathbf{A}_{p4} \mathbf{T}_{p4}(\psi_y) \mathbf{z}_{p4} + \mathbf{B}_{q4} \boldsymbol{\tau}_{q4} + \mathbf{K}_{p4} (\mathbf{y}_4 - \mathbf{y}_{p4}) + \mathbf{K}_f \hat{\mathbf{a}}_f, \\ \mathbf{y}_{p4} &= \mathbf{C}_{p4} \mathbf{z}_{p4} + \mathbf{D}_{q4} \boldsymbol{\tau}_{q4}, \end{aligned} \quad (\text{A.35})$$

Assume that

- 1) $|\dot{\psi}_y| \leq r_{\max}$ provided that r_{\max} is sufficiently small, and
- 2) The observer gain matrices $\mathbf{K}_{p4} \in \mathbb{R}^{10 \times 6}$, $\mathbf{K}_f \in \mathbb{R}^{10 \times 3}$, and $\mathbf{T}_f^{-1} \in \mathbb{R}^{2 \times 2}$ such that \mathbf{A}_{p4} in (A.35) is Hurwitz.

Then the nonlinear observer (A.35) is ULES. If r_{\max} is larger than any physical upper limit for $|\dot{\psi}_y(t)|$, (A.35) is said to be UGES.

Proof. If the two conditions in Theorem C.1 are satisfied, then the estimation error dynamics is ULES. Moreover, if the additional condition r_{\max} is larger than any physical upper limit for $|\dot{\psi}(t)|$, then the estimation error dynamics is UGES. The ULES and UGES of the estimation error dynamics are provided in Theorem A.1.

A.4 Proof of Proposition 1

The proof is divided into three parts: the ISS of the injected system in calm and moderate seas, extreme seas and transition regime (high seas).

Part 1

Consider the hybrid DP system with two controllers, in calm or moderate seas, where $\sigma = \rho = i$, for $i = 1, 2$. The state-space model of the injected system is found by copying the observer equations, (6.15), and the controller, (6.19)-(6.20), that is

$$\dot{\mathbf{z}}_{pi} = \mathbf{T}_{pi}^T(\psi_y) \mathbf{A}_{pi} \mathbf{T}_{pi}(\psi_y) \mathbf{z}_{pi} + \mathbf{B}_{qi} \boldsymbol{\tau}_{qi} + \mathbf{K}_{pi} (\mathbf{y}_i - \mathbf{y}_{pi}), \quad (\text{A.36})$$

$$\mathbf{y}_{pi} = \mathbf{C}_{pi} \mathbf{z}_{pi}, \quad (\text{A.37})$$

$$\dot{\xi}_{qi} = \hat{\boldsymbol{\eta}}, \quad (\text{A.38})$$

$$\dot{\boldsymbol{\tau}}_{qi} = -\mathbf{K}_{ii} \mathbf{R}^T(\psi_y) \xi_{qi} - \mathbf{K}_{pi} \mathbf{R}^T(\psi_y) \hat{\boldsymbol{\eta}} - \mathbf{K}_{di} \hat{\mathbf{v}}. \quad (\text{A.39})$$

By collecting the state $\mathbf{x}_{\rho\sigma} \in \mathbb{R}^{19}$ according to

$$\mathbf{x}_{\rho\sigma} = \begin{bmatrix} \xi_{qi}^T & \mathbf{z}_{pi}^T \end{bmatrix}^T, \quad (\text{A.40})$$

the state-space model of the injected system becomes

$$\begin{aligned} \dot{\mathbf{x}}_{\rho\sigma} &= \mathbf{T}_{\rho\sigma}^T \mathbf{A}_{\rho\sigma} \mathbf{T}_{\rho\sigma} \mathbf{x}_{\rho\sigma} + \mathbf{K}_{\rho\sigma} (\mathbf{y}_i - \mathbf{y}_{pi}), \\ \mathbf{y}_{pi} &= \mathbf{C}_{\rho\sigma} \mathbf{x}_{\rho\sigma}. \end{aligned} \quad (\text{A.41})$$

The system matrix $\mathbf{A}_{\rho\sigma} \in \mathbb{R}^{19 \times 19}$, the transformation matrix $\mathbf{T}_{\rho\sigma} \in \mathbb{R}^{19 \times 19}$, $\mathbf{C}_{\rho\sigma} \in \mathbb{R}^{4 \times 19}$, and $\mathbf{K}_{\rho\sigma} \in \mathbb{R}^{19 \times 4}$ are given by

$$\mathbf{A}_{\rho\sigma} = \begin{bmatrix} \mathbf{0}_{33} & \mathbf{0}_{36} & \mathbf{I}_{33} & \mathbf{0}_{33} & \mathbf{0}_{33} & \mathbf{0}_{31} \\ \mathbf{0}_{63} & \mathbf{A}_w & \mathbf{0}_{63} & \mathbf{0}_{63} & \mathbf{0}_{63} & \mathbf{0}_{61} \\ \mathbf{0}_{33} & \mathbf{0}_{33} & \mathbf{0}_{33} & \mathbf{0}_{33} & \mathbf{I}_{33} & \mathbf{0}_{31} \\ \mathbf{0}_{33} & \mathbf{0}_{33} & \mathbf{0}_{33} & -\mathbf{T}_b^{-1} & \mathbf{0}_{33} & \mathbf{0}_{31} \\ -\mathbf{M}^{-1} \mathbf{K}_{ii} & \mathbf{0} & -\mathbf{M}^{-1} \mathbf{K}_{pi} & -\mathbf{M}^{-1} & -\mathbf{M}^{-1} (\mathbf{D}_L + \mathbf{K}_{di}) & \mathbf{0}_{31} \\ \mathbf{0}_{13} & \mathbf{0}_{13} & \mathbf{0}_{13} & \mathbf{0}_{13} & \mathbf{0}_{13} & 0 \end{bmatrix}, \quad (\text{A.42})$$

$$\mathbf{T}_{\rho\sigma} = \text{diag}(\mathbf{R}^T, \mathbf{T}_{pi}), \quad (\text{A.43})$$

$$\mathbf{K}_{\rho\sigma} = \begin{bmatrix} \mathbf{0}_{41}^T & \mathbf{K}_{pi}^T \end{bmatrix}^T, \quad (\text{A.44})$$

$$\mathbf{C}_{\rho\sigma} = \begin{bmatrix} \mathbf{0}_{41} & \mathbf{C}_{pi} \end{bmatrix}. \quad (\text{A.45})$$

It is noted that the input to the injected system (A.41) is the estimation errors ($\mathbf{y}_i - \mathbf{y}_{pi}$). If the controller gains $\mathbf{K}_{ii} \in \mathbb{R}^{3 \times 3}$, $\mathbf{K}_{pi} \in \mathbb{R}^{3 \times 3}$, and $\mathbf{K}_{di} \in \mathbb{R}^{3 \times 3}$ are chosen such that the system

$$\dot{\mathbf{x}}_{\rho\sigma} = \mathbf{T}_{\rho\sigma}^T \mathbf{A}_{\rho\sigma} \mathbf{T}_{\rho\sigma} \mathbf{x}_{\rho\sigma}, \quad (\text{A.46})$$

is asymptotically stable, then the injected system (A.41) is ISS. The asymptotical stability of (A.46) is given by the Theorem A.1.

Part 2

In extreme seas, state-space model of the injected system is found by copying the observer equations, (6.43), and the controller, (6.46)-(6.48), where $\sigma = \rho = 4$, that is

$$\begin{aligned} \dot{\hat{\mathbf{a}}}_f &= \mathbf{T}_f^{-1} \left[-\hat{\mathbf{a}}_f + (\mathbf{y}_{24} - \mathbf{y}_{2p4}) \right], \\ \dot{\mathbf{z}}_{p4} &= \mathbf{T}_{p4}^T (\psi_y) \mathbf{A}_{p4} \mathbf{T}_{p4} (\psi_y) \mathbf{z}_{p4} + \mathbf{B}_{q4} \boldsymbol{\tau}_{q4} + \mathbf{K}_{p4} (\mathbf{y}_4 - \mathbf{y}_{p4}) + \mathbf{K}_f \hat{\mathbf{a}}_f, \\ \mathbf{y}_{p4} &= \mathbf{C}_{p4} \mathbf{z}_{p4} + \mathbf{D}_{q4} \boldsymbol{\tau}_{q4}, \end{aligned} \quad (\text{A.47})$$

$$\dot{\xi}_{q4} = \hat{\mathbf{n}}_T, \quad (\text{A.48})$$

$$\dot{\mathbf{a}}_f = \mathbf{A}_f \mathbf{a}_f + \mathbf{B}_f \Upsilon_3 \hat{\mathbf{v}}, \quad (\text{A.49})$$

$$\dot{\boldsymbol{\tau}}_{q4} = -\mathbf{K}_{i4} \mathbf{R}^T (\psi_y) \xi_{q4} - \mathbf{K}_{p4} \mathbf{R}^T (\psi_y) \hat{\mathbf{n}}_T - \mathbf{K}_{d4} \hat{\mathbf{v}}_T - \mathbf{K}_a^{PID} \mathbf{a}_f. \quad (\text{A.50})$$

By collecting the state $\mathbf{x}_{\rho\sigma} \in \mathbb{R}^{17}$

$$\begin{aligned} \mathbf{x}_{\rho\sigma} &= \left[\xi_{q4}^T \ \mathbf{z}_{p4}^T \ \hat{\mathbf{a}}_f^T \ \mathbf{a}_f^T \right]^T, \\ &= \left[\xi_{q4} \ \hat{\mathbf{n}}_T^T \ \mathbf{b}^T \ \hat{\mathbf{v}}_T^T \ \hat{\omega}_p \ \hat{\mathbf{a}}_f^T \ \mathbf{a}_f^T \right]^T. \end{aligned} \quad (\text{A.51})$$

the state-space model of the injected system becomes

$$\begin{aligned} \dot{\mathbf{x}}_{\rho\sigma} &= \mathbf{T}_{\rho\sigma}^T \mathbf{A}_{\rho\sigma} \mathbf{T}_{\rho\sigma} \mathbf{x}_{\rho\sigma} + \mathbf{K}_{\rho\sigma} (\mathbf{y}_4 - \mathbf{y}_{p4}), \\ \mathbf{y}_{p4} &= \mathbf{C}_{\rho\sigma} \mathbf{x}_{\rho\sigma}. \end{aligned} \quad (\text{A.52})$$

The system matrix $\mathbf{A}_{\rho\sigma} \in \mathbb{R}^{17 \times 17}$, the transformation matrix $\mathbf{T}_{\rho\sigma} \in \mathbb{R}^{17 \times 17}$, $\mathbf{C}_{\rho\sigma} \in \mathbb{R}^{6 \times 17}$, and $\mathbf{K}_{\rho\sigma} \in \mathbb{R}^{17 \times 6}$ are given by

$$\mathbf{A}_{\rho\sigma} = \begin{bmatrix} \mathbf{0}_{33} & \mathbf{I}_{33} & \mathbf{0}_{33} & \mathbf{0}_{33} & \mathbf{0}_{31} & \mathbf{0}_{32} & \mathbf{0}_{32} \\ \mathbf{0}_{33} & \mathbf{0}_{33} & \mathbf{0}_{33} & \mathbf{I}_{33} & \mathbf{0}_{31} & \mathbf{0}_{32} & \mathbf{0}_{32} \\ \mathbf{0}_{33} & \mathbf{0}_{33} & -\mathbf{T}_b & \mathbf{0}_{33} & \mathbf{0}_{31} & \mathbf{0}_{32} & \mathbf{0}_{32} \\ -\mathbf{M}^{-1}\mathbf{K}_{i4} & -\mathbf{M}^{-1}\mathbf{K}_{p4} & -\mathbf{M}^{-1} & -\mathbf{M}^{-1}(\mathbf{D}_L + \mathbf{K}_{d4}) & \mathbf{0}_{31} & \mathbf{K}_a & -\mathbf{M}^{-1}\mathbf{K}_a^{PID} \\ \mathbf{0}_{13} & \mathbf{0}_{13} & \mathbf{0}_{13} & \mathbf{0}_{13} & 0 & \mathbf{0}_{12} & \mathbf{0}_{32} \\ \mathbf{0}_{33} & \mathbf{0}_{33} & \mathbf{0}_{33} & \mathbf{0}_{33} & \mathbf{0}_{31} & -\mathbf{T}_f^{-1} & \mathbf{0}_{32} \\ -\mathbf{B}_M \mathbf{K}_{i4} & -\mathbf{B}_M \mathbf{K}_{p4} & -\mathbf{B}_M & -\mathbf{B}_M(\mathbf{D}_L + \mathbf{K}_{d4}) & \mathbf{0}_{31} & \mathbf{0}_{32} & \mathbf{A}_f - \mathbf{B}_M \mathbf{K}_a^{PID} \end{bmatrix}, \quad (\text{A.53})$$

$$\mathbf{T}_{\rho\sigma} = \text{diag}(\mathbf{R}_{\psi_y}^T, \mathbf{T}_{p4}, \mathbf{I}_{44}), \quad (\text{A.54})$$

$$\mathbf{C}_{\rho\sigma} =$$

$$\begin{bmatrix} \mathbf{0}_{33} & \mathbf{I}_{33} & \mathbf{0}_{33} & \mathbf{0}_{33} & \mathbf{0}_{31} & \mathbf{0}_{32} & \mathbf{0}_{32} \\ -\mathbf{M}_{Y_3} \mathbf{K}_{i4} \mathbf{R}_{\psi_y}^T & -\mathbf{M}_{Y_3} \mathbf{K}_{p4} \mathbf{R}_{\psi_y}^T & -\mathbf{M}_{Y_3} \mathbf{R}_{\psi_y}^T & -\mathbf{M}_{Y_3}(\mathbf{D}_L + \mathbf{K}_{d4}) & \mathbf{0} & Y_3 \mathbf{K}_a & -\mathbf{M}_{Y_3} \mathbf{K}_a^{PID} \\ \mathbf{0}_{13} & \mathbf{0}_{13} & \mathbf{0}_{13} & \mathbf{0}_{13} & 1 & \mathbf{0}_{12} & \mathbf{0}_{12} \end{bmatrix}, \quad (\text{A.55})$$

$$\mathbf{K}_{\rho\sigma} = \begin{bmatrix} \mathbf{0}_{33} & \mathbf{K}_{2p3}^T & \mathbf{K}_{3p3}^T & \mathbf{K}_{4p3}^T & \mathbf{0}_{31} & \mathbf{0}_{32} & \mathbf{0}_{32} \\ \mathbf{0}_{23} & \mathbf{0}_{23} & \mathbf{0}_{23} & \mathbf{0}_{23} & \mathbf{0}_{21} & \mathbf{T}_f^{-T} & \mathbf{0}_{22} \\ \mathbf{0}_{13} & \mathbf{0}_{13} & \mathbf{0}_{13} & \mathbf{0}_{13} & 0 & \mathbf{0}_{12} & \mathbf{0}_{12} \end{bmatrix}^T, \quad (\text{A.56})$$

where $\mathbf{B}_M = \mathbf{B}_f \mathbf{I} \mathbf{M}^{-1} \in \mathbb{R}^{2 \times 3}$; $\mathbf{M}_{Y_3} = Y_3 \mathbf{M}^{-1} \in \mathbb{R}^{2 \times 3}$; and $\mathbf{R}_{\psi_y}^T = \mathbf{R}^T(\psi_y) \in \mathbb{R}^{3 \times 3}$.

It can be seen that the input to the injected system (A.52) is the estimation errors ($\mathbf{y}_4 - \mathbf{y}_{p4}$). If the controller gains $\mathbf{K}_{i4} \in \mathbb{R}^{3 \times 3}$, $\mathbf{K}_{p4} \in \mathbb{R}^{3 \times 3}$, $\mathbf{K}_{d4} \in \mathbb{R}^{3 \times 3}$ and $\mathbf{K}_a^{PID} \in \mathbb{R}^{3 \times 2}$, and the observer gains $\mathbf{K}_a \in \mathbb{R}^{3 \times 2}$, $\mathbf{T}_f^{-1} \in \mathbb{R}^{2 \times 2}$ are chosen such that the system

$$\dot{\mathbf{x}}_{\rho\sigma} = \mathbf{T}_{\rho\sigma}^T \mathbf{A}_{\rho\sigma} \mathbf{T}_{\rho\sigma} \mathbf{x}_{\rho\sigma}, \quad (\text{A.57})$$

is asymptotically stable, then the injected system (A.41) is ISS. The asymptotical stability of (A.57) is provided in Theorem A.1.

Part 3

In the transition regime between moderate and extreme seas, state-space model of the injected system is found by copying the observer equations, (6.15) and (6.43), and the controller, (6.51), where $\rho = \sigma = 3$, that is

$$\dot{\mathbf{z}}_{p2} = \mathbf{T}_{p2}^T(\psi_y) \mathbf{A}_{p2} \mathbf{T}_{p2}(\psi_y) \mathbf{z}_{p2} + \mathbf{B}_{q2} \boldsymbol{\tau}_{q2} + \mathbf{K}_{p2} (\mathbf{y}_2 - \mathbf{y}_{p2}), \quad (\text{A.58})$$

$$\mathbf{y}_{p2} = \mathbf{C}_{p2} \mathbf{z}_{p2}, \quad (\text{A.59})$$

$$\begin{aligned} \dot{\hat{\mathbf{a}}}_f &= \mathbf{T}_f^{-1} \left[-\hat{\mathbf{a}}_f + (\mathbf{y}_{24} - \mathbf{y}_{2p4}) \right], \\ \dot{\mathbf{z}}_{p4} &= \mathbf{T}_{p4}^T(\psi_y) \mathbf{A}_{p4} \mathbf{T}_{p4}(\psi_y) \mathbf{z}_{p4} + \mathbf{B}_{q4} \boldsymbol{\tau}_{q4} + \mathbf{K}_{p4} (\mathbf{y}_4 - \mathbf{y}_{p4}) + \mathbf{K}_f \hat{\mathbf{a}}_f, \end{aligned} \quad (\text{A.60})$$

$$\mathbf{y}_{p4} = \mathbf{C}_{p4} \mathbf{z}_{p4} + \mathbf{D}_{q4} \boldsymbol{\tau}_{q4}, \quad (\text{A.61})$$

$$\hat{\boldsymbol{\tau}}_{q3} = \alpha_1(\hat{\omega}_p) \hat{\boldsymbol{\tau}}_{q2} + \alpha_2(\hat{\omega}_p) \hat{\boldsymbol{\tau}}_{q4}. \quad (\text{A.62})$$

By collecting the state $\mathbf{x}_{\rho\sigma} \in \mathbb{R}^{35}$ according to

$$\mathbf{x}_{\rho\sigma} = \left[\begin{array}{c|c|c|c|c|c|c|c|c|c} \xi_{q2}^T & \xi_{q4}^T & \mathbf{p}_w^T & \hat{\mathbf{n}}^T & \hat{\mathbf{b}}_1^T & \hat{\mathbf{v}}^T & \hat{\mathbf{n}}_T^T & \hat{\mathbf{b}}_2^T & \hat{\mathbf{v}}_T^T & \hat{\mathbf{a}}_f^T & \mathbf{a}_f^T & \hat{\omega}_p^T \end{array} \right]^T, \quad (\text{A.63})$$

the state-space model of the injected system becomes

$$\begin{aligned} \dot{\mathbf{x}}_{\rho\sigma} &= \mathbf{T}_{\rho\sigma}^T \mathbf{A}_{\rho\sigma} \mathbf{T}_{\rho\sigma} \mathbf{x}_{\rho\sigma} + \mathbf{K}_{\rho\sigma} (\mathbf{y}_3 - \mathbf{y}_{p3}), \\ \mathbf{y}_{p3} &= \mathbf{C}_{\rho\sigma} \mathbf{x}_{\rho\sigma}. \end{aligned} \quad (\text{A.64})$$

The system matrix $\mathbf{A}_{\rho\sigma} \in \mathbb{R}^{35 \times 35}$, the transformation matrix $\mathbf{T}_{\rho\sigma} \in \mathbb{R}^{35 \times 35}$, $\mathbf{C}_{\rho\sigma} \in \mathbb{R}^{6 \times 35}$, and $\mathbf{K}_{\rho\sigma} \in \mathbb{R}^{35 \times 9}$ are given by

$$\mathbf{A}_{\rho\sigma} = \begin{bmatrix} \mathbf{0}_{3 \times 3} & \mathbf{0}_{3 \times 3} & \mathbf{A}_{\rho\sigma}^{13} & \mathbf{0}_{3 \times 13} & \mathbf{0}_{3 \times 1} \\ \mathbf{0}_{3 \times 3} & \mathbf{0}_{3 \times 3} & \mathbf{0}_{3 \times 15} & \mathbf{A}_{\rho\sigma}^{24} & \mathbf{0}_{3 \times 1} \\ \mathbf{A}_{\rho\sigma}^{31} & \mathbf{0}_{15 \times 3} & \mathbf{A}_{\rho\sigma}^{33} & \mathbf{0}_{15 \times 13} & \mathbf{0}_{15 \times 1} \\ \mathbf{0}_{13 \times 3} & \mathbf{A}_{\rho\sigma}^{42} & \mathbf{0}_{13 \times 15} & \mathbf{A}_{\rho\sigma}^{44} & \mathbf{0}_{13 \times 1} \\ \mathbf{0}_{1 \times 3} & \mathbf{0}_{1 \times 3} & \mathbf{0}_{1 \times 15} & \mathbf{0}_{1 \times 13} & 0 \end{bmatrix}, \quad (\text{A.65})$$

$$\mathbf{T}_{\rho\sigma} = \text{diag}(\mathbf{R}^T, \mathbf{R}^T, \mathbf{R}^T, \mathbf{R}^T, \mathbf{R}^T, \mathbf{R}^T, \mathbf{I}_{33}, \mathbf{R}^T, \mathbf{R}^T, \mathbf{I}_{88}), \quad (\text{A.66})$$

$$\mathbf{C}_{\rho\sigma} = \left[\begin{array}{ccccc} \mathbf{0}_{6 \times 3} & \mathbf{C}_{\rho\sigma}^{12} & \mathbf{C}_{\rho\sigma}^{13} & \mathbf{C}_{\rho\sigma}^{14} & \mathbf{C}_{\rho\sigma}^{15} \end{array} \right], \quad (\text{A.67})$$

$$\mathbf{K}_{\rho\sigma} = \left[\begin{array}{ccccc} \mathbf{0}_{9 \times 6} & \mathbf{0}_{9 \times 3} & (\mathbf{K}_{\rho\sigma}^{31})^T & (\mathbf{K}_{\rho\sigma}^{41})^T & \mathbf{0}_{9 \times 1} \end{array} \right]^T, \quad (\text{A.68})$$

where $\mathbf{A}_{\rho\sigma}^{13} \in \mathbb{R}^{3 \times 15}$, $\mathbf{A}_{\rho\sigma}^{24} \in \mathbb{R}^{3 \times 13}$, $\mathbf{A}_{\rho\sigma}^{33} \in \mathbb{R}^{15 \times 15}$, $\mathbf{A}_{\rho\sigma}^{31} \in \mathbb{R}^{15 \times 3}$, $\mathbf{A}_{\rho\sigma}^{42} \in \mathbb{R}^{13 \times 3}$, $\mathbf{A}_{\rho\sigma}^{44} \in \mathbb{R}^{13 \times 13}$, $\mathbf{C}_{\rho\sigma}^{12} \in \mathbb{R}^{6 \times 3}$, $\mathbf{C}_{\rho\sigma}^{13} \in \mathbb{R}^{6 \times 15}$, $\mathbf{C}_{\rho\sigma}^{14} \in \mathbb{R}^{6 \times 13}$, $\mathbf{C}_{\rho\sigma}^{15} \in \mathbb{R}^{6 \times 1}$, $\mathbf{K}_{\rho\sigma}^{31} \in \mathbb{R}^{15 \times 9}$, and $\mathbf{K}_{\rho\sigma}^{41} \in \mathbb{R}^{13 \times 9}$ are given by

$$\mathbf{A}_{\rho\sigma}^{13} = [\mathbf{0}_{36} \quad \mathbf{I}_{33} \quad \mathbf{0}_{33} \quad \mathbf{0}_{33}],$$

$$\mathbf{A}_{\rho\sigma}^{24} = [\mathbf{I}_{33} \quad \mathbf{0}_{33} \quad \mathbf{0}_{33} \quad \mathbf{0}_{32} \quad \mathbf{0}_{32}],$$

$$\mathbf{A}_{\rho\sigma}^{33} = \begin{bmatrix} \mathbf{A}_w & \mathbf{0}_{63} & \mathbf{0}_{63} & & \mathbf{0}_{63} \\ \mathbf{0}_{36} & \mathbf{0}_{33} & \mathbf{0}_{33} & & \mathbf{I}_{33} \\ \mathbf{0}_{36} & \mathbf{0}_{33} & -\mathbf{T}_b^{-1} & & \mathbf{0}_{33} \\ -\alpha_1 \mathbf{M}^{-1} \mathbf{K}_{p2} & \mathbf{0}_{33} & -\alpha_1 \mathbf{M}^{-1} & -\alpha_1 \mathbf{M}^{-1} (\mathbf{D}_L + \mathbf{K}_{d2}) & \end{bmatrix},$$

$$\mathbf{A}_{\rho\sigma}^{31} \begin{bmatrix} \mathbf{0}_{63} \\ \mathbf{0}_{33} \\ \mathbf{0}_{33} \\ -\alpha_1 \mathbf{M}^{-1} \mathbf{K}_{i2} \end{bmatrix}, \quad \mathbf{A}_{\rho\sigma}^{42} = \begin{bmatrix} \mathbf{0}_{33} \\ \mathbf{0}_{33} \\ \mathbf{0}_{23} \\ -\alpha_2 \mathbf{B}_M \mathbf{K}_{i4} \end{bmatrix},$$

$$\mathbf{A}_{\rho\sigma}^{44} = \begin{bmatrix} \mathbf{0}_{33} & \mathbf{0}_{33} & \mathbf{I}_{33} & \mathbf{0}_{32} & \mathbf{0}_{32} \\ \mathbf{0}_{33} & -\mathbf{T}_b & \mathbf{0}_{33} & \mathbf{0}_{32} & \mathbf{0}_{32} \\ -\alpha_2 \mathbf{M}^{-1} \mathbf{K}_{p4} & -\mathbf{M}^{-1} & -\alpha_2 \mathbf{M}^{-1} (\mathbf{D}_L + \mathbf{K}_{d4}) & \mathbf{K}_a & -\alpha_2 \mathbf{M}^{-1} \mathbf{K}_a^{PID} \\ \mathbf{0}_{23} & \mathbf{0}_{23} & \mathbf{0}_{23} & -\mathbf{T}_f^{-1} & \mathbf{0}_{22} \\ -\alpha_2 \mathbf{B}_M \mathbf{K}_{p4} & -\alpha_2 \mathbf{B}_M & -\alpha_2 \mathbf{B}_M (\mathbf{D}_L + \mathbf{K}_{d4}) & \mathbf{0}_{22} & \alpha_2 (\mathbf{A}_f - \mathbf{B}_M \mathbf{K}_a^{PID}) \end{bmatrix},$$

$$\mathbf{C}_{\rho\sigma}^{12} = \begin{bmatrix} \mathbf{0}_{33} \\ \mathbf{0}_{33} \\ -\mathbf{M}_{Y_3} \mathbf{K}_{i4} \mathbf{R}_{Y_y}^T \\ \mathbf{0}_{13} \end{bmatrix}, \quad \mathbf{C}_{\rho\sigma}^{13} = \begin{bmatrix} \mathbf{C}_w & \mathbf{I}_{33} & \mathbf{0}_{33} & \mathbf{0}_{33} \\ \mathbf{0}_{36} & \mathbf{0}_{33} & \mathbf{0}_{33} & \mathbf{0}_{33} \\ \mathbf{0}_{26} & \mathbf{0}_{23} & \mathbf{0}_{23} & \mathbf{0}_{23} \\ \mathbf{0}_{16} & \mathbf{0}_{13} & \mathbf{0}_{13} & \mathbf{0}_{13} \end{bmatrix},$$

$$\mathbf{C}_{\rho\sigma}^{14} = \begin{bmatrix} \mathbf{0}_{33} & \mathbf{0}_{33} & \mathbf{0}_{33} & \mathbf{0}_{32} & \mathbf{0}_{32} \\ \mathbf{I}_{33} & \mathbf{0}_{33} & \mathbf{0}_{33} & \mathbf{0}_{32} & \mathbf{0}_{32} \\ -\mathbf{M}_{Y_3} \mathbf{K}_{p4} \mathbf{R}_{Y_y}^T & -\mathbf{M}_{Y_3} \mathbf{R}_{Y_y}^T & -\mathbf{M}_{Y_3} (\mathbf{D}_L + \mathbf{K}_{d4}) & Y_3 \mathbf{K}_a & -\mathbf{M}_{Y_3} \mathbf{K}_a^{PID} \\ \mathbf{0}_{13} & \mathbf{0}_{13} & \mathbf{0}_{13} & \mathbf{0}_{12} & \mathbf{0}_{12} \end{bmatrix},$$

$$\mathbf{C}_{\rho\sigma}^{15} = \begin{bmatrix} \mathbf{0}_{31} \\ \mathbf{0}_{31} \\ \mathbf{0}_{21} \\ 1 \end{bmatrix}, \quad \mathbf{K}_{\rho\sigma}^{31} = \begin{bmatrix} \mathbf{K}_{1p2} & \mathbf{0}_{63} & \mathbf{0}_{62} & \mathbf{0}_{61} \\ \mathbf{K}_{2p2} & \mathbf{0}_{33} & \mathbf{0}_{32} & \mathbf{0}_{31} \\ \mathbf{K}_{3p2} & \mathbf{0}_{33} & \mathbf{0}_{32} & \mathbf{0}_{31} \\ \mathbf{K}_{4p2} & \mathbf{0}_{33} & \mathbf{0}_{32} & \mathbf{0}_{31} \end{bmatrix}, \quad \mathbf{K}_{\rho\sigma}^{41} = \begin{bmatrix} \mathbf{0}_{33} & \mathbf{K}_{2p4} & \mathbf{0}_{32} & \mathbf{0}_{32} \\ \mathbf{0}_{33} & \mathbf{K}_{3p4} & \mathbf{0}_{32} & \mathbf{0}_{32} \\ \mathbf{0}_{33} & \mathbf{K}_{4p4} & \mathbf{0}_{32} & \mathbf{0}_{32} \\ \mathbf{0}_{23} & \mathbf{0}_{23} & \mathbf{T}_f^{-1} & \mathbf{0}_{22} \\ \mathbf{0}_{23} & \mathbf{0}_{23} & \mathbf{0}_{22} & \mathbf{0}_{22} \end{bmatrix}.$$

It can be seen that the input to the injected system (A.64) is the estimation errors ($\mathbf{y}_3 - \mathbf{y}_{p3}$). If the controller gains $\mathbf{K}_{i2} \in \mathbb{R}^{3 \times 3}$, $\mathbf{K}_{p2} \in \mathbb{R}^{3 \times 3}$, $\mathbf{K}_{d2} \in \mathbb{R}^{3 \times 3}$, $\mathbf{K}_{i4} \in \mathbb{R}^{3 \times 3}$, $\mathbf{K}_{p4} \in \mathbb{R}^{3 \times 3}$, $\mathbf{K}_{d4} \in \mathbb{R}^{3 \times 3}$ and $\mathbf{K}_a^{PID} \in \mathbb{R}^{3 \times 2}$; and the observer gains $\mathbf{K}_a \in \mathbb{R}^{3 \times 2}$, $\mathbf{T}_f^{-1} \in \mathbb{R}^{2 \times 2}$ are chosen such that the system

$$\dot{\mathbf{x}}_{\rho\sigma} = \mathbf{T}_{\rho\sigma}^T \mathbf{A}_{\rho\sigma} \mathbf{T}_{\rho\sigma} \mathbf{x}_{\rho\sigma}, \quad (\text{A.69})$$

is asymptotically state, then the injected system (A.69) is ISS. The asymptotical stability of (A.69) is provided in Theorem A.1.

Appendix B Marine Cybernetics Laboratory.

The Marine Cybernetics Laboratory (MCLab) is a joint laboratory between Department of Engineering Cybernetics and Department of Marine Technology of Norwegian University of Science and Technology (NTNU) for testing the model marine structures such as vessels, pipelines, underwater vehicles, propulsion system, etc. The basin of MCLab has the dimension of $L \times B \times D = 40 \text{ m} \times 6.45 \text{ m} \times 1.5 \text{ m}$ (Figure B.1).

The DHI wave maker (www.dhi.dk/products/modeltesting/wavegeneration.htm) as shown in Figure B.2 is single flap type where the distance from the hinge to the water surface is 0.75 m for generating regular, irregular waves, e.g. PM, JONSWAP, etc. and impulse waves. The regular waves generated by the wave maker can have the period $T = 0.3 - 3.0 \text{ s}$, maximum wave height $H_{\max} = 0.3 \text{ m}$ (for $T = 1.3 - 1.5 \text{ s}$), and the optimum waves for $T = 0.6 - 1.5 \text{ s}$. The irregular waves can have the dominating period $T_p = 0.6 - 1.5 \text{ s}$, maximum significant wave height $\max(H_p) = 0.15 \text{ m}$ (for $T_p = 1.0 - 1.5 \text{ s}$), and the optimum waves for $T = 0.6 - 1.5 \text{ s}$.

Four cameras mounted on the towing carriage for capturing position of model vessel (Figure B.3).



Figure B.1. The basin of the MCLab.



Figure B.2. The single flap wave generator of the MCLab.

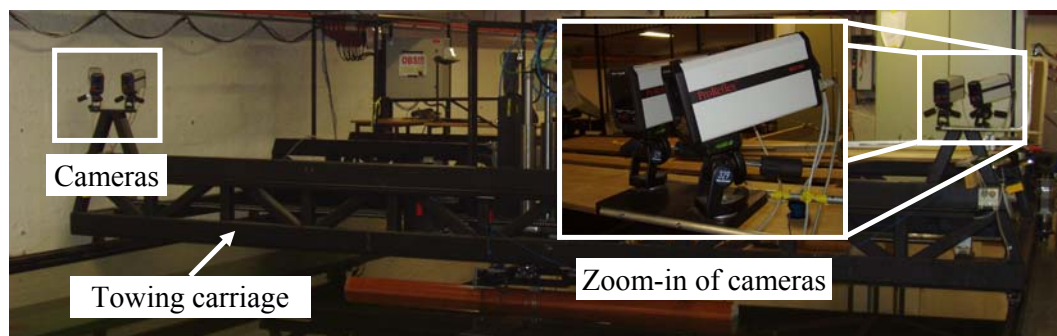


Figure B.3. Four cameras mounted on the towing carriage for capturing position of model vessel.

Appendix C Cybership III

C.1 General Configurations of Cybership III

Cybership III has been developed in MCLab for testing dynamic position system and navigational system. The early version of Cybership III was the Cyberships I and II. The Cybership I is a 1:70 scaled model of a supply vessel having a mass of $m = 17.6$ kg, length of $L = 1.19$ m and equipped with 2 aft azimuth thrusters and 2 fore azimuth thrusters. The Cybership II is a 1:70 scaled model of a supply vessel having a mass of $m = 15$ kg, length of $L = 1.15$ m and equipped with 2 aft azimuth thrusters with 2 rudders, 1 fore azimuth thruster and 1 tunnel thruster at the bow. The drawbacks of these two Cybership are the limitations in configuration due to their small size.

Cybership III (Figure C.1), which is a 1:30 scaled model of the supply vessel in Table C.1, having a mass of $m = 75$ kg, length of $L = 2.27$ m and breadth of $B = 0.4$ m. Mechanical and electric configuration/installation of Cybership III were developed by Nilsen (2003). The vessel is equipped with two main aft azimuth propellers, one tunnel thruster and one fore azimuth thruster. The internal hardware architecture is controlled by an onboard computer which can communicate with onshore PC through a WLAN. The PC onboard the ship uses QNX real-time operating system (target PC). The control system is developed on a PC in the control room (host PC, see Figure C.2) under Simulink/Opal and downloaded to the target PC using automatic C-code generation and wireless Ethernet.

An onboard accelerometer provides body-fixed acceleration (Figure C.1). The accelerometer manufactured by Sherborne Sensor Limited is able to measure the acceleration in x - and y -directions within ± 0.25 g. The output of the accelerometer is the voltage and therefore must be linearly converted to accelerometer by multiplying

factors of 19.963 and 19.957 Volts/g for x - and y -directions, respectively. The accelerometer was calibrated in the temperature of 22.8°C and its shifted reading due to different temperature is less than 0.01% /°C.

The motion capture unit (MCU) manufactured by ProReflex™ provides Earth-fixed position and heading of the vessel. The MCU consists of onshore 4-cameras (Figure B.3) mounted on the towing carriage and a number of markers mounted on the vessel (Figure C.1). The cameras emit infrared light and receive the light reflected from the markers. The 3-dimensional positions of the markers are calculated from the 2-dimensional markers' positions appearing simultaneously in the four cameras which were arranged in different positions.

Table C.1. Supply vessel main particulars.

V_{dis}	Displacement volume	2376 m ³
m	Mass	2433 tons
L_{oa}	Overall length	68.10 m
L_{pp}	Length between perpendiculars	59.13 m
B	Breadth	13.724 m
T	Design draught	4.59 m
$(\tau_{\text{surge}})_{\max}$	Maximum thrust force in surge	0.3×10^6 N
$(\tau_{\text{sway}})_{\max}$	Maximum thrust force in sway	0.12×10^6 N
$(\tau_{\text{yaw}})_{\max}$	Maximum thrust force in yaw	9.7×10^6 Nm

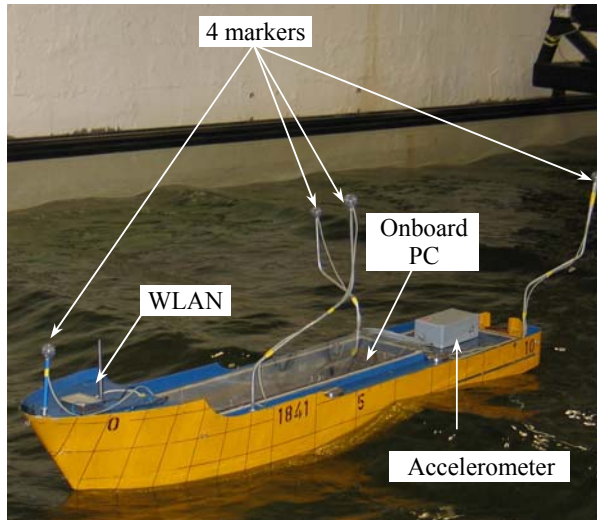


Figure C.1. Cybership III.

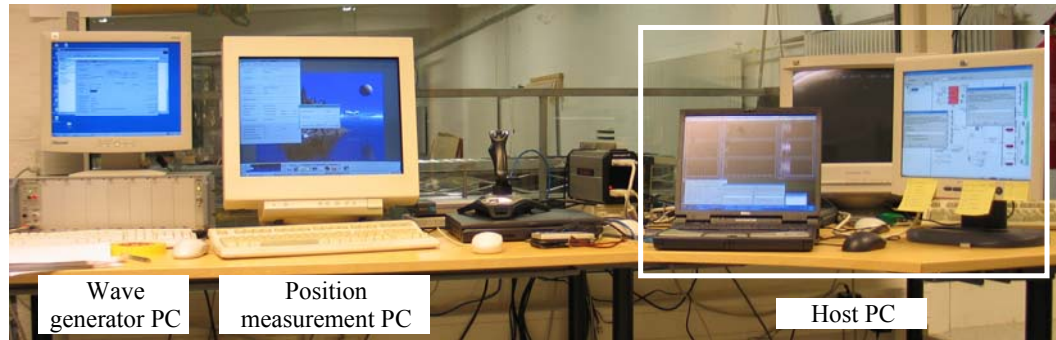


Figure C.2. PC in control room.

C.2 Bollard Pull Tests of Cybership III.

C.2.1 Cybership III Thruster Configuration

Arrangement of the four thrusters on the Cybership III is shown in Figure C.3.

Two main (port and starboard) azimuth thrusters locate at the stern of the vessel while one azimuth and one tunnel thruster are arranged at the bow of the vessel. The specifications of the four thrusters are shown in Table C.2.

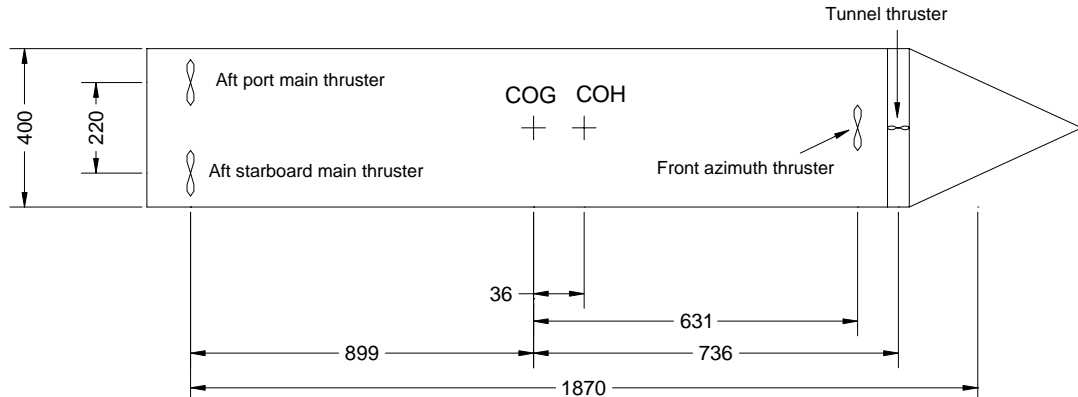


Figure C.3. Thruster distance.

Table C.2. Thruster specifications

Specifications	Aft port main thruster	Aft starboard main thruster	Front azimuth thruster	Front tunnel thruster
Number of blades	4	4	4	3
Diameter (D)	9 cm	9 cm	4 cm	3 cm
Propeller disc area (A_p)	62.6 cm^2	62.6 cm^2	12.6 cm^2	7.1 cm^2
Max shaft speed	1000 rpm	1000 rpm	2500 rpm	2300 rpm

C.2.2 Experimental Setup

There are seven Tests to determine the thrust characteristics of the four thrusters in different angles: (a) Port Main thruster at 0° , (b) Starboard Main thruster at 0° , (c) Port Main thruster at 30° , (d) Starboard Main thruster at 30° , (e) Front Azimuth thruster at 0° , (f) Front Azimuth thruster at 90° , and (g) Tunnel thruster. The setups for the first five Tests and the last two Tests are shown in Figures C.4 and C.5, respectively

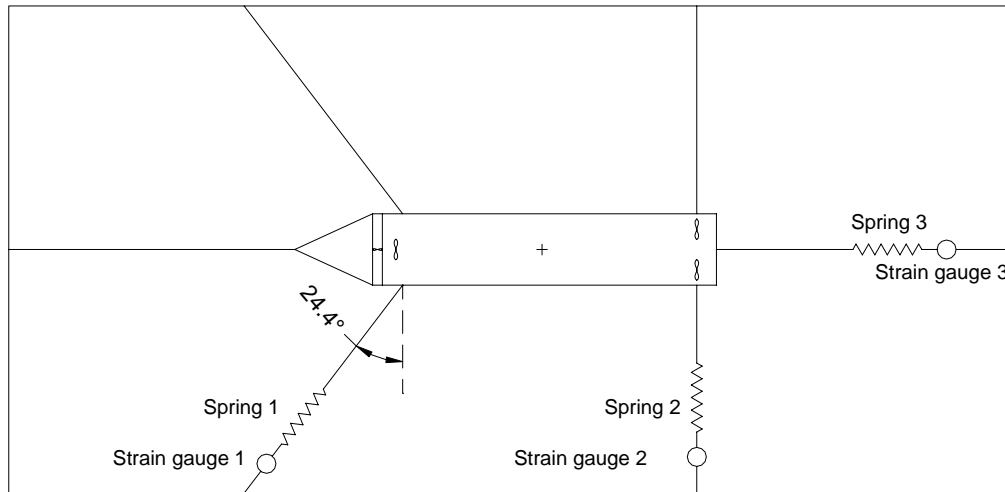


Figure C.4. Experimental setup for test (a) Port Main thruster at 0° , (b) Starboard Main thruster at 0° , (c) Port Main thruster at 30° , (d) Starboard Main thruster at 30° , and (e) Front Azimuth thruster at 0° .

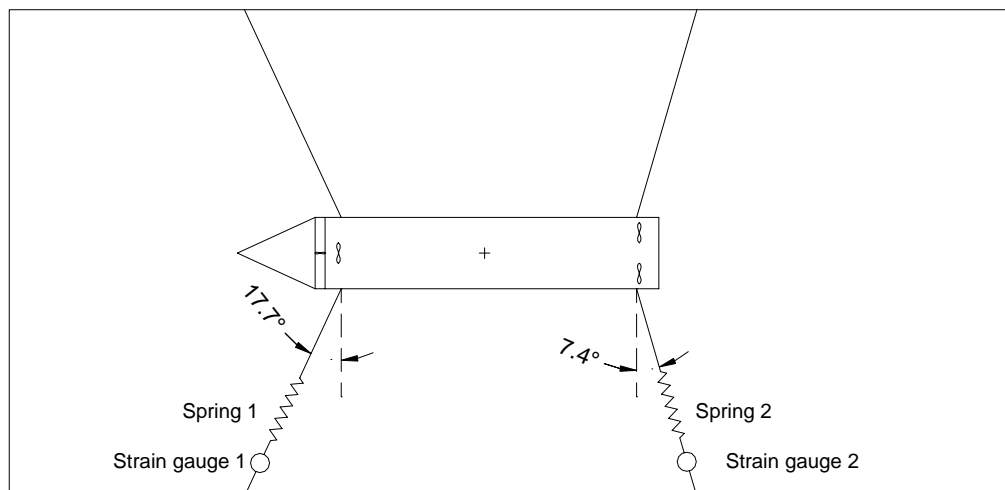


Figure C.5. Experimental setup for test (f) Front Azimuth thruster at 90° , and (g) Tunnel thruster.

C.2.3 Thruster Characteristics

The thrust characteristics of the four thrusters in different angles are shown in Figure C.6 and Table C.3.

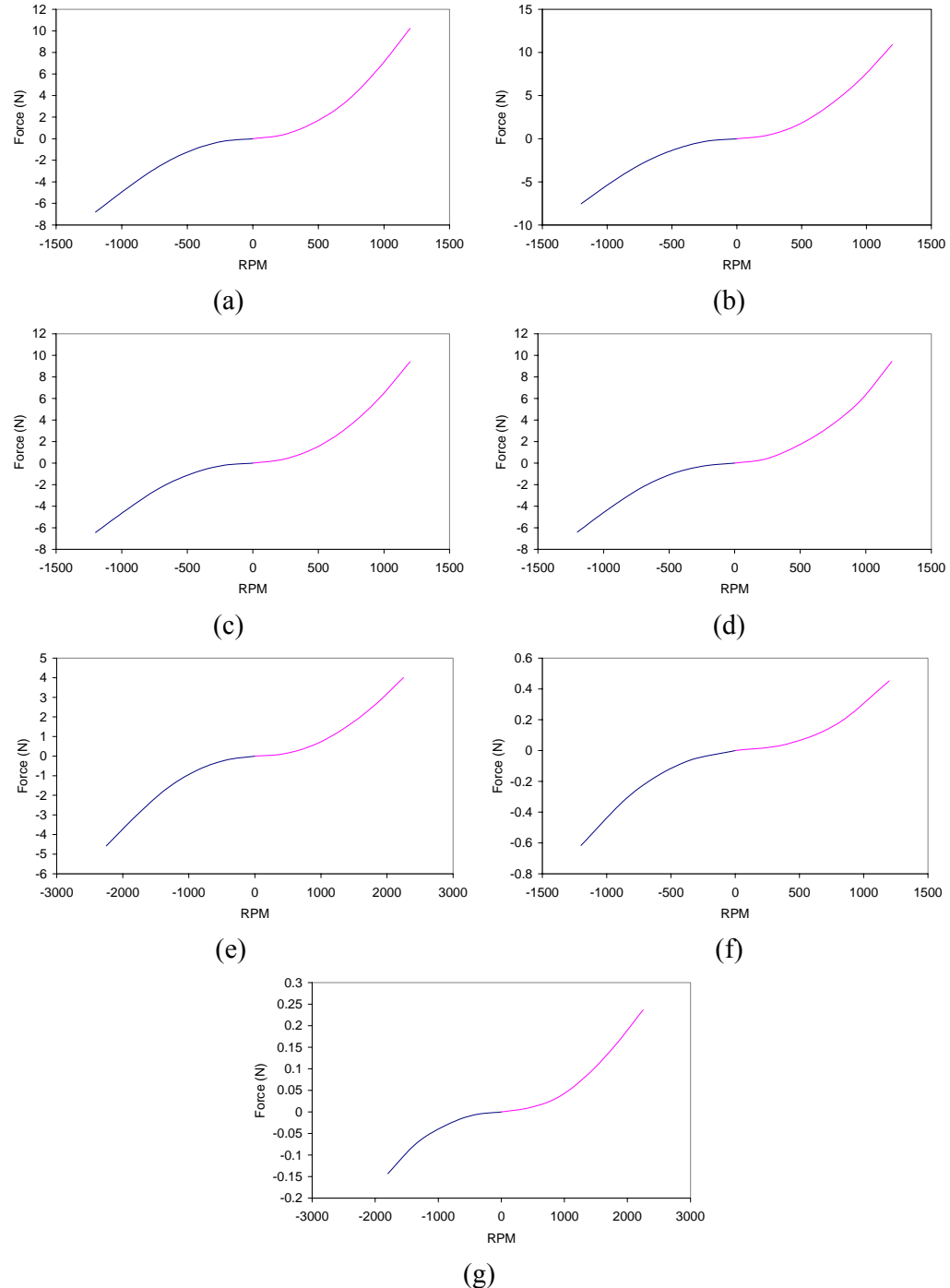


Figure C.6. Thrust characteristics for (a) Port Main at thruster 0° , (b) Starboard Main thruster at 0° , (c) Port Main thruster at 30° , (d) Starboard Main thruster at 30° , (e) Front Azimuth thruster at 0° , (f) Front Azimuth thruster at 90° , and (g) Tunnel thruster.

Table C.3. Thrust characteristics.

Test no.	Thruster	Thrust coefficient for negative RPM K_{Tn} (N/RPM ²)	Thrust coefficient for positive RPM K_{Tp} (N/RPM ²)
1	Port Main at 0°	4.7656E-06	7.1256E-06
2	Starboard Main at 0°	5.2602E-06	7.6005E-06
3	Port Main at 30°	4.5211E-06	6.5442E-06
4	Starboard Main at 30°	4.4819E-06	6.4645E-06
5	Front Azimuth at 0°	9.0737E-07	7.9927E-07
6	Front Azimuth at 90°	4.2357E-07	3.1817E-07
7	Tunnel	4.4126E-08	4.7201E-08

Appendix D Marine Systems Simulator

D.1 Introduction

The Marine Systems Simulator (MSS) has been developed by Professors, Master students, and PhD students in NTNU. MSS is a platform developed in Matlab/Simulink® environment for simulating different floating structures with focus on the control system design. MSS is a combination of three toolboxes: Marine GNC (Guidance and Navigation Control), MCSim (Marine Cybernetics Simulator), and DCMV (Dynamics and Control of Marine Vehicles) Toolboxes. Marine GNC was mainly developed by Fossen (2002). MCSim first introduced in Sørensen et al. (2003) was primarily to simulate the DP marine vessels. DCMV was developed by Perez and Blanke (2003) for autopilot design.

According to Perez et al. (2005) MSS has 2 main blocks that are dynamic model of the vessel (equation of motions of the vessel and sub-blocks for environment simulations) and control system blocks including the dynamics of the propulsion system. Figure D.1 shows main blocks from MSS library for simulating a DP vessel. It is noted that each block contains sub-blocks.

D.2 Simulation of Second-Order Wave Load for DP Vessel

Accessibility and flexibility of MSS due to its modular development in Matlab/Simulink® make users able to modify the standard library and/or add more blocks to the library to satisfy the users' preferred model. The second-order wave loads acting on the vessel in the current version of MSS are simulated by mean wave-drift loads while it should contain both mean wave-drift and slowly-varying wave loads.

Objective of this Appendix is to add second-order slowly-varying wave load to second-order mean wave load in LF model simulation of MSS.

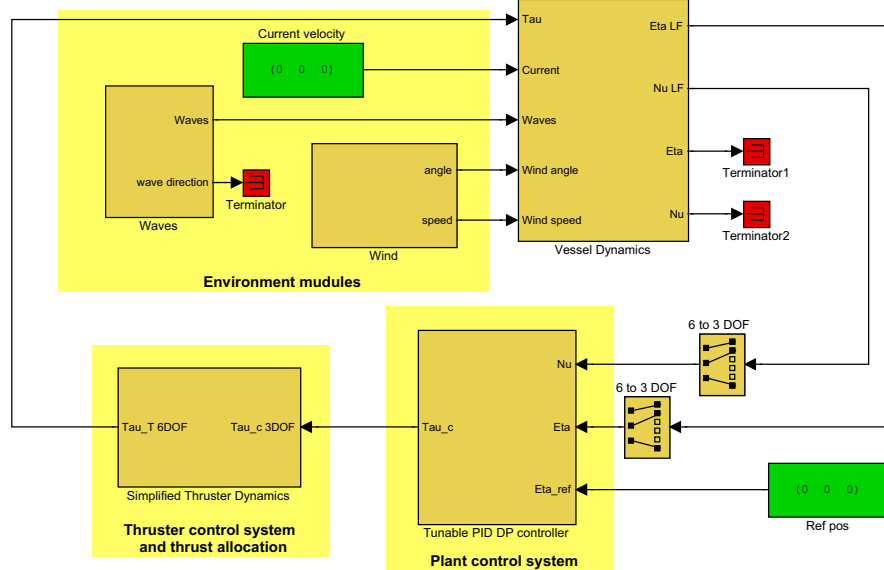


Figure D.1. An example of to simulating DP vessel using MSS.

D.2.1 Formulation

The second-order wave effects are divided into mean, and slowly-varying (difference frequencies) loads. The second-order wave effects can be done by means of quadratic transfer functions (Faltinsen, 1990), according to

$$\begin{aligned} \tau_{iwave2} &= \bar{\tau}_{wm}^i + \tau_{wsy}^i \\ &= \sum_{j=1}^N \sum_{k=1}^N A_j A_k \left[T_{jk}^{ic} \cos((\omega_k - \omega_j)t + \varepsilon_k - \varepsilon_j) + T_{jk}^{is} \sin((\omega_k - \omega_j)t + \varepsilon_k - \varepsilon_j) \right], \end{aligned} \quad (\text{D.1})$$

where $\bar{\tau}_{wm}^i$ and τ_{wsy}^i are mean and slowly-varying wave load, respectively. ω_j is the wave frequency, A_j is the wave amplitude and ε_j is a random phase angle. The superscript c and s denote cos and sin, respectively. The quadratic transfer functions T_{jk} are dependent on both the first and second order velocity potentials, which require a nonlinear panel methodology. For 3DOF, i is 1 for surge, 2 for sway, 3 for yaw. The

subscripts k and j denote k th and j th frequency components obtained by dividing the sea wave spectrum into N equal intervals.

Newman (1974) proposed simplification for second order wave load, given by

$$\begin{aligned}\tau_{iwave2} &= \bar{\tau}_{wm}^i + \tau_{wsy}^i \\ &= 2 \left(\sum_{j=1}^N A_j |T_{jj}^i|^{1/2} \cos(\omega_j t + \varepsilon_j) \right)^2.\end{aligned}\quad (\text{D.2})$$

The second order transfer function is interpolated based on given wave frequency and relative angle between wave angle and vessel's heading angle, according to

$$T_{jj}^i = T_{jj}^i(\omega_j, \beta_{wave} - \psi). \quad (\text{D.3})$$

It is noted that only mean wave drift load is considered in MCSim®, given by

$$\bar{\tau}_{wm}^i = \sum_{j=1}^N A_j^2 T_{jj}^i. \quad (\text{D.4})$$

D.2.2 Simulation results

There are two simulation Cases: (a) the fixed supply vessel ($L_{pp} = 80\text{m}$, $B = 17.4\text{m}$, $T = 5.6\text{ m}$) and (b) the same vessel kept in fixed position and heading $[x, y, \psi]^T = [0, 0, 0]^T$ by DP system. Only wave excitation is considered. Wave attacks at 135° . The ship is exposed to wave $H_s = 2.5\text{m}$, $T_p = 9.24\text{s}$ during 30000s.

The results are compared to MSS in which only mean wave drift is considered. Spectral analysis is used to check the LF motion frequency. The simulation results of Cases (a) are shown in Table D.1 and Figure D.2. The simulation results of Cases (b) are shown in Table D.2 and Figures from D.3 to D.6.

a) Case 1: Fixed vessel at position and heading $\eta = [0, 0, 0]^T$

Table D.1. Simulation results of Case (a): the fixed vessel.

	Force in Surge (kN)	Force in Sway (kN)	Yaw (kNm)
Mean wave drift force calculated by (D.4)	-6.4704	11.0112	176.3973
Mean wave drift force calculated by (D.2) over 30000s	-6.4761	11.0200	177.0093
Mean wave drift force calculated by (D.2) with filtered high frequency components over 30000s	-6.4758	11.0195	177.0010

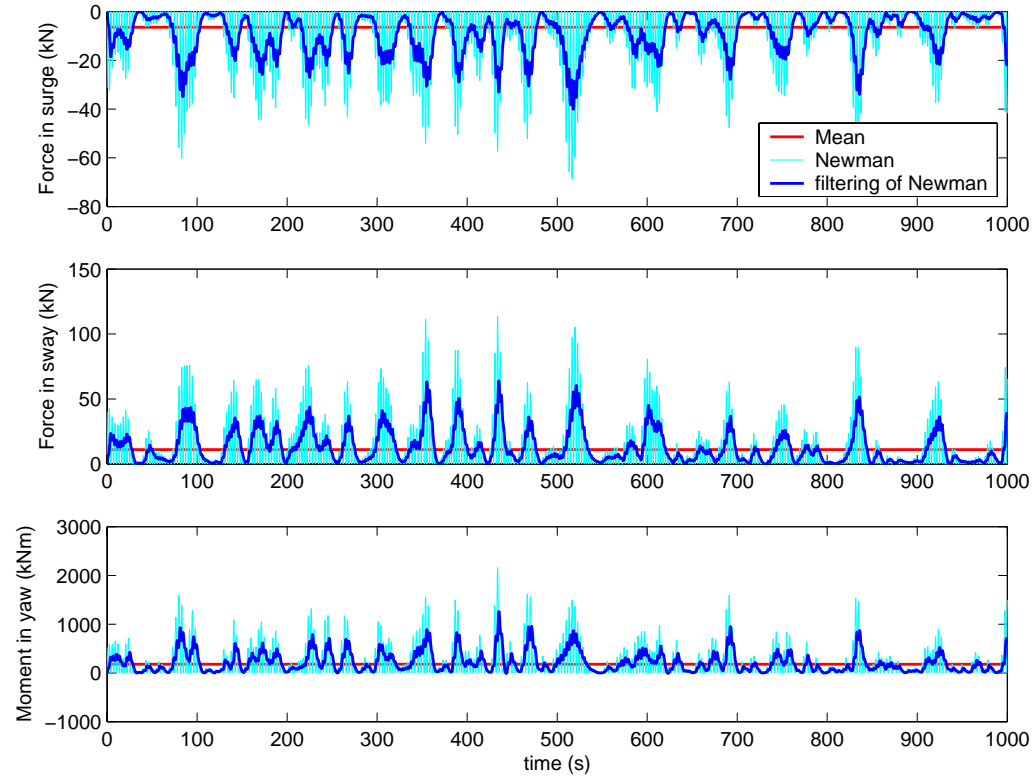


Figure D.2. Second-order wave-drift load acting on fixed vessel.

b) Case 2: DP vessel at desired position and heading $\eta = [0, 0, 0]^T$

Table D.2. Simulation results of Case (b): the DP vessel.

	Force in Surge (kN)	Force in Sway (kN)	Yaw (kNm)
Mean wave drift force calculated by (D.4)	-6.7402	10.982	171.29
Mean wave drift force calculated by (D.2) over 30000s	-6.7252	10.987	171.35
Mean wave drift force calculated by (D.2) with filtered high frequency components over 30000s	-6.7245	10.985	171.34

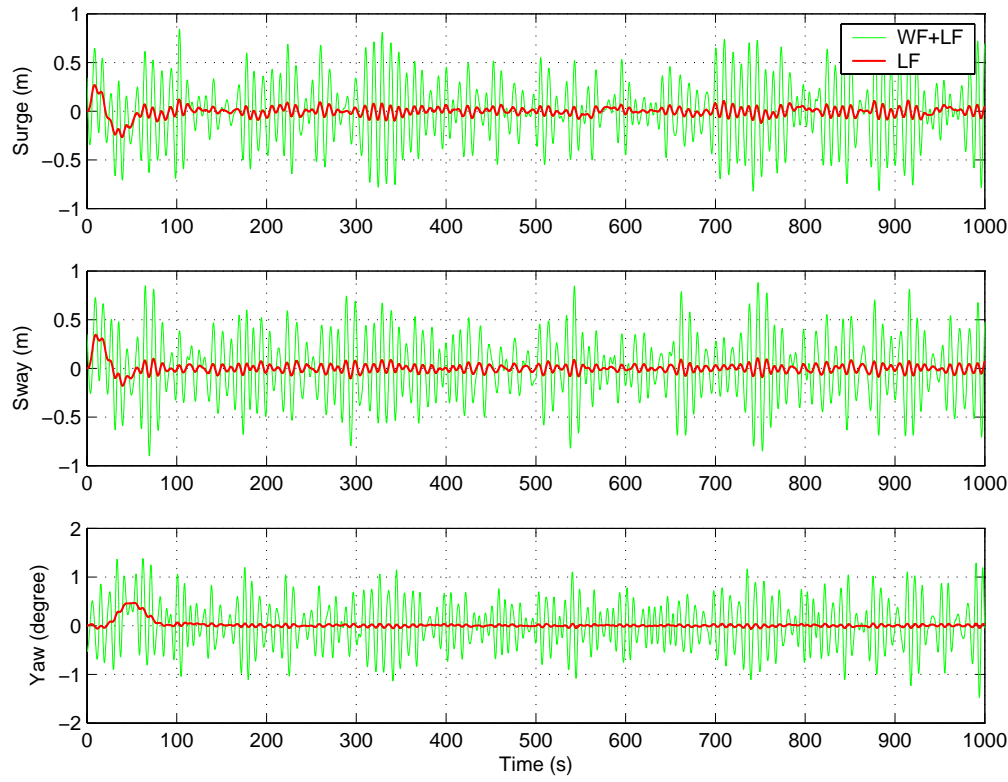


Figure D.3. Performance of DP vessel with mean wave-drift load simulation.

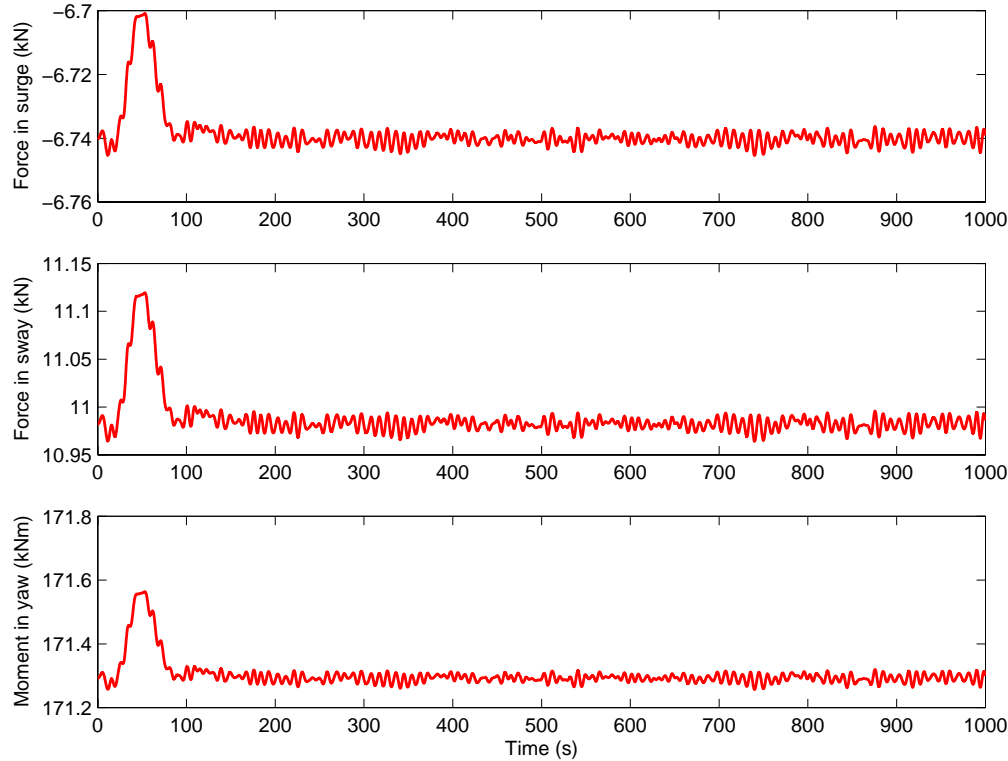


Figure D.4. Mean wave-drift load acting on the DP vessel.

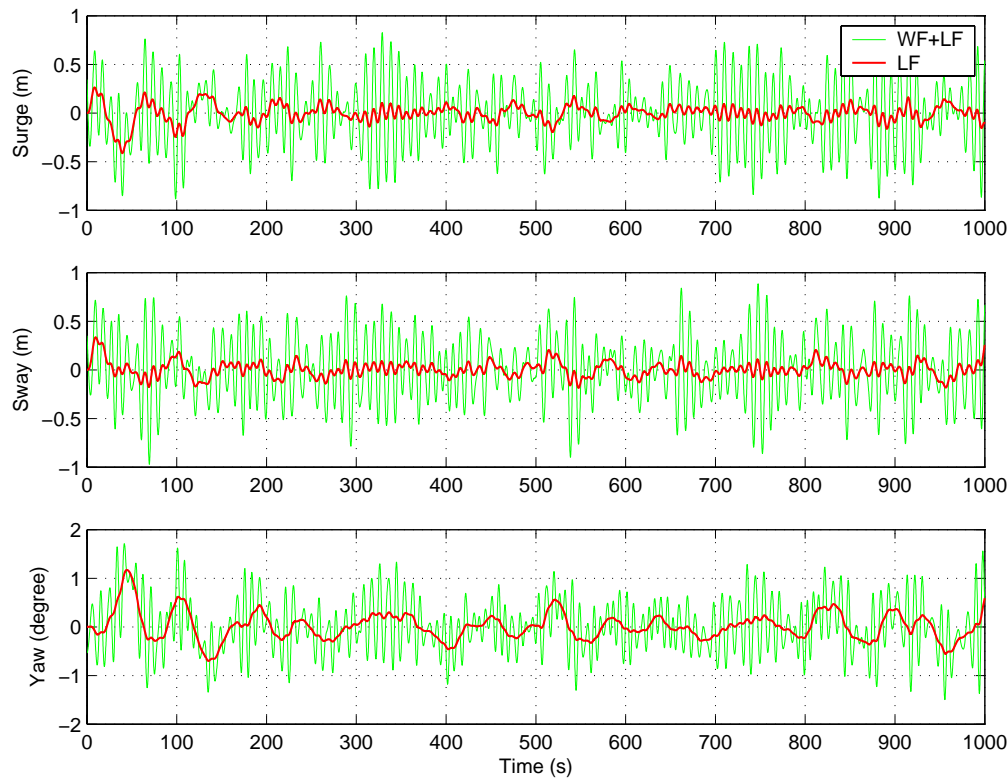


Figure D.5. Performance of DP vessel with *filtered* Newman second-order wave-drift load simulation.

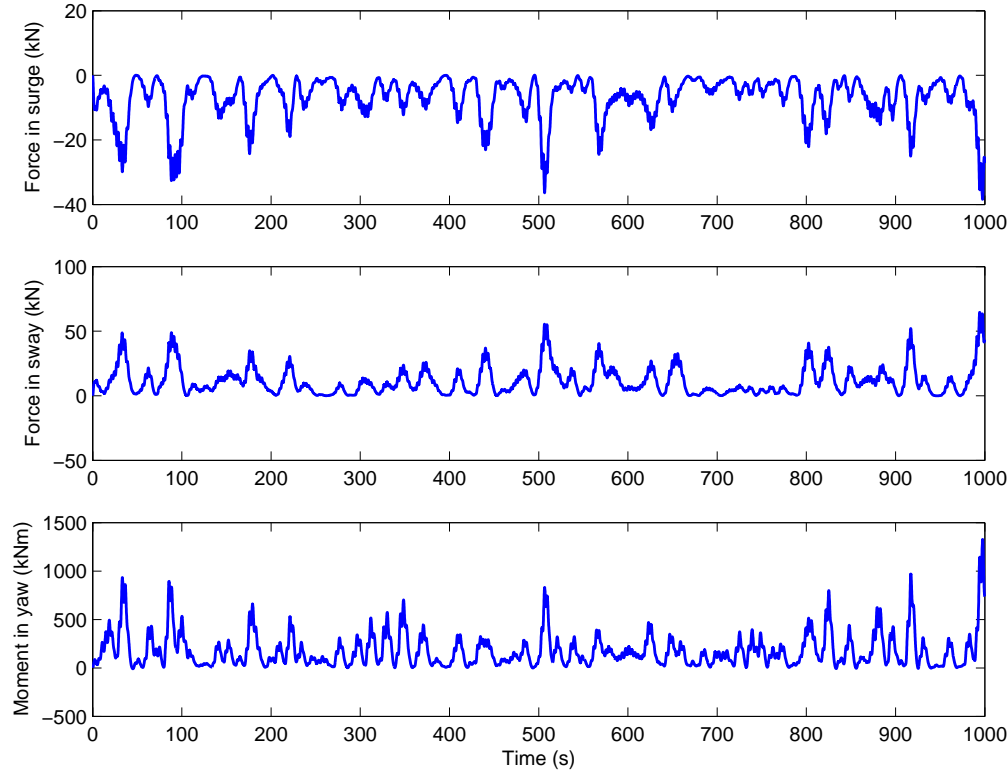


Figure D.6. Filtered Newman second-order wave-drift load acting on the DP vessel.

Appendix E Publications and Submitted Paper during this Period

E.1 Journal papers

- [1] Nguyen T. D., Sørensen A. J. and Quek S. T. (2005a). Multi-Operational Hybrid Controller Structure for Station Keeping and Transit Operations of Marine Vessels. *Submitted to IEEE Transaction on Control System Technology*.
- [2] Nguyen T. D., Sørensen A. J. and Quek S. T. (2005b). Design of High Level Hybrid Controller for Dynamic Positioning from Calm to Extreme Sea Conditions. *Submitted to Automatica*.

E.2 Conference papers

- [3] Nguyen T. D. and S. T. Quek (2003). Dynamic Position Control of Floating Structures via Slow-Drift Force Ensemble Simulations. *In Proceedings of KKCNN Symposium on Civil Engineering*, Korea, December 8-10.
- [4] Nguyen T. D. and S. T. Quek (2004). Position control of floating structures via slow-drift force ensemble simulations. *In Proceedings of 23rd International Offshore Mechanics and Arctic Engineering Conference, ASME, OMAE2004-51607*, Vancouver, Canada, June 20-25.
- [5] Nguyen T. D., A. J. Sørensen and S. T. Quek (2004). Observer for Dynamic Positioning of Floating Structures in Extreme Seas. *In Proceedings of KKCNN Symposium on Civil Engineering*, Thailand, December 13-15.
- [6] Sørensen A. J., S. T. Quek and T. D. Nguyen (2005). Improved Operability and Safety of DP Vessels Using Hybrid Control Concept. *In Proceeding of International Conference on Technology and Operation of Offshore Support Vessels – OSV 2005*, National University of Singapore, Singapore, 20-21 September.
- [7] Nguyen T. D., A. J. Sørensen and S. T. Quek (2005c). Hybrid Controller for Dynamic Positioning from Calm to Extreme Seas – Experiments with a Model Ship. *In Proceedings of KKCNN Symposium on Civil Engineering*, Taiwan, December 18-21.